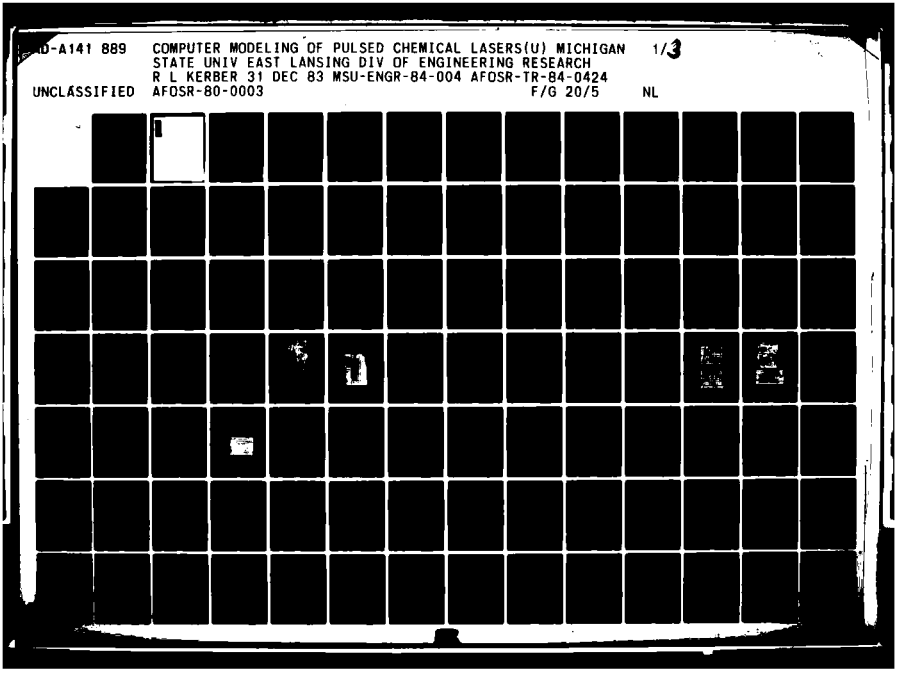
D-A141 889 COMPUTER MODELING OF PULSED CHEMICAL LASERS(U) MICHIGAN 1/3
STATE UNIV EAST LANSING DIV OF ENGINEERING RESEARCH
R L KERBER 31 DEC 83 MSU-ENGR-84-004 AFOSR-TR-84-0424
UNCLASSIFIED AFOSR-80-0003 F/G 20/5 NL

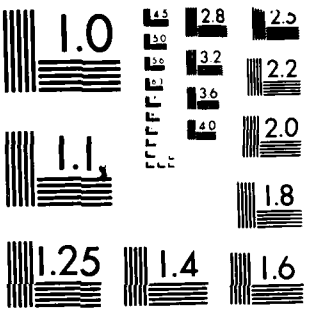

unclassified
SECURITY CLASSIFICATION OF THIS PAGE

REPORT DOCUMENTATION PAGE

1a. REPORT SECURITY CLASSIFICATION: unclassified	1b. RESTRICTIVE MARKINGS
2a. SECURITY CLASSIFICATION AUTHORITY	3. DISTRIBUTION/AVAILABILITY OF REPORT: Approved for public release, distribution unlimited
2b. DECLASSIFICATION/DOWNGRADING SCHEDULE	
4. PERFORMING ORGANIZATION REPORT NUMBER(S): MSU-ENGR-84-004	5. MONITORING ORGANIZATION REPORT NUMBER(S): AFOSR-TR- 84-0424
6a. NAME OF PERFORMING ORGANIZATION: Michigan State University; 6b. OFFICE SYMBOL (If applicable)	7a. NAME OF MONITORING ORGANIZATION: Air Force Office of Scientific Research
6c. ADDRESS (City, State and ZIP Code): East Lansing, MI 48824	7b. ADDRESS (City, State and ZIP Code): Bldg. 410 Bolling AFB, DC 20332
8a. NAME OF FUNDING/SPONSORING ORGANIZATION: Air Force Off. Sci. Research; 8b. OFFICE SYMBOL (If applicable): NC	9. PROCUREMENT INSTRUMENT IDENTIFICATION NUMBER: AFOSR-80-0003
8c. ADDRESS (City, State and ZIP Code): Bldg. 410 Bolling Air Force Base	10. SOURCE OF FUNDING NOS. — PROGRAM ELEMENT NO.: 61102F; PROJECT NO.: 2303; TASK NO.: B1; WORK UNIT NO.:
11. TITLE (Include Security Classification): Computer Modeling of Pulsed Chemical Lasers	
12. PERSONAL AUTHOR(S): Ronald L. Kerber	
13a. TYPE OF REPORT: Final; 13b. TIME COVERED FROM 11/1/79 TO 10/31/83	14. DATE OF REPORT (Yr., Mo., Day): December 31, 1983; 15. PAGE COUNT: 285
16. SUPPLEMENTARY NOTATION	
17. COSATI CODES — FIELD / GROUP / SUB. GR.	18. SUBJECT TERMS (Continue on reverse if necessary and identify by block number): chemical lasers, kinetic lasers

19. ABSTRACT (Continue on reverse if necessary and identify by block number)

A computer modeling study of pulsed H_2+F_2 and D_2+F_2 chemical lasers has been conducted. This work was directed toward understanding the role of kinetic rotational relaxation and vibrational-rotational relaxation mechanisms in HF and DF lasers. This study resulted in very comprehensive computer models that could predict spectral characteristics of pulsed laser performance using kinetic rate equation data and experimental conditions.

In addition, experiments were conducted on a flash initiated pulsed H_2+F_2 laser facility to generate data to compare with the models developed in this study. Models were also developed that demonstrated the performance of pulsed laser driven amplifiers and optical resonance transfer lasers. Finally, simple models were constructed that permit efficient prediction of pulse energy and pulse power.

(over)

20. DISTRIBUTION/AVAILABILITY OF ABSTRACT: UNCLASSIFIED/UNLIMITED ☒ SAME AS RPT. ☒ DTIC USERS ☐	21. ABSTRACT SECURITY CLASSIFICATION: unclassified
22a. NAME OF RESPONSIBLE INDIVIDUAL: Lee E Myers, Capt, USAF	22b. TELEPHONE NUMBER (Include Area Code): (202) 767-4963; 22c. OFFICE SYMBOL: NC

DD FORM 1473, 83 APR — EDITION OF 1 JAN 73 IS OBSOLETE.

UNCLASSIFIED
SECURITY CLASSIFICATION OF THIS PAGE

Results of these studies are contained in the technical publications, technical reports and theses listed in the Completed Project Summary.

Model predictions continue to improve as our understanding of the kinetic mechanisms improves. It is felt that these models are sufficiently comprehensive in kinetic mechanisms that no future model development is required. However, this study has pointed out a need for two follow-on efforts.

(1) The models should be expanded to include kinetics associated with $H_2/O_2/F_2$ mixtures since many systems use O_2 as a prereaction inhibitor.

(2) More work is required to improve the comparison of the comprehensive model predictions with experiment.

SUMMARY

A computer modeling study of pulsed H_2+F_2 and D_2+F_2 chemical lasers has been conducted. This work was directed toward understanding the role of kinetic rotational relaxation and vibrational-rotational relaxation mechanisms in HF and DF lasers. This study resulted in very comprehensive computer models that could predict spectral characteristics of pulsed laser performance using kinetic rate equation data and experimental conditions.

In addition, experiments were conducted on a flash initiated pulsed H_2+F_2 laser facility to generate data to compare with the models developed in this study. Models were also developed that demonstrated the performance of pulsed laser driven amplifiers and optical resonance transfer lasers. Finally, simple models were constructed that permit efficient prediction of pulse energy and pulse power.

Results of these studies are contained in the technical publications, technical reports and theses listed in Tables 1, 2, and 3, respectively.

The remainder of this report is the Ph.D. thesis of Paul E. Sojka. This study represents the capstone of the present work which ties the modeling to experimental results.

Model predictions continue to improve as our understanding of the kinetic mechanisms improves. It is felt that these models are sufficiently comprehensive in kinetic mechanisms that no future model development is required. However, this study has pointed out a need for two follow-on efforts.

(1) The models should be expanded to include kinetics associated with $H_2/O_2/F_2$ mixtures since many systems use O_2 as a prereaction inhibitor.

(2) More work is required to improve the comparison of the comprehensive model predictions with experiment.

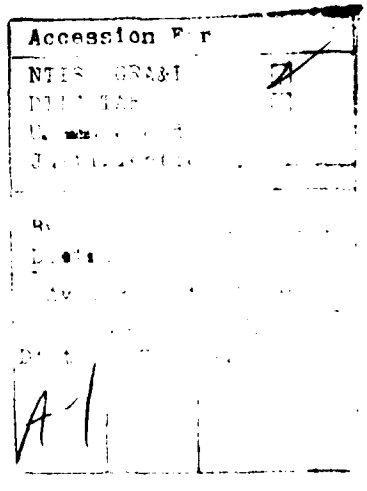

TABLE 1

TECHNICAL PUBLICATIONS

Computer Modeling of Pulsed Chemical Lasers
AFOSR Grant 80-003

J. J. T. Hough and R. L. Kerber, "Theoretical investigation of the effect of rotational nonequilibrium on predicted performance of pulsed HF chemical lasers," IEEE J. Quantum Electron. QE-11, 699 (1975).

R. L. Kerber, "Modeling of rotational nonequilibrium effects in pulsed HF chain reaction lasers," Proceedings of AFOSR/AFWL Workshop on the Numerical Solution of Ordinary Differential Equations, Albuquerque, New Mexico (May 6-7, 1976).

J. J. T. Hough and R. L. Kerber, "Rotational nonequilibrium mechanisms in pulsed H_2 + F_2 chain reaction lasers, I. effect on gross laser performance parameters," Appl. Optics 17, 2369 (1978).

R. C. Brown, K. Emery, and R. L. Kerber, "Rotational nonequilibrium mechanisms in pulsed H_2 + F_2 chain reaction lasers, 2: Effect of VR energy exchange," Appl. Optics 19, 292 (1980).

D. H. Stone and R. L. Kerber, "A statistical model for $H_2(D_2)$ + F_2 product distributions using information theory," Proceedings of LASERS '79, Society for Optical and Quantum Electronics, Edited by V. J. Corcoran, pp. 167-177, STS Press, McLean, VA, 1980.

R. C. Brown and R. L. Kerber, "An analysis of the role of kinetic mechanisms affecting H_2 + F_2 laser performance," Journal de Physique C9, Supplement 11, p. C9-9, (1980).

P. E. Sojka and R. L. Kerber, "Time resolved spectra and small signal gain in HF: An experimental and theoretical investigation," Proceedings of the Fourth International Symposium on Gas Flow and Chemical Lasers, Stresa, Italy, September 13-17, 1982.

R. C. Brown and R. L. Kerber, "A study of the effect of vibrational to rotational to translational relaxation mechanisms in pulsed H_2 + F_2 lasers," accepted for publication in Applied Optics.

P. E. Sojka and R. L. Kerber, "Time resolved spectroscopy and small signal gain in a pulsed HF laser: Experiment," to be published.

P. E. Sojka and R. L. Kerber, "Time resolved spectroscopy and small signal gain in a pulsed HF laser: Theory," to be published.

TABLE 2

TECHNICAL REPORTS
Computer Modeling of Pulsed Chemical Lasers
AFOSR Grant 80-003

J. J. T. Hough, W. Jaul, and R. L. Kerber, "Modeling of rotational nonequilibrium effects in pulsed HF chain reaction lasers," Proceedings of the AFWL/AFOSR Workshop on the Numerical Solution of Stiff Systems of Ordinary Differential Equations, pp. 179-206, AFWL TR-76-328, August, 1977.

R. L. Kerber, "Rotational nonequilibrium mechanisms in pulsed H_2 + F_2 chain reaction lasers," AFOSR Interim Progress Report, October, 1977.

R. C. Brown and R. L. Kerber, "DF Alband: A simple pulsed D_2 + F_2 laser model," AFOSR Interim Progress Report, June, 1978.

K. Emery, R. Brown, P. Sojka, and R. L. Kerber, "Preliminary results in modeling VR mechanisms and laser diagnostics in pulsed H_2 + F_2 lasers," AFOSR Interim Progress Report, July, 1979.

R. C. Brown, K. A. Emery, and R. L. Kerber, "Rotational mechanisms in pulsed H_2 + F_2 chain reaction lasers, 2: Effect of VR energy exchange," AFOSR Interim Progress Report, August, 1979.

R. L. Kerber, "Computer modeling of pulsed chemical lasers," AFOSR Final Report, December, 1979.

R. C. Brown and R. L. Kerber, "A study of the effect of vibrational to rotational to translational relaxation mechanisms in pulsed H_2 + F_2 lasers," AFOSR Interim Progress Report, No. MSU ENGR-80-004, July, 1980.

R. C. Brown and R. L. Kerber, "Kinetic model of a single pass pulsed H_2 + F_2 amplifier," AFOSR Interim Progress Report No. MSU-ENGR-80-005, July, 1980.

R. C. Brown and R. L. Kerber, "Parametric study of rotational nonequilibrium models of pulsed HF and DF chain reaction chemical lasers," AFOSR Interim Progress Report No. MSU-ENGR-80-013, January, 1980.

R. L. Kerber, "Rotational nonequilibrium mechanisms in pulsed H_2 + F_2 chain reaction lasers," AFOSR Interim Progress Report, 1980.

W. K. Jaul and R. L. Kerber, "A theoretical assessment of the kinetic limitations of the chemically pumped HF optical resonant transfer laser," Report No. MSU-ENGR-82-018, August, 1982.

S. T. Amimoto, J. S. Whittier, G. Harper, R. Hofland, Jr., J. M. Walters, Jr., T. a. Barr, Jr., W. K. Jaul, and R. L. Kerber, "High-performance DF-CO_2 chain-reaction laser," Air Force Systems Command Report No. SD-TR-83-05, February, 1983.

TABLE 3

Ph.D. Theses
AFOSR Grant 80-003

Joseph J. T. Hough
"Theoretical and Experimental Investigation of the Pulsed HF Chemical Laser," 1975

David H. Stone
"An Information Theory Approach to Hydrogen Halide Reaction Product Distribution," 1980

Robert C. Brown
"A Theoretical Assessment of Vibrational to Rotational Energy Exchange in the Hydrogen Fluoride Chemical Laser," 1980

Paul E. Sojka
"Time Resolved Spectroscopy and Small Signal Gain in a Flash Initiated Pulsed HF Laser," 1983

M.S. Thesis
AFOSR Grant 80-003

Keith A. Emery
"A Theoretical Investigation of Rotational Nonequilibrium Phenomena in the Pulsed Hydrogen Fluoride Laser System," 1979

TIME RESOLVED SPECTROSCOPY AND SMALL SIGNAL GAIN IN A FLASH INITIATED, PULSED HF LASER

By

Paul E. Sojka

A DISSERTATION

Submitted to
Michigan State University
in partial fulfillment of the requirements
for the degree of

DOCTOR OF PHILOSOPHY

Department of Mechanical Engineering

1983

ABSTRACT

TIME RESOLVED SPECTROSCOPY AND SMALL SIGNAL GAIN IN A FLASH INITIATED, PULSED HF LASER

By

Paul E. Sojka

An experimental and computer modeling investigation of a pulsed, flash photolysis initiated, $H_2 + F_2$ chemical laser was undertaken. Time resolved spectral (TRS) output, time history of small signal gain (SSG) and total pulse energy (TPE) were measured. Several experimental trends were noted.

For the TRS results, regular shifts of individual transition initiation, termination and peak intensity times with increasing rotational level are observed. Transition pulse duration increased with rotational level.

For the SSG results, regular shifts of positive gain initiation, termination and peak gain times with increasing rotational level were observed. Positive gain duration increased with rotational level.

The experimental TRS results were compared with those of other researchers and then with the results of computer simulations. Pulse duration in this work was longer than that reported elsewhere. This was most likely due to weak initiation of the $H_2 + F_2$ chain. No

reportable rotational lasing was observed. This is in contrast to other work but in agreement with model calculations.

In addition to the experimental study, an existing computer model was modified by the substitution of a wavelength dependent threshold gain in place of the previous wavelength independent threshold gain and by the addition of a flash photolysis initiation option. The modified model and a second, simplified, model were used to simulate the TRS and SSG experiments. Two model rate coefficients were varied to investigate the effects of the hot reaction vibrational pumping distribution and of the vibrational deactivation mechanism rate coefficients on the simplified model TRS and SSF results.

The experimental TRS and SSG results were compared to the calculations resulting from the two models.

The results of the simplified model, assuming Vibrational-Translational energy transfer, more closely duplicated experiment than did the results of the modified model (assuming Vibrational-Rotational energy transfer). This is in contrast to the currently accepted understanding of kinetic mechanisms.

Conclusions reached in this study were: (1) The time scales of SSG and TRS are not the same, SSG having much longer durations. (2) The trends of initiation, termination and peak gain or intensity times are similar for SSG and TRS. (3) Computer models are capable of accurately predicting the time resolved characteristics of gain and emission. (4) Further work is necessary to determine the form of V-R,T energy transfer.

TABLE OF CONTENTS

		Page
LIST OF TABLES		vii
LIST OF FIGURES		iix
1. INTRODUCTION		1
1.1	Background	1
1.2	Present Work	6
2. EXPERIMENTAL INVESTIGATION OF AN HF LASER		13
2.1	Introduction	13
2.2	Experimental Study	14
2.2.1	Flash Photolysis Laser	14
2.2.2	Diagnostics	26
2.3	Results of Time Resolved Spectroscopy Studies	38
2.3.1	Introduction	38
2.3.2	Time Resolved Spectroscopy Results for the Mixture $He:O_2:F_2:H_2$ = 20.8:1.0:4.6:1.2.	42
2.3.3	Time Resolved Spectroscopy Results for the Mixture $He:O_2:F_2:H_2$ = 22.0:1.0:2.7:1.0.	51
2.3.4	Results of Pure Rotational Lasing Studies	55
2.3.5	Discussion	57
2.4	Results of Small Signal Gain Studies	66
2.4.1	Introduction	66
2.4.2	Results of Small Signal Gain Studies for the Mixture $He:O_2:F_2:H_2$ = 20.8:1.0:4.6:1.2.	70
2.4.3	Results of Small Signal Gain Studies for the Mixture $He:O_2:F_2:H_2$ = 22.0:1.0:2.7:1.0.	72
2.4.4	Discussion	75
2.5	Results of Total Pulse Energy Studies	80

Page

3. COMPUTER SIMULATION OF AN HF LASER AND COMPARISON WITH EXPERIMENT. 81

3.1 Introduction. 81

3.2 Computer Modeling Results of Time Resolved Spectroscopy and Comparison with Experiment 88

3.2.1 Introduction. 88
3.2.2 Comparison of VT Modeling Results for Time Resolved Spectroscopy with Experiment: Initial Rate Package. 88
3.2.3 Comparison of VT Modeling Results for Time Resolved Spectroscopy with Experiment: Modified Vibrational Pumping Distribution . 91
3.2.4 Comparison of VT Modeling Results for Time Resolved Spectroscopy with Experiment: Modified Vibrational Pumping Distribution and Modified V-T Deactivation 93
3.2.5. Comparison of VR2OJ Modeling Results for Time Resolved Spectroscopy with Experiment. 95
3.2.6. Summary of Time Resolved Spectroscopy Modeling Results. 97

3.3 Computer Modeling Results of Small Signal Gain and Comparison with Experiment. 104

3.3.1 Introduction. 104
3.3.2 Comparison of VT Model Small Signal Gain Results with Experiment 105
3.3.3 Comparison of VR2OJ Model Small Signal Gain Results with Experiment 110
3.3.4 Summary of Small Signal Gain Modeling Results 113

4. SUMMARY AND CONCLUSIONS 120

APPENDIX A: COMPUTER MODEL FORMULATION 126

APPENDIX B: DETERMINATION OF INITIAL HF CONCENTRATION DUE TO PREREACTION 138

APPENDIX C: MODEL RATE COEFFICIENTS. 140

APPENDIX D: ERROR ANALYSIS FOR PROBING SMALL SIGNAL GAIN OFF LINE CENTER 144

APPENDIX E: RAW DATA FOR TIME RESOLVED SPECTROSCOPY PLOTS USED IN FIGURES 2.17 AND 2.21. 146

Page

APPENDIX F: TRS AND SSG PHOTOGRAPHES OF OSCILLOSCOPE DATA 149

REFERENCES 249

LIST OF TABLES

Table		Page
2.1	Summary of TRS Results from References [14, 17, 19, 42, 43, 52].	63
C.1	Current Rate Coefficients in $H_2 + F_2$ Systems.	141
C.2	VT Model Rate Coefficients for the $H_2 + F_2$ Chemical Laser.	143
E.1	Data for TRS presented in Figure 2.17	147
E.2	Data for TRS presented in Figure 2.21	148
F.1	SSG photographes, $He:O_2:F_2:H_2$=20.8:1.0:4.6:1.2, 102 torr.	149
F.2	TRS photographes, $He:O_2:F_2:H_2$=20.8:1.0:4.6:1.2, 36 torr .	152
F.3	TRS photographes, $He:O_2:F_2:H_2$=20.8:1.0:4.6:1.2, 102 torr.	158
F.4	TRS photographes, $He:O_2:F_2:H_2$=20.8:1.0:4.6:1.2, 331 torr.	165
F.5	SSG photographes, $He:O_2:F_2:H_2$=22.0:1.0:2.7:1.0, 102 torr.	172
F.6	SSG photographes, $He:O_2:F_2:H_2$=22.0:1.0:2.7:1.0, 331 torr.	179
F.7	TRS photographes, $He:O_2:F_2:H_2$=22.0:1.0:2.7:1.0, 36 torr .	187
F.8	TRS photographes, $He:O_2:F_2:H_2$=22.0:1.0:2.7:1.0, 102 torr.	199
F.9	TRS photographes, $He:O_2:F_2:H_2$=22.0:1.0:2.7:1.0, 331 torr, R_0=0.81	217
F.10	TRS photographes, He:O :F :H =22.0:1.0:2.7:1.0, 331 torr, R_0=0.97	233

LIST OF FIGURES

Figure		Page
2.1	Laser cell schematic.	15
2.2	Laser cell window configurations (a) laser cell window configuration for the mixture He:O_2:F_2:H_2= 20.8:1.0:4.6:1.2 (b) laser cell window configuration for the mixture He:O_2:F_2:H_2= 22.0:1.0:2.7:1.0.	16
2.3	Pulse discharge circuit schematic	19
2.4	Trigger circuit block diagram	20
2.5	Laser cell gas handling schematic	21
2.6	Hydrogen radial "sting" injection configuration	23
2.7	System photographs (a) mixing tube (b) laser cell.	24
2.8	Rotameter panel photograph.	25
2.9	Time resolved spectroscopy experimental configuration . .	27
2.10	Small signal gain experimental configuration.	28
2.11	Total pulse energy experimental configuration	29
2.12	Data photographs (a) typical TRS intensity trace (b) typical SSG trace	31
2.13	Photographs of experimental setup (a) photograph of monochromators (b) photograph of oscilloscopes	32
2.14	CW probe laser used in small signal gain tests.	34
2.15	Flashlamp intensity measurement experimental configuration	36

Figure		Page
2.16	Typical flashlamp intensity trace	37
2.17	Time resolved spectral output: He:O_2:F_2:H_2= 20.8:1.0:4.6:1.2 (a) 36 torr pressure (b) 102 torr pressure (c) 331 torr pressure	41
2.18	Spectral time history: He:O_2:F_2:H_2= 20.8:1.0:4.6:1.2, 36 torr pressure.	43
2.19	Spectral time history: He:O_2:F_2:H_2= 20.8:1.0:4.6:1.2, 102 torr pressure	44
2.20	Spectral time history: He:O_2:F_2:H_2= 20.8:1.0:4.6:1.2, 331 torr pressure	45
2.21	Time resolved spectral output: He:O_2:F_2:H_2= 22.0:1.0:2.7:1.0 (a) 36 torr, R_0 = 0.97 (b) 102 torr, R_0 = 0.97 (c) 331 torr, R_0 = 0.97 (d) 331 torr, R_0 = 0.81	53
2.22	Small signal gain time history: He:O_2:F_2:H_2=20.8:1.0:4.6:1.2 (a) v = 1-0 band, 102 torr (b) v = 2-1 band, 102 torr.	71
2.23	Small signal gain time history: He:O_2:F_2:H_2=22.0:1.0:2.7:1.0, (a) v = 1-0 band, 102 torr (b) v = 2-1 band, 102 torr (c) v = 1-0 band, 331 torr (d) v = 2-1 band, 331 torr.	73
3.1	Time resolved spectral output: comparison of VT model results and experiment using rate package VT (standard rates), He:O_2:F_2:H_2 = 20.8:1.0:4.6:1.2 (a) experimental results, 36 torr (b) experimental results, 102 torr (a) experimental results, 331 torr (d) model results, 36 torr (e) model results, 102 torr (f) model results, 331 torr	89

Figure

Page

3.2 Time resolved spectral output: comparison of VT model results and experiment using rate package VT2, $He:O_2:F_2:H_2$ = 20.8:1.0:4.6:1.2
(a) experimental results, 36 torr
(b) experimental results, 102 torr
(c) experimental results, 331 torr
(d) model results, 36 torr
(e) model results, 102 torr
(f) model results, 331 torr 92

3.3 Time resolved spectral output: comparison of VR20J and VT model results (with rate package VT3) with experiment, $He:O_2:F_2:H_2$ = 20.8:1.0:4.6:1.2
(a) experimental results, 102 torr
(b) VT model results using rate package VT3, 102 torr
(c) VR20J model results, 102 torr 94

3.4 Individual derivative contributions for mechanisms reducing population inversion on $P_2(5)$, $He:O_2:F_2:H_2$=20.8:1.0:4.6:1.2
(a) VT model results for rate package VT3, 102 torr
(b) VR20J model results, 102 torr 103

3.5 Small signal gain time histories: comparison of experimental and VT model results using rate package VT (standard rates), $He:O_2:F_2:H_2$ = 20.8:1.0:4.6:1.2
(a) experimental results, v = 1-0 band, 102 torr
(b) model results, v = 1-0 band, 102 torr
(c) experimental results, v = 2-1 band, 102 torr
(d) model results, v = 2-1 band, 102 torr 106

3.6 Small signal gain time histories: comparison of experimental and VT model results using rate package VT2, $He:O_2:F_2:H_2$ = 20.8:1.0:4.6:1.2
(a) experimental results, v = 1-0 band, 102 torr
(b) model results, v = 1-0 band, 102 torr
(c) experimental results, v = 2-1 band, 102 torr
(d) model results, v = 2-1 band, 102 torr 107

3.7 Small signal gain time histories: comparison of experimental and VT model results using rate package VT3, $He:O_2:F_2:H_2$ = 20.8:1.0:4.6:1.2
(a) experimental results, v = 1-0 band, 102 torr
(b) model results, v = 1-0 band, 102 torr
(c) experimental results, v = 2-1 band, 102 torr
(d) model results, v = 2-1 band, 102 torr 108

Figure		Page
3.8	Small signal gain time histories: comparison of experimental and VR20J results (a) experimental results, v = 1-0 band, 102 torr (b) model results, v = 1-0 band, 102 torr (c) experimental results, v = 2-1 band, 102 torr (d) model results, v = 2-1 band, 102 torr	111
A.1	Total flashlamp intensity vs time	134
A.2	Reflectivity vs wavenumber for the output coupler with nominal 97% reflectivity.	136
A.3	Reflectivity vs wavenumber for the output coupler with nominal 81% reflectivity.	137

CHAPTER 1

INTRODUCTION

1.1 Background

A chemical laser is defined as a laser whose population inversion is produced by energy liberated during a chemical reaction [1]. The first chemical laser emission was observed by Kasper and Pimentel [2] in 1965 in an exploding mixture of hydrogen and chlorine. The first hydrogen-fluoride (HF) chemical laser emission was observed by Kompa and Pimentel [3] in 1967. Both lasers were initiated by flash photolysis of molecular fluorine.

The chemical lasers of most interest are those operating on diatom-radical exchange reactions of the form:

$$A + BC = AB^{*} + C \qquad \Delta H<0 \qquad (1.1)$$

where ΔH is the reaction enthalpy released in chemical bond rearrangement. Reactions of this type have several advantages for chemical lasers. First, they tend to be highly exothermic making large amounts of chemical energy available for producing population inversions. Second, the activation energy is often only a few multiples of k_bT (k_b is Boltzmann's constant). This allows easy initiation and provides a very fast rate of reaction. These very fast reaction rates are necessary to overcome processes deactivating the excited product species AB^{*}. Third, in diatom-radical exchange reactions, a large fraction of

the reaction enthalpy is channeled into vibrational excitation of the product AB^* [4]. Moreover, this type of reaction tends to selectively channel that enthalpy into higher excited vibrational states in a non-Boltzmann distribution creating the population inversions necessary for lasing. In some cases, population is deposited in the highest vibrational level thermodynamically allowed [1, 5, 6]. Fourth, a wealth of initiation schemes (to produce initial concentrations of radical A) are available. To date, reactions that yield lasing have been initiated by flash photolysis, pulsed electric discharge, electron beam impact and laser photolysis [1].

The external initiation provided by flash photolysis, electric discharge or electron beam impact is not strictly necessary in a chemical laser. A prime example of a chemical laser which does not utilize an external initiation source is the CW (Continuous Wave) HF laser. External initiation is desirable though, as it provides a precise means of controlling laser turn on time for pulsed devices. External initiation has the additional advantage of assisting in the avoidance of prereaction. Prereaction is the uncontrolled formation of HF prior to the mixture entering the laser cavity. Control of prereaction is accomplished by forcing the pulse to begin before the effects of prereaction can become important.

HF lasers, the subject of this study, are of the diatom-radical type. The enthalpy liberated for both system reactions is very high:

$$F + H_2 = HF(v \leq 3) + H \qquad \Delta H = -31.7 \text{ kcal/mole} \qquad (1.2)$$

$$H + F_2 = HF(v \leq 8) + F \qquad \Delta H = -97.7 \text{ kcal/mole} \qquad (1.3)$$

It is customary to denote Equation (1.2) as the "cold" reaction and Equation (1.3) as the "hot" reaction in view of their relative exothermicities. The activation energies for the two reactions are low. For the hot reaction, E_a = 2.4 kcal/mole and for the cold reaction, E_a = 1.7 kcal/mole. This is four times k_bT, or less, at room temperature. Finally, the fraction of reaction enthalpy channeled into vibration is particularly large: 66% for the cold reaction [7] and 53% for the hot reaction [8].

The HF laser has further advantages, the foremost being production of excited HF by a chain reaction. Laser emission from the first chain reaction lasers was observed by Batovskii, et al [9] and Basov, et al [10] in 1969.

Two benefits of the chain reaction mechanism can be seen by inspecting Equations (1.2) and (1.3). If a small amount of atomic fluorine (or atomic hydrogen) is formed, the two reactions cycle, the product radical H of Equation (1.2) initiating Equation (1.3) and the resulting product radical F of Equation (1.3) reinitiating Equation (1.2). In principle, the reactions will cycle until all reactants are depleted. The initiation energy is low for chain reactions as the energy required per reaction step is inversely proportional to the chain length [11]. Initial F atoms generated are used several times in a chain reaction implying that a small initiation energy will generate a large laser output energy, yielding very high efficiencies [12, 13, 14]. In addition, in the $H_2 + F_2$ laser, energy is liberated by the chain reaction through Equation (1.3) as well as through Equation (1.2).

Operation on a chain reaction mechanism has the additional advantage of the reaction continuing after initiation has ceased. Thus, it

is unnecessary to exactly uniformly initiate the entire lasing volume: If the medium is initiated in a small portion of its volume the reaction will propagate throughout the whole medium volume due to collisions and diffusion and due to thermal effects [15]. Two disadvantages of non-uniform initiation are poor beam quality due to index of refraction gradients within the mixture and a lack of repeatability in the laser output. A lesser advantage of the HF system is the large stimulated emission cross section.

Research on HF chemical lasers also contributes to the understanding of two other chemical laser systems of interest: DF and DF/CO_2. The DF laser emits in an atmospheric transmission window providing good beam propagation at lower altitudes and has slower rates of deactivation than HF.

The chemical kinetics of the DF molecule are greatly complicated by its high density of states. This high density of states increases the number of relevant reaction pathways and makes it very difficult to measure the relevant reaction rates. However, one can apply results gained from studying HF lasers to the DF and DF/CO_2 laser systems by making use of the isotope effect between HF and DF and by making use of surprisal analysis techniques for analagous reactions in the HF and DF systems [16].

In this work, initiation of the HF laser pulse was by photolysis of molecular fluorine using flashlamps. The initiation reaction proceeded as:

$$F_2 + h\nu_p = 2F \qquad (1.4)$$

with ν_p being an ultraviolet photodissociating photon of frequency ν_p.

After generating an initial fluorine atom concentration, the chain reaction proceeds as stated above.

It is known that highly diluted H_2 + F_2 systems initiated flash photolytically permit detailed analyses of the kinetic mechanisms [17]. Electric discharge initiation, on the other hand, produces unwanted charged species, complicating the chemistry [4, 18].

For the conditions of this study, the medium absorbing the ultraviolet flash photolysis photons can be characterized as optically thin. This is equivalent to stating that the photolysis signal passes through the medium with its intensity nearly constant: absorption by F_2 is minimal. In that case, flash photolysis has the advantage of generating a homogeneous fluorine atom concentration as a function of time over a wide range of fluorine partial pressures and mixture total pressures, even when mixed with non-absorbing gases [19]. There are no charged species involved. Consequently, lasers initiated by flash photolysis are easier to model numerically than those using another form of initiation and are thus well suited to studies gaining insight into competing kinetic mechanisms. One potential complication is the possibility of "hot" F atom formation during the photolysis process. "Hot" atoms are those with a thermal energy significantly greater than 3/2 $k_b T$. If such atoms are formed, it is felt they could significantly alter the vibrational state-product distribution of Equations (1.2) and (1.3)[20]. Furthermore, since the ultraviolet light required for initiation is difficult to produce, and since it is difficult to couple more than a small fraction of the ultraviolet light produced by the flashlamps into the medium, the initiation efficiency is poor and the

rate of fluorine atom production is less than that of other initiation schemes.

A further disadvantage of photolytic initiation arises if the medium is not optically thin. This occurs if significant absorption of the photolysis signal occurs as it traverses the medium. This would be caused by an overlarge absorption path length or an increase in the pressure of the absorbing species (F_2). Either of these would lead to inhomogeneous absorption and initiation of the medium, and hence, poor beam quality and lack of repeatability.

Additional disadvantages of HF lasers are the very efficient deactivation processes of HF itself and other collision partners [21] and the poor beam transmission through the atmosphere [22]. In addition, there are very strong analogies between the mechanisms in HF and DF lasers. Since lasing on DF occurs in an atmospheric transmission window and is of great interest, research on HF lasers continues.

1.2 Present Work

Evaluation of the performance of chemical lasers requires an understanding of the chemical, radiative and relaxation kinetic mechanisms that pump and deactivate the energy levels associated with lasing. The detailed representation of the mechanisms necessary for accurate prediction of laser performance requires a mix of experimental and computer modeling investigations.

The main limitation in the comparison of computer models with experiment is the lack of a well defined and characterized experiment.

Such an experiment should have sufficient diagnostics to monitor as many time histories of HF(v,J) populations as is feasible. Previous experimental endeavors consist of time resolved spectra recorded at only one pressure, using one mixture composition and employing only one value of outcoupling. This is insufficient. A more comprehensive study is necessary.

This work presents the results of a comparison of such a set of detailed experimental observations with computer simulations to facilitate the understanding of the kinetic mechanisms involved in the H_2 + F_2 laser. To that end, experiments have been performed to fully characterize a pulsed H_2 + F_2 flash photolysis laser at selected, well controlled operating conditions. A systematic experimental study was conducted where: (1) the time-resolved small signal gain on eleven lines, (2) the total P-branch laser emission, and (3) the total pulse energy were measured for an H_2 + F_2 laser.

Specific objectives of this study were:

(1) To measure small signal gain and time resolved spectra at three cavity pressures (36, 102, and 331 torr).

(2) To measure small signal gain and time resolved spectra for two mixture compositions ($He:O_2:F_2:H_2$ = 20.8:1.0:4.6:1.2 and 22.0:1.0:2.7:1.0).

(3) To measure time resolved spectra using two different output couplers (nominal 81% and 97% reflectivity).

A minimum of three detailed data sets were to be developed from the results of objectives 1-3.

Finally, all experimental results were to be compared with the results of a computer modeling study. This very comprehensive computer model includes V-V, V-R,T and R-R,T relaxation channels, and P-branch and pure rotational lasing [23]. The model was modified by inserting the latest available rate data [24-27], and adding a wavelength dependent threshold gain.

Many investigators have already completed studies of P-branch time resolved spectra. Several initiation schemes have been used including laser photolysis [28, 29] ultraviolet spark photolysis [30], electron beams [12], electric discharge and flash photolysis. A multitude of reacting species have been used. In the case of flash photolysis initiation this included:

$F_2O + H_2$ [31], $UF_6 + H_2$ [18, 32], $XeF_4/SbF_5 + H_2/CH_4$ [33], $MoF_6 + H_2$ [18, 34, 35], $WF_6 + H_2$ [36], and $F_2 + H_2$ [11, 17-19, 35, 37-43].

Individual transition intensity traces are shown in several of these studies: References 18, 31, 33 and 41 show "cold band" lasing while References 14, 17, 42 and 43 show both "hot band" and "cold band" lasing.

In the case of electric discharge initiation, reacting species used included:

$H_2 + SF_6$ [44, 45], $CH_4 + SF_6$ [44, 46], $C_3H_8 + SF_6$ [47-49], $HI + SF_6$ [50], H_2 + freons [51] and $H_2 + F_2$ [14, 51-54].

Several studies utilizing electric discharge initiation show individual intensity traces for cold band lasing [44-46, 50, 51, 55, 56] while two show individual intensity traces for hot band and cold

band lasing [17, 52].

The literature available on oure rotational time resolved spectra is not as extensive as that on P-branch time resolved spectra. Nonetheless, several studies have been completed. Pure rotational lasing has been observed in mixtures of $H_2 + CF_4$ [57], $H_2 + BF_3$ [58], $CH_4 + SF_6$ [46] and $H_2 + SF_6$ [49, 59, 60] initiated by electric discharge. Pure rotational lasing has also been observed in flash photolytically initiated mixtures of CF_3I/CF_3Br with C_2H_2/CH_3C_2H [61] and in flash photoelimination of hydrocarbons [62]. Both of these groups present traces of individual transition intensities. There have been no reports of pure rotational lasing in $H_2 + F_2$ laser mixtures to date.

There are few reports of small signal gain measurements. Two authors give values for peak gain on a single transition in $SF_6 + H_2$ mixtures initiated by electric discharge [63, 64]. Another study presents a gain averaged over all transitions available from a multiline probe laser [15]. Small signal gain has been measured versus position in CW HF lasers (cf. Reference 65). The only study to date reporting time history of small signal gain is for the $D_2 + F_2/CO_2$ system of Reference 66. Reference 67 reports P-branch and pure rotational gains in CO_2 lasers.

A number of studies are available which compare computer modeling predictions to experimental results. These include References 23, 39-41, 68-70. These works compare only P-branch time resolved spectra.

This work compares time resolved spectra and time history of small signal gain at three pressures and two mixtures. This is the first

time such a well diagnosed experiment and such a detailed computer model have been compared.

The results, in conjunction with computer simulations, will be used to evaluate weaknesses in the four kinetic relaxation modes.

These four relaxation modes of interest are Vibrational to Translational (V-T), Vibrational to Rotational (V-R), Vibrational to Vibrational (V-V), and Rotational to Rotational and Translational (R-R,T).

Vibrational to Translational relaxation

$$HF(v,J) + M = HF(v-1,J) + M \qquad E \sim 3500\ cm^{-1} \qquad (1.4)$$

is assumed to occur with the product rotational levels being in thermal equilibrium at the translational temperature. The resulting energy defects for HF V-T processes are approximately 3500 cm^{-1}.

Similar to V-T, V-R relaxation

$$HF(v,J) + M = HF(v-1,\ J+\Delta J) + M \qquad E \sim 150\ cm^{-1} \qquad (1.5)$$

also assumes a portion of the vibrational energy is transferred into rotational energy of the product molecule. However, the product molecule rotational energy contribution is much higher for V-R than for V-T. In fact, for V-R, if the product rotational state is assumed to minimize the reaction energy defect, high rotational levels will result with very little contribution to translational energy. Thus, V-T and V-R have essentially complementary fractions of rotational and translational energy in their product molecules: V-T product molecules have nearly all the energy transferred from vibration going into translation, while V-R molecules have nearly all the energy transferred from vibration going into rotation.

Current kinetic understanding implies that a combination of V-R and V-T energy transfer represents the vibrational deactivation mode in HF lasers. This combination is denoted V-R,T, the vibrational energy transferred to rotation and to translation in the product molecules are of the same order of magnitude.

In contrast to V-T, V-R and V-R,T, all of which are mechanisms for removing vibrational quanta, Vibrational to Vibrational energy transfer is concerned with rearranging the distribution of vibrational energy while conserving the number of vibrational quanta.

$$HF(v_1,J_1) + HF(v_2,J_2) = HF(v_1-\Delta v,J_1) + HF(v_2+\Delta v,J_2)$$

$$E \sim 450\ cm^{-1} \qquad (1.6)$$

It is assumed that there is no change in rotational state for V-R *exchange*.

The last relaxation mode of importance is R-R,T. This mechanism is assumed to consist of single quantum rotational exchange (R-R)

$$HF(v_1,J_1) + HF(v_2,J_2) = HF(v,J_1-1) + HF(v_2,J_2+1) \qquad (1.7)$$

and single and double quantum R-T.

$$HF(v,J) + M = HF(v,J-\Delta J) + M \qquad J = 1,2 \qquad (1.8)$$

As in the case of vibrational energy transfer, R-T removes quanta and R-R conserves quanta while rearranging the distribution of rotational energy. Current practice is to assume that R-T contributes approximately two thirds of the total R-R,T rate. The other one third is comprised of R-R.

In summary, the goal of this work was to examine in a systematic manner the dominate kinetic mechanisms in a pulsed $H_2 + F_2$ laser: i.e. to develop a collection of consistent time resolved data to use in

evaluating the weaknesses in kinetic models which are in turn used to guide laser system development.

CHAPTER 2

EXPERIMENTAL INVESTIGATION OF AN HF LASER

2.1 Introduction

Since the advent of the HF chemical laser in 1967, there has been much research devoted to answering fundamental questions regarding laser performance. However, after sixteen years of effort, there are still areas to be explored. This work attempts to address several areas of concern.

One such area is the impact of lasing on pure rotational transitions. This is important in large scale devices as even a small fraction of the total output power being emitted at pure rotational transition wavelengths could severly damage optical components [71]. It is thus necessary to know the extent of lasing on pure rotational transitions.

Another area of concern is in the examination of the time history of small signal gain (SSG) on P-branch transitions. This is pertinent to applications involving laser amplifiers, the gain being the single most important parameter in studies of laser amplifiers. There have been reports of wavelength averaged [15] and peak [63, 64] gains measured for HF lasers and measurements of gain time histories for CO_2 lasers [66]. This is the first study to combine measurements of TRS and SSG and a computer simulation, all on a single device.

In the remainder of this chapter, an experimental basis for answering these questions will be presented. In the next chapter, the results of computer simulations of the experiment will be introduced and compared with the experimental results of this chapter. Further conclusions will be drawn from the comparison of the experimental and simulation results and explanations will be proposed for the areas of concern listed above.

2.2 Experimental Study

2.2.1 Flash Photolysis Laser

A schematic of the flash photolysis laser cell used in this study is shown in Figure 2.1. Referring to this figure, the laser cell consisted of a 100 cm long aluminum cavity of 10 cm x 10 cm cross section. Two 1.6 cm diameter inlet ports were located in one cavity sidewall 10 cm from one cavity end and two 1.6 cm diameter outlet ports were symmetrically located in the opposite cavity sidewall 10 cm from the opposite cavity end. The gas mixture was fed in through the inlets, flowed 80 cm longitudinally through the cavity and exhausted through the outlets. A 10 cm diameter dump port was opened after each run to rapidly exhaust the cavity of combusted gases.

The ultraviolet light necessary for initiation of the gas mixture was coupled into the cavity through 11 cm x 11 cm x 2 cm synthetic quartz windows (Suprasil II). Two different window configurations were used (see Figure 2.2). In one configuration, five quartz windows were mounted on the top side of the cavity and five quartz windows were mounted on the bottom side of the cavity (Figure 2.2a). In the other configuration, the five quartz windows mounted on the bottom side of

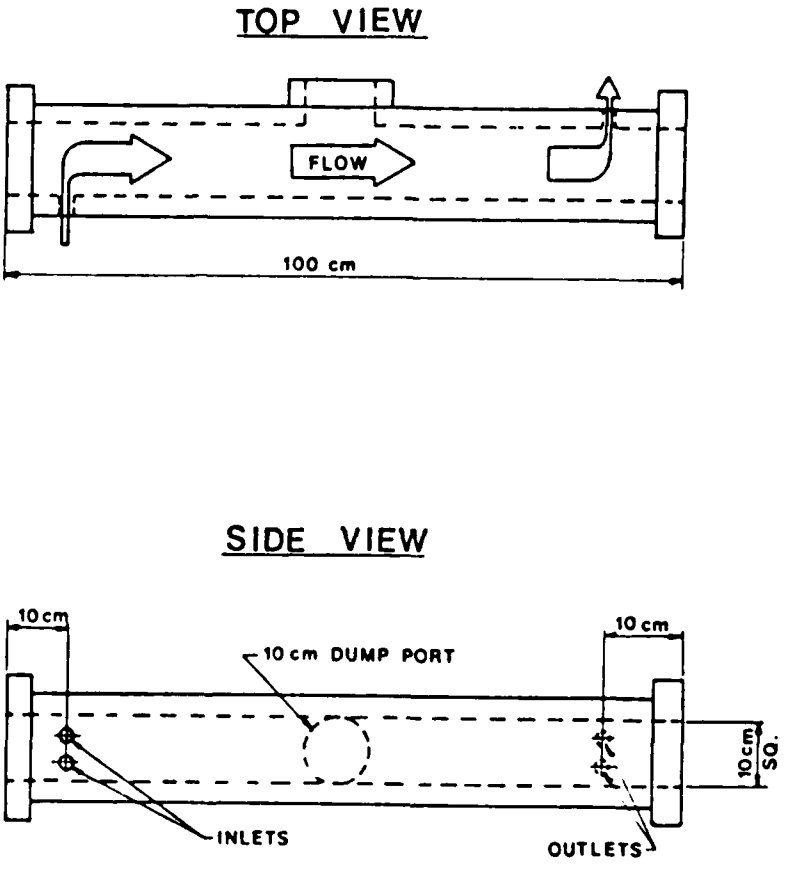

Figure 2.1 Laser cell schematic

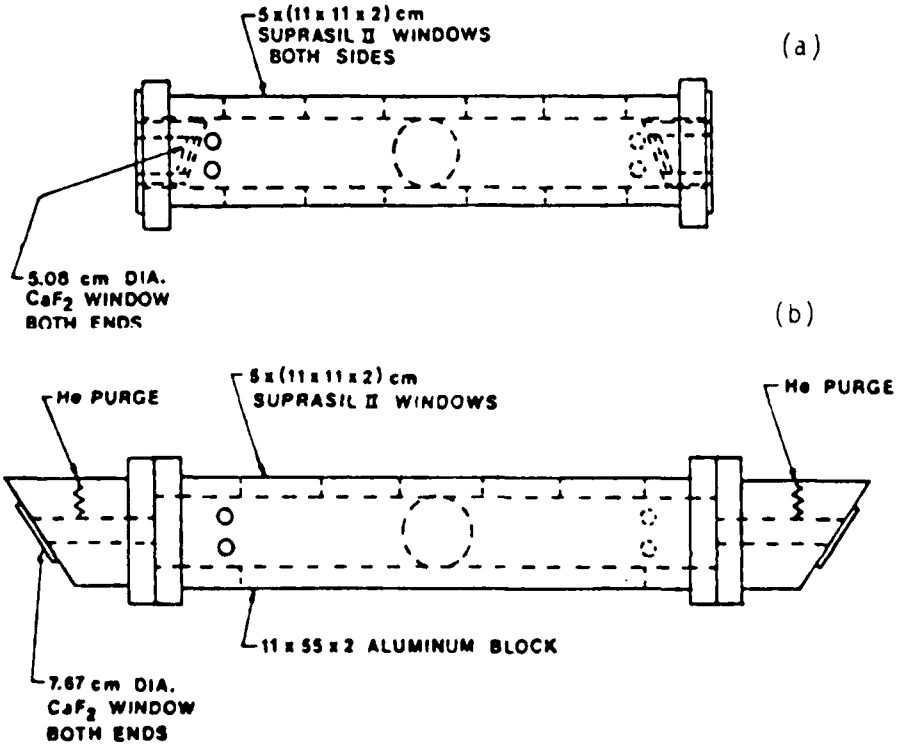

Figure 2.2 Laser cell window configurations

(a) laser cell window configuration for the mixture $He:O_2:F_2:H_2$= 20.8:1.0:4.6:1.2
(b) laser cell window configuration for the mixture $He:O_2:F_2:H_2$= 22.0:1.0:2.7:1.0

the cavity were replaced by one 55 cm x 11 cm x 2 cm aluminum plate (Figure 2.2b). In each case, the quartz windows were sealed to the cavity with viton o-rings and clamped in place by aluminum brackets.

A CaF_2 window at the brewster angle was attached to each end of the cavity by an aluminum mount. Two different brewster window configurations were used (see Figure 2.2). In one case, internal brewster mounts were used to hold the 5.08 cm diameter CaF_2 windows in place. The window spacing was 81 cm and there was no window path to purge (see Figure 2.2a). In the second case, external brewster mounts were used to hold the 7.67 cm diameter CaF_2 windows in place. The window spacing was 121 cm and the window paths were purged with helium (see Figure 2.2b). All window-to-brewster mount and brewster mount-to-cavity surfaces were sealed with viton o-rings.

The entire cavity-quartz window-brewster window assembly was passivated by exposing it to increasing concentrations of fluorine (initially 10%, increased in 10% increments, to 50%, F_2 in He, total pressure 400 torr) for periods of one-half hour.

The optical resonator was of a stable configuration and external to the cavity. The maximum reflector was a 15.2 cm diameter, 500 cm radius of curvature copper mirror. Two flat dielectric output couplers were used. Corresponding to Figure 2.2a, an output coupler with maximum 81% reflectivity (see Figure A.3) was used. The mirror spacing was 121 cm for this case. Corresponding to Figure 2.2b, an output coupler with maximum reflectivity of 97% (see Figure A.2) was used. For this case, the mirror spacing was 180 cm.

The ultraviolet light necessary for laser initiation was supplied by a high voltage discharge through four flashlamps (ILC: 56 cm long,

0.9 cm diameter, filled with 50 torr Xe). The lamps were mounted in pairs directly above and below the cavity, outside the quartz windows. The high voltage pulse was produced by charging four capacitors (Maxwell: 31161, 0.7 microfarads, 45 kV maximum) to between 30 kV and 35 kV and discharging two of them through each pair of flashlamps using spark gaps (Maxwell: 40060, 75 kV maximum). The spark gaps were simultaneously triggered by a high voltage trigger generator (Maxwell: KV50-805). A schematic of the upper half of this circuit is shown in Figure 2.3. The lower half of this circuit was identical to the upper half.

The signal from the trigger generator to the spark gaps was controlled in the following manner. The square wave output from a rotating wheel chopper (Ithaco: 383) and the manual triggering signal from the laser control panel were input to a pulse generator (Hewlett-Packard: 214A). The pulse generator served as an "and gate", firing the high voltage trigger generator. The high voltage trigger generator then fired the spark gaps as mentioned, simultaneously triggering the fast risetime oscilloscope (Tektronix: 400 MHz, 7844). A block diagram of the trigger circuit is shown in Figure 2.4.

Figure 2.5 is a schematic of the gas handling system. The gases used were:

(1) electrolytically pure oxygen (99.98% minimum purity)

(2) fluorine (98.2% minimum purity)

(3) helium and hydrogen (98% minimum purities).

Batch analysis of the fluorine showed the following inpurities:

HF	<0.4 molar percent
Air	1.69 molar percent

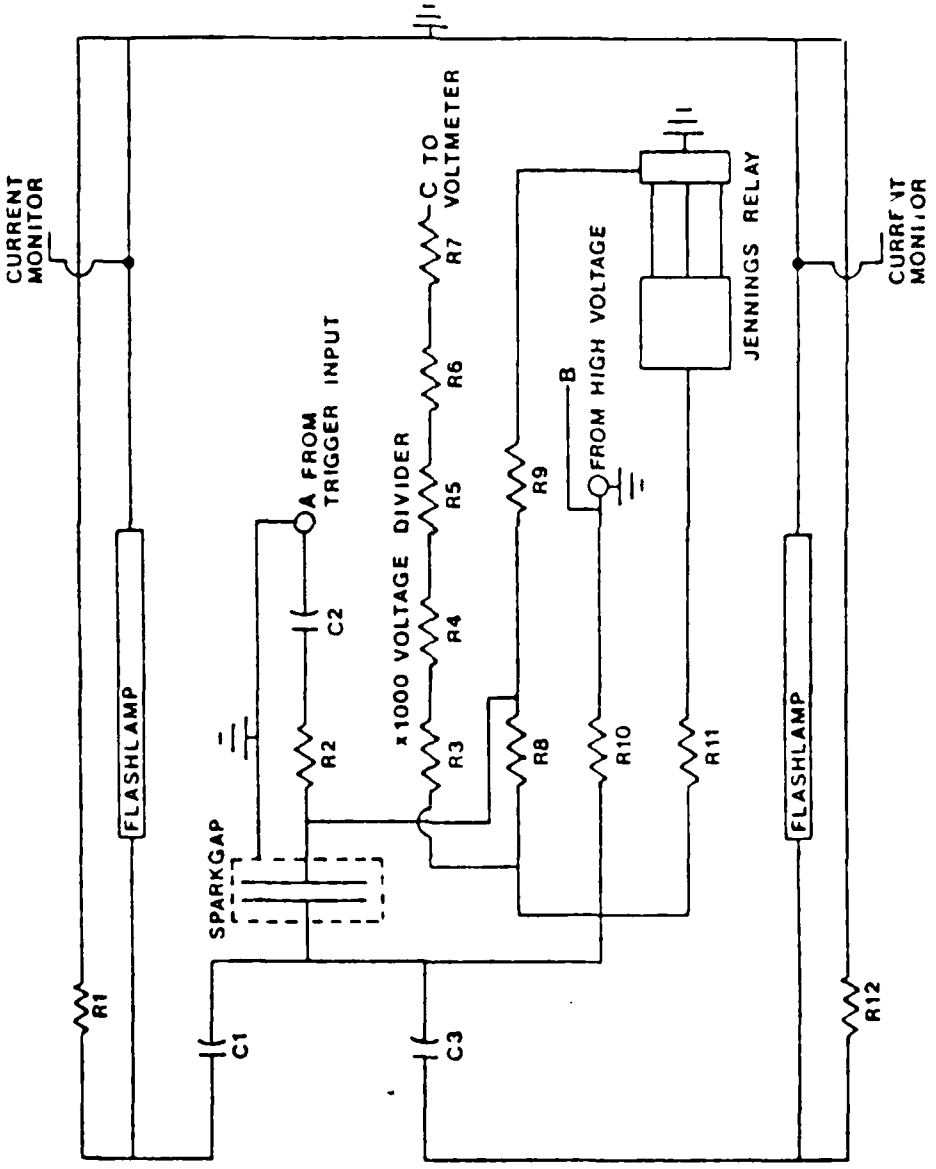

Figure 2.3 Pulse discharge circuit schematic

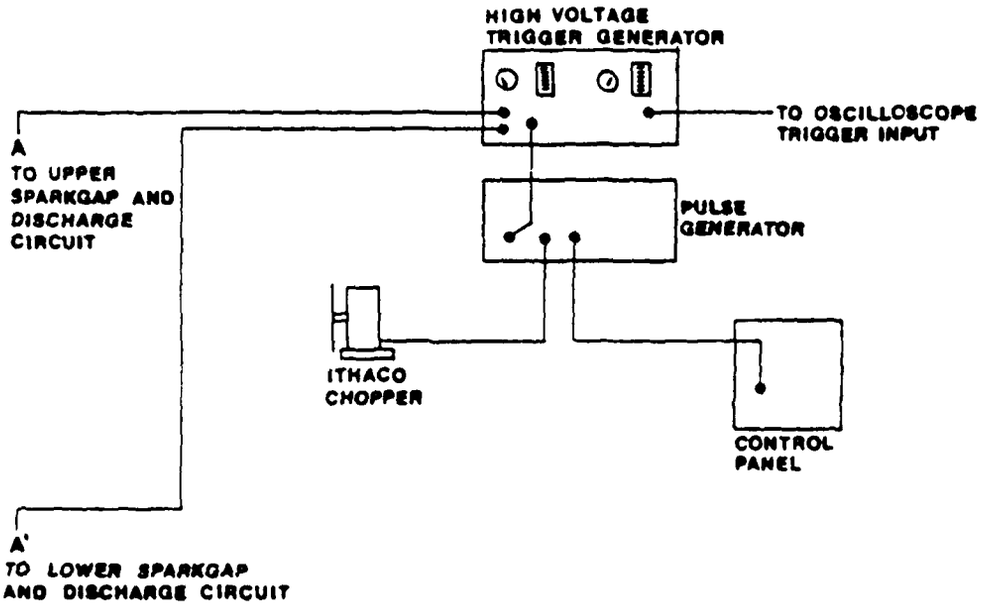

Figure 2.4 Trigger circuit block diagram

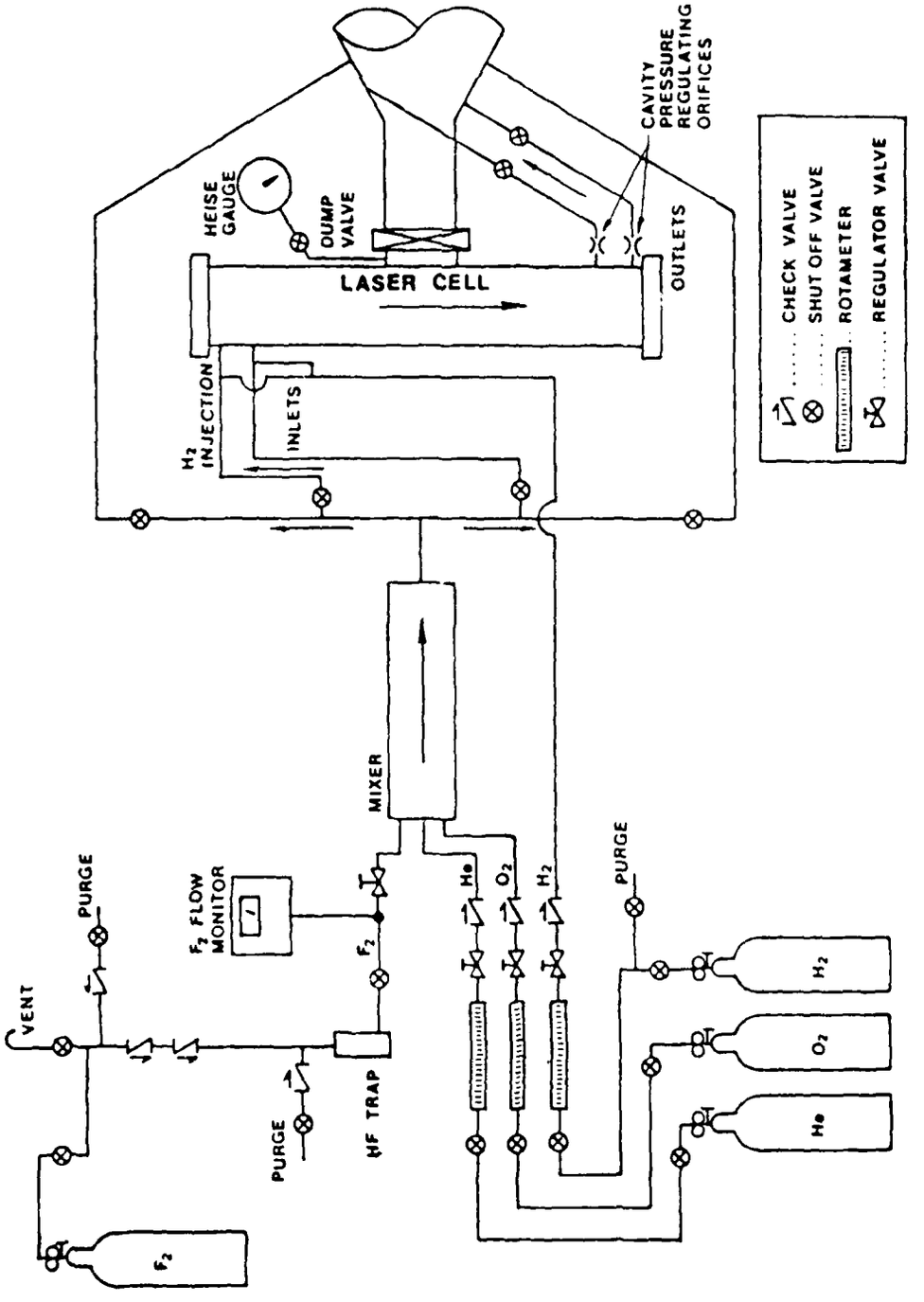

Figure 2.5 Laser cell gas handling schematic

CO_2 443 molar ppm

CF_4 301 molar ppm

SF_6 10 molar ppm

The helium, oxygen and hydrogen flows were monitored using rotameter flow meters (Matheson 7400 series) and the flowrates were controlled using fine metering valves (Nupro). The fluorine flow was monitored using a linear mass flowmeter (Matheson: 8611) and the flowrate was controlled using a bellows seal valve (Nupro Severe Service). A hydrogen fluoride trap (Matheson), using NaF_2 pellets, was installed in the fluorine delivery line to minimize the initial cavity HF concentration. The helium, oxygen and fluorine flows were mixed in a 5.1 cm diameter, 76.2 cm long stainless steel tube as shown in Figure 2.5. This mixture was routed to the cavity in two 1.9 cm OD stainless steel lines. The hydrogen flow was injected into the helium-oxygen-fluorine mixture 20 cm upstream of the laser cavity using the radial "sting" arrangement shown in Figure 2.6. The complete helium-oxygen-fluorine-hydrogen mixture then flowed into the cavity where lasing took place.

The cavity pressure was measured using a Bourdon tube gauge (Heise: Cu-Be) and was controlled by two orifices located 20 cm downstream of the cavity exits in the two 1.9 cm OD exhaust lines. The combusted product gases were exhausted through these two lines to a 15.2 cm OD vacuum duct and then to a triplex pump (Kinney: KT-500B, 500 cfm). Photographs of the mixing tube, cavity and rotameter flow controllers are shown in Figures 2.7 and 2.8 respectively.

Experiments were run at three cavity pressures: 36, 102, and 331 torr, and two gas mixtures: $He:O_2:F_2:H_2$ = 22.0:1.0:2.7:1.0 and 20.8:1.0:4.6:1.2. The cavity Reynolds numbers were calculated to be

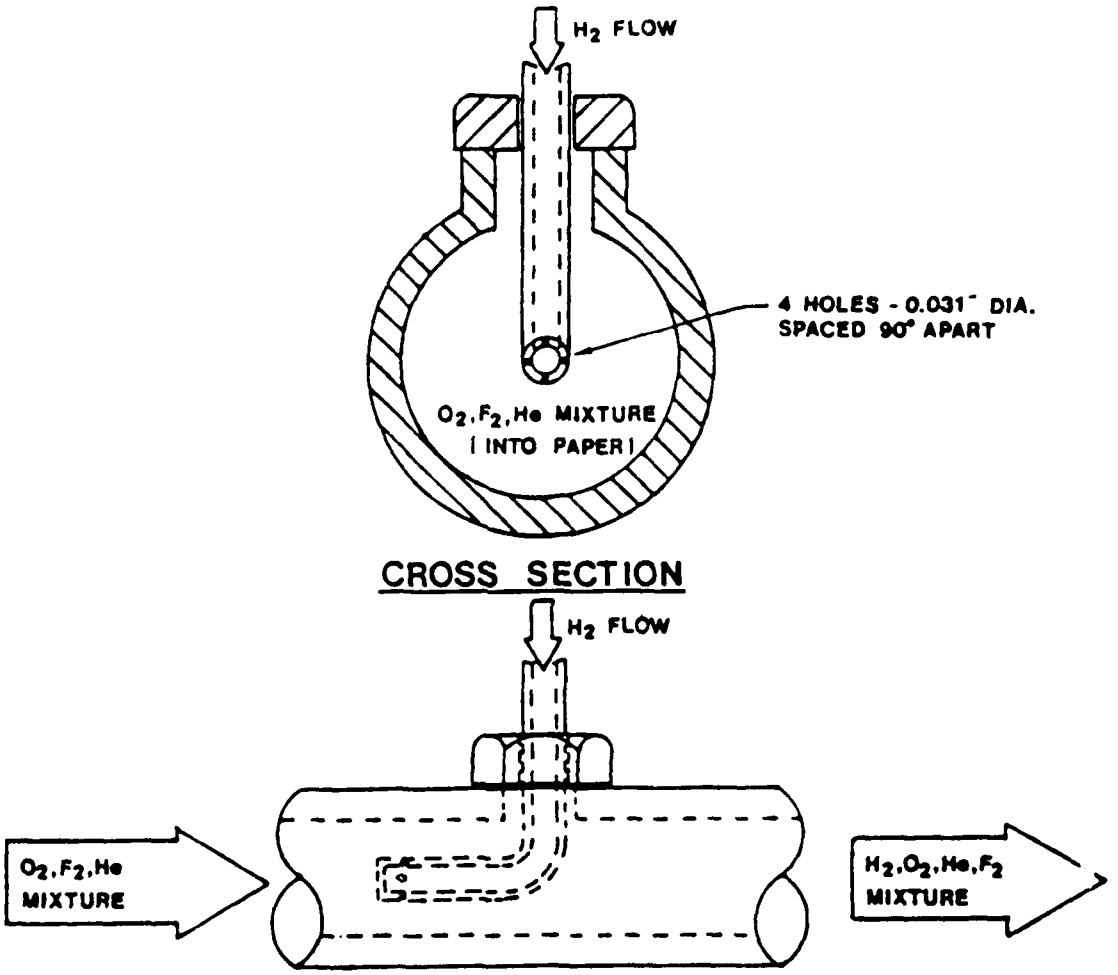

Figure 2.6 Hydrogen radial "sting" injection configuration

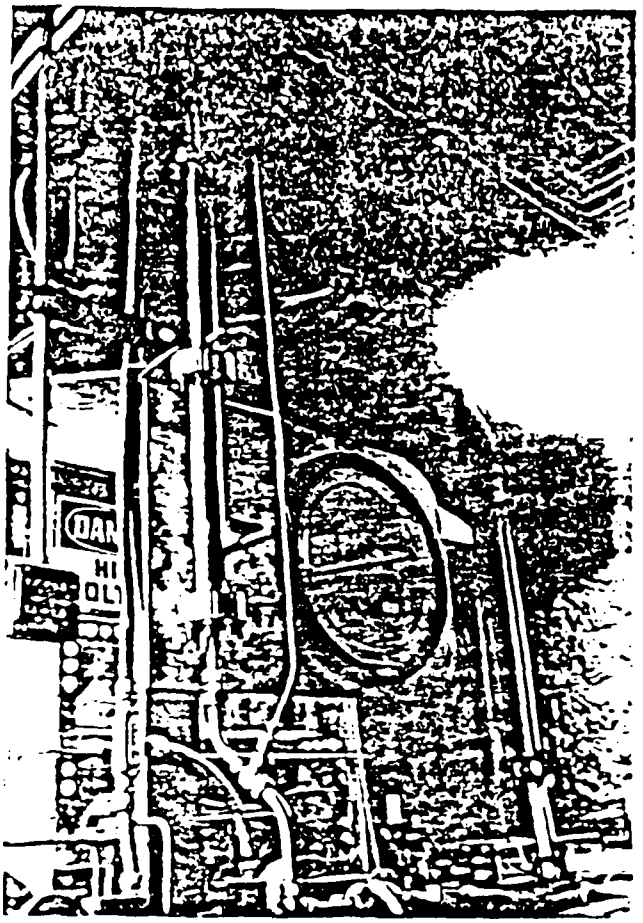

(a)

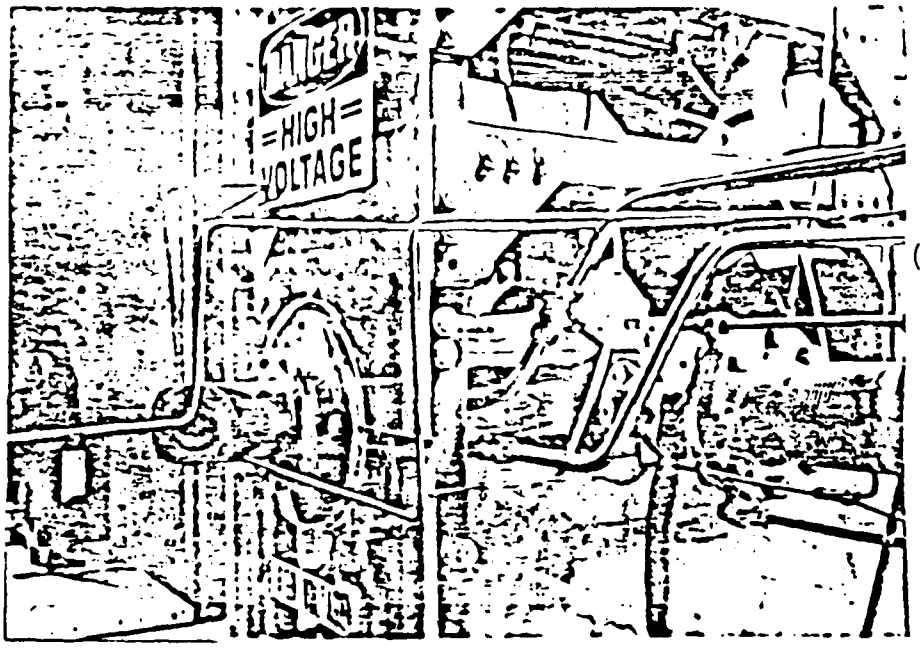

(b)

Figure 2.7 System photographs

(a) mixing tube
(b) laser cell

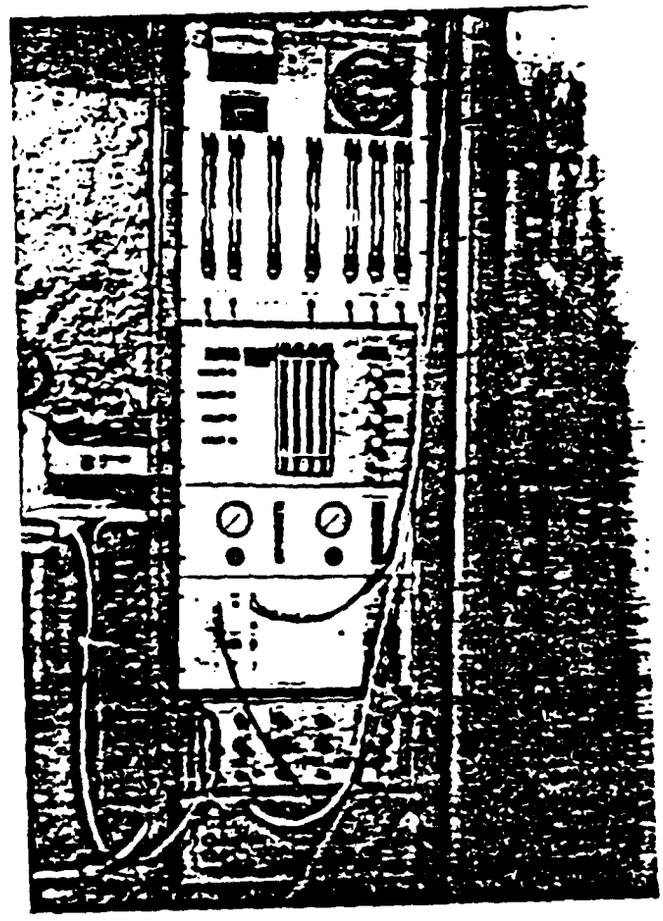

Figure 2.8 Rotameter panel photograph

23,000 for the 331 and 102 torr cases and 9,200 for the 36 torr case. Thus, the flow is turbulent for most of the cavity length [72].

2.2.2 Diagnostics

Three types of diagnostic measurements were performed on the laser medium described in Section 2.2.1: measurement of the Time Resolved Spectra (TRS), Time History of P-branch Small Signal Gain (SSG) and Total Pulse Energy (TPE). See Figures 2.9, 2.10 and 2.11 respectively for schematic representations of each experimental configuration.

In the TRS experiments, the laser was used exactly as described in Section 2.2.1. For this case, the laser beam left the output coupler and entered the first of two enclosed, dry nitrogen purged optical paths. The purpose of these purged paths was to decrease atmospheric water vapor absorption of the laser beam as it traveled from the output coupler to the detector. Upon exiting the first purged path, the beam was focused by a CaF_2 lens and steered into the second purged path. On leaving the second purged path, the beam entered the electromagnetic interference (EMI) shielded room. Once inside, the beam was steered through another CaF_2 lens and focused onto the entrance slit of a monochromator (GCA-McPherson: 218, 0.3 m). The monochromator diffraction grating (GCA-McPherson: 150 grooves/mm, 4.0 micron blaze) dispersed the desired component of the total beam through the monochromator exit slit and onto a biased, liquid nitrogen cooled Ge:Au detector (Raytheon: QKN-1568, 200 nsec risetime). The change in detector bias current was displayed on a fast risetime, EMI shielded oscilloscope (Tektronix: 7844) with fifty ohm vertical amplifier plugins (Tektronix: 7A19). A picture was taken of each data run with

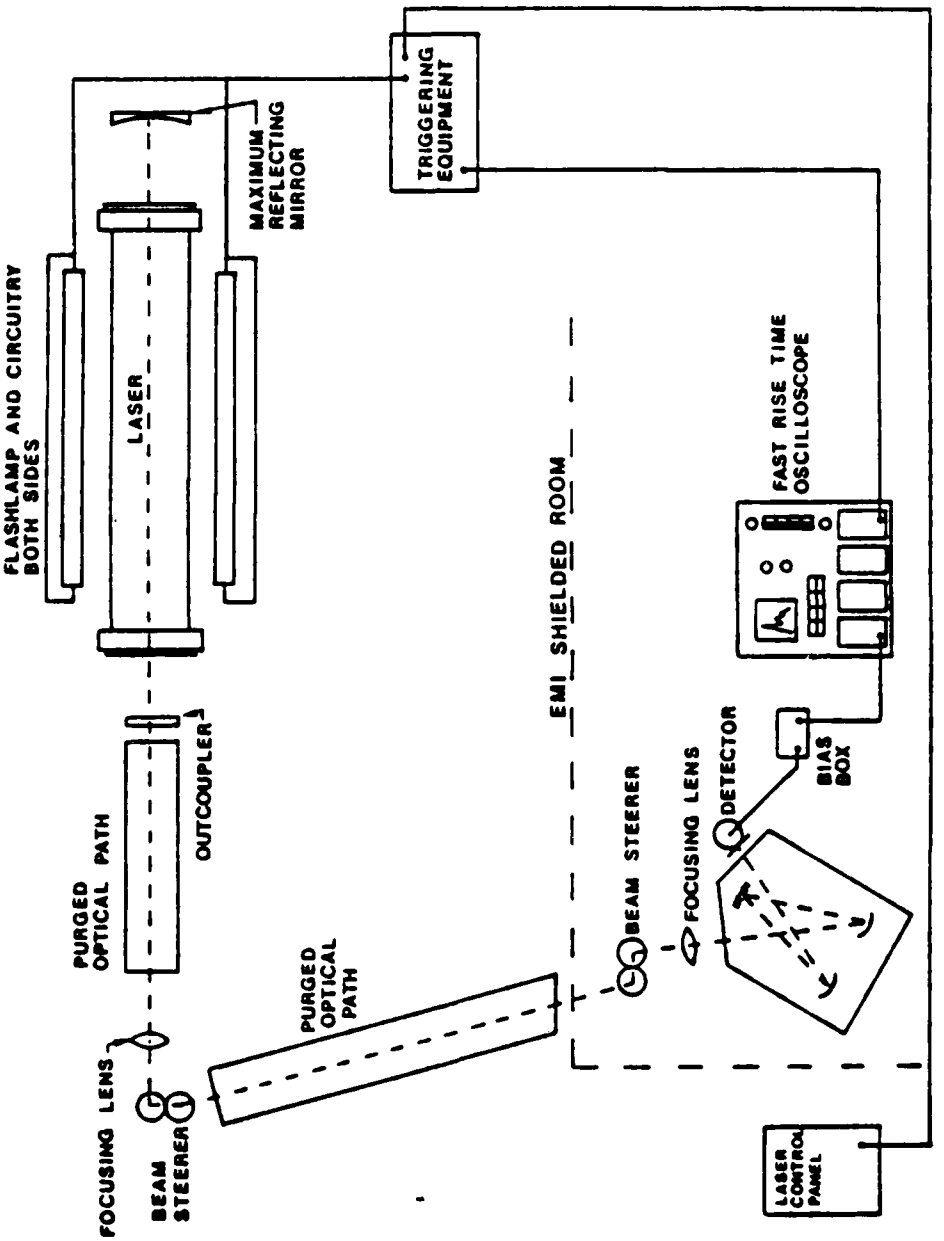

Figure 2.9 Time resolved spectroscopy experimental configuration

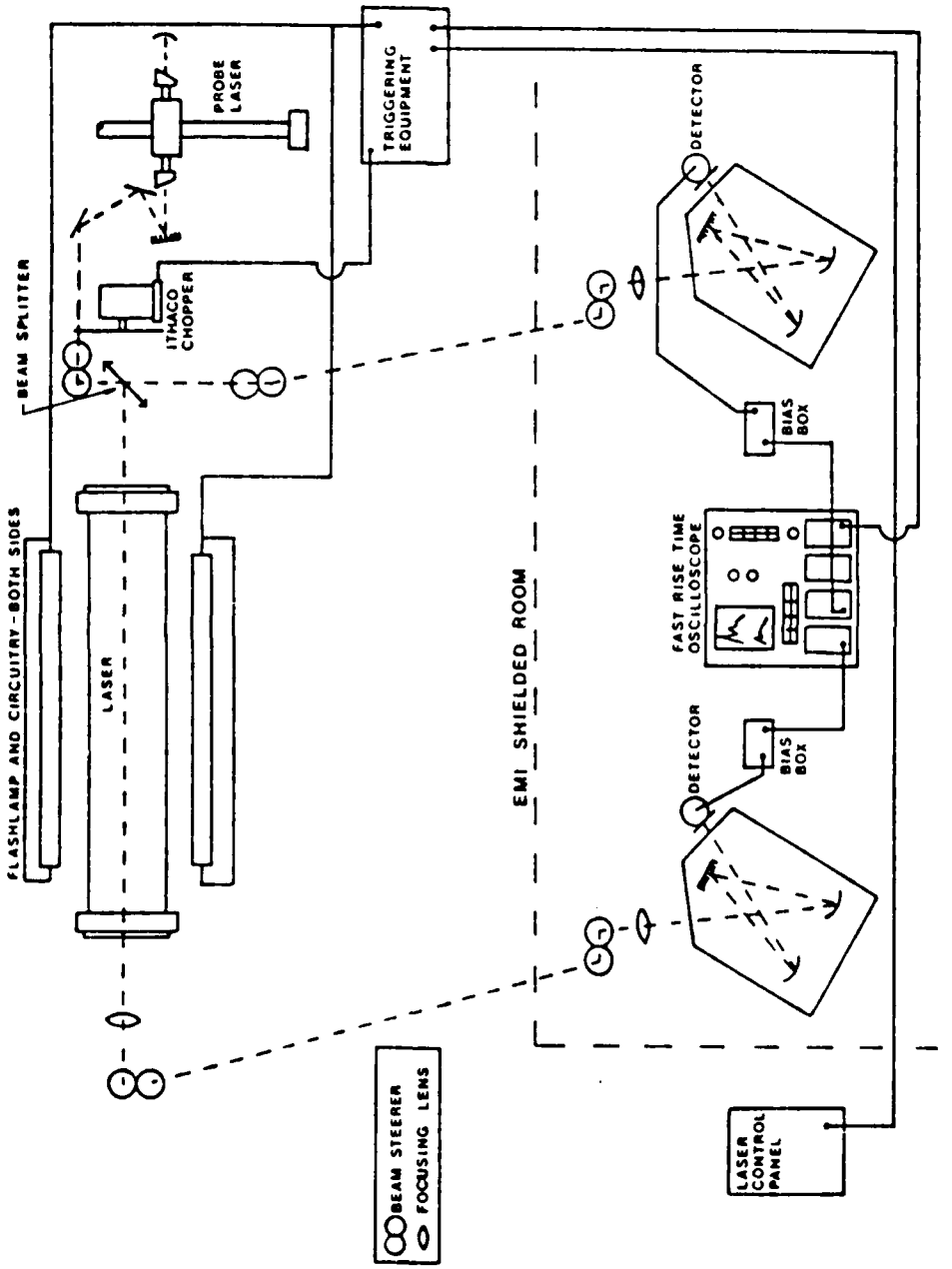

Figure 2.10 Small signal gain experimental configuration

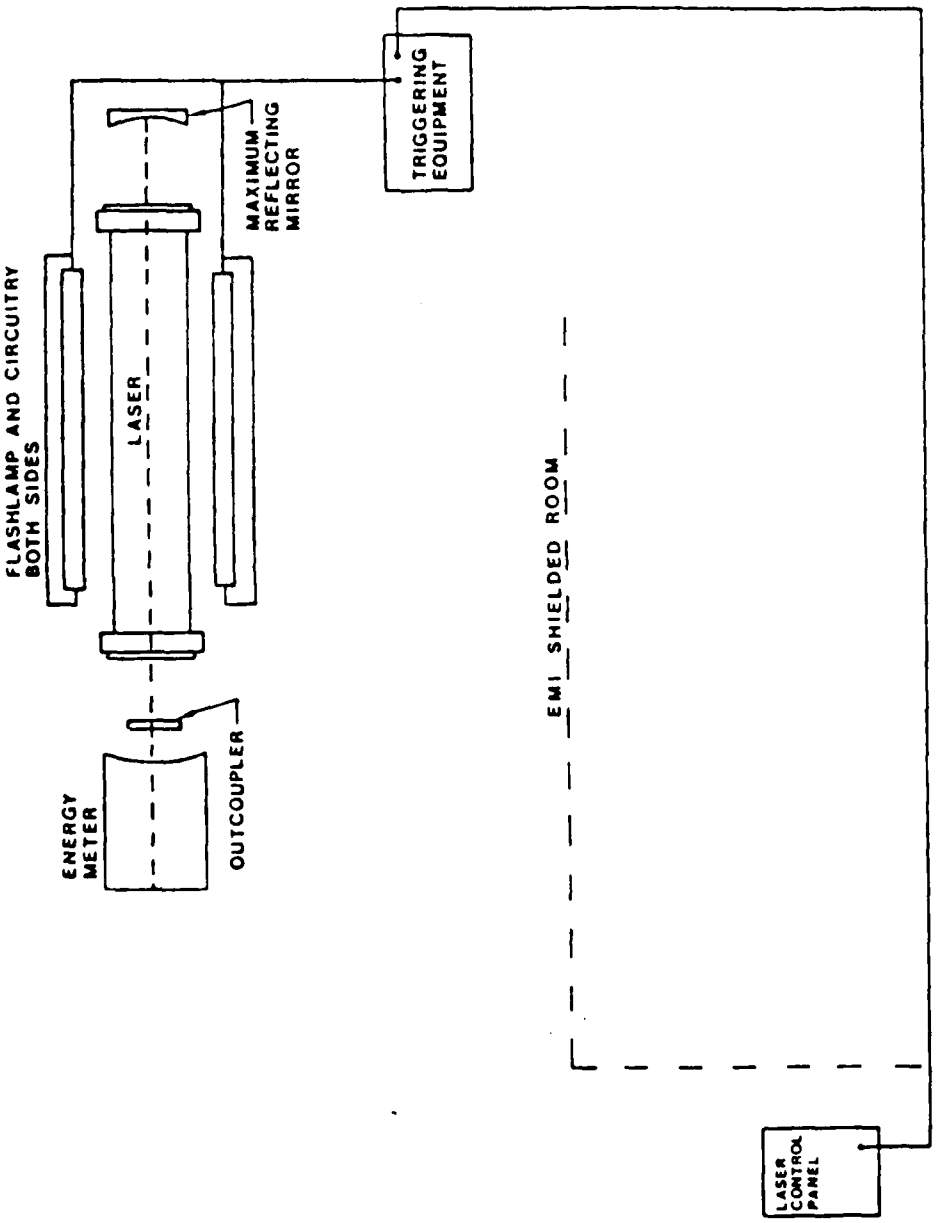

Figure 2.11 Total pulse energy experimental configuration

a sample shown in Figure 2.12a. Photographs of the monochromators and the oscilloscope are shown in Figure 2.13.

Time resolved spectroscopy measurements of pure rotational lasing intensities were also performed. The experimental apparatus was that of the P-branch lasing case with three exceptions:

(1) The CaF_2 brewster windows were replaced with NaCl brewster windows having much improved transmission in the pure rotational lasing region of the spectrum,

(2) The 150 grooves/mm, 4.0 micron blaze monochromator diffraction grating was replaced by a 75 grooves/mm, 16.0 micron blaze monochromator diffraction grating, and

(3) The Ge:Au detector and biasing system was replaced by a liquid nitrogen cooled HgCdTe detector (SBRC: 40742, 200 nsec risetime) and applicable biasing circuit. See Figure 2.9 for a schematic of this setup.

A slightly different system was used during the SSG experiments. The laser cell of Section 2.2.1 was modified by removing the optical resonator. A commercially available continuous wave (CW) HF laser (Helios: CLI) was employed to probe the laser medium. This laser utilized an electric discharge in a mixture of SF_6, O_2, He and H_2 to produce laser emission. The probe laser resonator consisted of a gold coated 200 cm radius of curvature maximum reflecting mirror and a grating output coupler which allowed single line operation. Transitions available for probing from this laser were: $P_1(3)$, $P_1(4)$, $P_1(5)$, $P_1(6)$, $P_1(7)$, $P_1(8)$, $P_1(9)$, $P_1(10)$, $P_2(5)$, $P_2(6)$, $P_2(7)$, $P_2(8)$. This probe laser is discussed further in Reference 73. Pictures of the probe

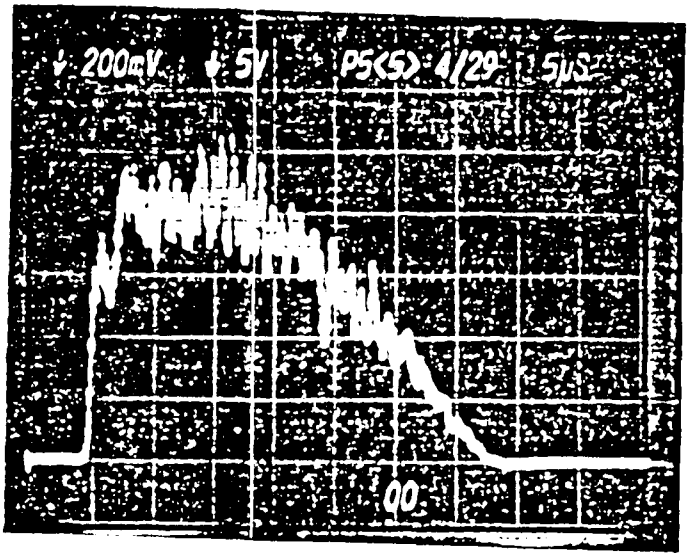

(a)

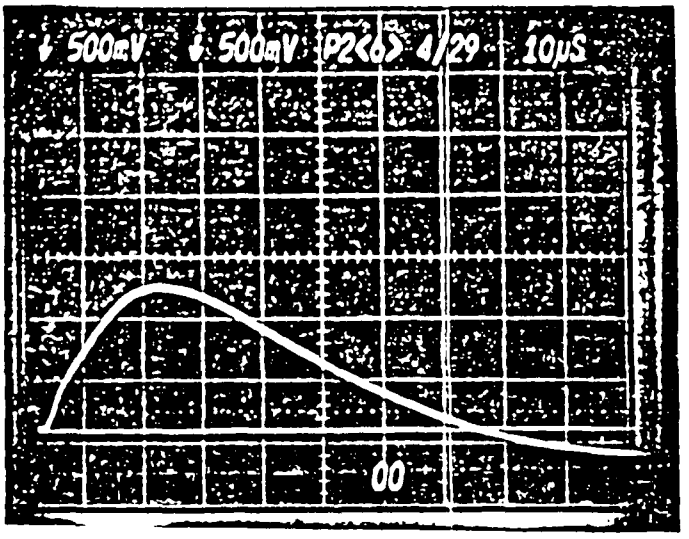

(b)

Figure 2.12 Data photographs

(a) typical TRS intensity trace
(b) typical SSG trace

(a)

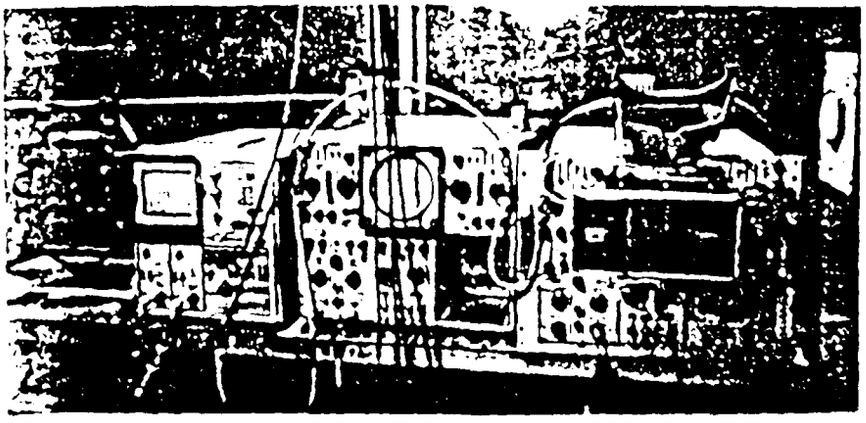

(b)

Figure 2.13 Photographs of experimental setup

(a) photograph of monochromators
(b) photograph of oscilloscopes

laser and its control panel are shown in Figures 2.14 and 2.8 respectively.

The small signal gain diagnostics were performed as follows. The probe laser was tuned to a specific transition using the probe laser resonator grating. The output was then chopped by the rotating wheel chopper and steered onto a beam splitter. The resulting two output beams were designated as the reference beam and the signal beam. They will be described separately (see Figure 2.10).

The signal beam was that portion of the probe laser beam that was reflected off the beam splitter. It traversed a path through the laser medium collinear with the path of the laser emission described in the TRS section above. The time dependent chemistry occurring within the laser medium perturbed the signal beam. The resulting perturbed signal beam then traveled to the detector following the path described for the TRS beam.

The reference beam was that portion of the probe laser beam that was transmitted through the beam splitter. Upon exiting the beam splitter, the reference beam was focused using a CaF_2 lens and steered into the EMI shielded room. Once inside the room, the reference beam was focused again by another CaF_2 lens and steered into a monochromator diffraction grating-detector-bias circuit system identical to that in the signal beam's path.

A dual beam, EMI shielded oscilloscope (Tektronix: 7844) with two fifty ohm vertical amplifier plugins (Tektronix: 7A19) monitored the two signals simultaneously. Pictures were taken of each data run with a sample shown in Figure 2.12b. Pictures of the monochromatic-diffraction grating-detector-bias circuit are shown in Figure 2.13a.

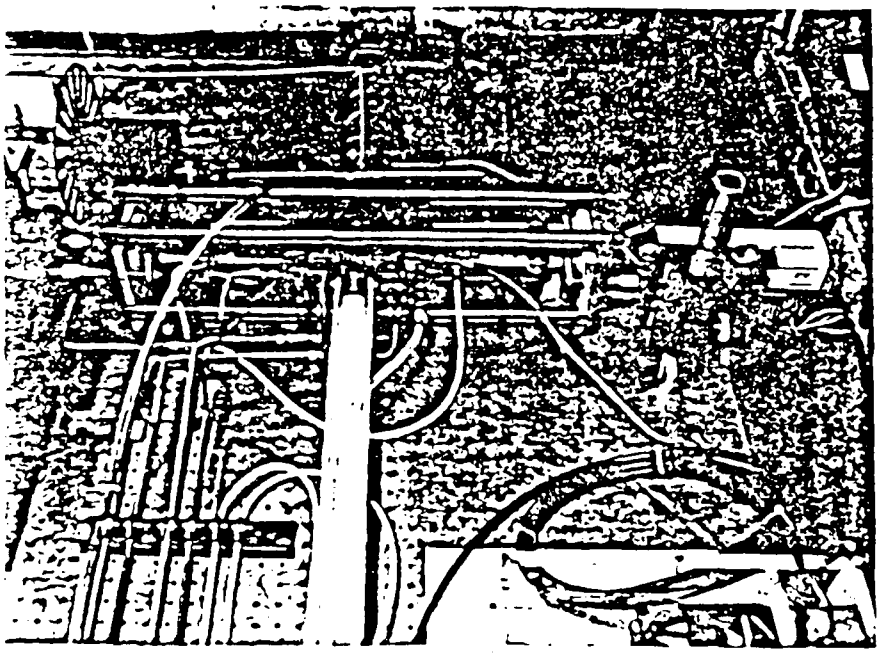

Figure 2.14 CW probe laser used in small signal gain tests

The total pulse energy diagnostic was performed on the laser cell while it was in the configuration described in the TRS section. However, the output beam was routed into a calorimeter (Scientech: 364, 10.2 cm diameter) immediately after exiting the output coupler (see Figure 2.11).

It was also necessary to experimentally characterize the flashlamp emission properties. It was important to know flashlamp pulse duration and wavelength distribution as a function of time for the modeling studies. Measurement of these parameters was accomplished in the following manner (see Figure 2.15).

The CaF_2 brewster window was removed from one end of the cavity. A quartz lens was positioned inside the cavity, focusing the ultraviolet light pulses from the flashlamps onto the entrance slits of a monochromator (GCA-McPherson: 218, 0.3 m). A diffraction grating (GCA-McPherson: 2400 grooves/mm, 0.2 micron blaze) dispersed the desired wavelength component through the exit slit onto a photomultiplier tube (RCA: 4832). Voltage was supplied to the photomultiplier tube (PMT) and the resulting signal displayed on an EMI shielded, fast risetime oscilloscope (Tektronix: 7844) with a one megaohm vertical amplifier (Tektronix: 7A16A). Flashlamp intensities vs time at 0.1 micron intervals in the region 0.25 micron to 0.40 micron were recorded (see Figure 2.16).

EXPERIMENTAL CONFIGURATION FOR MEASUREMENT OF $I_{\lambda_i}(t)$

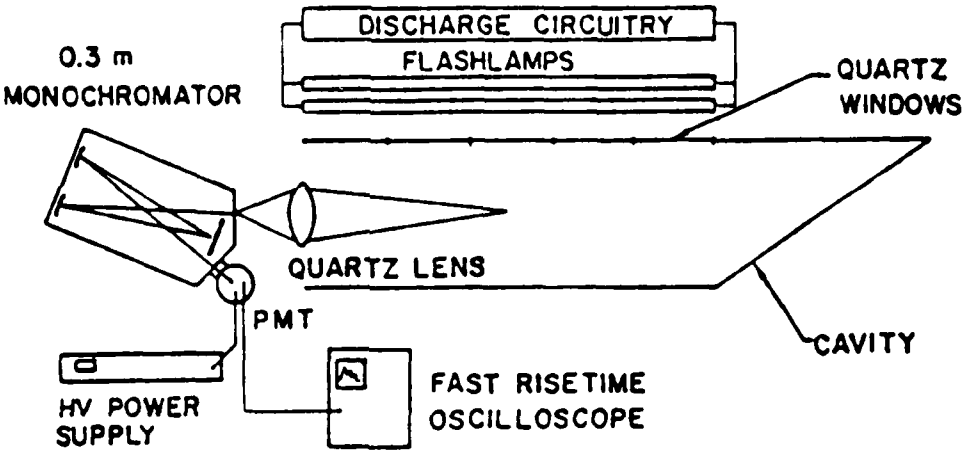

Figure 2.15 Flashlamp intensity measurement experimental configuration

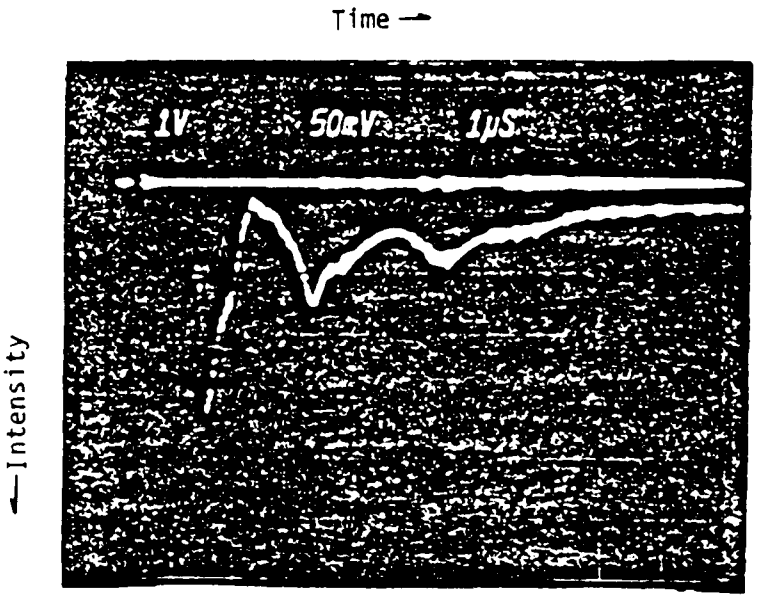

Figure 2.16 Typical Flashlamp intensity trace

2.3 Results of Time Resolved Spectroscopy Studies

2.3.1 Introduction

Time resolved spectra measurements were recorded at three pressures and two mixtures using two values of outcoupler reflectivity. Results for the two mixtures will be discussed separately. Some general considerations will be presented first.

It is widely known that mixtures of H_2 and F_2 will spontaneously form HF. For laser mixtures this is known as prereaction and has been reported by many authors (cf. Reference [64]). The HF formed by prereaction rapidly equilibrates, depositing population in low rotational levels in the ground vibrational state. This population, already present when initiation of the remainder of the H_2 + F_2 mixture takes place, is undesirable for several reasons. (1) The equilibrated population acts as an absorber on several low J transitions in the v = 1-0 band, increasing their threshold gains. These increased threshold gains are a loss mechanism robbing the laser pulse of a portion of its energy [74]. (2) Hydrogen fluoride is a very efficient self deactivator. It is the most efficient rotational deactivator [68] and one of the most efficient vibrational deactivators [75]. Hydrogen fluoride population, formed prior to initiation, reduces total pulse power, energy and duration by increasing the relaxation rate of the nascent population distribution [76]. (3) Finally, the laser pulse loses additional power and energy because any HF formed and deactivated prior to pulse initiation cannot contribute to pulse energy and pulse power. For these reasons, it is desirable to minimize prereaction in a laser. For this study, there is another important reason: (4) Because of the large HF Einstein coefficient for stimulated emission (and consequently, the

large absorption coefficient) and the long length of the active medium (53 cm), gain measurements were extremely sensitive to initial HF concentration. In fact, a concentration of 0.5 mtorr of HF could be detected by probing on the $P_1(3)$ transition. See Appendix B for a description of this technique.

This sensitivity to initial HF concentration necessitated a much more stringent prereaction requirement for this study than in other works. Suchard [14], for instance, claimed prereaction of less than five percent initial mixture F_2. If this criterion were used, up to 295 mtorr HF could be present initially for the lowest pressure case. This would have prevented measurements using the gain detection system by totally absorbing the probe laser signal.

Historically, to minimize prereaction, O_2 is added to the $H_2 + F_2$ mixture [1, 17, 30, 42, 77, 78]. The rate of formation of HF is reduced by the presence of O_2, in some cases insuring stability [78]. It is believed that O_2 removes chain carriers (H and F atoms) from the mixture [79]. Unfortunately, Taylor, et al [79] have shown that in the absence of prereaction, increasing O_2 concentration reduces laser performance by removing the H and F atom chain carriers. Thus, O_2 concentration has to be balanced between the minimum amount required to reduce prereaction to an acceptable level and the maximum amount tolerable to laser performance.

Reduction of prereaction was deemed to be of primary importance so O_2 was added until the initial concentration of HF was below 1 mtorr. This necessitated an unusually high concentration of O_2.

In addition to problems associated with prereaction, HF lasers suffer problems with parasitic oscillations (cf. Reference 70). A

parasitic oscillation is defined as undesirable stimulated emission occurring within the laser medium. Normally, this means lasing between surfaces other than the cavity mirrors. This can be a large loss mechanism as emission produced by parasitic oscillation is not emitted in the output beam; parasitic power and energy are lost. Two attempts were made to reduce parasitics.

One attempt was to cant the cavity end surfaces such that single pass oscillation could not exist between the Brewster window mounts. This should have eliminated parasitic oscillations in the lasing axis direction.

Another attempt was to coat all cavity interior surfaces with absorbant black paint (3M: Nextel). This was expected to eliminate parasitic oscillations between surfaces normal to the lasing axis [39]. The disadvantage of this technique was that the ultraviolet initiation photons hitting the cavity interior surfaces were essentially all absorbed. Since initiation was low with the absorbant black paint in place, it was removed. Removal of the paint helped increase initiation efficiency, always desirable in a flash photolysis case [1].

While precautions were taken to minimize parasitic oscillations, there is no absolute evidence that parasitic oscillations did not exist. There is the possibility that undetected parasitic oscillations did exist because the system exhibits high gain and because the laser cavity walls and windows are not perfectly transmitting. In addition, Suchard, et al. [39] have discussed the existence of circumferential and axial modes of parasitic oscillations and shown them to be important under certain conditions. They have shown that axial grazing modes can be

particularly detrimental to laser performance. Calculations similar to those of Suchard, et al. [39] for axial grazing modes were performed. The resulting parasitic oscillation threshold gain for this mode is 0.019 cm^{-1}. This is lower than the experimental peak gain reported here for all transitions except $P_1(7)$ and $P_1(6)$. Potential parasitic threshold gains presented here are comparable to gains measured here implying parasitic oscillations may well be important.

For the time resolved spectroscopy runs, the data taking procedure was as follows: (1) The cavity was purged with He for approximately two minutes to flush out residual HF. (2) The dump valve was closed and the cavity was evacuated to less than 1 torr. (3) Metered flows of He and O_2 were admitted. At this point, in rapid succession, (4) the F_2 flow was turned on, the capacitors were charged, the H_2 was added, and flows were permitted to stabilize. (5) The capacitors were discharged, pulsing the flashlamps and initiating lasing. (6) All gas flows except the He were turned off and the dump valve was opened. Step (1) was then repeated. The duration between shots was timed to be five minutes. This allowed sufficient time to remove all combustion products from the cavity between runs.

All the time resolved spectra data was taken in the form of pictures of oscilloscope traces. A sample is shown in Figure 2.12a. All the data for one mixture at one pressure were then reduced to a plot like Figure 2.17. In this figure, the horizontal lines show the measured duration of each transition, displayed horizontally at the v and J corresponding to the transition's lower level. The time of each transition's peak intensity is denoted as a closed circle. To aid in the visualization of pulse development, selected transition intensity

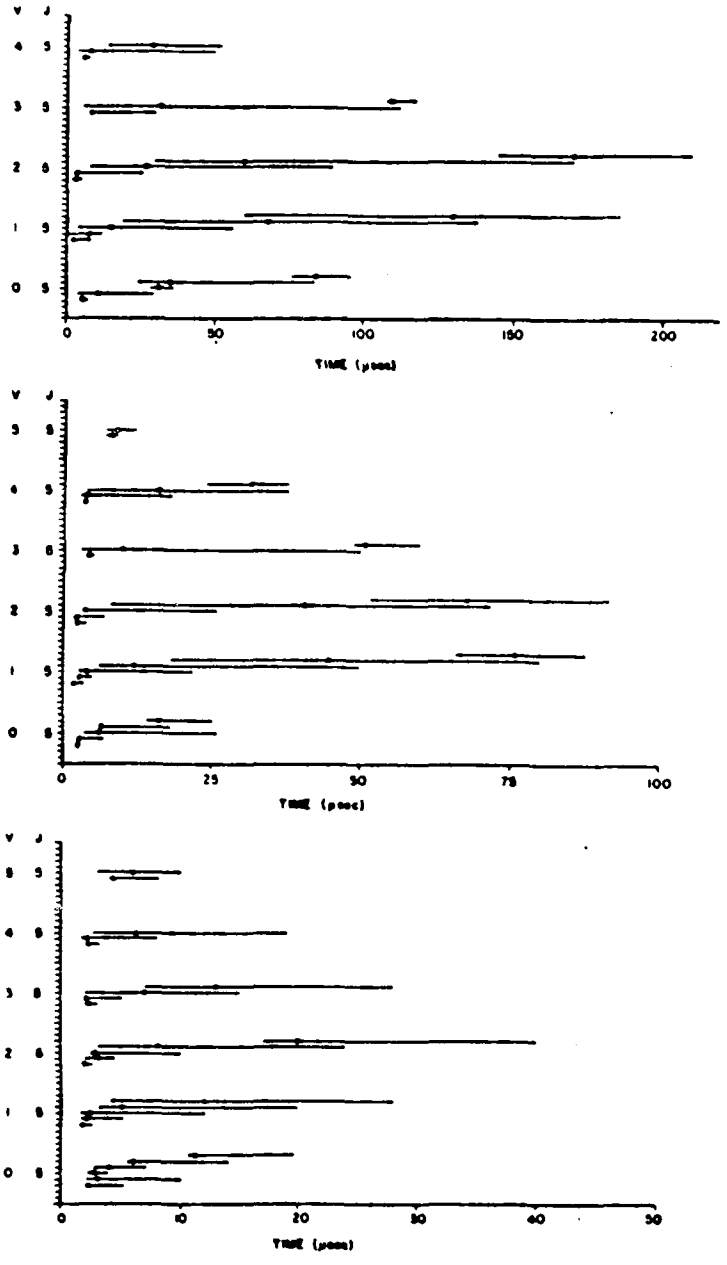

Figure 2.17 Time resolved spectral output: $He:O_2:F_2:H_2$ = 20.8:1.0:4.6:1.2
(a) 36 torr pressure
(b) 102 torr pressure
(c) 331 torr pressure

time histories were plotted in Figures 2.18, 2.19 and 2.20. Figures 2.18, 2.19 and 2.20 show relative intensities only.

Using the aforementioned data taking procedure, day-to-day repeatability was about 20% for peak intensities, about 15% for pulse durations and about 20% for pulse energies. Shot-to-shot repeatability was better: 10% for peak intensities, 10% for durations and 15% for pulse energies.

Most of this variation can be attributed to two causes: (1) The variation of capacitor charging voltage from run-to-run, and (2) The lack of repeatability in cavity mixture and pressure. The first would cause a change in initiation strength from shot-to-shot by varying the photolysis energy supplied to the mixture. This would perturb all pulse characteristics. The second would cause a change in the chemistry and relaxation processes, also perturbing all pulse characteristics.

2.3.2 Time Resolved Spectroscopy Results for the Mixture

$$He:O_2:F_2:H_2 = 20.8:1.0:4.6:1.2$$

For all runs, there is a strong trend of shifting of the transition peak intensity times with rotational level in all bands. There is also a strong trend toward shifting of the transition initiation and termination times with rotational level in all bands. In addition, one observes an increase in pulse duration in all bands with an increase in rotational level up to $P_v(6)$. Pulse duration shows a decrease at transtions above $P_v(6)$. Finally, there is also a general decrease in peak intensity with increasing rotational level.

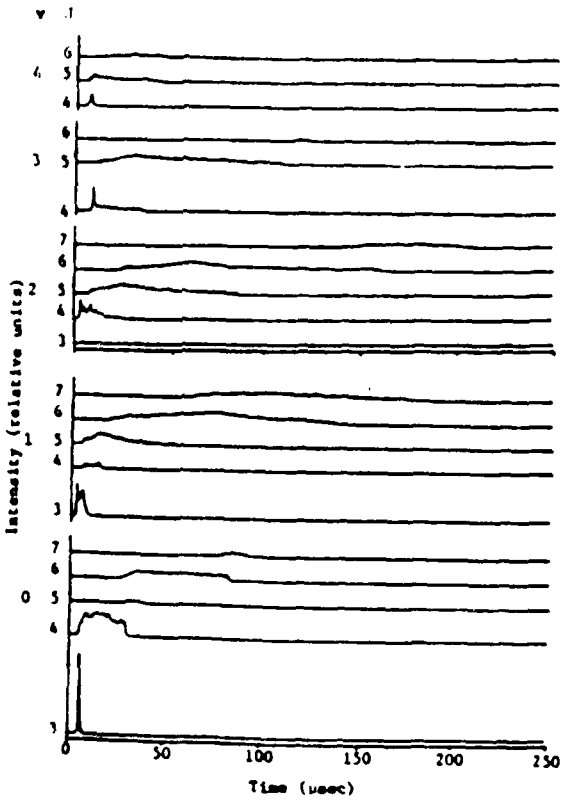

Figure 2.18 Spectral time history: $He:O_2:F_2:H_2$ = 20.8:1.0:4.6:1.2, 36 torr pressure

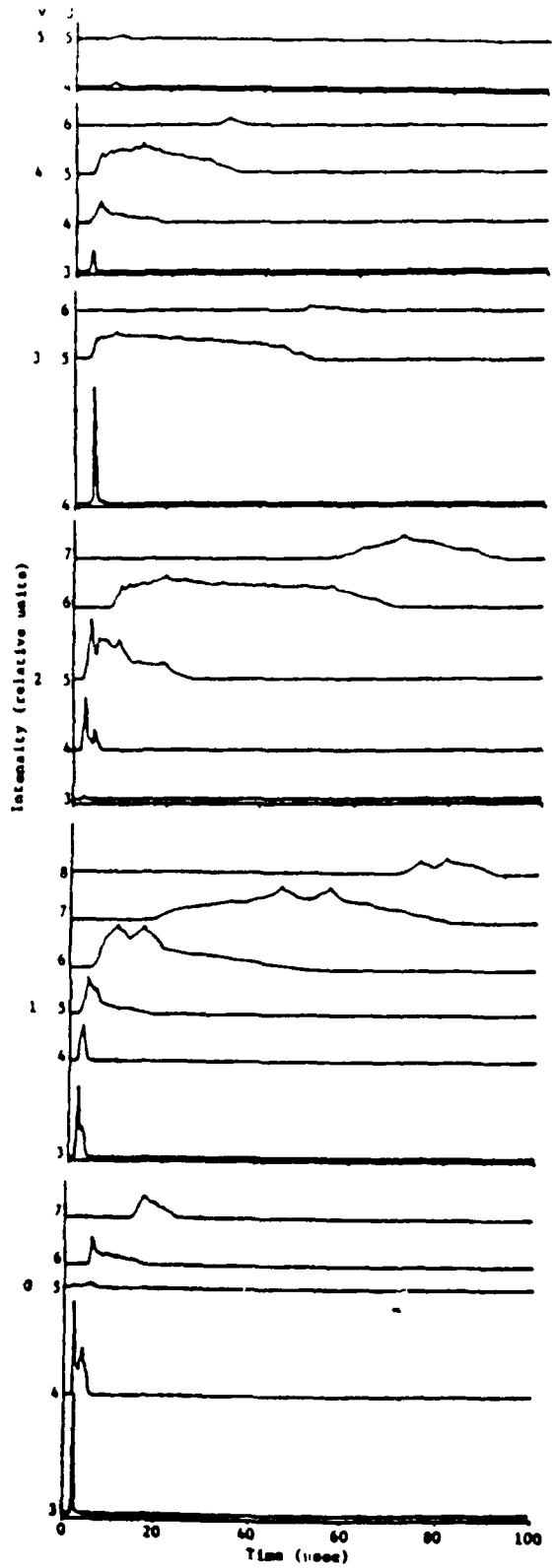

Figure 2.19 Spectral time history: $He:O_2:F_2:H_2$ = 20.8:1.6:4.6:1.2, 102 torr pressure

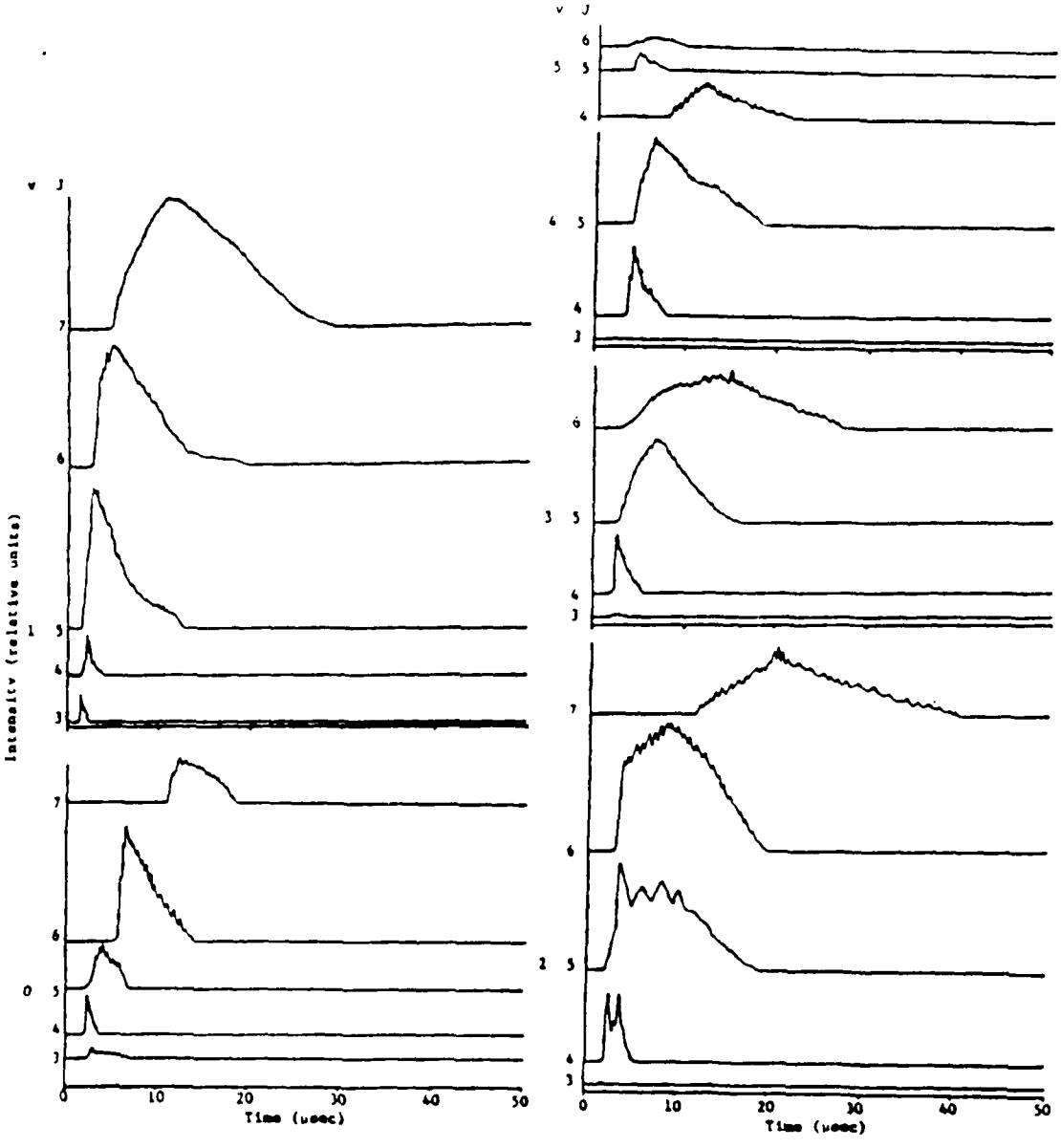

Figure 2.20 Spectral time history: $He:O_2:F_2:H_2$ = 20.8:1.0:4.6:1.2, 331 torr pressure

The observed monotonic trends of shifting transition initiation, termination and peak intensity times are strong evidence of a rotational distribution approximating Boltzmann. Furthermore, peak intensity within a given band generally appears on the transition with the maximum upper level population in that band consistent with a Boltzmann distribution of rotational levels at about 400 K. Nevertheless, nonequilibrium rotational populations are evidenced by simultaneous lasing on adjacent transitions.

There appears to be cascading linking the transitions $P_2(3)$ and $P_1(4)$, $P_3(4)$ and $P_2(5)$ and $P_5(3)$ with $P_4(4)$ and $P_3(5)$.

Cascading is a phenomena due to lasing where the stimulated emission flux on one transition assists in the inversion buildup, and subsequent lasing, of a second transition. The two transitions are linked by a common, intermediate energy level: HF(v = 1, J = 3) for instance. When lasing occurs on the $P_2(3)$ transition, population is radiatively transferred from HF(v = 2, J = 2) to HF(v = 1, J = 3). This population transfer helps to build up an inversion between HF(v = 1, J = 3) and HF(v = 0, J = 4), leading to lasing on the $P_1(4)$ transition. $P_2(3)$ and $P_1(4)$ are then said to be cascade linked transitions.

For each of these pairs of transitions linked by cascading, a peak in the upper transition stimulated emission intensity is closely followed by a peak in the lower transition stimulated emission intensity. This is particularly noticeable for the 36 torr pair $P_2(3)$ and $P_1(4)$. Initially $P_1(4)$ rises just after $P_2(3)$ rises, falls just after $P_2(3)$ falls, and rises again just after $P_2(3)$ rises for the second time.

Also note that lasing is observed on transitions in the v = 6-5 band. No such lasing was observed for the 36 torr case. This behavior

is probably a result of a more favorable competition at 102 torr between the net result of pumping plus deactivation and the cavity loss mechanisms. As the pressure increases for a fixed gas composition, the net inversion produced by pumping minus deactivation increases. From the results presented in Figure 2.17 for the 102 torr case, it appears that for this case, the inversion exceeded the threshold gain due to cavity losses while for the 36 torr case it did not.

This increased rate of stimulated emission on the v = 6-5 band for the 102 torr case would help to explain the anomalous behavior of the $P_5(5)$ transition. This transition has a significantly higher peak than $P_5(4)$, hence, it does not follow the trend of decreasing peak intensity with increasing rotational level. This could be explained by cascading from $P_6(3)$. Another possible explanation is that the assumed pumping distribution is in error. An alternative pumping distribution is suggested in Chapter 3.

The v = 6-5 band behavior also appears anomalous for the 331 torr case. Here, none of the trends observed for the other levels are obeyed. Because of the high rate of hot pumping into v = 6 [8], one would expect stronger lasing. However, because hot reaction pumping into v = 7 is much less than the pumping into v = 6, V-V exchange and reverse V-R,T (R-V) energy transfer may be transferring a significant amount of population between v = 6 and v = 7. This would diminish the v = 6-5 inversion. Furthermore, since V-R,T energy transfer is thought to scale as $v^{2.7}$ [25], fast V-R,T relaxation will also contribute to the reduction of the v = 6-5 inversion. These mechanisms may account for the behavior of the v = 6-5 band.

The unique time history of the v = 6-5 band may also be explained by cascading. It appears that lasing on $P_6(4)$ is strongly dependent on the behavior of lasing on $P_5(5)$. $P_6(4)$ does not initiate lasing until $P_5(5)$ reaches its peak intensity. Thus $P_5(5)$ lasing would assist in $P_6(4)$ lasing by improving the population inversion by cascading. Recall that cascading occurs when the lower transition lases, removing population from the lower level of the upper transition, which then lases. In addition, $P_6(4)$ terminates shortly after $P_5(5)$ terminates. This implies that when the mechanism assisting the population inversion terminates, so does the laser pulse.

If the behavior of $P_6(4)$ were neglected, $P_6(5)$ and $P_6(6)$ would follow the observed trends well. These two transitions exhibit behavior in agreement with the trends for peak intensity and termination times. They disobey the trend for initiation time only slightly.

It is clear that the intensity, initiation and termination times, and duration of $P_1(5)$ do not fit the observed trends. A possible explanation is partial absorption of the $P_1(5)$ signal by a foreign species. This absorption would tend to decrease the signal intensity while leaving the peak position unchanged. This would effectively shorten the pulse duration. This behavior is consistent with that observed for $P_1(5)$: An initiation time later than predicted by the trends, a termination time earlier than predicted by the trends, a peak intensity lower than predicted by the trends but a peak position in agreement with the trends. Possible candidates as absorbers are impurities in the F_2 supply (SF_6, CO_2, O_2, N_2 or CF_4) or products generated during lasing (OH or H_2O).

Oxygen and nitrogen can be eliminated immediately since they have no transitions which absorb in the 2.7 μm region[80].

Sulfur hexafluoride can also be eliminated from consideration. First, it has no infrared active transitions near 2.7 μm [81], and second, the reported absorption coefficient at the $P_1(5)$ wavelength is 1.3×10^{-5} cm^{-1} $torr^{-1}$ [82]. Coupled with the estimated SF_6 impurity in the F_2 supply and the 100 cm absorption pathlength accounted for, this would yield only 7.0×10^{-7}% absorption of the $P_1(5)$ signal over the entire cavity length.

Carbon tetrafluoride can also be eliminated. It has only continuum absorption in this region of the spectrum [83]. This continuum absorption would affect all transitions in this spectral region equally and would not be responsible for the anomalous behavior of a single line.

The hydroxl radical has infrared active transitions in the 2.7 μm region of the spectrum, however none are within 3 cm^{-1} of the reported $P_1(5)$ transition wavelength [84]. Since the linewidths of both OH and HF should be considerably less than 3 cm^{-1}, even for the 331 torr case, OH should have negligible absorption for the $P_1(5)$ transition.

Carbon dioxide also has infrared active transitions in the 2.7 μm region of the spectrum [80]. There are three transitions near the measured wavelength of $P_1(5)$: 3741.4598 cm^{-1} [85]. These are transitions at 3741.445 cm^{-1}, 3741.471 cm^{-1} and 3741.368 cm^{-1} corresponding to transitions occuring in the 14^41-04^40, 22^21-12^20 and $10^\circ1$-$00^\circ0$ bands respectively. Although these three transitions lie within the $P_1(5)$ line profile, they probably do not contribute significantly to $P_1(5)$ absorption. First, the 14^41-04^40 and 22^21-12^20 transitions are hot bands and will have very little population in their lower levels for temperatures encountered here. Their absorption will thus be negligible [86]. Second, the remaining transition, $10^\circ1$-$00^\circ0$, is a combination band with

a very low absorption coefficient. Approximately 100 torr of CO_2 would be needed in the laser cavity to produce the absorption necessary to diminish $P_1(5)$ [86]. Consequently, CO_2 absorption does not appear to be the cause of anomalous $P_1(5)$ behavior.

Water vapor has an infrared active absorption line near 3741.4598 cm^{-1}. Fraley and Rao [87], report an 001→000 transition at 3741.3088 cm^{-1}. This is within the line profile of $P_1(5)$ and could account for the observed absorption.

Other investigators have credited water vapor absorption with perturbing $P_1(5)$ intensities. Ultee [88] and Jacobson, et al [89] credit water vapor absorption with being responsible for anomalous behavior of their reported $P_1(5)$ intensities, although they do not list the water vapor transition responsible. Galochian, et al [29] and Greiner, et al [50] also report $P_1(5)$ intensities inconsistent with the remainder of their observations. They do not suggest a cause.

Due to the evidence presented, it is likely that the anomalously low $P_1(5)$ intensities observed are due to water vapor absorption of the signal.

For the 331 torr case, the behavior of $P_1(5)$ may seem inconsistent with the partial water vapor absorption of the signal as was suggested for the 36 torr and 102 torr cases. However, careful inspection of the $P_1(5)$ trace reveals the peak intensity is barely in accord with the trend of increasing peak intensity with increasing rotational level up to $J = 6$ within a given band. An increase in peak height for this transition would still be consistent with the trend observed for the 331 torr case. Thus, partial water vapor absorption of $P_1(5)$ is still a viable explanation for the observed behavior.

2.3.3 Time Resolved Spectroscopy Results for the Mixture $He:O_2:F_2:H_2 = 22.0:1.0:2.7:1.0$

For this mixture composition, there is monotonic shifting of both transition peak intensity times and transition termination times with increasing rotational level. These trends are well obeyed except for the 81% outcoupler reflectivity 331 torr case. In addition, transition initiation time increases with rotational level within a band. This is generally obeyed for all pressures with the following exceptions: $P_3(5)$ starts before $P_3(4)$, $P_4(4)$ starts before $P_4(3)$, and $P_5(4)$ starts before $P_5(3)$. Pulse duration also increases with an increase in rotational level. This behavior is strongest for the 331 torr case with 97% outcoupler reflectivity and for the 36 torr case. It is obeyed up to $P_v(6)$ for the remaining two cases.

Cascade linked transitions are apparent for all three cases utilizing the 97% reflectivity outcoupler. There is no apparent cascading for the 331 torr case using the 81% reflectivity output coupler. Furthermore, cascading is more evident at 36 torr than at 102 torr and more important at 102 torr than at 331 torr. This is based on the observation that the number of cascade linked transition pairs decreases with pressure.

It should be noted that no lasing is observed on v = 6-5 band transitions. The absence of v = 6-5 lasing is most likely explained by the steep dropoff of the output coupler reflectivity with increasing wavelength. See Figure A.2. It is possible that the resultant increase in threshold gain with wavelength is such that the v = 6-5 transition population inversions are insufficient to attain threshold.

Figure 2.21 Time resolved spectral output: He:O_2:F_2:H_2 = 22.0:1.0:2.7:1.0
(a) 36 torr, R_0 = 0.97
(b) 102 torr, R_0 = 0.97
(c) 331 torr, R_0 = 0.97
(d) 331 torr, R_0 = 0.81

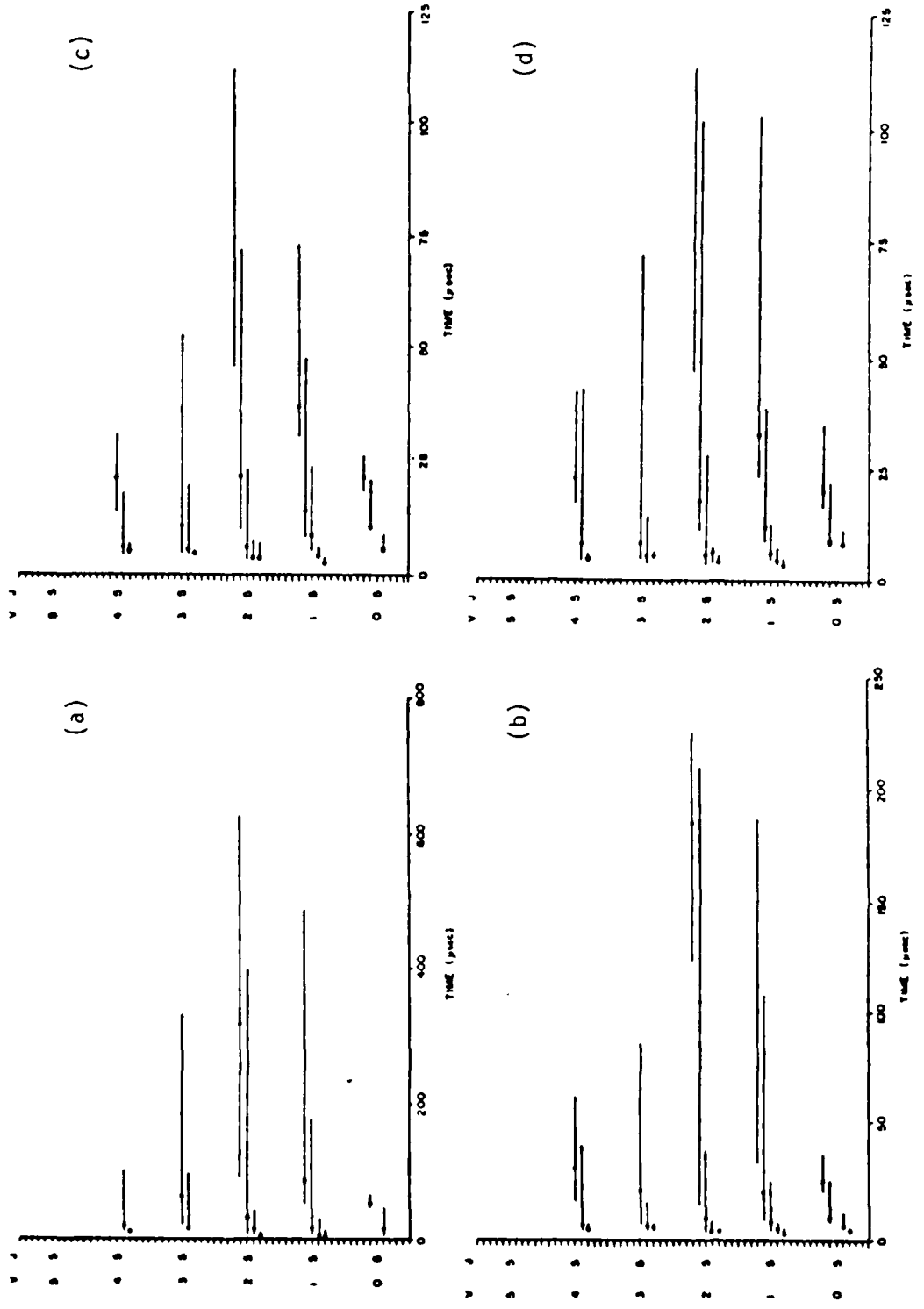

Figure 2.21

As mentioned in Section 2.3.2, the observation of increasing pulse duration with increasing rotational level, shifting of initiation time, and monotonic shifting of peak and termination times with increasing rotational level, are evidence of a near Boltzmann distribution of rotational population within a given vibrational level. Since these trends are also observed here, it is likely that a near Boltzmann distribution of rotational levels exists for this case too.

It should also be noted that $P_1(5)$ is absent. This again, is probably attributable to water vapor absorption. In this case, it appears that absorption is so strong, $P_1(5)$ never attains threshold.

Upon comparison of the two cases at 331 torr, it is evident that a change in output coupler reflectivity has no effect on the number of transitions lasing, the number being the same in each case. Hence, for this case, output coupler reflectivity has little effect on an individual transition's initiation time or on an individual transition's termination time. Outcoupler reflectivity causes a slight effect on pulse duration: of the nineteen transitions observed to lase, ten have longer durations using the 81% reflectivity output coupler, seven have longer durations using the 97% reflectivity output coupler, and two have durations essentially unchanged. This behavior runs counter to the expected result that an increase in the value of output coupler reflectivity would lower threshold gain, leading to increased pulse durations and an increase in the number of transitions lasing. There appears to be no explanation for this lack of agreement.

2.3.4 Results of Pure Rotational Lasing Studies

As noted in Section 2.1, the portion of laser power emitted at pure rotational wavelengths is of prime importance to researchers and development engineers interested in high power applications. Pure rotational lasing has also been shown to be linked to V-R,T energy transfer [61, 62, 80]. For these reasons, attempts were made to measure the time solved spectroscopy of pure rotational lasing transitions.

The experimental configuration used to investigate pure rotational lasing was discussed in 2.2.2. Two changes were made: (1) The 4 micron blazed monochromator diffraction grating employed in the P-branch lasing studies was replaced by a 16 micron blazed grating. (2) A long pass interference filter was inserted into the optical path immediately prior to the monochromator entrance slit. This filter had a 9 micron cut on point with <0.1% transmission below 9 microns and nominal 50% transmission from 9 microns to 20 microns. The interference filter served to eliminate all P-branch lasing signals, passing only radiation due to pure rotational lasing transitions.

Initial testing was done with the mixture $He:O_2:F_2:H_2$ = 22.0:1.0:2.7:1.0. At first, the 81% and 97% peak reflectivity output couplers were used. No rotational lasing was observed for any of the three pressure cases using these two output couplers. This could be due to the drop in output coupler reflectivity above 4 microns. This decrease in reflectivity continued out into the middle IR such that at 16 microns, the center of the pure rotational transition wavelengths, the reflectivity was below 20%. A 20% reflectivity would yield a threshold gain of 0.012 per cm. It appeared that pure rotational lasing transitions never exceeded threshold gain.

To correct for this, an output coupler with approximately 95% reflectivity at 16 microns was substituted for those used previously. This lowered the threshold gain for pure rotational lasing to approximately 0.0011 per cm. This output coupler had low reflectivity in the P-branch region of the spectrum: Nominally 40%.

The monochromator was tuned to transitions originating on J = 13,14,15 and 16 for vibrational levels v = 0, 1 and 2. These levels were chosen by noting the results of other researchers who had reported pure rotational lasing [57, 58, 60, 91], most notably Pimentel and coworkers [62,90]. Note that this rotational lasing was not observed from mixtures of $H_2 + F_2$, but from boron trihalides, vinyl fluoride, 1,1-difluoroethene, $ClF_x + H_2$, freons + H_2, CF_3I or CF_3Br + hydrocarbons and in optically pumped HF. Transitions above J = 16-15 could not be detected due to detector wavelength limitations.

For this mixture, no rotational lasing was recorded for either the 36 torr or 331 torr cases. Intermittent pure rotational lasing was detected at 102 torr for the transition v = 1, J = 15-14. Lasing was observed to occur only three times out of twenty-four trials. This is not sufficient evidence to report TRS for pure rotational lasing. However, this investigation does imply the existence of pure rotational lasing.

An investigation of pure rotational lasing was also conducted for the mixture $He:O_2:F_2:H_2$ = 20.8:1.0:4.6:1.2. The same transitions were examined as for the other mixture. All three output couplers were used. Pure rotational lasing was not observed for any of these three pressure cases.

The conclusions to be drawn from the examination of pure rotational lasing are: (1) For higher F_2/H_2 ratios, hence stronger initiation, pure rotational lasing is unimportant and probably does not exist. (2) For more strongly diluted systems with F_2/H_2 approaching stoichiometric, rotational lasing may exist. (3) If output coupler reflectivity is low, near 25% for pure rotational wavelengths, pure rotational lasing is negligible for all compositions reported here.

2.3.5 Discussion

Several trends become apparent upon comparing the runs presented in Sections 2.3.2 and 2.3.3.

(1) As expected, individual transition pulse durations show a decrease with an increase in mixture pressure. All but two transitions exhibit this behavior for the mixture composition $He:O_2:F_2:H_2$ = 20.8:1.0:4.6:1.2. For the mixture composition $He:O_2:F_2:H_2$ = 22.0:1.0:2.7:1.0, the trend is observed for transitions which terminate on rotational levels above J = 4. No pattern is evident for transitions which terminate on rotational levels J = 3 and 4.

(2) Individual transition pulse durations decrease with an increase in initial percentage of mixture F_2. This behavior is observed for both the 36 torr and 102 torr cases, there being only one exception to each. It is not observed for the 331 torr case.

(3) The number of transitions lasing within a given band increases with an increase in initial percentage of mixture F_2. This is stricly true for the 36 torr case. It is also true

for the 1-0, 3-2, 5-4 and 6-5 bands at 102 torr and for the 1-0, 4-3, 5-4 and 6-5 bands at 331 torr.

Two more trends become apparent upon comparing the raw data used to generate the figures in Sections 2.3.2 and 2.3.3.

(4) As one would expect, individual transition peak intensities increase with an increase in mixture pressure. There are no exceptions when comparing the 36 torr and 102 torr cases, but there are four exceptions when comparing the 102 torr and 331 torr cases on rotational levels above J = 4.

(5) Individual transition peak intensities increase with an increase in initial percentage of mixture F_2. As in (3) above, there are no exceptions for the 36 torr case. This behavior is generally true for the 102 torr and 331 torr cases. However, there are several sets of intensities which do not follow this pattern for both cases.

The increase of individual transition peak intensity and the decrease of individual transition pulse duration with increasing pressure are probably due to binary scaling of the chemical pumping and relaxation kinetic processes. Binary scaling would yield faster pumping and relaxation causing increased rates of fuel and oxidizer consumption and increased rates of product deactivation. This, in turn, is probably responsible for the shortened individual transition pulse durations. The increased rate of chemical pumping would also allow the population inversions generated to compete more favorably with threshold gain loss mechanisms and with stimulated emission allowing higher intensity build-ups. This would result in larger transition peak intensitites.

We conclude the remaining trends, (3), (4) and (5), are due to an increase in the initial percentage of mixture F_2. However, the effects of increasing initial mixture F_2 are probably distorted by the change in outcoupler reflectivity between the two mixtures. A discussion of these two effects follows.

Only two variable are changing during the comparison of the runs at the two mixture compositions. The first is the percentage of initial F_2 in the mixture. The second is the nominal output coupler reflectivity. These changes in initial mixture F_2 percentage and output coupler reflectivity should affect pulse behavior in opposite ways.

One of the effects of increasing the initial percentage of mixture F_2 to increase the rate of chemical pumping. This leads directly to an increase in the consumption rates of fuel and oxidizer and a consequent shortening of the pulse duration. Another consequence is more favorable competition between inversion buildup and losses through deactivation and radiation. Hence, one notes: (1) an increase in the number of transitions lasing and (2) increased peak intensities. The conclusion is that an increase in the initial percentage of mixture F_2 is partly responsible for observations (3) and (4). It is not clear what the effect of increasing initial mixture F_2 percentage would be on observation (5).

Changing the output coupler reflectivity has the opposite effect on pulse behavior for (3) and (4). Increasing the output coupler reflectivity decreases the threshold gain, lowering cavity losses, allowing more favorable competition between pumping and losses, yielding a greater number of transitions lasing and leading to increased

transition durations. This is not observed. There are two possible explanations.

The first, as stated in Section 2.3.3, is that the effect of the change in outcoupler reflectivity under these mixture conditions is minimal. The second is that the effect of increasing the initial percentage of mixture F_2 dominates the effect of the outcoupler reflectivity.

There are further observations to be made. One is that for all pressures and all mixture compositions, the time resolved spectra results indicate a nearly thermalized, or near Boltzmann, distribution of rotational levels. This is due to observed shifts in pulse initiation, pulse termination and pulse peak intensity times with increasing rotational level. Additional evidence is the increase of pulse duration with an increase in rotational level.

As previously stated in both Sections 2.3.2 and 2.3.3, these nearly thermalized rotational distributions are evidence of a rotational relaxation mechanism that is fast compared to chemical pumping and V-V and V-R,T relaxation.

Rotational relaxation may be much faster than chemical pumping and vibrational transfer and relaxation, but it is slower than the stimulated emission buildup time. Kerber, et al. [70] report the stimulated emission buildup time to be on the order of 2L/c. For this work, $2L/c = 9.5 \times 10^{-9}$ sec while model results show the rotational relaxation time to be 5.0×10^{-8} sec at 331 torr. The rotational relaxation times at 102 torr and 36 torr are longer than that at 331 torr.

Another observation is that $P_1(5)$ lasing is present only for the mixture $He:O_2:F_2:H_2$ = 20.8:1.0:4.6:1.2. The proposed increase in pump percentage rate with increased initial mixture F_2, presented above, is consistent with this. It is possible that this increase in pumping ra would overcome the absorption losses which are present for $P_1(5)$.

A final observation is that the relative importance of stimulated emission as a population transfer mechanism is increasing with an increase in mixture pressure. This is more evident for the mixture composition $He:O_2:F_2:H_2$ = 20.8:1.0:4.6:1.2.

For this mixture, cascade effects increase with pressure. More transitions are linked by cascading and cascading is more dominant at higher pressures, especially for higher vibrational bands: compare v = 6-5 at 331 torr and 102 torr for this mixture composition. Peak intensities for individual transitions also increase with pressure. As expected, population transfer due to stimulated emission increases with pressure. The latter two effects are related to the increase in cascading.

As mentioned in Section 1.2, there are six other studies reporti time resolved spectra for $H_2 + F_2$ systems. Of these six, four [14, 1 42, 43] utilized flash photolysis initiation and two [17, 52] used electric discharge. Only the results of one of the electric discharg works will be compared: those of Parker and Stevens [17]. Basov, et al. [52] do not present a complete set of spectra, but instead presen only selected transitions time histories. A meaningful comparison between that work and the results presented here is not possible. Co sequently, only the work of five authors will be presented: Referenc 14, 19, 42, 43, 17. These results will be compared individually with

the results of the present work. All pertinent information for each of these five works is presented in Table 2.1.

Suchard, et al. [14] present results for a 75 cm long, 1.2 cm diameter tube filled with 50 torr of a $He/F_2/H_2$ mix of composition $He:F_2:H_2 = 60:1:1$. The resonator configuration was a 310 cm radius, 98% reflector separated by 100 cm from a 0.2 cm hole outcoupler. A photolysis pulse 55 μsec long initiated the reaction, dissociating approximately 1% of the initial F_2.

Greiner [19] presents results for a 15 cm long, 0.7 cm diameter tube filled with 45.5 torr of a $O_2/F_2/H_2$ mix of composition $O_2:F_2:H_2 = 1:10:11.0$. A photolysis pulse 18 μsec long initiated the reaction, dissociating an estimated 0.75% of the initial F_2. This resulted in a pulse 8 μsec long with individual transitions having a mean duration of 2 μsec. Lasing was observed only for the lowest four bands: 4-3, 3-2, 2-1, 1-0. There was some evidence of cascading. Greiner [19] gives no information on the configuration of his optical cavity, but does note that the lasing mixture was originally cooled to 200K to 218K.

The work of Suchard [42] is very similar to that of Suchard, et al. [14]. According to Suchard [42], the differences are a different optical cavity configuration, a different gas composition and a different cavity length. The values from Reference 42 are a 43.5 cm cavity, a mixture consisting of $He:F_2:H_2 = 80:2:1$ and an optical cavity consisting of a 90% reflectivity outcoupler separated by 90.5 cm from the 98% reflectivity, 310 cm radius mirror, also used in the study of Reference 14.

Table 2.1 Summary of TRS Results from References [14, 17, 19, 42, 43, 52]

Reference Number	Initiation Method, Duration (μsec), Energy Density (J/cm³)	Gas Composition ($He:O_2:F_2:H_2$ *), Pressure (torr)	F_2 Dissociation (Estimated %)	Cavity Length, Cavity Diameter, Mirror Spacing (cm)	Mirror Reflectivities (Nominal %) Mirror Radii (cm)	Bands Observed, Lines Per Band	Total Pulse Duration, Mean Transition Duration (μsec)	Cascade Transitions
14	Flash Photolysis 55 3.45	60:0:1:1 50	1	75 1.2 100	98 310 Hole Outcoupler -	1-0, 6 2-1, 7 3-2, 8 4-3, 3	60 9	$P_2(3)/P_3(2)$ $P_3(3)/P_4(2)$ $P_3(4)/P_4(3)$
19	Flash Photolysis 18 >44	0:1:10:11.8 45.5	0.75	15 0.7 -	- - -	1-0, 6 2-1, 8 3-2, 5 4-3, 1	8 2	$P_1(7)/P_2(6)/P_3(5)$ $P_1(8)/P_2(7)/P_3(6)$ $P_2(8)/P_3(7)$
42	Flash Photolysis - -	80:0:2:1 50	-	43.5 - 90.5	90 310 90 -	1-0, 6 2-1, 8 3-2, 7 4-3, 7 5-4, 6 6-5, 4	32 9	$P_1(6)/P_2(5)$ $P_1(7)/P_2(6)$ $P_1(8)/P_2(7)$ $P_1(9)/P_2(8)$ $P_2(4)/P_3(3)$ $P_6(1)/P_9(2)$
43	Flash Photolysis >30 39	9:2:3:1 114	-	75 .2.4 -	96 - 6 -	1-0, 6 2-1, 8 3-2, 6 4 3, 4	4 1.7	$P_1(7)/P_2(6)$ $P_1(8)/P_2(7)/P_3(6)$ $P_1(9)/P_2(8)/P_3(7)/P_4(6)$ $P_2(9)/P_3(8)$ $P_2(11)/P_3(10)$ $P_4(8)/P_6(7)$
17	Electric Discharge 0.2 - 0.7 0.0015	10:0.25:1:1 36	2.5	1 x 0.8 x 15 60	- 300 80 -	1-0, 11 2-1, 11 3-2, 7 4-3, 5 5-4, 4 6-5, 2	6 2.3	Much Cascading

Borisov, et al [43] report TRS for a 114 torr mixture of $He:O_2:F_2:H_2$ = 0:2:3:1 contained in a 75 cm long 2.4 cm diameter cavity. The optical cavity consisted of two flat mirrors of 96% and 6% reflectivity. The flash photolytically initiated pulse had a total duration of 4 μsec with individual transitions having a mean duration of 1.7 μsec.

The previous four authors all used flash photolysis for laser initiation. The remaining work used a pulsed electric discharge for initiation. As mentioned in the introduction, electric discharge initiation produces charged species which can complicate the medium chemistry. This difference in chemistry could be responsible for a difference in results between electrically and photolytically initiated systems.

Parker and Stevens [52] present results for a 36 torr mixture of $He:O_2:F_2:H_2$ = 10:0.25:1:1 flowing through a 1 x 0.8 x 15 cm long channel. A 300 cm radium "high reflector" and 80% reflectivity flat mirror comprised the optical cavity. Electric discharge pulses of 0.2 → 0.7 μsec produced laser pulses of 6 μsec total length with a mean transition duration of approximately 2.3 μsec. The authors claim an initial F_2 dissociation of about 2.5%.

Our 36 torr, mixture $He:O_2:F_2:H_2$ = 20.8:1.0:4.6:1.2, TRS results are consistent with the results of Greiner [19] and Parker and Stevens [17]. These studies report durations less than that presented here: 8 μsec and 4 μsec vs. 200 μsec, respectively. This is to be expected as:

(1) Both studies report fluorine dissociation values over two orders of magnitude less than this study. Pulse duration is known to decrease strongly with initiation strength [70].

(2) Both studies report cavity lengths less than this work. Pulse duration has also been shown to decrease with decreased cavity length.

(3) Greiner [19] has a much less dilute mixture, also leading to a decrease in pulse duration relative to this work.

Our 36 torr, mixture $He:O_2:F_2:H_2$ = 22.0:1.0:2.7:1.0, TRS results are consistent with the results of Suchard and coworkers [14, 42]. The durations reported there are shorter due to the higher level of initiation reported (1% vs the 0.0025% reported here) and their slightly higher cavity total pressures. The mixtures employed by Suchard and coworkers are more dilute than this case, which could lead to some lengthening of their pulse duration compared with this. However, it is expected that this will be a much smaller effect than the over two order of magnitude difference in initiation strength.

The results of Borisov et al. are consistent with our 102 torr results with mixture composition $He:O_2:F_2:H_2$ = 20.8:1.0:4.6:1.2. They report shorter pulse durations because of higher threshold gain and a much less dilute mixture. The former is due to the low (6%) outcoupler reflectivity employed and leads to a decrease in pulse duration [70]. The latter has also been shown to lead to a decrease in pulse duration.

2.4 Results of Small Signal Gain Studies

2.4.1 Introduction

Small signal gain was measured on this laser at three pressures and two mixtures. Results from the two mixtures will be discussed separately.

For the case with nominal mixture $He:O_2:F_2:H_2$ = 22.0:1.0:2.7:1.0 small signal gain could not be measured at 36 torr. The small signal gain was too low to cause a noticable perturbation in the amplitude of the signal beam. All attempts showed neither positive nor negative gain. Small signal gain was not measured for $P_1(6)$, $P_2(3)$ or $P_2(4)$ at 102 torr and for $P_1(3)$, $P_2(3)$ or $P_2(4)$ at 331 torr. This was due to an old and erratic probe laser which refused to lase on these transitions. Several different probe laser gas mixtures and discharge currents/voltages were tried in an effort to get the probe laser to oscillate on these transitions. All failed.

For the mixture $He:O_2:F_2:H_2$ = 20.8:1.0:4.6:1.2 small signal gain was measured only at 102 torr. In addition, small signal gain was not measured for $P_2(6)$, $P_2(7)$, $P_2(8)$, $P_1(3)$ or $P_1(8)$ for the reason stated in the paragraph above.

It was originally proposed to probe small signal gain (SSG) on the v = 2-1 and v = 1-0 transitions with the Helios SF_6/H_2 probe laser and to probe SSG on all other bands with a Laser Analytics Tunable Diode Laser (TDL). Upon the advice of Butler of Laser Analytics [92], the latter was dropped. It was felt that there would be two insurmountable problems. The first was attenuation of the weak (<1 microwatt) TDL probe signal. This would have been caused by scattering off optical elements and atmospheric dust particles and absorption by optical

reflecting and transmitting elements and by the atomsphere. It was felt the signal level would be too low to register on the detectors. The second, and more serious problem, was electromagnetic interference (EMI) of the TDL power supply. High transient currents in the flashlamp discharge circuitry would produce time varying magnetic and electric fields which would in turn perturb circuit elements within the sensitive TDL power supply. This would result in mode hopping of the TDL causing a shift in probe laser signal frequency. This could not be tolerated. For these reasons, the TDL probe was not used.

One alternative to the TDL as a gain probe was to use SF_6 + HI in the existing SF_6/H_2 Helios probe laser. This was suggested by Jeffers [93]. Due to previous results using the SF_6 + HI mixture [50], Jeffers felt this mixture might produce lasing on transitions up to v = 6-5 using the probe laser described in Section 2.2.2.

There were three reasons why no measurements were attempted using this technique. First, iodine atoms remaining as products from the reaction F + HI = HF + I could combine with fluorine atoms to form IF, and subsequently, IF_5 and IF_7 [94]. These compounds are potentially very damaging to vacuum pumps. It is believed that the IF_5 and IF_7 rapidly decompose vacuum pump oil and seals often leading to vacuum pump failure [93, 94]. Second, Jeffers believed any HI not consumed in the probe laser reaction zone would have an effect on the vacuum pumps similar to that of IF_5 and IF_7 [94]. Third, there was a lack of sufficient facility time to complete the TRS and SSG measurements at the two mixtures presented here and undertake SSG measurements for the higher vibrational bands. It was felt that the TRS and SSG measurements

presented here were more important than the SSG measurements for the higher vibrational bands. Thus, facility time was utilized in a manner consistent with these goals.

A second alternative to the TDL as a gain probe was the F-center laser marketed by Burleigh, Inc. This system consists of an argon-ion or krypton-ion pump laser and frequency shifting crystal which produce tunable light in the 2.1 to 3.3 micron region of the spectrum. Several transitions of interest in the v = 3-2, v = 4-3 and v = 5-4 bands would be accessible using this device. However, because the combined cost of the ion pump laser and frequency shifting crystal was high, this system was not tried due to lack of funds.

There were no further substitute sources available which would oscillate in the required region of the spectrum. Hence, gain was not measured for bands above v = 2-1.

The data taking procedure for the SSG runs was identical to that of the TRS study. This procedure was described in Section 2.3.1. For the SSG runs, it was necessary to synchronize the firing of the flashlamps with the presence of the probe laser beam in the laser cavity. This was accomplished by gating the lamp signal to the probe laser signal via a HP 214A pulse generator. The lamps would fire only when they simultaneously received a ready signal from the probe laser and the operator.

All small signal data was taken in the form of oscilloscope trace pictures. A sample is shown in Figure 2.12b. For each run, both the signal intensity and reference intensity traces were digitized at approximately twenty discrete points. The results of digitization were used to calculate the small signal gain at each point. The gain points

were plotted and a smooth curve was drawn through the result. Gains for all transitions measured in each band were then graphed on a single figure.

There are two main sources of uncertainity in the gain measurements. One of these is associated with the uncertainty in the frequency of the probe laser. This uncertainty arises from the possibility of the probe laser "mode-hopping"; shifting from one cavity longitudinal mode to a cavity longitudinal adjacent mode. This would cause a shift in probe laser frequency. Since medium gain is highly frequency dependent, through the lineshape profile term, this could lead to measurement of a significantly different gain. Mode hopping should not have been caused by thermal effects as the cavity was constructed of material (INVAR) with an extremely low thermal expansion coefficient. However, it could have been caused by vibrations from the probe laser vacuum pump. If these vibrations were transmitted to the probe laser resonator optical elements, mode hopping could occur.

A second cause of uncertainty would be due to lack of measurement precision when reducing data. Measurement precision is limited by the ability to resolve oscilloscope traces from the data photographs. For this work, the minimum resolvable intensity quotient was approximately 1.04. This, coupled with a gain measurement length of 53 cm, yielded an uncertainty of 0.00074 per cm.

Using the data collection and reduction techniques discussed resulted in shot-to-shot repeatability of approximately 15%. Day-to-day repeatablilty was nearly 25%. It is expected that probe laser mode hopping affects gain magnitudes by less than 25%. See Appendix D.

Much of the day-to-day variation can be attributed to a lack of repeatability in cavity mixture and pressure conditions and to a variation in capacitor charging voltage. The major effect would be to vary initiation strength by varying F_2 concentration and by varying F/F_2 due to initiation. As will be seen in the following sections, varying F_2 concentration can alter the gain behavior significantly.

One possible source of error that was eliminated was saturation of the medium by the probe signal. Saturation was shown to be unimportant by the following experiment. Two sets of gain measurements were made at 102 torr. The probe laser intensity was varied by a factor of ten between the two cases. In both instances, the SSG time histories were in good agreement. Since the SSG time histories were independent of probe intensity, the transitions under investigation should not be saturated. In addition, since the 102 torr case should saturate easier than the 331 torr case, saturation should not be important in either case.

2.4.2 Results of Small Signal Gain Studies for the Mixture $He:O_2:F_2:H_2 = 20.8:1.0:4.6:1.2$

For this case, gain was measured at 102 torr only. There are several points of interest.

First, gain initiation time increases with increasing rotational level. In addition, time to peak gain and gain termination time also increase with increasing rotational level. Gain duration increases with increasing rotational level while peak gain magnitude decreases with increasing rotational level.

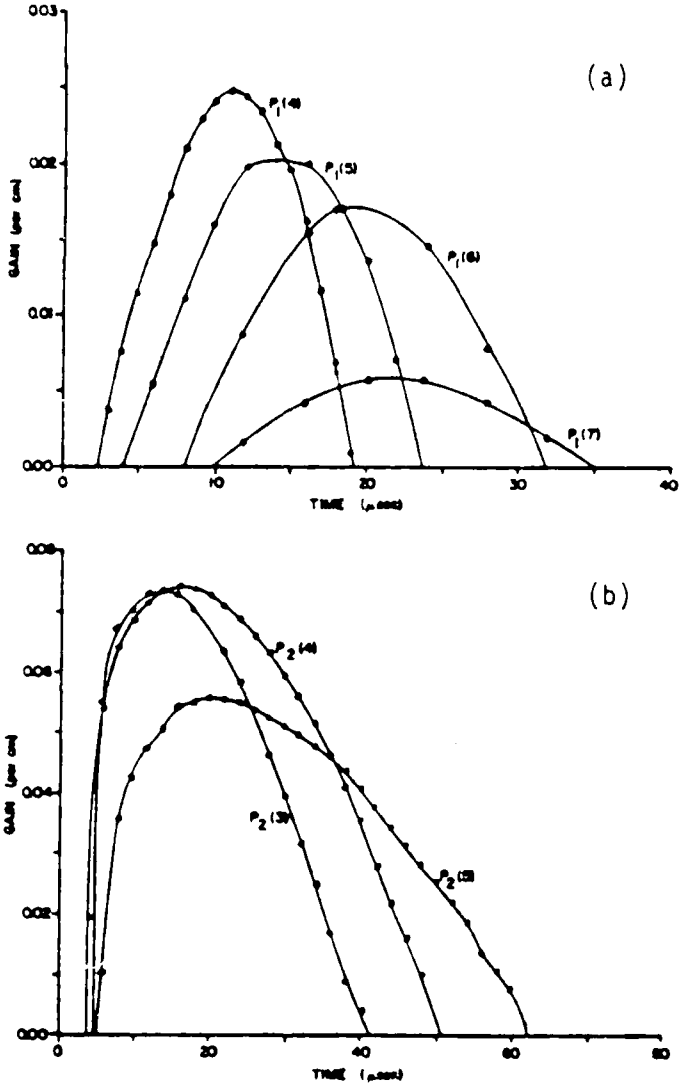

Figure 2.22 Small signal gain time history: $He:O_2:F_2:H_2$ = 20.8:1.0:4.6:1.2,
(a) v=1-0 band, 102 torr
(b) v=2-1 band, 102 torr

Prereaction of the initial cavity mixture is observed. Evidence is seen in the initial gains for the v = 1-0 band being negative at time zero. This implies more population in v = 0 than in v = 1. Since the rate of pumping into v = 0 is believed to be negligible [85], this must be population deposited into levels by pumping and subsequently relaxing to v = 0. This must be occuring before initiation and hence, is prereaction.

Analysis of the trends observed implies strong rotational relaxation of the nascent pumping distribution. This is evident from the behavior of the v = 1-0 band transitions. This sequential transition history is probably caused by a near Boltzmann distribution of rotational levels in a system whose temperature is monotonically increasing. This behavior is analogous to the rigid sequencing of transitions in a given band for rotational equilibrium based computer simulations [70]. This trend is not as pronounced for the v = 2-1 band.

Conclusions drawn from this section are: Prereaction exists, even with the addition of large amounts of O_2 as an inhibitor. The R-R,T mechanism is important for both levels, possibly rapid enough to make nonlasing mixtures appear rotationally equilibrated in the v = 1-0 band.

2.4.3 Results of Small Signal Gain Studies for the Mixture $He:O_2:F_2:H_2$ = 22.0:1.0:2.7:1.0

For this case, gain was measured at pressures of 102 torr and 331 torr.

For the 102 torr case, there exists a general increase

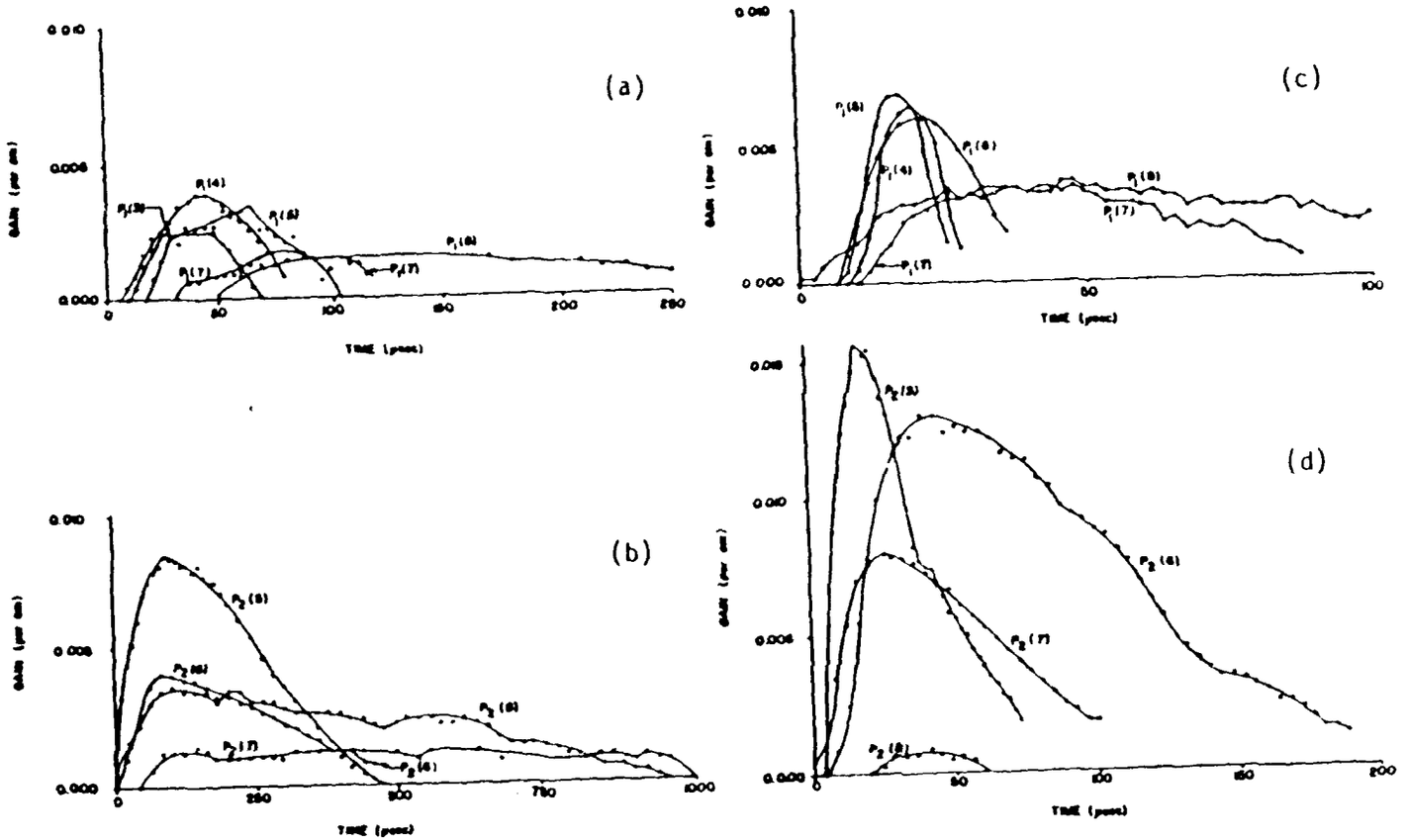

Figure 2.23 Small signal gain time history: $He:O_2:F_2:H_2$ = 22.0:1.0:2.7:1.0, (a) v=1-0 band, 102 torr, (b) v=2-1 band, 102 torr, (c) v=1-0 band, 331 torr, (d) v=2-1 band, 331 torr

in gain initiation time with increasing rotational level. This is not observed for the 331 torr case. There is an increase in peak gain time with increasing rotational level and an increase in gain termination time with an increase in rotational level for the 102 torr pressure case. In addition, gain duration increases with increasing rotational level for the 102 torr case, but not for the 331 torr case.

Gain on the v = 1-0 band is negative at time zero for both cases. As before, this implies initial absorption and hence prereaction of the H_2, F_2, He, O_2 mixture. The technique used in this work to measure small signal gain is sensitive enough to detect HF concentrations above 0.5 mtorr. See Appendix B for details. Measurements of prereaction show a concentration of 1.5 mtorr of HF per 0.5 torr of F_2 initially in the cavity. This is approximately 0.016 molar percent HF in the F_2 supply and is consistent with the F_2 supply batch analysis presented in Section 2.2.1. Prereaction is more important at 331 torr than at 102 torr.

Analysis of the trends for this case show strong rotational nonequilibrium effects. Since it was the observed regular shifting of gain initiation, peak and termination times that was given as evidence of rotational thermalization, and hence, strong rotational relaxation, their absence implies a less important rotational relaxation mechanism for this case.

AD-A141 889 COMPUTER MODELING OF PULSED CHEMICAL LASERS(U) MICHIGAN 1/3
STATE UNIV EAST LANSING DIV OF ENGINEERING RESEARCH
R L KERBER 31 DEC 83 MSU-ENGR-84-004 AFOSR-TR-84-0424
UNCLASSIFIED AFOSR-80-0003 F/G 20/5 NL

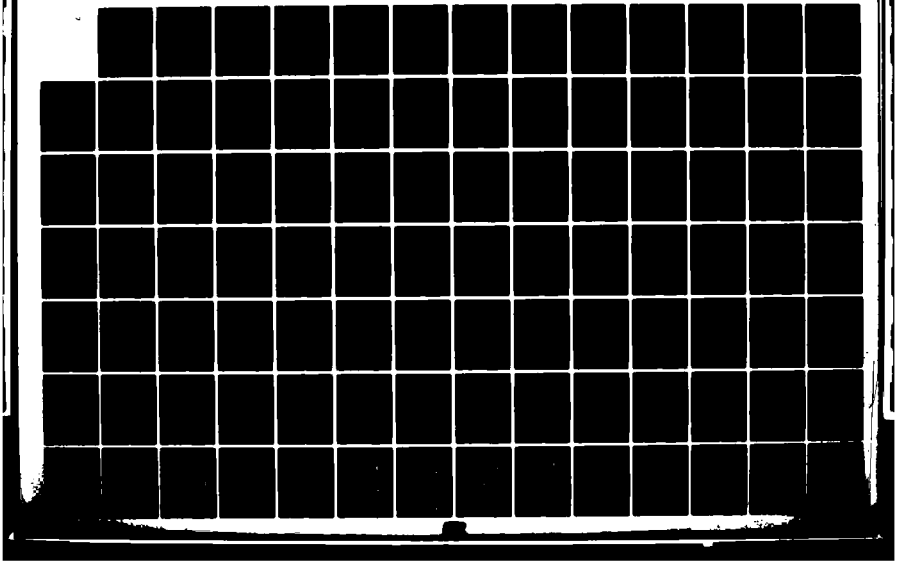

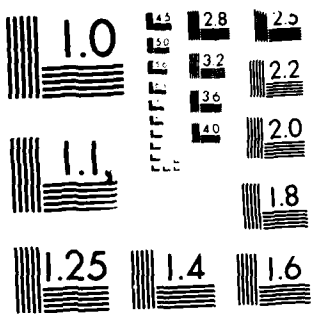

For this case, it can be concluded that prereaction still exists and that the R-R,T mechanism is less important than for this pressure at the mixture $He:O_2:F_2:H_2$ = 20.8:1.0:4.6:1.2.

2.4.4 Discussion

The effects of increasing the percentage of F_2 in the mixture and the effect of increasing mixture pressure can be determined by comparing the results of the three cases presented. This will be done below. The two 102 torr cases will be presented first to determine the effects of an increase in the percentage of mixture F_2. The two cases for $He:O_2:F_2:H_2$ = 22.0:1.0:2.7:1.0 will be compared next to determine the impact of increasing pressure.

Upon comparing the gains of the two 102 torr cases, several points arise:

(1) Increasing the percentage of F_2 in the mixture increases the peak gain. As the percentage of F_2 climbs from 10.1% to 16.7% the peak gain rises by about a factor of 7. Thus, in this range, peak gain appears to be very sensitive to the percentage of F_2 in the mixture. Note that this is not due to a concurrent increase in F/F_2 ratio with the increase in mixture F_2 percentage. As shown in Appendix A.2, F/F_2 ratio is independent of initial F_2 concentration for the conditions of this work.

(2) Increasing the percentage of F_2 in the mixture decreases gain duration and decreases the time

to peak gain and the gain initiation time. Gain duration is quite sensitive to the percentage of F_2 in the mixture in this range. Increasing the percentage of F_2 from 10.1% to 16.7% decreases the pulse duration by a factor of 7 for the v = 1-0 band and by a factor of 15 for the v = 2-1 band. Both of these observations can be attributed to the increased rate of chemical pumping which is due to the increased F_2 concentration. This effect has been documented by many authors (cf. Reference 70). An increase in F_2 concentration causes an increase in fluorine atom production rate, as in Equation (1.4). The increase in F production rate causes a subsequent increase in the rates of Equation (1.2), and hence, Equation (1.3). This accelerates the rate of production of HF, speeds the formation of and increases the magnitude of the population inversions required for lasing, and hence, decreases the gain initiation time, increases the peak gain, and decreases the gain duration. The latter occurs because the fuel and oxidizer are consumed at a faster rate.

(3) Perhaps the most interesting observation is the effect of increasing the percentage of F_2 in the mixture on the shapes of the individual gain pulses. For the case using the lower concentra-

tion of initial mixture F_2 (10.1%), the individual pulse shapes appear erratic. Upon increasing the initial mixture concentration of F_2 to 16.7%, the pulse shapes become more regular, approaching a common, somewhat parabolic shape.

The observed patterns for increasing peak gain, decreasing gain duration, decreasing gain initiation time and decreasing time to peak gain with increasing rotational level are more evident as the percentage of F_2 in the mixture increases.

It is possible that this phenomenon is due to the larger temperature rise for the 16.7% mixture F_2. The larger percentage of mixture F_2 would increase the chemical pumping, as mentioned above, which would increase the enthalpy production, hence increasing the temperature.

Directly related to the temperature rise is a shift in the relative importance of the various relaxation mechanisms. Careful inspection of the rate coefficients for the V-R,T and R-R,T channels shows a decrease in the HF V-R,T self-relaxation rate with a temperature increase up to 1040 K and an increase in the HF R-R,T total relaxation rate with a temperature increase up to 1370 K. These temperatures are considerably higher than results of model calculations at these conditions. The model predicts final pulse temperatures ranging from 360° K to 400° K.

To a good approximation, the HF V-R,T self-relaxation rate is equivalent to the V-R,T total relaxation rate. This is due to: (1) The rate constants for H, F, and HF V-R,T deactivation of HF all being of the same order of magnitude and significantly higher than the rate coefficients due to F_2, H_2 and chaperone gases [85]. (2) Prereaction

causing the concentration of HF to be consistently two orders of magnitude higher than either the H or F concentrations. Thus, the HF self-relaxation rate for V-R,T should dominate the total V-R,T rate and be a good approximation to the total rate for purposes of comparison.

It is clear from these arguments that the relaxation contribution of R-R,T is increasing relative to the contribution due to V-R,T. This is consistent with the increase in the strength of trends in gain initiation, peak and termination times with an increase in F_2 concentration. This increase in R-R,T contribution to relaxation leads to the nearly thermalized distribution which leads in turn to the rigid J-shifting behavior of the gain.

Since R-R,T relaxation decreases with J, this leads to an increased gain duration with an increase in rotational level. It is assumed that R-R,T relaxation scales as exp-(ΔE/RT) with ΔE being the rotational level energy gap. The value of ΔE increases with increasing rotational level decreasing the relaxation rate. This decreases the total relaxation rate with increasing rotational level and leads to an increase in gain duration.

Upon comparing SSG for the two cases with composition $He:O_2:F_2:H_2$ = 22.0:1.0:2.7:1.0, the following arise:

(1) Gain duration on each transition decreases with an increase in mixture pressure.

(2) Peak gain on each transition increases with an increase in mixture pressure.

These observations are consistent with our understanding. The increase in pressure leads to increases in the pumping rate and the rates of relaxation. These increased rates cause a quicker consumption of fuel

and oxidizer and also a sharper termination rate. The combination of the two reduces gain duration. Since all dominant chemical and relaxation kinetic reactions are binary, this is simply binary scaling. This decrease in gain duration is probably due to binary scaling.

The peak gain increase with pressure is probably another manifestation of binary scaling: As pressure increases, the rate of chemical pumping increases as the pressure squared. This would cause formation of larger population inversions due to an increase in total population (even if population ratios remain constant). These larger inversions would lead to larger gains.

2.5 Results of Total Pulse Energy Studies

The experimental configuration utilized for the total pulse energy (TPE) measurements is described in Section 2.2.2 and displayed in Figure 2.11. Total pulse energy measurements were made only for the 331 torr case with mixture composition $He:O_2:F_2:H_2$ = 20.8:1.0:4.6:1.2. For these conditions, 175 mJ of laser energy was measured. This can be converted to an energy density by dividing by the resonator mode volume and by the mixture pressure in atmospheres. The resonator mode volume can be approximated as the volume of a truncated right circular cone whose radius is equal to the distance at which the beam intensity is 1% of its centerline value. This is a radius equivalent to five times the intensity 1/e point radius. The latter can be determined using formulae found in Gross and Bott [1]. For the case considered here, flat output coupler and 5 m radius of curvature mirror with an active medium length of 53 cm, the mode volume is 75 cm^3. This gives a value of 5.4 J/l-atm as the measured energy density.

The value reported here lies between the reported values of 80 J/l-atm of Chen, et al [41] and 2.9 J/l atm of Hess [11]. This is to be expected as energy density increases with the fraction of mixture H_2 and F_2. Hess [11] reports results for a very dilute mixture of $He:F_2:H_2$ = 40:1:1 while Chen, et al [41] show results for a mixture of $He:F_2:H_2$ = 8:1:1. The mixture used here lies between the two, and closer to that of Hess [11]: $(He + O_2):F_2:H_2$ = 18.2:3.7:1.0. This is as expected.

CHAPTER 3

COMPUTER SIMULATION OF AN HF LASER AND COMPARISION WITH EXPERIMENT

3.1. Introduction

The computer model used to simulate the HF laser is described in detail in References 23 and 68. A brief description is given in Appendix A. This model will be referred to as the VR model.

The VR model was modified initially from that of References 23 and 68 by including wavelength dependence of the output mirror reflectivity and by modifying the flash photolysis temporal profile. The wavelength dependence of the output mirror reflectivity caused a wavelength dependent variation of the threshold gain. The flash photolysis temporal profile was changed from a sinusoidal distribution to one resembling the measured flashlamp intensity time history. See Figure 2.16 and Appendix A, Figure A.1, for further details.

In addition to the modifications stated in the preceding paragraph, an update of the model kinetic rate package was performed. The most significant changes from that of Reference 23 were: (1) Removal of the multiquanta V-R,T energy transfer channels for HF self-deactivation. This was recommended by the work of Jursich and Crim [24] and Foster and Crim [25]. The remaining single quantum V-R,T energy transfer rates for HF self-deactivation were determined by using the HF V-V self-relaxation rates of Wilkins [96] and the total HF V-V,R,T self-relaxation rate of

Foster and Crim [25]. This reflects previously accepted kinetics where V-V deactivation was asssumed to be a separate mechanism, independent of V-V,R,T. In addition to this, (2) revised hot and cold pumping rates were used reflecting the work of Heidner, et al [26] and Wurzberg and Houston [27]. Some additional minor changes were made including: (3) slightly different rates for recombination of F and H atoms and, (4) new rates for V-V transfer between H_2 and HF [75]. The remainder of the rate coefficients are those of Cohen [95], excluding the endothermic cold pumping back reactions which are those of Bartoszek, et al [97]. A table of the rate coefficients used is given in Appendix C, Table C.1. This is the basic rate package and excursions were made from it.

Model runs were attempted using the VR model modified as stated above. It was discovered that in order for a run to integrate to completion, an inordinately small step size had to be chosen. This step size would have caused excessive CPU time usage had the case been run to completion. A modification was performed in an attempt to solve this problem.

The most likely cause of the stepsize problem was "stiffness" in the system of differential equations, due in this case to the choice of input conditions necessary to simulate the experiments [98]. Moreover, the model appeared to be spending excessive time calling and using the derivative computation subroutines. For this reason, an approximation was inserted to allow the derivative computation subroutines to be called only 10% as often. It was hoped that this would speed up execution, reducing the amount of CPU time required for a complete run. The result was that the model refused to integrate.

At this point, a simplified version of the VR model, denoted the VT model, was run in an attempt to simulate the experiments. The VT model is similar to the VR model except it neglects the V-R portion of the V-R,T energy transfer mechanism approximating it as a completely V-T mechanism. The V-T model also approximates all rotational relaxation as R-T relaxation, instead of R-R,T [99]. The rates used in the VT model are also given in Appendix C, Table C.2.

Two final modifications were implemented on the VR model. First, the subroutine computing the population derivatives due to V-R,T energy transfer was rewritten to take advantage of the removal of the multiquanta V-R,T mechanism. This had no noticeable effect on the required CPU time. Second, the number of rotational levels considered per vibrational band was reduced from 30 to 20. This was justified by the prior removal of the multiquanta V-R,T relaxation mechanism since this mechanism is the only one that populates rotational levels above $J = 20$. The model with no multiquanta V-R,T deactivation and only twenty rotational levels was denoted VR20J. The inclusion of these last two modifications reduced CPU time necessary for a complete run by about a factor of two. Hence, in this study, two separate models were used, denoted as the VT and the VR20J models.

In all computer modeling studies, it is necessary to determine the model input conditions. For this work, that was done in the following manner.

An area of uncertainty in most modeling studies is an uncertainty in the rate of fluorine atom production due to photolysis. Several researchers have undertaken studies to determine the efficiency of various photolysis sources [100] and the importance of various lamp

characteristics in photolyzing molecular fluorine [36]. Various types of sources have been compared in detail by Berry [101]. All have reached the conclusion that it is important to be able to quantify the fluorine atom production rate. Unfortunately, there appears to be no accurate, nonintrusive experimental technique available to determine fluorine atom concentrations. Furthermore, the techniques used to infer fluorine atom production rates, from fluorine molecule disappearance rates, are inaccurate. Thus, there is no viable experimental method to determine this important laser characteristic.

In this work, the fluorine atom production rate due to photolysis was estimated using the VT computer model with the original rate package in the following way. The parameters η_ρ and l_α in Equation (A.26) were varied, systematically changing the rate of fluorine atom production. Values of η_ρ and l_α were chosen which provided best fit agreement between model predictions of SSG and TRS and those recorded experimentally. This method is in contrast to other workers who have employed a variety of techniques to measure fluorine atom production rates.

Perhaps the most common experimental method is actinometric measurements on F_2. Greiner [102] has used thermal actinometry and Suchard and Sutton [103] have used laser actinometry to attempt to measure the rate of disappearance of F_2. These techniques suffer in accuracy because of the small amount of F produced, less than 0.5%. One is thus attempting to determine a small number by differencing two large numbers, where errors in the large numbers are comparable to the result desired. The laser actinometry technqiue also suffers because the F_2 absorption coefficient is strongly temperature dependent. Under normal laser

conditions, this temperature dependence will have a stronger effect on the absorption signal than the disappearance of 0.5% of F_2 [104].

Other workers have attempted to use multidimensional radiative transfer computer codes [76, 100] to estimate the fluorine atom production rate. Adjustable parameters in these codes are based on experimental measurements similar to those of [103] and hence experience the same problems.

It is because of the uncertainties and ir ent errors in the above methods that the fluorine atom production rat s estimated in the manner stated herein.

The model required several input parame.. in addition to knowledge of the F/F_2 ratio produced through photolysis. A description of how these were determined is presented below.

The gas inlet composition was determined from measurements of the cavity partial pressures of each of the constituents prior to a run. This gave pressures for He, H_2, F_2 and O_2. The value for SF_6 was determined from a knowledge of the F_2 supply batch analysis, provided by the gas supply company (Matheson), and the cavity initial F_2 pressure. For example, the inlet F_2 pressure for the 36 torr case of composition $He:O_2:F_2:H_2$ = 20.8:1.0:4.6:1.2 was measured to be 6.0 torr. From the batch analysis, presented in Section 2.2.1, the SF_6 concentration is 0.001 molar percent yielding 0.00006 torr SF_6, initially. The initial concentrations of air, CF_4 and CO_2 were determined in the same manner. These constituents were assumed to be inert and were, hence, added to the initial He pressure. This was necessary as the model does not include kinetics for the species CF_4, CO_2 and air. In addition, the

partial pressure of O_2 was also added to the He pressure. Again, as for CF_4, CO_2 and air, there are no kinetics for O_2 in the model so it was accounted for by treating it as an inert species.

The cavity active medium length was determined to be the length of active medium illuminated by the flashlamps. This was the lamp length (56 cm) minus the length blocked by the aluminum brackets securing the quartz windows to the cavity (3 cm). See Figure 2.2. The result was an active medium length of 53 cm.

The mirror spacing was measured to be 121 cm, and the initial mixture temperature was assumed to be 300° K.

The output coupler reflectivity was measured at the AFWL metrology lab. It was nominally 81%. A curve of reflectivity vs wavelength is presented in Figure A.3

The copper mirror reflectivity was stated by the manufacturer to be 99%. This value was multiplied by the measured Brewster window transmission values of 99% each, yielding an effective mirror reflectivity of 95%. The effective reflectivity was used as an input to the model.

The results of the measurements of flashlamp emission properties were used to determine the flash photolysis temporal profile. This procedure is described in detail in Appendix A. The resulting fit to the flashlamp intensity time history was used as a model input.

After having determined the input parameters, the VT model was run for the conditions $He:O_2:F_2:H_2$ = 20.8:1.0:4.6:1.2 at 36 torr, 102 torr, and 331 torr simulating the three TRS cases presented. The results of this set of model runs is presented in Figure 3.1.

The model rate package was then modified by changing the vibrational pumping distribution suggested by Cohen [95] to an updated distribution, also suggested by Cohen [105]. See Table C.2, Appendix C.
The original hot reaction vibrational pumping distribution [95] increased monotonically from v=3 to v=6. Pumping to all other vibrational levels was assumed to be zero. The updated vibrational pumping distribution [105] also increased monotonically form v = 3 to v = 6. In the updated case though, the pumping distribution was assumed to be monotonically decreasing from its peak at v = 6 to v = 8. Pumping was again assumed to be zero for all other levels. Cohen [105] also suggested leaving the total pumping rate summed over all vibrational levels unchanged from Reference 85. The model was again run at 36 torr, 102 torr and 331 torr for the mixture composition $He:O_2:F_2:H_2$ = 20.8:1.0:4.6:1.2. The results of this set of model runs are presented in Figure 3.2 and compared with experiment.

The model rate package was modified one final time. Here, the vibrational deactivation mechanism was changed to reflect the current belief that the total vibrational deactivation rate is a sum of the V-R,T rate and the V-V rate. The V-R,T rate was then determined by subtracting the V-V contribution, reported by Wilkins [96], from the total vibrational deactivation rate of Foster and Crim [25]. This, in effect, reduced the V-R,T rate from $1.1 \times 10^{10}\ e^{1030/RT}\ T^{0.5}$ to $3.3 \times 10^{9}\ e^{1030/RT}\ T^{0.5}$. For this rate package, the model was run only at 102 torr. The results are presented in Figure 3.3

The rate package mentioned directly above was then used with model VR2OJ to simulate the 102 torr case for mixture composition $He:O_2:F_2:H_2$ = 20.8:1.0:4.6:1.2. The results are presented in Figure 3.3

All model results will be discussed in the following two sections.

3.2 Computer Modeling Results of Time Resolved Spectroscopy and Comparison with Experiment

3.2.1 Introduction

The results of the VT model TRS computer simulations using the initial rate package are presented in Figure 3.1 in Section 3.2.2. The results of the VT model TRS computer simulations using the modified vibrational pumping distribution are presented in Figure 3.2 in Section 3.2.3. The results of the VT model TRS computer simulations using the modified vibrational pumping distribution and the modified V-T deactivation rates are presented in Figure 3.3 in Section 3.2.4. The results of the VR2OJ model TRS computer simulations using the modified pumping distribution and the modified vibrational deactivation rates are also presented in Figure 3.3 and are discussed in Section 3.2.5.

All results are plotted identically to those of Sections 2.3.2 and 2.3.3. Experimental results are repeated with the presentation of model results to facilitate comparison. They will be discussed individually below.

3.2.2 Comparison of VT Modeling Results of Time Resolved Spectroscopy with Experiment: Initial Rate Package

A comparison of the model predictions for this composition with experiment (see Figure 3.1) shows good agreement for transitions pumped strongly by the cold pumping reaction, Equation (1.2) and only fair agreement for transitions pumped by the hot pumping reaction,

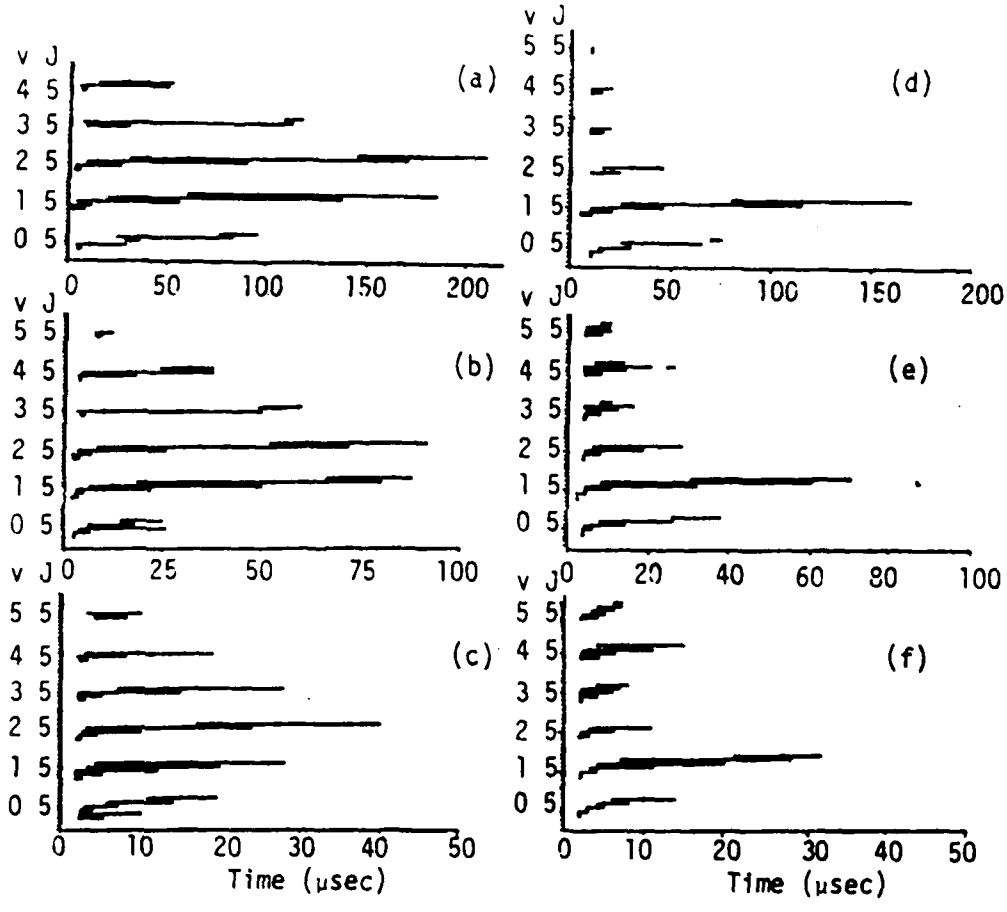

Figure 3.1 Time resolved spectral output: comparison of VT model results and experiment using rate package VT (standard rates)
(a) experimental results, 36 torr
(b) experimental results, 102 torr
(c) experimental results, 331 torr
(d) model results, 36 torr
(e) model results, 102 torr
(f) model results, 331 torr

Equation (1.3).

It is apparent that the model results agree well with the general trends observed experimentally regarding pulse initiation, termination and peak intensity times, peak intensities and pulse durations. Furthermore, agreement between model and experimental magnitudes is generally good for the v = 1-0 band and very good for the v = 2-1 band. For these two bands, the model underpredicts pulse durations, giving intiation times which are late and termination times which are early. The area of least agreement for the v = 1-0 band is in the behavior of $P_1(5)$.

Experimentally, $P_1(5)$ is a short duration transition with weak intensity. It does not obey the pulse initiation time, pulse duration or peak intensity trends. In Section 2.3.2, it was stated that this behavior was due to water vapor absorption of the $P_1(5)$ signal. The model results support this contention.

According to the model, $P_1(5)$ should obey the observed trends for pulse initiation time, pulse duration and peak intensity. That this is not observed experimentally leads to the conclusion that the anamolous $P_1(5)$ behavior is due to some effect other than laser cavity chemistry. This effect is probably due to water vapor absorption and could be investigated by including oxygen kinetics in the model.

As noted in the preceding paragraphs, agreement between the model and experimental results is generally very good for the lower two bands. This is not true for the higher bands. It is interesting to note that the VT model overpredicts the number of lasing transitions observed. Some of these predicted transitions are weak and may well have intensities below the experimental detector sensitivity limit. As a further note, the model agrees with experiment by predicting the

absence of lasing on pure rotational lasing transitions.

It is noteworthy that the entire VT model results for the v = 1-0 band at 102 torr and all bands at 331 torr appear to be shifted upward one rotational level: i.e. the observed behavior of $P_1(4)$ in the model corresponds to the experimental $P_1(3)$, etc. There is no apparent explanation for this behavior.

3.2.3 Comparison of VT Modeling Results for Time Resolved Spectroscopy and Comparison with Experiment: Modified Vibrational Pumping Distribution

A comparison of the model predictions with experiment in Figure 3.2 shows excellent agreement for the transitions in the v = 2-1 and v = 5-4 bands. In general, one observed the same qualitative features for the remaining bands. However, the model does not quantitatively agree with the measured spectra. This is more evident for the v = 3-2, v = 1-0 and v = 6-5 bands.

It is apparent that the model results agree very well with the general trends observed experimentally regarding pulse initiation, termination and peak intensity times and pulse durations. This holds for both hot band and cold band lasing. Furthermore, agreement between model and experimental magnitudes agree very well for all bands except v = 3-2 and v = 6-5 in general. The model accurately predicts initiation and termination times, as well as pulse durations for the v = 2-1, v = 4-3 and v = 5-4 bands. In addition, the model predicts lasing on all the transitions that are observed to lase experimentally

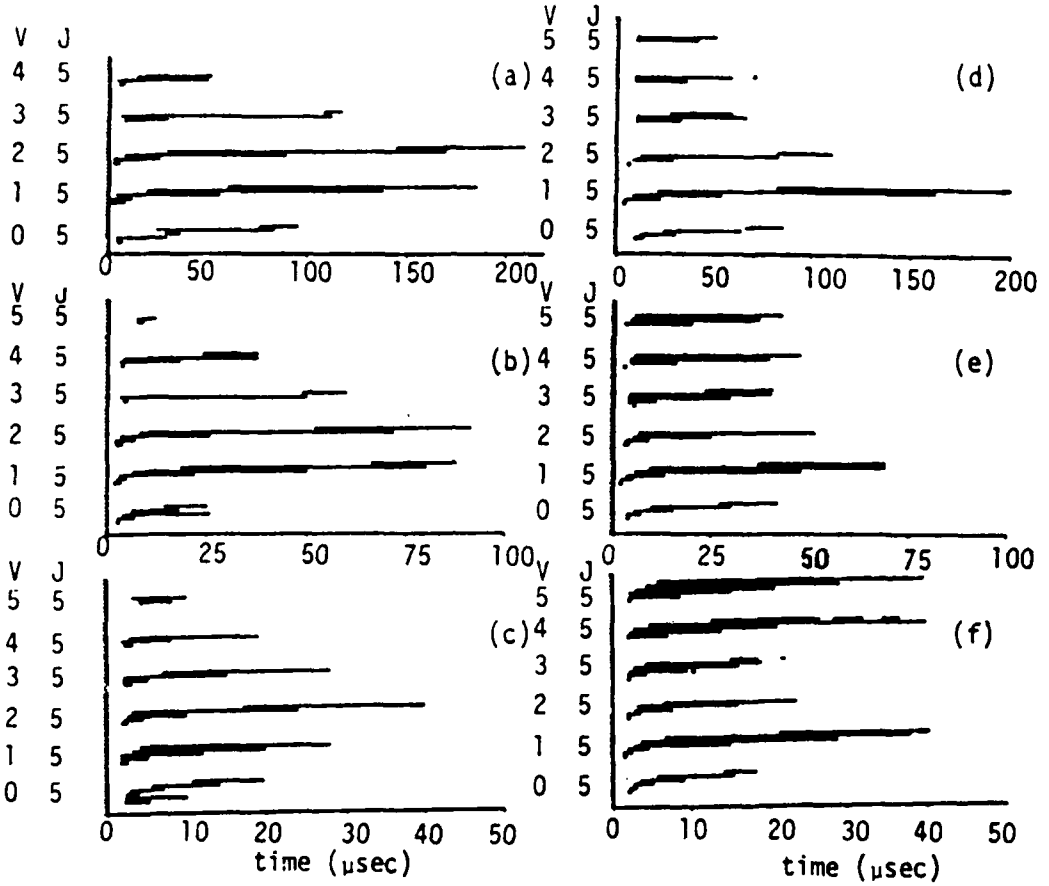

Figure 3.2 Time resolved spectral output: comparison of VT model results and experiment using rate package VT2, $He:O_2:F_2:H_2$ = 20.8:1.0:4.6:1.2
(a) experimental results, 36 torr
(b) experimental results, 102 torr
(c) experimental results, 331 torr
(d) model results, 36 torr
(e) model results, 102 torr
(f) model results, 331 torr

The model does not agree in its prediction of the $P_1(5)$ behavior. Experimentally, $P_1(5)$ is a short duration pulse with weak intensity. The model predicts a much longer, more intense, pulse. This result supports the supposition of water vapor absorption of the $P_1(5)$ signal.

For the 331 torr case, the model overpredicts the number of lasing transitions. This overprediction occurs in every band and generally consists of prediction of one or two transitions at high rotational levels not observed experimentally. In many cases, these transitions are weak, but that is not always the case.

A minor discrepancy between model and experiment at 331 torr is that the model predicts transitions shifted one J level relative to experiment. This observation could be a thermal effect resulting from a small change in P(v,J), i.e. reaction enthalpy or specific heat capacity.

3.2.4 Comparison of VT Modeling Results of Time Resolved Spectroscopy with Experiment: Modified Vibrational Pumping Distribution and Modified V-T Deactivation

Only the 102 torr pressure case was modeled using the modified vibrational pumping distribution and modified V-T deactivation rate package. The results, and comparison with experiment, are presented below.

A comparison of the model predictions for the 102 torr case with experiment (see Figure 3.3) shows good agreement for all the bands. Once again, the model very accurately predicts the observed trends of increasing pulse initiation, peak intensity and termination times, and pulse duration with increasing rotational level. The model also shows

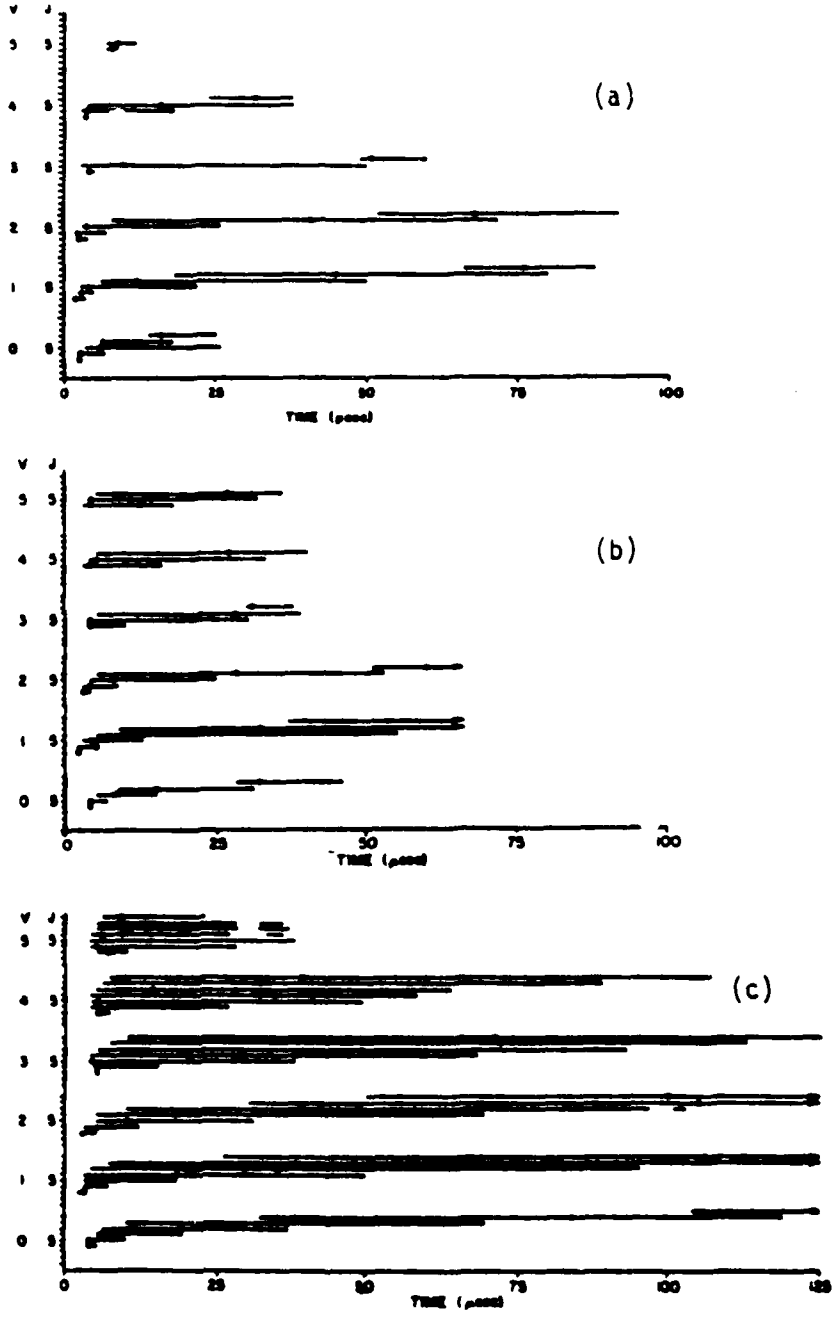

Figure 3.3 Time resolved spectral output: comparison of VR20J and VT model results (with rate package VT3) with experiment, $He:O_2:F_2:H_2$ = 20.8:1.0:4.6:1.2
(a) experimental results, 102 torr
(b) VT model results using rate package VT3, 102 torr
(c) VR20J model results, 102 torr

good agreement when comparing initiation, peak intensity and termination time positions.

The model is in agreement with experiment for the bands v = 2-1, v = 3-2 and v = 5-4. No extra transitions are predicted and predicted durations are consistent with experiment.

Although predictions for the remaining bands do not match as well, overall model predictions reflect experimental TRS results better than all previous attempts.

Again, $P_1(5)$ behavior does not match the experimental results. As before, the model predictions are all shifted up one rotational level.

3.2.5 Comparison of VR20J Modeling Results for Time Resolved Spectroscopy with Experiment

The 102 torr TRS and SSG cases were modeled using the VR20J model discussed in Section 3.1. The kinetic rate package was that of Section 3.2.4 with the additional modification of changing V-T deactivation to V-R,T. As in Section 3.2.4, only the 102 torr TRS and SSG cases with mixture composition $He:O_2:F_2:H_2$ = 20.8:1.0:4.6:1.2 were modeled. The results are presented below.

The predictions of the VR20J model are much poorer than those of the VT model (see Figure 3.3). The VR20J model does not consistently predict all the trends observed experimentally: increasing pulse initiation, termination and peak intensity times and increasing pulse duration, all with increasing rotational level. Also, the VR20J model considerably overpredicts pulse durations, listing termination times which are consistently too long. Finally, the VR20J model

overpredicts the number of lasing transitions. In particular, the model predicts lasing on high rotational transitions (J = 7, 8, 9) not observed experimentally.

3.2.6 Summary of Time Resolved Spectroscopy Modeling Results

A comparison of the 102 torr model results for the different kinetics packages will be presented below. The effects of changes in the V-T rate coefficient and the hot reaction pumping distribution will be discussed.

Upon comparing VT model results for the initial rate package with the rate package containing the modified vibrational pumping distribution (denoted rate package VT2), it is apparent that changing to the VT2 rate package causes a general increase in transition durations. This is particularly so for the bands v = 6-5 through v = 3-2. There also appears to be more lasing energy emitted by "hot band" transitions, and, the pulse energy nearly doubles, increasing by 81%. There is also a general increase in peak intensities with rate package VT2. This is especially true for the hot bands. Finally, the mixture temperature is less for the VT2 rate package than for the standard rates.

Changing the model rate package from VT2 to the rate package containing both the modified vibrational pumping distribution and the modified V-T deactivation rate (denoted rate package VT3) affects results by generally decreasing the duration of hot band lasing transitions while leaving cold band transition durations unaffected. In addition, the hot band peak intensities decrease slightly, the cold band intensities increase slightly, and intensities of the individual transition pulse shapes change very little. For the change from VT2 to VT3, the pulse energy increases by 7%. Finally,

the mixture temperature decreases when rate package VT3 is substituted for rate package VT2.

A comparison of the rate package VT3 results with those of the VR20J model show clear increases in transition durations, the appearance of more lasing transitions and transitions at higher rotational levels for the VR20J results. In addition, the VR20J results show a decreased transition intensity for low rotational transitions and a increased intensity for high J transitions as compared to the VT3 results. The VR20J results also exhibit a pulse energy three times greater than the VT3 results and a final mixture temperature that is lower.

The differences in spectral content, pulse energy and mixture final temperature for the different rate packages can be explained in the following manner.

The change in spectral behavior between the standard rate package and rate package VT2 must be due to the modified vibrational pumping distribution as this was the only change made. This change did not alter the pumping rate into $v = 3$ or $v = 4$ but did increase the pumping rates into $v = 7$ and $v = 8$ at the expense of pumping into $v = 5$ and $v = 6$. This modification of the pumping distribution increases the total rate of vibrational quanta produced by the hot pumping reaction by approximately 10%. This increase in the rate of vibrational quanta produced occurs at the expense of heat liberation during pumping and may contribute to the observed temperature reduction.

The decrease in pumping rates into $v = 5$ and $v = 6$ are probably responsible for the decrease in the number of observed transitions in

the VT2 case. The decrease in pumping rates would lessen the inversions produced, probably causing the missing transitions to fall below threshold. It also appears that the increased rate of pumping into v = 7 and v = 8 and subsequent V-T relaxation into v = 6, 5, and 4 is responsible for the increased pulse lengths observed for the v = 6-5, v = 5-4 and v = 4-3 bands.

A change from rate package VT2 to VT3 resulted in only a reduction of the V-T relaxation rate by a factor of 3.3. This must then be responsible for the change in pulse characteristics.

A decrease in the V-T deactivation rate would explain the observed decrease in mixture temperature as fewer quanta of vibrational energy would be transformed into translational energy with a necessarily smaller rise in mixture temperature. This decrease in V-T relaxation rate would also explain the increase in pulse energy, since with fewer vibrational quanta being converted into translational energy, more quanta would be available for emission, increasing the pulse energy.

The decrease in the V-T rate could also explain the appearance of $P_4(3)$ and $P_5(3)$. As losses go down it becomes easier for transitions to build up a population inversion sufficient to attain threshold and achieve lasing. The V-T decrease does not appear to be able to explain the disappearance of $P_3(7)$.

Finally, the change in V-T deactivation rate could also explain the shorter hot band transition durations observed for the VT3 case. If, as suggested in the discussion of VT2 vs standard rate package results, the hot band transition durations are dependent on pumping into v = 7 and v = 8 and subsequent V-T relaxation as a means of population inversion enhancement, it is likely that a decrease in V-T

deactivation could account for the shorter hot band transition durations observed in the VT3 case. This could occur through a decrease in the rate of transfer of population from v = 7 and v = 8 to v = 6, 5 and 4, lessening the ability of the v = 6-5, v = 5-4 and v = 4-3 bands to attain threshold. This would cause earlier termination times.

The change from rate package VT3 and the VT model to the VR20J model resulted in a change in the relaxation channel structure of the vibrational deactivation mechanism. As discussed in the introduction, this change is essentially from a Boltzmann distribution of product rotational states to a rotational distribution centered about the rotational level possessing rotational energy equal to one half the energy of a vibrational quantum. This change effectively shifts the rotational product manifold upward approximately seven quanta. The consequences of this change have been documented by Kerber, et al. [96]. They observed an increase in individual transition durations, a decrease in individual transition intensities and an increase in the number of transitions attaining threshold. The latter was especially true for high rotational transitions. Their results are consistent with what is observed here.

In addition, the results presented here show a factor of three increase in pulse energy for the VR20J results vs the VT3 rate package results. This must be due to the change from V-T to V-R,T deactivation, and can probably be explained as follows. Since the V-R,T mechanism transfers approximately 50% of a quantum of vibrational energy to rotation, while the V-T mechanism transfers roughly 5% of a quantum of vibrational energy to rotation, a "pool" of rotational energy can build up for the V-R,T case. Some of this energy can be converted back

to vibrational energy through reverse V-R,T (R-V) energy transfer. These R-V processes are potentially much faster than reverse V-T processes, and combined with the available pool of rotational energy produced by V-R,T relaxation, could explain the increased pulse energy.

It is important to note that Kerber, et al. [23] show a strong coupling between the effectiveness of V-R,T energy transfer as a vibrational deactivator and the relative rates of V-R,T and R-R,T relaxation. They state that the effective vibrational relaxation rate will decrease if R-R,T relaxation is much slower than V-R,T. This is because population builds up in the high rotational levels, rapidly reaching a state of equilibrium with the initial vibrational state.

It was stated in Section 3.2.5 that there appears to be a correlation between either mixture diluent concentration or mixture O_2 concentration and observed trends in the TRS results. In particular, the results of Greiner [19], Borisov, et al. [43] and Parker and Stevens [52] all exhibit increasing pulse initiation, termination and peak intensity times with J. These studies all utilized O_2 for prereaction control and had a He diluent concentration less than 83%. In contrast, the data of Suchard and coworkers [17, 42] show no noticable patterns in the TRS behavior. In their work, there is no O_2 and the diluent concentration is quite high: greater than 96% in both cases. It would appear that either high diluent concentration or lack of O_2 caused the erratic behavior observed in References 17 and 42. Inclusion of O_2 kinetics in the VR2OJ model may assist in explaining this observation.

As a final explanation, the observations of Suchard and coworkers [17, 42] may be anomalies. No other studies have reported the behavior observed therein.

In Section 2.3.5 it was suggested that the TRS trends observed were those of well thermalized rotational levels. It was also suggested that these well thermalized rotational levels were due to the rotational relaxation rate being much faster than chemical pumping, vibrational transfer and vibrational relaxation, but slower than lasing. Evidence for these statements is presented in Figure 3.4.

Figure 3.4 displays derivative contributions to the rate of change of the population difference associated with $P_2(5)$. The vertical bars represent mechanisms producing and reducing the population difference associated with $P_2(5)$ lasing. Two cases are compared: Model VR20J and the V-T model using rate package VT3. In both instances, it is clear that rotational relaxation (R-R or R-T) is very fast once lasing has initiated. At 8 μsec and 20 μsec, R-R,T is faster than all other deactivation processes with the exception of lasing, for the VR20J and VT model results. This also holds at 50 μsec for the V-T model results. In addition, R-R,T is faster than pumping at 8, 20 and 50 μsec for the V-T model and at 20 μsec for the VR20J model. Finally, in no instance is R-R,T faster than stimulated emission while lasing is occurring (8 and 20 μsec). These plots show the influence of rotational relaxation mechanisms on lasing.

The conclusions to be drawn from comparing the various sets of model results are: (1) The VT model seems to more accurately predict the experimental spectral behavior. The VT2 and VT3 rate packages seem to produce results in closest agreement to the TRS results. (2) The VT model with either rate package VT2 or VT3 predicts the experimentally observed trends of initiation, termination and peak intensity times.

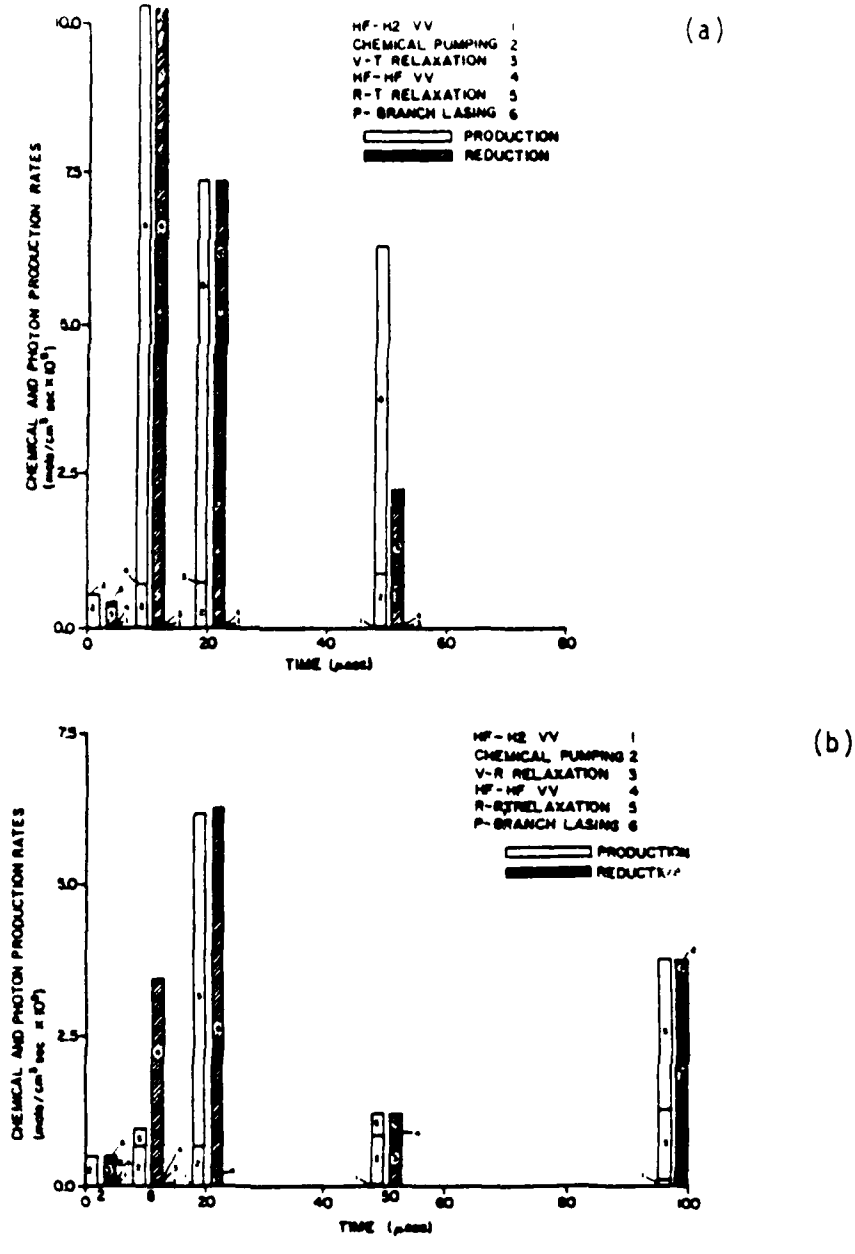

Figure 3.4 Individual derivative contributions for mechanisms reducing population inversion on $P_2(5)$, $He:O_2:F_2:H_2=20.8:1.0:4.6:1.2$
(a) VT model results for rate package VT3
(b) VR20J model results

The VR20J predictions are not as consistently accurate as the VT predictions. (3) It would be desirable to include O_2 kinetics in the model. The inclusion of O_2 kinetics may assist in the interpretation of the results of Suchard and coworkers [17, 42].

Although the results presented here show best agreement between experiment and model for the VT2 and VT3 rate packages, this is counter to presently accepted kinetic thinking. The importance of V-R,T energy transfer has been shown by the results of Pimentel and coworkers [62, 80] and Wilkins [96]. However, refer to Section 3.3.4 for a discussion of how the choice of initiation parameters can affect relative model results.

3.3 Computer Modeling Results for Small Signal Gain and Comparison with Experiment

3.3.1 Introduction

The results of the VT model SSG computer simulations are presented in Figure 3.5 in Section 3.3.2. The VT model computer simulation results using the initial rate package (Figure 3.5) are presented first, the computer simulation results using the modified vibrational pumping distribution (Figure 3.6), are presented next, and the computer simulation results using the modified vibrational pumping distribution and modified V-T deavtivation (Figure 3.7) are presented last.

The results of the VR20J model SSG computer simulations are presented in Figure 3.7, in Section 3.3.2. There is only one kinetic rate package used for the VR20J results, that being the VR20J equivalent of the modified vibrational pumping distribution and modified V-T deactivation rate package.

3.3.2 Comparison of VT Model Small Signal Gain Results with Experiment

The results of the model small signal gain simulations are presented in Figures 3.5, 3.6, and 3.7. The results of the computer simulation using the initial rate package, Figure 3.5, are presented first.

A comparison of the model results with the experimental results reveals the following: (1) The agreement between model and experiment for the trends of gain initiation time, peak gain time, gain termination time and gain duration is excellent. For all three pressure cases, the model accurately predicts the experimental behavior. (2) The model predicts the experimentally observed shift of peak gain with J.

A comparison of the standard rate package results with experiment shows that for the v = 1-0 band, the experimental gain duration is within 21% of the model gain duration and the experimental peak gain is within 37% of the model peak gain for all lines. Comparison of the v = 2-1 model results with experiment shows even better correspondence. The experimental gain duration is within 19% of the model gain duration and the experimental peak gain is within 16% of the model peak gain for all transitions.

A comparison of the VT2 rate package predictions and experimental results shows that for the v = 1-0 band, the experimental gain duration is within 34% of the model gain duration and the experimental peak gain is within 38% of the model peak gain for all lines. Comparison of the v = 2-1 band model and experimental results show even better correspondence. The experimental gain duration is within 29% of the model gain duration and the experimental peak gain is within 37% of the model peak gain for all transitions.

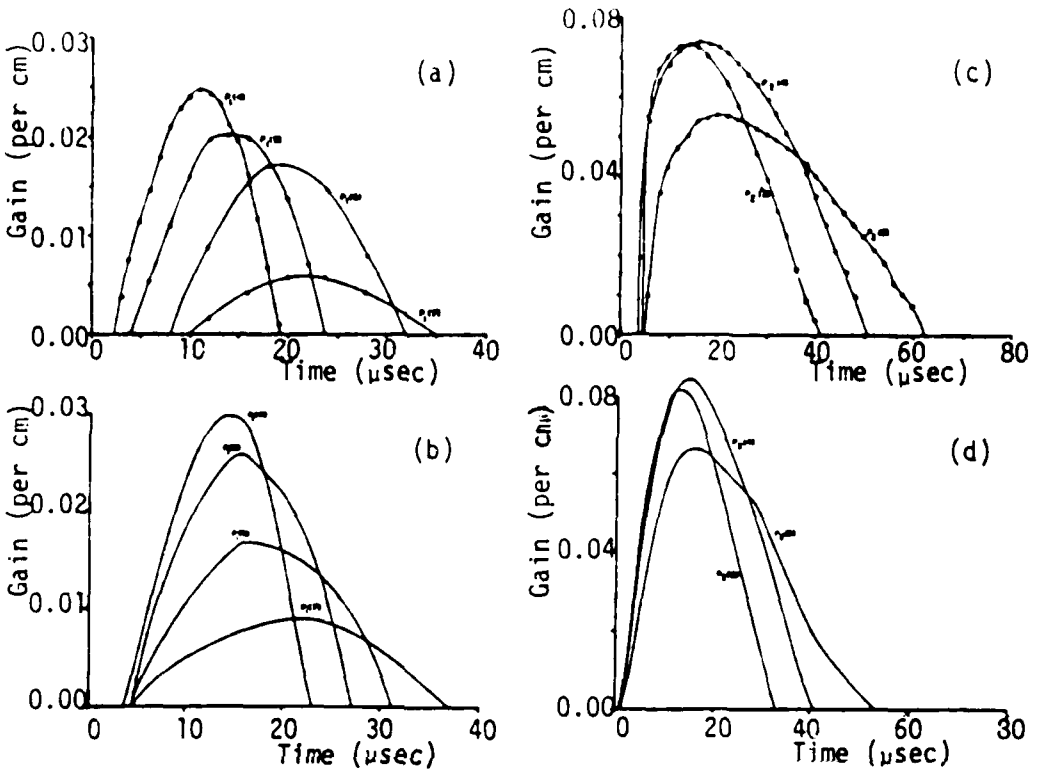

Figure 3.5 Small signal gain time histories: comparison of experimental and VT model results using rate package VT (standard rates), $He:O_2:F_2:H_2$= 20.8:1.0:4.6:1.2
(a) experimental results, v = 1-0 band
(b) model results, v = 1-0 band
(c) experimental results, v = 2-1 band
(d) model results, v = 2-1 band

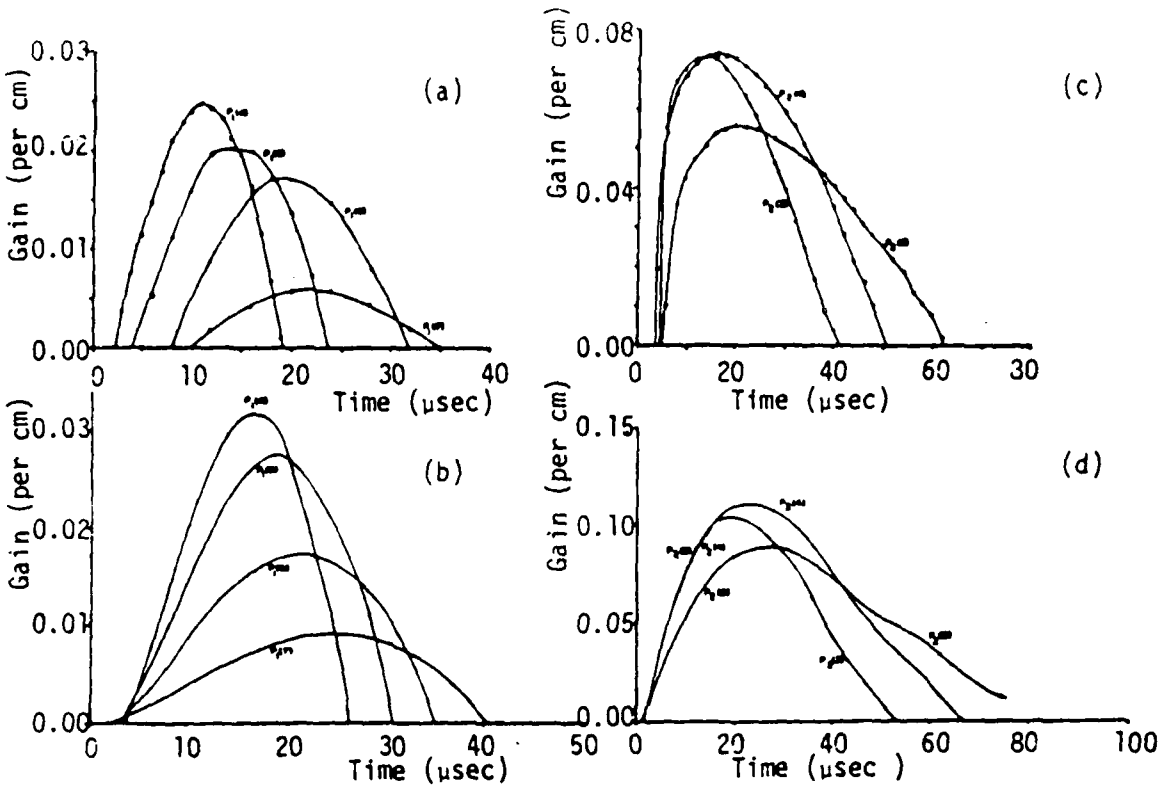

Figure 3.6 Small signal gain time histories: comparison of experimental and VT model results using rate package VT2, $He:O_2:F_2:H_2$=20.8:1.0:4.6:1.2
(a) experimental results, v = 1-0 band
(b) model results, v = 1-0 band
(c) experimental results, v = 2-1 band
(d) model results, v = 2-1 band

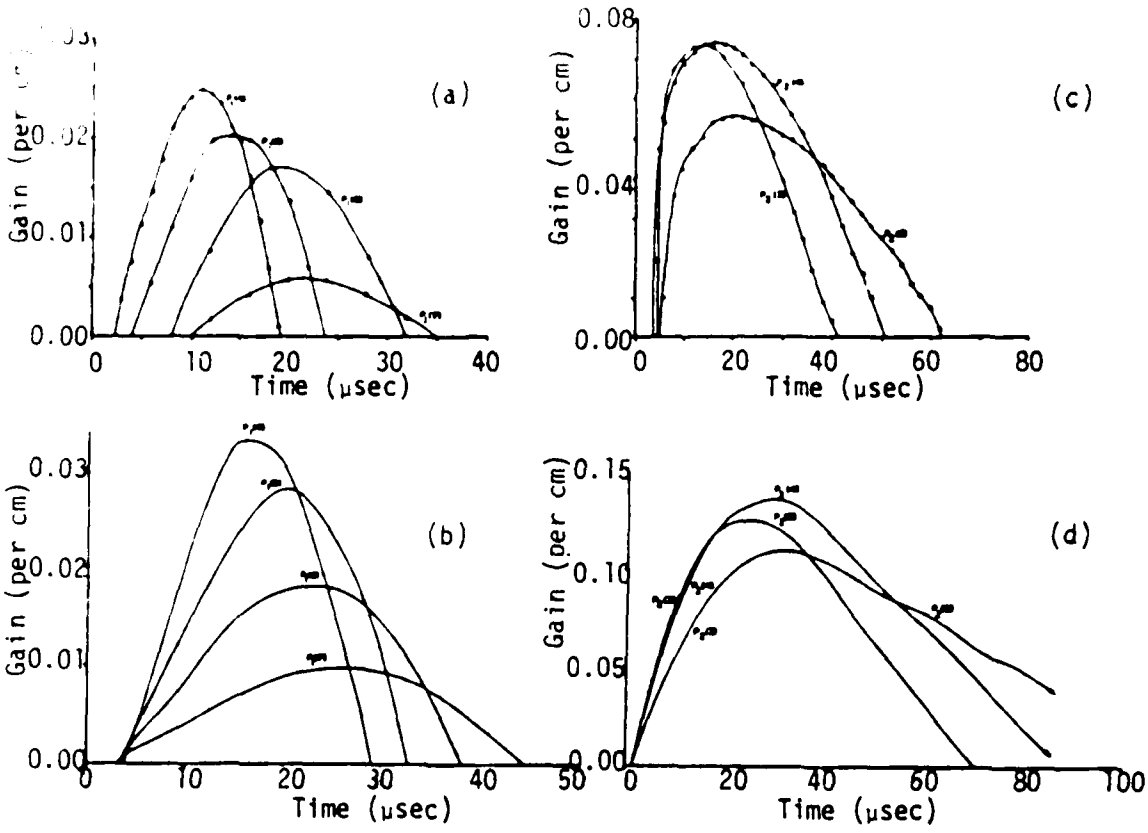

Figure 3.7 Small signal gain time histories: comparison of experimental and VT model results using rate package VT3, $He:O_2:F_2:H_2$=20.8:1.0:4.6:1.2
(a) experimental results, v = 1-0 band
(b) model results, v = 1-0 band
(c) experimental results, v = 2-1 band
(d) model results, v = 2-1 band

A comparison of the VT3 model predictions and experimental results show that for the v = 1-0 band, the experimental gain duration is within 34% of the model gain duration and the experimental peak gain is within 41% of the VT model gain for all lines. The v = 2-1 model and experimental results do not compare as well as the v = 1-0. The experimental peak gain is within 47% of the model gain duration and the experimental peak gain is within 49% of the model peak gain for all transitions.

3.3.3 Comparison of VR2OJ Model Small Signal Gain Results with Experiment

The results of the VR2OJ model small signal gain simulations are presented in Figure 3.8 The VR2OJ model was run with only one kinetic rate package. This rate package was the VR equivalent of the modified vibrational pumping distribution and modified VT deactivation rate package.

A comparison of the model and experimental results reveals the following: (1) The agreement between model and experiment for the shift of initiation time, peak gain time, gain termination time and gain duration with J is excellent. (2) The agreement between model and experiment for the peak gain magnitude shift with J is also excellent.

A comparison of the predicted and experimental magnitudes involved shows that the VR2OJ model considerably overpredicts peak gains for both bands. The model peak gain is consistently a factor of three higher than that observed experimentally for the v = 2-1 band. For the v = 1-0 band, the model predicts peak gains between two and three times that observed experimentally.

The VR2OJ model also overpredicts gain durations. The v = 2-1 band gain durations are consistently overpredicted by almost a factor of two. The v = 1-0 band gain durations are overpredicted by factors greater than two.

As previously stated, there are few reports of HF small signal gain measurements. No one has reported time histories of HF small signal gain and only Deutsch [63] and Jones [64] report gain measurements on individual transitions in HF. Unfortunately, these studies are for

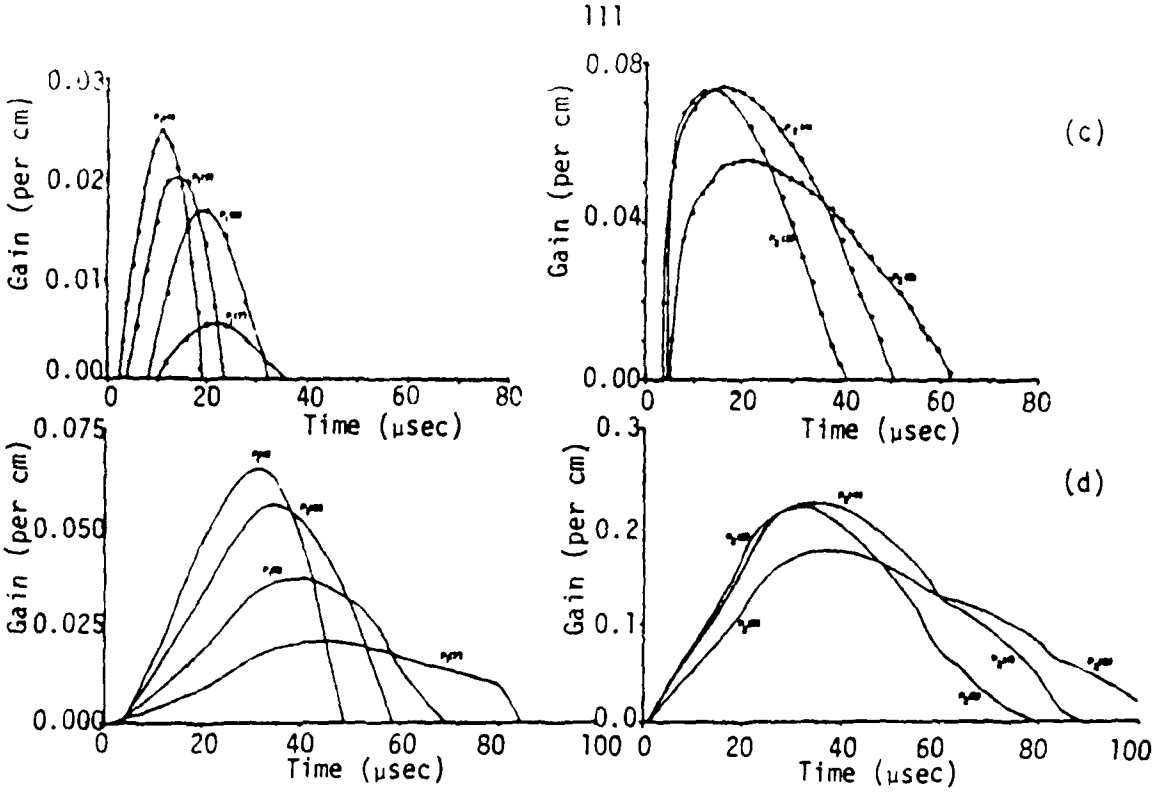

Figure 3.8 Small signal gain time histories: comparison of experimental and VR20J results
(a) experimental results, v = 1-0 band
(b) model results, v = 1-0 band
(c) experimental results, v = 2-1 band
(d) model results, v = 2-1 band

mixtures of SF_6 and H_2 initiated by electric discharge. The chemistry of SF_6 + H_2 systems is markedly different than that of F_2 + H_2 systems as the latter operates on a chain reaction mechanism while the former does not. This difference has been shown to substantially effect pulse behavior [1]. Consequently, comparison with the present work would be difficult.

To further complicate matters, Jones [64] reports results for a total pressure of only 24 torr and with a mixture composition of $He:SF_6:H_2$ = 10:1:1. This pressure is over four times smaller than the pressure reported here, and the H_2 partial pressure is double that reported here. Kerber, et al [70] have shown that pulse duration and pulse energy are both very sensitive to H_2 partial pressure for H_2 lean mixtures. This mismatch in total mixture pressure and in H_2 partial pressure further hinder comparison with the current results.

Deutsch [63], presents results for a 140.5 torr mixture of composition $He:SF_6:H_2$ = 30.9:8.3:1.0. This mixture has an H_2 partial pressure that is approximately half that employed in this study. As mentioned above, this inhibits meaningful comparison of results.

Finally, neither Deutsch [63] or Jones [64] reports a value for their F atom production rates. As initiation strength is known to strongly affect pulse duration [70], lack of this informtion is an added difficulty when attempting to compare results.

One consistency between results presented here and those of Deutsch [63] is in position of peak gain. Deutsch [63] reports peak gains on all transitions observed ($P_2(2)$, $P_2(3)$, $P_2(4)$, $P_2(5)$, $P_2(6)$) to occur at approximately 1.5 μsec. This is much shorter than the approximate observations of 20 μsec reported here. This is consistent for two reasons.

First, the partial pressure reported by Deutsch [63] is approximately half that reported here. Since both systems are H_2-lean, pulse duration should scale proportional to H_2 -partial pressure [70]. Thus, Deutsch should see shorter durations and earlier occurring peaks.

Second, Deutsch uses a non-chain reaction system with an initiation pulse length of 0.6 μsec. In this work, a chain reaction system is used with an initiation pulse length of 4.4 μsec. This two effects would, generally, shorten the pulse duration, and hence, the position of peak gain.

One area where results reported here compare extremely well with those of Deutsch [63] is in relative peak gains. Deutsch [63] reports gains of 0.177, 0.174 and 0.134 per cm for $P_2(3)$, $P_2(4)$ and $P_2(5)$ respectively. The ratios are 1.00:0.98:0.76. We find ratios of 0.98:1.00:0.76 for the mixture $He:O_2:F_2:H_2$ = 20.8:1.0:4.6:1.2. Considering the possible differences in initiation and differences in H_2 partial pressure and in chemistry, this agreement is most likely coincidental.

3.3.4 Summary of Small Signal Gain Modeling Results

A comparison of the model results for the different kinetics packages used will be presented below. The effects of changes in rate coefficients will be discussed.

Upon comparing VT model results for the initial rate package with results for the rate package with the modified vibrational pumping distribution, denoted rate package VT2, it is apparent that changing to the VT2 rate package increases gain duration, increases peak gain time and gives higher peak gain magnitudes. The increase in gain

duration is especially pronounced for the v = 2-1 band, while the increase in peak gain is seen to be strongest for the lower rotational level transitions in the v = 1-0 band.

Changing the model rate package from rate package VT2 to the rate package with both the modified vibrational pumping distribution and the modified V-T deactivation rate, denoted rate package VT3, affects the SSG time histories similar to the change from the initial rate package to rate package VT2: Gain durations and peak gain times are increased further, as are peak gain magnitudes. However, here, the time to peak gain for $P_1(4)$ is nearly the same for both cases. As in the comparison of the previous rate packages, the increase in gain duration is pronounced for the v = 2-1 band.

Finally, a comparison between rate package VT3 and the VR20J model results shows a large increase in peak gain magnitudes along with increased peak gain times and gain durations. The VR20J peak gain magnitudes are approximately a factor of 2 and 3 higher for v = 2-1 and v = 1-0 bands respectively. Furthermore, the gain duration and peak gain time increases are greater for the v = 1-0 band than for the v = 2-1 band.

The differences in gain behavior for the different rate packages can be explained in the following manner.

The model results show that changing from the initial rate package to rate package VT2 gives an increase in mixture temperature at gain termination. For the initial rate package, the termination temperature is 344°K, while for rate package VT2, it is 368°K. This increase temperature will simultaneously increase the hot and cold pumping rates while decreasing the V-T deactivation rate. The combination of these

two effects should lead to increased peak gain and longer duration, as chemical pumping can compete more favorably with deactivation. This is what is observed.

In addition, the modified vibrational pumping distribution effectively increases the average number of HF vibrational quanta produced per $H + F_2$ collision from 5.15 to 5.69. This is due to a shift in product state population from v = 5 and 6, 7 and 8. Thus, even if the total rate of HF formation into all vibrational levels was the same for both cases, the number of vibrational quanta produced would be 10% larger for rate package VT3. The fact that the total rate is higher for rate package VT2 emphasized the effect of changing the vibrational pumping distribution. This combination of increased rate and increased average product quanta per collision assist in the increased gain peak magnitude and duration.

The model results also show a gain pulse termination temperature that is higher for the VT3 rate package than for the VT2 rate package. In this case, the V-T rate coefficient has been reduced by a factor of 3.3, the VT3 rate package having the smaller rate coefficient. This reduction in V-T reduces the major pulse termination mechanism: removal of vibrational quanta. This allows favorable competition between pumping and deactivation to occur for a greater length of time, thus consuming more fuel and oxidant. Model results verify this. The VT2 results show consumption of 1.31% of the initial F_2 in 74 μsec while the VT3 results show consumption of 1.60% of the initial F_2 in 86 μsec. This decrease in V-T deactivation in concert with the increase in fuel and oxidant consumption lead to the observed increases in peak gain magnitudes and gain durations.

A comparison of the results for the VT3 rate package and the VR20J model show changes similar to those described in the previous paragraph.

The pulse termination temperature increases from 382 °K to 387 °K and the percentage initial F_2 consumed increases from 1.60% to 1.85%. In both cases, the larger values correspond to the VR20J results.

As stated in the comparison of the VT2 and VT3 rate packages, the increase in temperature increases the rate of chemical pumping while decreasing the rate of V-R,T deactivation. However, there is an even stronger effect contributing than the rise in temperature. This effect is the change in the vibrational relaxation mechanism from V-T to V-R,T.

Brown [68] has shown that increasing the V-T portion of the V-R,T rate decreases pulse duration. Conversely, transforming a portion of the V-T rate into V-R,T, i.e. changing from rate package VT3 to VR20J should increase pulse duration. This is precisely what is observed. Thus, it is likely that the modeling of V-T deactivation as V-R,T is responsible for the increased pulse durations observed.

The VT and VR20J models consistently overpredict pulse duration and peak gain magnitude. That may be attributed to the following factors.

First, all models neglect oxygen kinetics. Inclusion of oxygen kinetics in the model of Taylor, et al. [79] has shown that oxygen decreases pulse duration by acting as a chain reaction terminator. Inclusion of oxygen in the experimental apparatus would also result in water vapor formation within the laser cavity concurrent with the desired laser medium chemistry.

Second, the models calculate gains at line center. This is the maximum gain possible for a given transition consistent with boradening of the emitting line. In contrast, gain is probably not measured experimentally at line center. Since it is rare for a longitudinal laser cavity mode to coincide precisely with transition line center, the probe laser itself will not oscillate at transition line center, but at a frequency shifted slightly to one side or the other. In consequence, gain probing of the medium is probably done at a frequency shifted slightly off line center. Thus, due to the strong variation of gain with frequency for a given transition, this can result in an experimentally measured gain value substantially less than that for line center and hence substantially less than the model predicts. To complicate matters further, the gain at a frequency shifted slightly from line center will change relative to the line center gain during the laser pulse. This is due to changes in cavity temperature and changes in chemical species concentrations with time which alter line broadening and hence transition line shape. The result is that measured gain should be less than line center gain in all cases. Errors of up to 26% in gain magnitude are possible due to this effect. In addition, there should be no discernible pattern to this effect since whether or not a probe laser longitudinal cavity mode falls on, near, or off line center is random. This is discussed further in Appendix D.

As one would expect, agreement between the two sets of modeling results and experiment is dependent upon the model that is used to evaluate the unknown F atom dissociation parameters, n_ρ and l_α. In this work, the V-T model with the standard rate package was used to determine n_ρ and l_α through best fits of computer TRS and SSG results to the

experimental data. Consequently, V-T model results agreed very well with experiment while VR2OJ results did not. However, if this procedure had been reversed, with the VR2OJ model being used to determine n_p and l_a, agreement between VR2OJ results and experiment would not have been significantly improved, for the following reasons.

The V-R model overpredicts gain and spectral durations and peak gain magnitudes. To bring the model durations into agreement with experiment, a higher percentage of fluorine dissociation would have to be assumed in the model. This would in turn increase the peak gain magnitude, decreasing agreement between model and experimental gain magnitudes.

If attempts were made to match peak gain magnitudes between model and experimental results, the assumed model precentage of fluorine dissociation would have to be decreased. This would in turn lengthen the model gain and spectral durations, decreasing agreement in this case.

It is important to note that the model verifies several of the points noted in earlier discussions of the gain experiments.

Two features of the model are inclusion of chain reaction pumping and inclusion of prereacted HF. Parametric studies showed that it was necessary to include an initial concentration of HF (prereaction) to get reasonable agreement between the model and experimental results for both SSG and TRS. This was determined by comparing VT model results using the initial rate package with the experimental TRS and SSG results. With initial HF due to prereaction absent, it was observed that the model v = 1-0 gain and lasing durations were too long relative to the

v = 2-1 gain and lasing durations. Thus, without prereaction, it was not possible to generate model results in good agreement with experiment for both the v = 2-1 and v = 1-0 bands. The inclusion of prereaction rectified this by reducing v = 1-0 durations for SSG and TRS to values consistent with the v = 2-1 SSG and TRS durations.

The conclusions to be drawn from this are as follows: (1) The model accurately predicts all gain trends involving initiation, peak and termination times. The model also precisely predicts the gain duration trend. (2) The model predicts exactly the trend with rotational level for peak gain. (3) VT model gain magnitudes compare well with experimental gain magnitudes, VR20J gain magnitudes do not compare as favorably. (4) It is probably important to include the effects of oxygen kinetics in the model. (5) It would be desirable to be able to include calculations to determine gain off line center in the model. However, due to the extreme complexity of this problem, it is beyond the scope of current state of the art computer modeling.

CHAPTER 4

SUMMARY AND CONCLUSIONS

An experimental and computer modeling investigation of a flash photolytically initiated, pulsed $H_2 + F_2$ chemical laser was undertaken. Time Resolved Spectra (TRS), time history of Small Signal Gain (SSG), and Total Pulse Energy (TPE) were recorded. The time resolved spectra were recorded at three pressures, 36 torr, 102 torr and 331 torr at each of two cavity mixture compositions, $He:O_2:F_2:H_2$ = 20.8:1.0:4.6:1.2 and $He:O_2:F_2:H_2$ = 22.0:1.0:2.7:1.0. The time history of small signal gain was measured for a total of eleven transitions in the v = 2-1 and v = 1-0 bands. The SSG measurements were performed at 102 torr for both of the cavity mixture compositions listed above, and at 331 torr for the cavity mixture composition $He:O_2:F_2:H_2$ = 22.0:1.0:2.7:1.0. Total pulse energy was measured at 331 torr with a cavity mixture composition of $He:O_2:F_2:H_2$ = 20.8:1.0:4.6:1.2.

Several trends are observed in the TRS results. First, individual transitions pulse durations increase with increasing mixture pressure and with increasing initial mixture F_2 concentration. Second, the number of lasing transitions within a given band increases with increasing initial mixture F_2 concentration. Third, individual transition peak intensities increase with increasing pressure and increasing initial mixture F_2 concentration. The first of these trends is probably due to binary scaling of the reaction processes

involved while the second and third are probably due to increased rates of chemical pumping. The increased chemical pumping rates would be due to the increased initial mixture F_2 concentration.

There are further observations to be made in addition to the trends mentioned above. These observations are that there is monotonic shifting of transition initiation, termination and peak intensity times, within a given vibrational band. These observations lead to the postulation of a nearly thermalized, or near Boltzmann, distribution of rotational levels. If this is so, it would seem that rotational relaxation is fast compared to chemical pumping and vibrational energy transfer. Model calculations verify this. Rotational relaxation is not fast compared to stimulated emission processes. Model calculations also verify this. Finally, it is probable that water vapor absorption is a strong loss mechanism for $P_1(5)$, significantly perturbing its spectral history.

The SSG results show that increasing the percentage of mixture F_2 increases peak gain, decreases gain duration, decreases time to peak gain and decreases gain initiation time. These trends are most likely attributable to the increased rate of chemical pumping which leads to an increased inversion and faster consumption of reactants.

The SSG results also show that there is a change in the shape of gain time histories with an increase in initial mixture F_2 concentration. This may be a result of an increased temperature rise with increased F_2 concentration. This temperature rise causes an increase

in the rate of R-R,T relaxation vs V-R,T relaxation. This would increase the thermalization of rotational levels and lead to the more distinct trends observed.

The SSG results also show that gain duration decreases and peak gain increases with increasing pressure. Binary scaling of the chemical reactions would explain both of these effects.

A total pulse energy of 5.4 J/l-atm was measured. This is consistent with other measured results.

A comparison of the time histories of gain and spectra show that the gain duration on a particular transition is much longer than the lasing duration for the same transition. The conclusion to be drawn is that gain magnitude data does not yield much information on TRS, except that the TRS duration will be shorter. Time resolved spectra durations are shorter than small signal gain durations because stimulated emission acts as an additional mechanism for reducing population inversions.

Although the magnitudes of TRS and SSG do not match, the trends do. Both TRS and SSG durations decrease with increasing pressure and initial mixture F_2 concentration. Initiation, termination and peak gain and intensity times increase with increasing rotational level, as do gain and intensity durations.

In addition to the experimental trends and results listed, computer simulations of the laser were run. An existing computer model was modified through substitution of a wavelength dependent threshold gain and by addition of a flash photolysis option. The modified model, denoted VR20J, was compared with the experimental results and with the

predictions of a second model. This second model, denoted VT, was a simplified version of the VR20J model. Both models simulate a spatially uniform mixture of H_2 + F_2 with He diluent. The mixture is assumed to be contained in a Fabry-Perot laser cavity. The models use a rate equation approach to determine individual species concentrations for HF, H_2, He, SF_6, F_2, F, H, plus the P-branch and pure rotational fluxes as well as the thermodynamic temperature. Detailed kinetic mechanisms are included in both models consisting of the H_2 + F_2 chain pumping reaction, dissociation-recombination and four modes of energy transfer. Both models include V-V exchange and R-R,T relaxation. The VT model assumes V-T vibrational deactivation while model VR20J assumes V-R,T vibrational deactivation.

The lastest available kinetic rate data was input to the models. Two rate coefficients were varied in a systematic manner: the hot reaction vibrational pumping distribution and the V-T deactivation rate. This combination yielded one V-R,T and three V-T rate packages.

The results of this parametric variation of rate coefficients showed that the VT model results using rate package VT2 were in closest agreement to experimental results for gain and pulse energy. This decision was based on a comparison of individual transition pulse durations and peak, initiation and termination times for TRS, plus, individual initiation, termination and peak times and peak gain magnitudes for SSG. The experimental spectra results agreed equally well with the VT model using eitner rate package VT2 or VT3. The model overpredicts pulse energy by 10% and is within 38% and 34% of predicting gain peak magnitude and duration.

The model does not always agree well with experiment. It predicts v = 6-5 lasing, not experimentally observed at 36 torr and overpredicts the number of lasing transition at 331 torr, especially at higher rotational levels. The model results are also shifted up one rotational level at 331 torr (model $P_1(5)$ being equivalent to experimental $P_1(4)$). A final point of disagreement is that of $P_1(5)$ TRS. The VT model shows $P_1(5)$ behavior in observance of the stated trends while experiment does not. This is most likely due to water vapor absorption of the $P_1(5)$ signal.

Other than the discrepancies noted in the preceeding paragraph, the VT model results closely follow experiment. In all cases, the VT model accurately predicts all trends observed experimentally in both the TRS and SSG measurements.

The VT modeling results clearly demonstrate the utility of computer simulations of $H_2 + F_2$ lasers as predictive tools.

It is important to realize that current chemical kinetic practice is to use V-R,T as the actual mechanism of vibrational deactivation in $H_2 + F_2$ lasers, not V-T. Thus, the fact that the VT model predictions are closer to experiment than V-R is surprising. The opposite would be expected to be true. This is a shortcoming of current models, and should be rectified. This does not invalidate the results of the model studies. Instead it provides direction for future chemical kinetics research and for further model development.

There is still uncertainty in the exact details of the V-R mechanism. The major question is what proportion of a vibrational quantum is transferred into rotational energy. Brown [68] suggests between 50% and 80% of each vibrational quanta should go into rotational energy.

Wilkins trajectory studies suggest even more than 80% [86] of each vibrational quanta should be transferred to rotation. The results presented here suggest less than 50% would yield best agreement.

This uncertainty in the V-R,T mechanism should be resolved. This could either be done via experiments, quantum ab initio potential surface calculations, or a combination of the two. In any case, further investigation of V-R,T energy transfer is necessary to improve computer modeling predictive capabilities.

The lack of H_2O vapor kinetics appears to be a serious model limitation. This is most evident when comparing VR20J model results with VT model and experimental results. Since the VR20J model includes the most recent rate data, it should match experimental results more closely than the VT model. The opposite is observed. In both SSG and TRS investigations, the VR20J results show durations that are much longer than experiment and real gains much higher than experiment. These results imply absence of a deactivation mechanism within the model. This could be H_2O kinetics.

Leone [106] shows that H_2O is a very efficient deactivator of HF, even more efficient than HF itself. This fact, coupled with the evidence of H_2O vapor present, through absorption of $P_1(5)$, supports the assertion that a major deactivation mechansim is missing from the model. Inclusion of H_2O vapor kinetics could bring model predictions in line with experiment.

APPENDICES

APPENDIX A

COMPUTER MODEL FORMULATION

APPENDIX A

COMPUTER MODEL FORMULATION

A.1 General Model Formulation

The computer model described here is similar to that of References 23 and 68. The model simulates a spatially homogeneous helium-fluorine-hydrogen gas mixture in a Fabry-Perot laser resonator. The kinetic processes are initiated by introducing a concentration of fluorine atoms. The model utilizes a rate equation approach to determine the time histories of:

(1) The individual species concentrations of the lowest seven vibrational levels (v = 0 to v = 6) of HF and their lowest twenty rotational levels (J = 0 to J = 19),

(2) The individual species concentrations of the lowest three vibrational levels (v = 0 to v = 2) of H_2,

(3) The species concentrations of He, SF_6, F_2, F and H,

(4) The P-branch laser photon fluxes for the lowest twelve transitions in the lowest six bands ($P_1(1)$ to $P_6(12)$),

(5) The pure rotational laser fluxes for the lowest nineteen transitions in the lowest seven vibrational levels, and

(6) The thermodynamic (or translational) temperature.

HF vibrational levels v = 7 and v = 8 are also included with their rotational levels assumed to be in equilibrium at the translational temperature.

The kinetic mechanisms used in the model are:

(1) The $H_2 + F_2$ chain

$$F + H_2 = HF(v, J) + H \quad (A1)$$

$$H + F_2 = HF(v, J) + F, \quad (A2)$$

(2) Vibrational to Rotational, Translational (V-R,T) energy transfer

$$HF(v, J) + M = HF(v', J') + M \qquad (v' = v-1), \quad (A3)$$

(3) Vibrational to Vibrational (V-V) energy transfer

$$HF(v_1, J_1) + HF(v_2, J_2) = HF(v_1-1, J_1) + HF(v_2+1, J_2), \quad (A4)$$

$$HF(v_1, J) + H_2(v_2) = HF(v_1-1, J) + H_2(v_2+1), \quad (A5)$$

(4) Rotational to Rotational (R-R) energy transfer

$$HF(v_1, J_1) + HF(v_2, J_2) = HF(v_1, J_1-\Delta J) + HF(v_2, J_2+\Delta J), \quad (A6)$$

(5) Rotational to Translational (R-T) energy transfer

$$HF(v, J) + M = HF(v, J-\Delta J) + M, \quad (A7)$$

(6) Dissociation - Recombination

$$F_2 + M = 2F + M \quad (A8)$$

$$H_2 + M = 2H + M \quad (A9)$$

$$HF(v, J) + M = H + F + M \quad (A10)$$

and both P-branch and pure rotational stimulated emission

$$HF(v+1, J-1) + h\nu_{v,J} = HF(v, J) + 2h\nu_{v,J} \quad (A11)$$

$$HF(v, J+1) + h\nu_J = HF(v, J) + 2h\nu_J \tag{A12}$$

where, $h\nu_{v,J}$ is a photon stimulated by P-branch emission while, $h\nu_J$ is a photon stimulated by pure rotational emission.

The chemical reactions are written as

$$\sum_i \alpha_{ri}[N_i] = \sum_i \beta_{ri}[N_i]. \tag{A13}$$

Here $[N_i]$, α_{ri} and β_{ri} are the molar concentrations and stoichiometric coefficients for the i^{th} species in reaction r. The forward and backward rate coefficients for the r^{th} reaction are k_r and k_{-r}.

The rate equations for the i^{th} nonlasing species concentrations, the HF(v, J) lasing species concentrations and both P-branch and pure rotational lasing fluxes (with lower lasing levels v, J) are respectively:

$$(1)\quad [\dot{N}_i] = X_i \tag{A14}$$

where $X_i = \prod_r(\alpha_{ri} - \beta_{ri})(k_r[N_j]^{\alpha_{rj}} - k_{-r}[N_j]^{\beta_{rj}})$,

$$\begin{aligned}(2)\quad [\dot{HF}(v, J)] = {} & X_i + P(v, J) + D_{V\text{-}R,T} + D_{R\text{-}R} \\ & + D_{R\text{-}T} + D_{V\text{-}V} + \alpha_{VR}(v, J)f_{VR}(v,J) \\ & - \alpha_{VR}(v-1, J+1)f_{VR}(v-1, J+1) \\ & + \alpha_{RR}(v, J)f_{RR}(v, J) \\ & - \alpha_{RR}(v, J-1)f_{RR}(v, J-1)\end{aligned} \tag{A15}$$

where $[\dot{HF}(v, J)]$ is the time rate of change of the molar concentration of HF(v, J), X_i is from Equation (A14) and P(v, J) is the rate of chemical pumping into level v, J. $D_{V\text{-}R,T}$ is the net rate of concentration change of level v, J due to vibrational to rotational, translational energy transfer, $D_{R\text{-}R}$ is the net rate of concentration change

of level v, J due to rotational to rotational energy transfer, D_{R-T} is the net rate of concentration change of level v, J due to rotational to translational energy transfer and D_{V-V} is the net rate of concentration change of level v, J due to vibrational to vibrational enery transfer. $\alpha_{VR}(v, J)$ is the gain of the P-branch laser transition with lower level v, J, $f_{VR}(v, J)$ is the photon flux of the P-branch laser transition with lower level v, J, $\alpha_{RR}(v, J)$ is the gain of the pure rotational laser transition with lower level v, J and $f_{RR}(v, J)$ is the photon flux of the pure rotational laser transition with lower level v, J.

(3) $\dot{f}(v, J) = c(\alpha(v, J) - \alpha_{thr}(v, J))f(v,J)\ell/L$ (A16)

where f(v, J) is the photon flux of the P-branch or pure rotational lasing transition, c is the speed of light in vacuum, ℓ is the laser active medium length, L is the resonator mirror spacing and α_{thr} is the (P-branch or pure rotational) threshold gain for the transition with lower level v, J. As given by Reference 69:

$$\alpha_{thr}(v, J) = -\ln(R_0R_L)/2\ell \quad (A17)$$

where R_0 and R_L are the wavelength dependent mirror reflectivities.

The gain of the P-branch or pure rotational transition, $\alpha(v, J)$, can be expressed as in Reference 107:

$$\alpha(v, J) = (hN_A\phi(v, J)B(v, J))/(4\pi\lambda(v, J))$$
$$(g_u[N_u]/g_l - [N_l]) \quad (A18)$$

where h is Planck's constant, N_A is Avogadro's number, $\lambda(v, J)$ is the wavelength of the P-branch or pure rotational transition with lower level v, J [108], $\phi(v, J)$ is the Voigt lineshape profile evaluated at line center [109] and B(v, J) is the Einstein isotropic absorption coefficient based on the intensity [110, 111]. The upper and lower

level species concentrations are $[N_u]$ and $[N_l]$ respectively and the corresponding level degeneracies are g_u and g_l.

For a constant density gas, conservation of energy yields [69]

$$\sum_i [N_i]\, C_{v_i}\, \dot{T} = -P_L - \sum_i [\dot{N}_i]\, H_i \qquad (A19)$$

Here, C_{v_i} and H_i are the molar constant volume specific heat and molar enthalpy for species i.

The power of an individual P-branch lasing transition is

$$P_{Lv,\,J} = (hcN_A\alpha(v,\,J)f(v,\,J))/\lambda(v,\,J) \qquad (A20)$$

A similar expression holds for pure rotational lasing.

For each transition, the fraction of generated power actually coupled out of the laser through mirror R_0, $P_{0v,\,J}$ is given by Reference[107] as

$$P_{0v,\,J} = P_{v,\,J}(1-R_0)/((1+\sqrt{R_0/R_L})(1-\sqrt{R_0/R_L})). \qquad (A21)$$

The energy extracted on each individual transition is determined by integrating $P_{0v,\,J}$ over the pulse length, t = 0 to t = t_c, where t_c is the pulse completion of time:

$$E_{v,\,J} = \int_{t_o}^{t_c} P_{0v,\,J}\,dt. \qquad (A22)$$

The energy extracted on a particular band is found by summing the energies of all transitions in that band

$$E_v = \sum_J E_{v,\,J}. \qquad (A23)$$

The total pulse energy extracted is calculated by summing the energies of all the bands

$$E = \sum_{v} E_{v}. \tag{A24}$$

Equations (A14), (A15), (A16), and (A19) are simultaneously numerically integrated using the fourth order Runge-Kutta code, RKF45, of Reference 112. This integration yields the time history of all the individual species concentrations, the intensities on all P-branch and pure rotational lasing transitions and the temperature. The gain on all P-branch and pure rotational transitions and the pressure is then calculated from the species concentrations and thermodynamic variables respectively.

A.2 Initiation

Initiation of the laser pulse is via flash photolysis of molecular fluorine. A rate equation for fluorine atom production is derived in a manner similar to that of Reference 113. In this work we generalize to a species which can absorb over a finite frequency interval.

We assume a spatially uniform flashlamp input intensity, $I_i(\lambda, t)$, a spatially uniform fluorine concentration within the laser cavity and that only fluorine is dissociated by the ultraviolet light pulse. This is consistent with the statement that the medium is optically thin. The rate of fluroine atom formation is then proportional to the flash-lamp photon flux lost in traversing the medium. Since two fluorine atoms are produced for each ultraviolet photon absorbed, we have on a per wavelength basis,

$$\dot{[F]} = 2(I_i(\lambda, t) - I_f(\lambda, t))n_p \tag{A25}$$

where $I_i(\lambda, t)$ and $I_f(\lambda, t)$ are the wavelength dependent flashlamp input and output intensities to the medium respectively. These are determined from a Beer's law analysis of the laser medium [114]

$$dI(\lambda, t)/dx = -\varepsilon_{F_2}(\lambda)I(\lambda, t)[F_2]. \tag{A26}$$

Here, $\varepsilon_{F_2}(\lambda)$ is the molecular fluorine absorption coefficient and $I(\lambda, t)$ is the flashlamp intensity per unit wavelength. Integrating Equation (A23) over the cavity absorption length, l_a, and assuming a spatially homogeneous mixture of F_2 gives

$$I_f(\lambda, t) = I_i(\lambda, t)e^{-\varepsilon_{F_2}(\lambda)[F_2]l_a}. \tag{A27}$$

The per unit wavelength terms are integrated across the spectral region of interest 0.25 to 0.40 microns, to find the total fluorine atom production rate:

$$[\dot{F}] = 2\eta_p \int I_i(\lambda, t)(1-e^{-\varepsilon_{F_2}(\lambda)[F_2]l_a})d\lambda. \tag{A28}$$

η_p is an empirically determined geometry dependent efficiency which characterizes the coupling of ultraviolet radiation to the medium, taking account of radiation losses to windows, wall absorption, variation of absorption path length due to multiple bounces and scattering.

To simplify the calculation of $[\dot{F}]$ and the evaluation of Equation (A25), $I_i(\lambda, t)$ was assumed to be separable into two parts: a time independent portion $I_i(\lambda)$ giving the distribution of $I_i(\lambda, t)$ vs wavelength and a time dependent portion i(t) determining the time response. Furthermore, for conditions considered here, the medium can be assumed to be optically thin allowing approximation of e^{-x} by 1-x. This approximation will break down only if the argument of the exponential, x, is

greater than 1/10. For this study, the worst possible case would be for light at the wavelength of maximum absorption, 2845Å, with the maximum F_2 concentration involved. Thus, $\epsilon_{F_2}(2845\text{Å}) = 6.09$/mole cm [115], $[F_2] = 55.0$ torr, $l_a = 5.0$ cm. The resultant argument, x, is 0.095. Equation (A25) then reduces to

$$[\dot{F}] = 2n_p i(t)[F_2] l_a \int I_i(\lambda)\epsilon_{F_2}(\lambda)d\lambda. \qquad \text{(A29)}$$

Note that the ratio $[\dot{F}]/[F_2]$ is independent of $[F_2]$ for these conditions. Since $[F_2]$ changes by less than 2.5% during the pulse, it can be assumed constant. Integrating Equation (A26) then shows that $[F]/[F_2]$ is independent of initial $[F_2]$ for this study.

Analytical expressions for $I_i(\lambda)$, i(t) and $\epsilon_{F_2}(\lambda)$ were determined by least squares fitting expressions to measured results for $I_i(\lambda)$ and i(t), see Figure (A.1), and to the data of Reference [115] for $\epsilon_{F_2}(\lambda)$:

$$\epsilon_{F_2}(\lambda) = Ae^{-B(\lambda-\lambda_0)^2}, \qquad \text{(A30)}$$

$A = 6.0$ liters/mole-cm

$B = 2.8788 \times 10^{-6}$ Å^{-2}

$\lambda_0 = 2845$Å,

$$\begin{aligned}
i(t) &= 0.685 \times 10^6\, t && 0.0<t<1.46\ \mu\text{sec}\\
i(t) &= -4.17 \times 10^6\, t + 7.0882 && 1.46<t<1.64\ \mu\text{sec}\\
i(t) &= 0.273 \times 10^6\, t - 0.17772 && 1.64<t<2.74\ \mu\text{sec}\\
i(t) &= -0.345 \times 10^6\, t + 1.51455 && 2.79<t<4.39\ \mu\text{sec}\\
i(t) &= 0.0 && t>4.39
\end{aligned} \qquad \text{(A31)}$$

$$I(\lambda) = -395.92 + 0.48671\lambda - 2.2172 \times 10^{-4}\lambda^2 + 4.4511 \times 10^{-8}\lambda^3 - 3.3262 \times 10^{-12}\lambda^4 \qquad \text{(A32)}$$

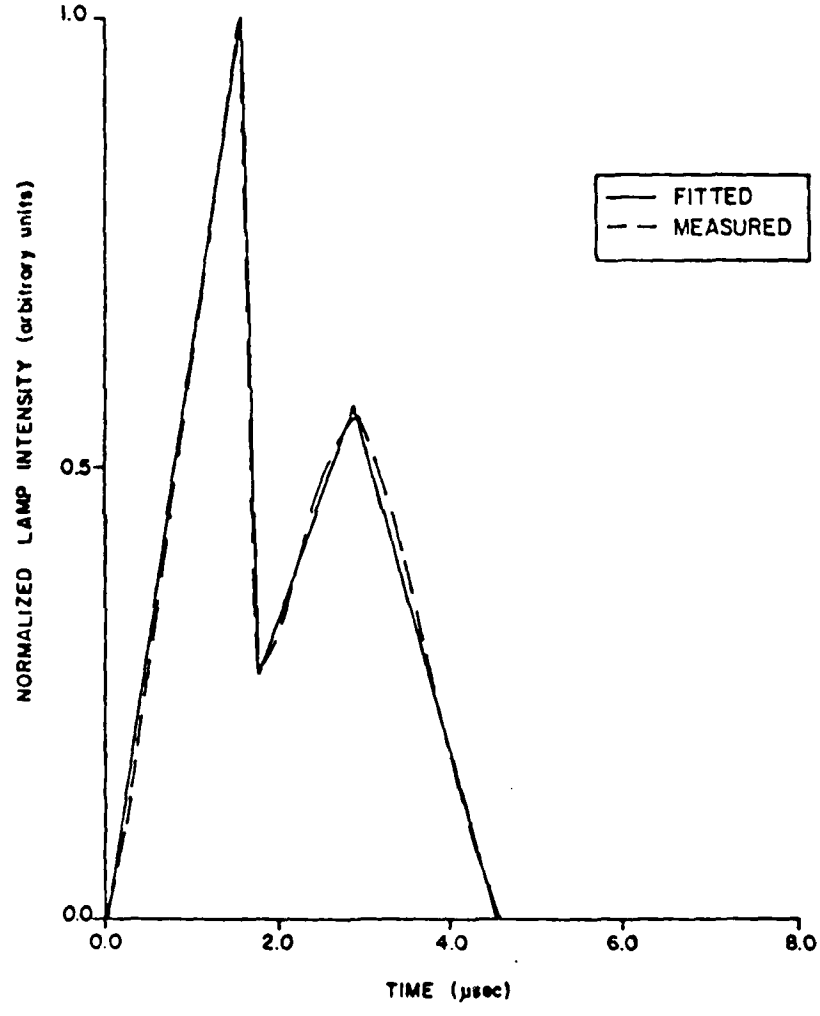

Figure A.1 Total flashlamp intensity vs time

A.3 Threshold Gain

The model of References 23 and 69 was modified to include a wavelength dependent threshold gain. Variations in output coupler reflectivity with wavelength made this modification necessary for accurate simulation of experimental results.

The reflectivity of the 5m radius of curvature copper mirror was assumed to be 99% for the region 2.5 microns to 4.0 microns. An analytical expression for output coupler reflectivity vs wavelength was least squares fit to the measured reflectivity vs wavelength curves of Figures (A2) and (A3). The form of the reflectivity was found to be

$$R_{97}(\lambda) = -22.794 + 0.020169\lambda - 5.7187 \times 10^{-6}\lambda^2 + 5.4066 \times 10^{-10}\lambda^3 \qquad \text{(A33)}$$

for the 97% maximum reflectivity output coupler and

$$R_{81}(\lambda) = -0.98008 + 0.0012030\lambda - 2.4912 \times 10^{-7}\lambda^2 + 1.4827 \times 10^{-11}\lambda^3 \qquad \text{(A34)}$$

for the 81% maximum reflectivity output coupler. Threshold gain as a function of wave number was computed using Equation (A17) with Equation (A30) substituted. α_{thr} is evaluated for each lasing transition.

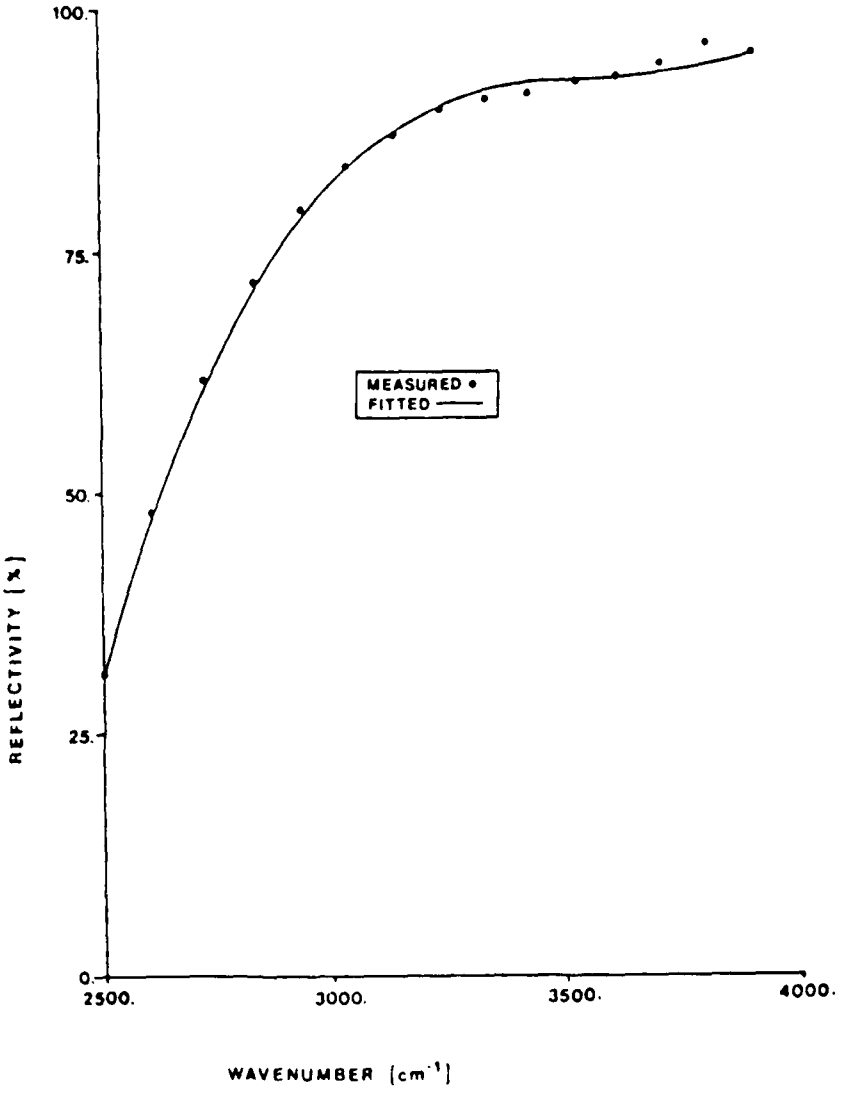

Figure A.2 Reflectivity vs wavenumber for the output coupler with nominal 97% reflectivity

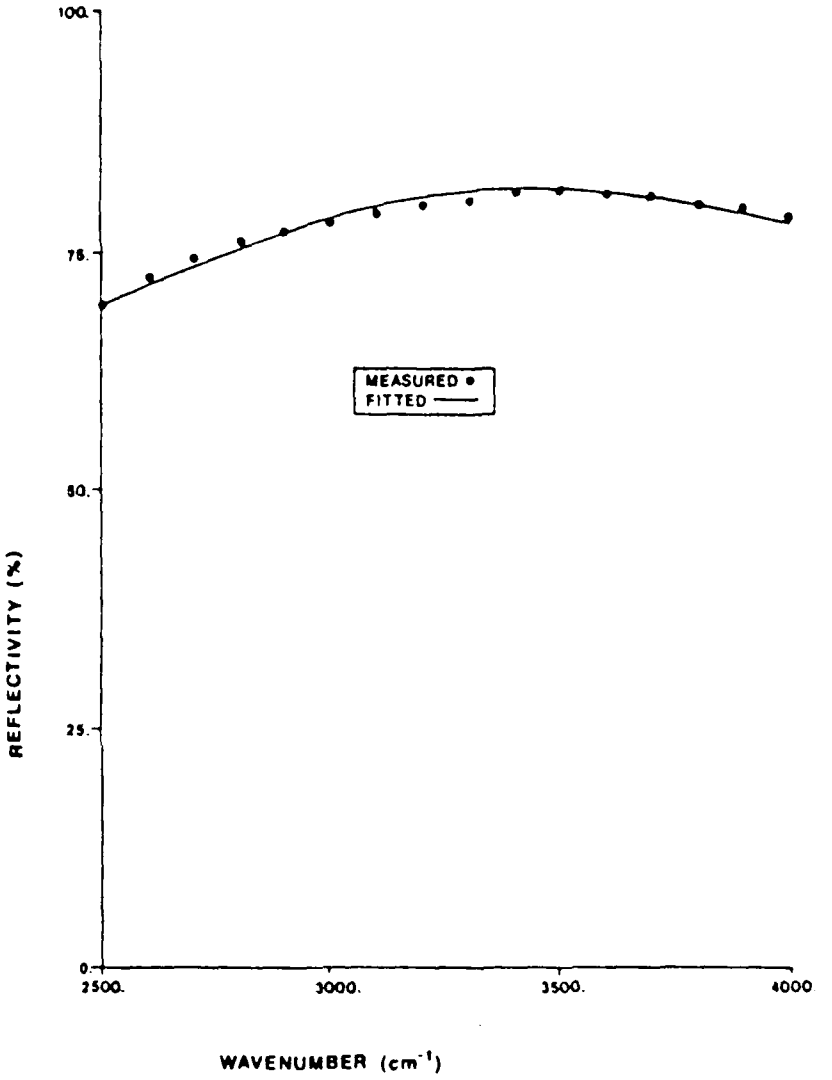

Figure A.3 Reflectivity vs wavenumber for the output coupler with nominal 81% reflectivity

APPENDIX B

DETERMINATION OF INITIAL HF CONCENTRATION DUE TO PREREACTION

APPENDIX B

DETERMINATION OF INITIAL HF CONCENTRATION DUE TO PREREACTION

The concentration of HF due to prereaction was determined in the following manner. The laser was set up in the small signal gain diagnostic configuration. See Section 2.2.2 and Figure 2.10 for further details. The cavity was first evacuated, then filled with a 36 torr mixture of $He:O_2:F_2:H_2:H_2$ = 22.0:1.0:2.7:1.0. The $P_1(3)$ absorption, or negative gain, was measured as 0.0035 per cm. A computer simulation was run using the above mixture composition with 1 mtorr HF added, all at 300 K. The $P_1(3)$ absorption was computed by the model to be 0.00404 per cm. A second computer simulation was run producing a value of 0.00364 per cm for the above mixture with 0.9 mtorr of HF added, again all at 300 K. The HF prereaction concentration was thus estimated at 0.9 mtorr for this case. Prereaction for the other cases was then scaled linearly with mixture F_2 pressure, using the value obtained for the 36 torr case as a baseline.

This gain technique has the sensitivity to measure even lower concentrations of HF. To see this, we write for the $P_1(3)$ transition:

$$dI/dx = \alpha I. \tag{B1}$$

Assuming constant gain over the entire absorption path,

$$\ln(I_1/I_2) = \alpha L_{12} \tag{B2}$$

Solving for α,

$$\alpha = [\ln(I_2/I_1)/L_{12}]. \qquad (B3)$$

In these tests, we were limited to $I_2/I_1<0.9$. $I_2/I_1 = 0.9$ was the largest ratio of intensities that could be accurately resolved from the photographs. For this work, L_{12} was 100 cm. This yielded a minimum detectable gain of approximately 0.001 per cm. Using the model again, as above, it was determined that this corresponded to an HF concentration of about 0.3 mtorr. This would be the minimum detectable concentration of HF.

APPENDIX C

MODEL RATE COEFFICIENTS

APPENDIX C

MODEL RATE COEFFICIENTS

The rate coefficients used in the VR computer model are listed in Table C.1. The rate coefficients used in the VT model are listed in Table C.2. These rate coefficients are listed by rate package: VT, VT2 and VT3.

Table C.1 Current Rate Coefficients in $H_2 + F_2$ Systems*

Reaction Number		Rate coefficient Units of cm, mole, sec, cal	M, v, A, g(v)
1a	$H_2(0) + M_2 = 2H + M_2$	$K_{-1a} = 6.2 \times 10^{17}\ T^{-0.95}$	M_2 = all species except $H + H_2$
1b	$H_2(0) + M_2 = 2H + M_2$	$K_{-1b} = 9.4 \times 10^{16}\ T^{-0.61}$	
1c	$H_2(0) + H = 2H + H$	$K_{-1c} = 1.2 \times 10^{14}\ T^{0.5}$	
2	$F_2 + M_3 = 2F + M_3$	$K_2^m = 5.0 \times 10^{13}$ exp(-35, 100/RT) $\times 10^{-(E_o - E_v)A_m}$	$A_F = 10$, $A_{F_2} = 2.7$, $A_{He} = 2$, $A_3 = 1$, all others
3	$HF(v) + M_3 = H + F + M_3$	$K_3(v) = \frac{1.2\ A_m}{n+1} \times 10^{19}\ T^{-1}$ exp(-135, 100/RT)	$A_F = A_H = A_{HF} = 5$, $A_m = 1$, all others: v = 0.....n
4	$F + H_2(0) = HF(v) + H$	$K_4 = g(v) \times 4.9 \times 10^{11}\ T^{0.8}$ exp(-600/RT)	v = 1, 2, 3; g(1) = 0.17, g(2) = 0.55, g(3) = 0.28; g(v) = 0, v >3
4b-1	$HF(4) + H = H_2(v') + F$	$K_{-4_{(v=4)}} = 6.0 \times 10^{11}\ T^{0.5}$	
4b-2	$HF(5) + H = H_2(v') + F$	$K_{-4_{(v=5)}} = 8.8 \times 10^{11}\ T^{0.5}$	
4b-3	$HF(6) + H = H_2(v') + F$	$K_{-4_{(v=6)}} = 1.6 \times 10^{12}\ T^{0.5}$	
5	$H + F_2 = HF(v) + F$	$K_5 = g(v) \times 3.0 \times 10^{9}\ T^{1.3}$ exp(-950/RT)	g(v) = 0, v = 0, 1, 2, g(3) = 0.08, g(4) = 0.13, g(5) = 0.35, g(6) = 0.44; g(v) = 0, v > 6
6	$HF(v) + HF = HF(v') + HF$	$K_{6a} = 1.1 \times 10^{10}\ v^{3.5}\ T^{0.5}$ exp(1030/RT)	v' = v-1
6b	$HF(v) + H_2 = HF(v') + H_2$	$K_{6_{bv}} = 6.0 \times 10^{7}\ v\ T$	v' = v-1
6c	$HF(v) + H = HF(v') + H$	$K_{6_{c(v,v')}} = g(v,v') \times 1.5 \times 10^{12}$ exp(-700/RT)	g(1,0) = 1, g(2,1) = g(2,0) = 1.8, g(v,v-1) = 360, v = 3, ..., 6, g(v,v-n) = 1.8, v = 3, ..., 6, n = 2...v
6d	$HF(v) + F = HF(v') + F$	$K_{6_{dv}} = 1.6 \times 10^{13}\ v\ e^{-2700/RT}$	v' = v-1
6e	$HF(v) + M = HF(v') + M$	$K_{6_{ev}} = 7.7 \times 10^{-7}\ v\ T^{5}\ A_M$	$A_{F_2} = A_{Ar} = 1.0$, $A_{He} = 2.0$

Table C.1 (Continued)

Reaction Number		Rate coefficient Units of cm, mole, sec, cal	M, v, A, g(v)
7	$HF(v) + HF(v') = HF(v+1) + HF(v'-1)$	$K_7(v, 1; v+1,0) = 3.6 \times 10^{15} v^{-1} T^{-1.0}$	$v = 1$, $v' = 1$
		$K_7(v, v', v+1, v'-1) = 3 \times 10^{15} v^{-1} T^{-1.0}$	$v = 2,\ldots,7$, $v' = 1,\ldots,6$
8a	$H_2(v) + M_{10} = H_2(v-1) + M_{10}$	$K_{8a} = 2.5 \times 10^{-4} v T^{4.3} A_M$	$A_{H_2} = 4$, $A_{10} = 1$ all others
			$v = 1, 2$
8b	$H_2(v) + H = H_2(v-1) + H$	$K_{8b} = 2 \times 10^{13} \exp(-2720.RT)$	$v = 1, 2$
9	$HF(v-n) + H_2(v'+n) = HF(v)$	$K_9 \quad 8 \times 10^{11} v$	$v = 1\ldots6$; $n = 1,\ldots, v$
10a	$HF(0,10) + HF(v,J) = HF(0,10-\Delta J) + HF(v,J)$	$K_{10a} = 1.023 \times 10^{16} T^{-0.805} e^{-2569/RT}$	
10b	$HF(1,10) + HF(v,J) = HF(1,10-\Delta J) + HF(v,J)$	$K_{10b} = 3.38 \times 10^{16} T^{-0893} e^{-2436/RT}$	

*The rate coefficients are taken primarily from Cohen [95] except where noted in the test.
+Equation (6a) represents the total V-R-T rate for level v for collisions with HF. The sum of this rate and that of reaction (9) equals the rate suggested by Crim for toal deactivation of HF(v).

Table C.2 VT Model Rate Coefficients for the $H_2 + F_2$ Chemical Laser

rate package VT

identical to VR rate package with the following exception:

Equation (6a) and Equation (9) are summed to give one V-T rate:

(6a') $K_{6a} = 1.1 \times 10^{10} v^{3.5} T^{0.5} \exp(1030/RT)$

rate package VT2

identical to VR rate package with the following exceptions:

Equation (6a) and Equation (9) are summed to give one V-T rate:

(6a') $K_{6a} = 1.1 \times 10^{10} v^{3.5} T^{0.5} \exp(1030/RT)$

Equation (5) has a revised pumping distribution:

(5') $K_5 = g(v) \times 3.0 \times 10^9 T^{1.3}$

$g(v) = 0$, $v = 0, 1, 2$;
$g(3) = 0.07$, $g(4) = 0.13$,
$g(5) = 0.22$, $g(6) = 0.32$,
$g(7) = 0.14$, $g(8) = 0.12$

rate package VT3

identical to VR rate package with the following exceptions:

Equations (6a) and Equation (9) are summed to give one V-T rate:

(6a") $K_{6a} = 3.3 \times 10^9 v^{3.5} T^{0.5} \exp(1030/RT)$

Equation (5) has a revised pumping distribution:

(5') $K_5 = g(v) \times 3.0 \times 10^9 T^{1.3}$

$g(v) = 0$, $v = 0, 1, 2$;
$g(3) = 0.07$, $g(4) = 0.13$,
$g(5) = 0.22$, $g(6) = 0.32$
$g(7) = 0.14$, $g(8) = 0.12$

APPENDIX D

ERROR ANALYSIS FOR PROBING SMALL SIGNAL GAIN OFF LINE CENTER

APPENDIX D

ERROR ANALYSIS FOR PROBING SMALL SIGNAL GAIN OFF LINE CENTER

In Section 3.3.2, it was stated that up to 26% error could be introduced by probing SSG off-line center with the system utilized here. This will be demonstrated below.

Yariv [116] gives the following expression for a pressure (Lorentz) broadened line:

$$\phi(\nu) = (\Delta\nu_L/\pi)/[(\nu-\nu_o)^2 + (\Delta\nu_L/2)^2] \qquad (D1)$$

where $\Delta\nu_L$ is the Lorentz full width at half maximum (FWHM) for the transition in question. $\Delta\nu_L$ is related to the binary collision frequency for the emitting molecule by:

$$\Delta\nu_L = Z/\pi \qquad (D2)$$

$$Z = 2\sigma^2 N_A\sqrt{2\pi k_B T[1/M_{HF} + 1/M_i]} \qquad (D3)$$

where σ^2 is the collision cross section between the emitting molecule and the i^{th} collision partner, N_A is Avogadro's number, k_B is Boltzmann's constant, T is the temperature and M_{HF} and M_i are the molecular masses of HF and the i^{th} collision partner respectively. For the 102 torr mixture $Z = 3.35 \times 10^8$ Hz.

To determine the maximum error due to probing SSG off-line center, it is first necessary to determine the maximum probe laser frequency deviation from line center and then determine the effect of this deviation on the measured SSG.

The maximum probe laser frequency deviation from line center must be equal to one half of the probe laser cavity longitudinal mode spacing. Yariv [116] gives an expression for the cavity longitudinal mode spacing:

$$\Delta\nu_c = c/2L \qquad (D4)$$

with c being the speed of light and L being the cavity mirror spacing. For the Helios probe lase used here, $\Delta\nu_c = 1 \times 10^8$ Hz.

The effect of this frequency shift on the gain is directly related to its effect on the line shape, $\phi(\nu)$. To determine the maximum error, it is thus sufficient to determine the difference between the line center value of the line shape function and that at the maximum frequency deviation. Substituting from Equation (D1) yields:

$$\text{max error} = 1 - (\Delta\nu_L/2)^2/[(\nu-\nu_o)^2 + (\Delta\nu_L/2)^2] \qquad (D5)$$

Inserting the values for $\Delta\nu_L$ and $\Delta\nu_c$ calculated above gives a value for the maximum error of 26.6%. Here, $(1/2)\Delta\nu_c = \nu-\nu_o$. This is the number quoted in Section 3.2.2.

APPENDIX E

RAW DATA FOR TIME RESOLVED
SPECTROSCOPY PLOTS USED IN
FIGURES 2.17 AND 2.21

APPENDIX E

RAW DATA FOR TIME RESOLVED SPECTROSCOPY

PLOTS USED IN FIGURES 2.17 AND 2.21

The raw data used to plot Figures 2.17 and 2.21 are presented in Tables E.1 and E.2 respectively.

Table E.1 Data for TRS presented in Figure 2.17

Transition	36 torr pressure					102 torr pressure					331 torr pressure				
	t_i[1]	t_p[2]	I_p[3]	t_c[4]	t_d[5]	t_i	t_p	I_p	t_c	t_d	t_i	t_p	I_p	t_c	t_d
$P_1(3)$	5.4	5.6	3200	6.6	1.2	2.2	2.4	5000	2.9	0.7	4.0	4.1	150	4.5	0.5
$P_1(4)$	4.0	11.0	900	29.0	25.0	2.4	2.5	4000	6.5	4.1	2.5	2.8	1000	7.0	4.5
$P_1(5)$	28.0	30.0	40	37.0	9.0	2.0	6.0	80	28.0	26.0	2.1	2.3	3400	3.7	1.6
$P_1(6)$	25.0	36.0	330	73.0	48.0	6.0	6.5	1250	18.0	12.0	2.4	3.9	3800	7.2	4.8
$P_1(7)$	76.0	84.0	140	96.0	20.0	15.0	17.0	900	25.0	10.0	5.7	6.0	10000	14.3	8.6
$P_1(8)$	---	---	---	---	---	---	---	---	---	---	11.0	12.3	3800	18.8	7.8
$P_2(3)$	2.4	2.5	1400	8.5	6.1	1.7	1.8	3200	3.3	1.6	1.5	1.6	2400	2.2	0.7
$P_2(4)$	5.0	11.0	200	16.0	11.0	2.1	2.9	1600	10.4	8.3	1.7	2.1	3600	4.0	2.3
$P_2(5)$	4.0	15.0	410	55.0	51.0	2.2	4.0	1700	18.0	15.8	1.6	2.2	12100	12.5	10.9
$P_2(6)$	18.0	69.0	320	135.0	127.0	6.0	11.0	1800	47.0	41.0	2.7	4.8	10400	20.0	17.3
$P_2(7)$	60.0	125.0	180	180.0	120.0	17.0	45.0	1300	81.0	64.0	5.0	11.0	11000	28.0	23.0
$P_2(8)$	---	---	---	---	---	68.0	76.0	540	90.0	22.0	---	---	---	---	---
$P_3(3)$	3.5	3.7	50	4.9	1.4	2.3	2.4	70	3.2	0.9	1.6	1.8	90	2.5	0.9
$P_3(4)$	3.0	3.2	840	26.0	23.0	2.0	2.2	2400	7.5	5.5	2.0	3.0	6100	4.7	2.7
$P_3(5)$	8.0	27.0	410	86.0	78.0	2.5	3.5	2600	26.5	24.0	2.1	3.4	9000	18.8	16.7
$P_3(6)$	25.0	60.0	360	170.0	145.0	8.0	42.0	1500	73.0	65.0	3.0	9.0	11000	25.0	22.0
$P_3(7)$	145.0	170.0	80	210.0	65.0	55.0	68.0	800	95.0	40.0	12.0	20.5	5700	40.0	28.0
$P_4(3)$	---	---	---	---	---	---	---	---	---	---	2.0	2.5	25	3.5	1.5
$P_4(4)$	9.0	26.0	1000	35.0	26.0	4.0	4.2	4800	9.0	5.0	2.5	2.8	4800	5.5	3.0
$P_4(5)$	10.0	104.0	320	114.0	104.0	4.0	10.0	1200	51.0	47.0	3.0	7.0	7000	16.0	13.0
$P_4(6)$	112.0	116.0	4	118.0	6.0	49.0	52.0	80	60.0	11.0	6.0	15.0	5000	27.0	21.0
$P_5(3)$	6.0	7.0	520	7.0	1.0	3.4	3.6	900	3.9	0.5	2.3	2.4	130	3.0	0.7
$P_5(4)$	6.0	45.0	280	45.0	39.0	3.0	4.0	960	19.0	16.0	3.6	4.2	6000	8.0	4.4
$P_5(5)$	14.0	50.0	70	50.0	36.0	4.0	16.0	1040	38.0	34.0	4.2	6.4	7000	19.0	14.8
$P_5(6)$	---	---	---	---	---	28.0	32.0	110	38.0	10.0	8.0	12.0	2800	21.5	13.5
$P_6(3)$	---	---	---	---	---	---	---	---	---	---	4.0	4.1	2100	8.0	4.0
$P_6(4)$	---	---	---	---	---	7.2	7.9	200	9.6	2.4	4.1	4.5	1100	7.2	3.1
$P_6(5)$	---	---	---	---	---	7.0	9.0	18	12.0	5.0	3.0	6.0	900	10.0	7.0

[1] Initiation time (μsec)

[2] Peak intensity time (μsec)

[3] Peak intensity (relative units)

[4] Termination time (μsec)

[5] Transition duration (μsec)

Table E.2 Data for TRS presented in Figure 2.21

Transition	36 torr pressure					102 torr pressure					331 torr pressure					331 torr pressure				
	t_i[1]	t_p[2]	I_p[3]	t_c[4]	t_d[5]	t_i	t_p	I_p	t_c	t_d	t_i	t_p	I_p	t_c	t_d	t_i	t_p	I_p	t_c	t_d
$P_1(3)$	---	---	---	---	---	3.9	4.2	2	5.8	1.9	---	---	---	---	---	---	---	---	---	---
$P_1(4)$	6.6	14.8	160	47.4	40.8	4.8	5.9	2400	11.5	6.7	8.1	8.3	1000	11.4	3.3	5.6	5.9	2100	8.9	3.3
$P_1(6)$	49.8	56.0	---	67.4	17.6	8.4	9.7	600	27.0	18.6	8.3	9.0	700	21.7	13.4	10.3	10.8	600	23.7	13.4
$P_1(7)$	---	---	---	---	---	21.8	26.8	400	37.3	15.5	16.5	20.0	720	36.3	17.8	19.1	24.8	300	26.0	6.9
$P_2(3)$	3.4	4.0	---	10.5	7.1	2.7	3.2	2700	4.6	1.9	3.2	3.4	2200	4.6	1.4	2.7	2.8	2200	4.3	1.6
$P_2(4)$	4.0	8.2	145	31.3	27.3	3.4	4.4	1300	6.3	2.9	3.8	4.5	820	6.6	2.8	4.0	4.2	740	6.5	2.5
$P_2(5)$	9.5	17.5	265	175.0	165.5	4.8	8.2	2300	25.8	21.0	5.0	6.1	2600	12.5	7.5	5.8	8.9	1900	24.0	18.2
$P_2(6)$	56.0	90.0	135	488.0	432.0	9.1	21.0	2100	113.0	103.9	9.0	12.0	1800	38.0	29.0	8.9	14.4	1800	48.0	39.1
$P_2(7)$	---	---	---	---	---	34.5	102.3	1400	188.0	153.5	23.0	32.0	1090	103.0	80.0	30.3	37.0	200	73.2	42.9
$P_3(3)$	5.5	5.9	42	7.3	1.8	4.3	4.6	270	5.4	1.1	3.8	4.0	100	4.7	0.9	3.8	4.0	220	7.3	3.5
$P_3(4)$	5.0	18.0	---	48.0	43.0	3.3	4.0	1500	8.8	5.5	4.0	6.2	900	7.4	3.4	3.9	3.9	1500	8.1	4.2
$P_3(5)$	8.3	34.5	200	400.0	391.7	6.0	10.0	3000	40.5	36.5	4.0	5.5	2600	27.5	23.5	3.7	6.4	2100	24.2	20.5
$P_3(6)$	95.0	320.0	85	625.0	530.0	15.7	38.7	1900	210.0	194.3	11.5	17.5	2300	102.0	90.5	10.5	22.0	2200	72.2	61.7
$P_3(7)$	---	---	---	---	---	125.0	185.0	180	225.0	100.0	46.0	---	---	113.0	67.0	46.0	---	---	112.0	66.0
$P_4(3)$	---	---	---	---	---	4.9	6.4	120	7.4	2.5	5.2	5.4	180	6.4	1.2	4.7	4.8	80	5.4	0.7
$P_4(4)$	15.3	16.8	230	99.7	84.4	5.8	6.5	1250	17.5	11.7	3.7	5.5	3100	11.6	7.9	5.0	5.8	500	19.7	14.7
$P_4(5)$	22.7	68.0	110	335.0	312.3	8.0	22.0	1500	87.0	79.0	5.0	8.0	1500	72.0	67.0	5.5	11.0	1400	53.0	47.5
$P_5(3)$	9.0	10.2	155	12.5	3.5	5.2	5.4	600	7.0	1.8	4.5	4.8	930	6.3	1.8	5.1	5.7	65	7.2	2.1
$P_5(4)$	11.0	17.0	200	107.0	96.0	5.5	7.4	1300	42.5	37.0	4.5	8.3	1400	42.0	37.5	4.9	6.5	1600	21.0	16.1
$P_5(5)$	---	---	---	---	---	18.0	32.0	130	64.0	46.0	17.3	22.5	200	41.0	23.7	14.3	21.2	270	31.3	17.0

[1] Initiation time (μsec)

[2] Peak intensity time (μsec)

[3] Peak intensity time (relative units)

[4] Termination time (μsec)

[5] Transition duration (μsec)

APPENDIX F

TRS AND SSG PHOTOGRAPHES OF OSCILLOSCOPE DATA

Table F.1 SSG photogrammes, $He:O_2:F_2$, [illegible], [illegible], 2, 102 torr

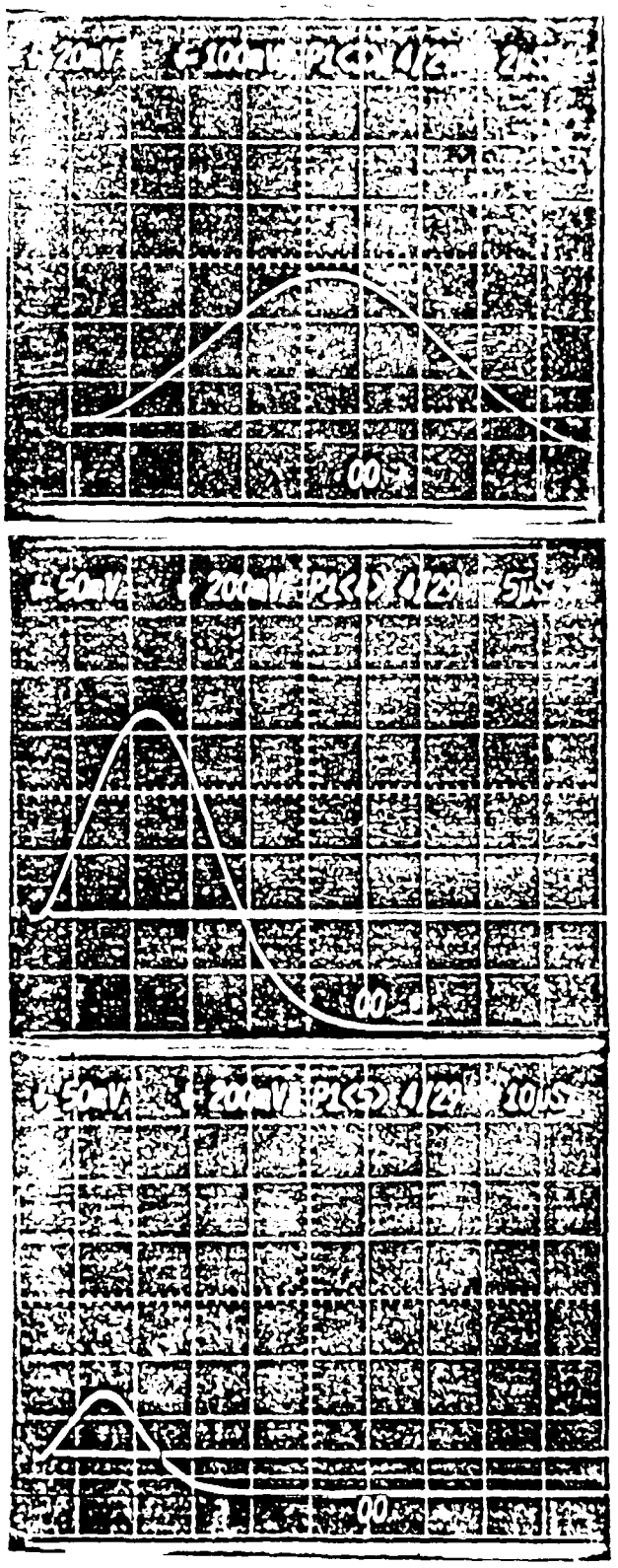

Table F.1 (Continued)

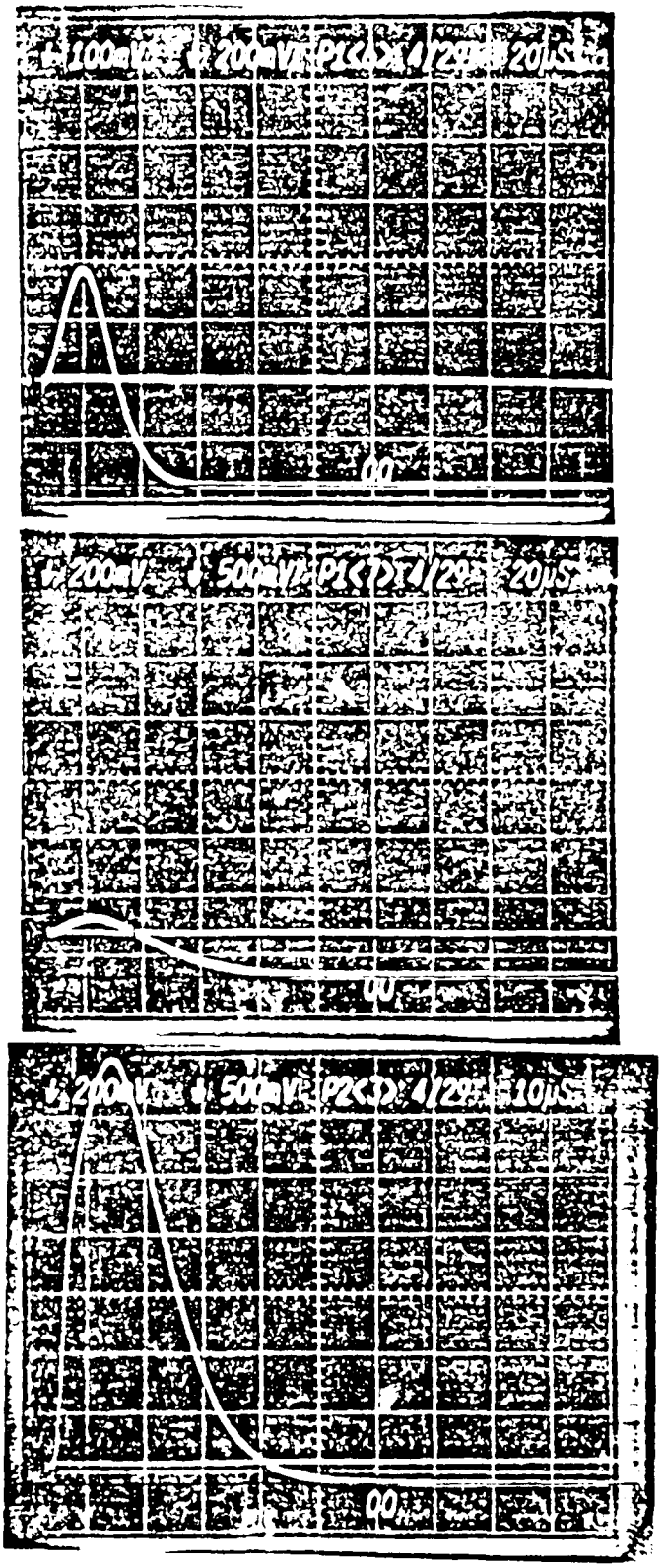

Table F.1 (Continued)

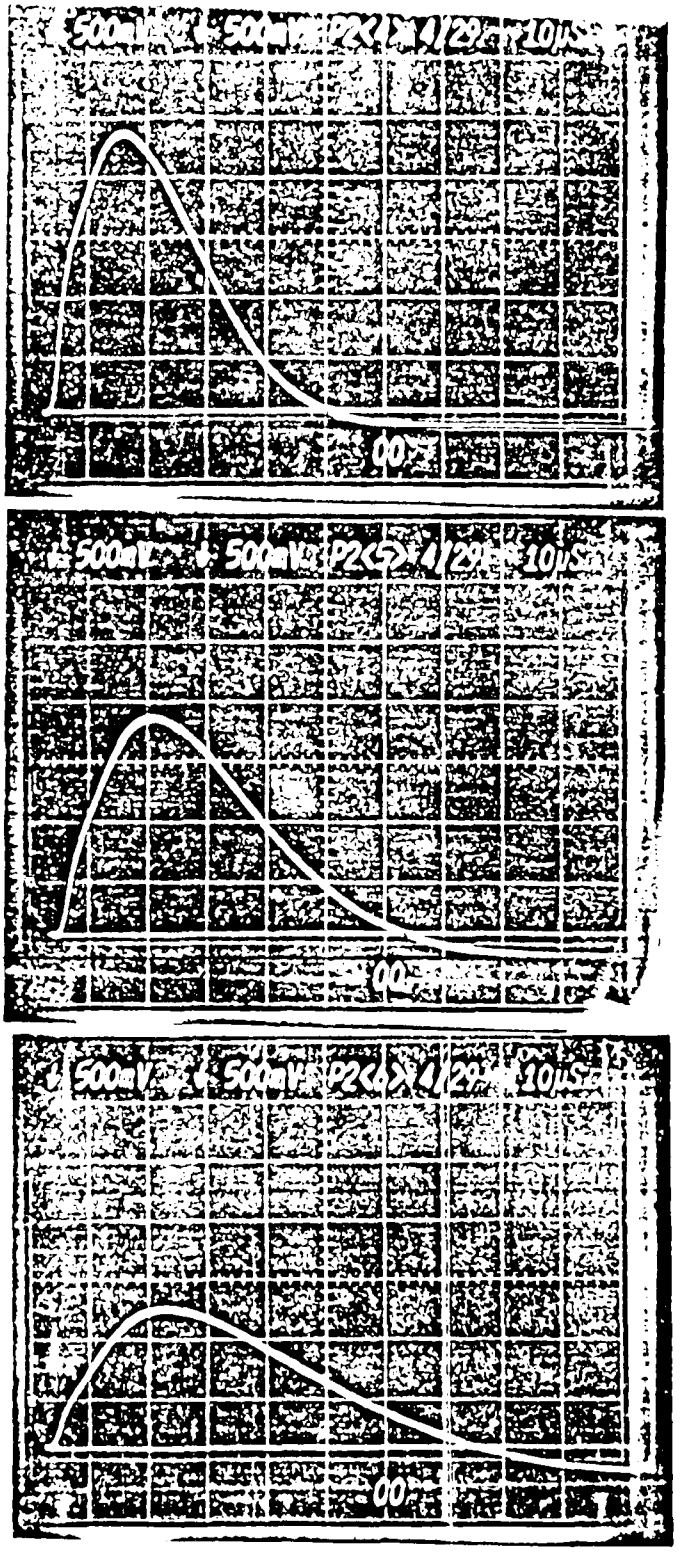

Table F.2 TRS photographes, $He:O_2:F_2:H_2$=20.8:1.0:4.6:1.2, 36 torr

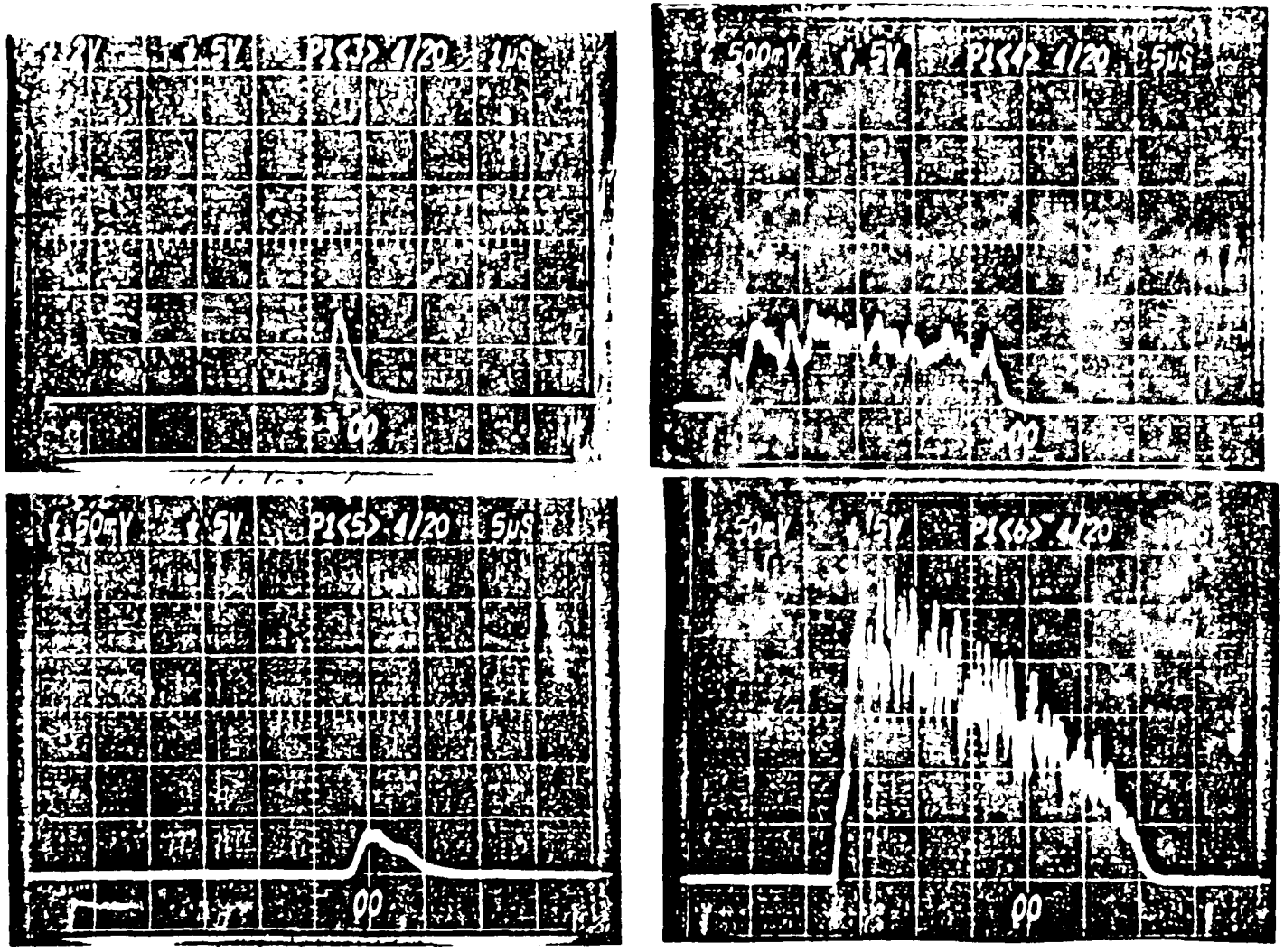

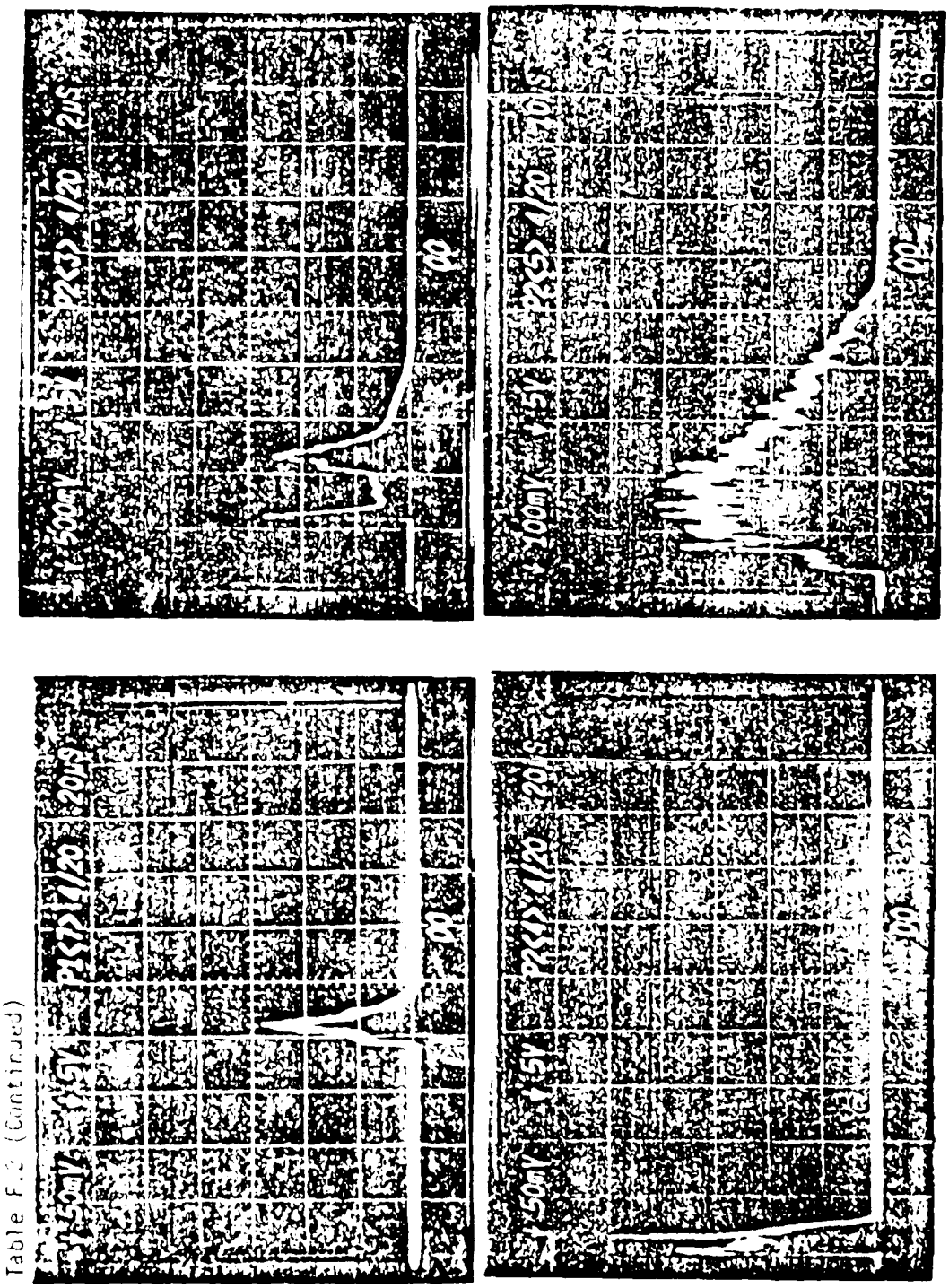

Table F.2 (Continued)

Table F.2 (Continued)

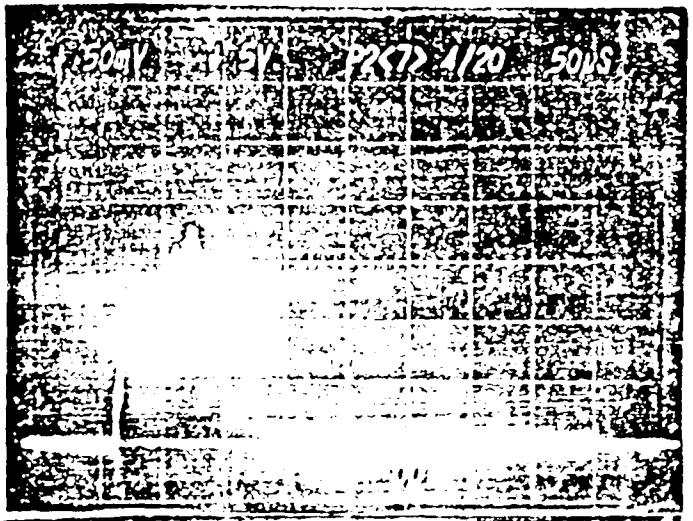

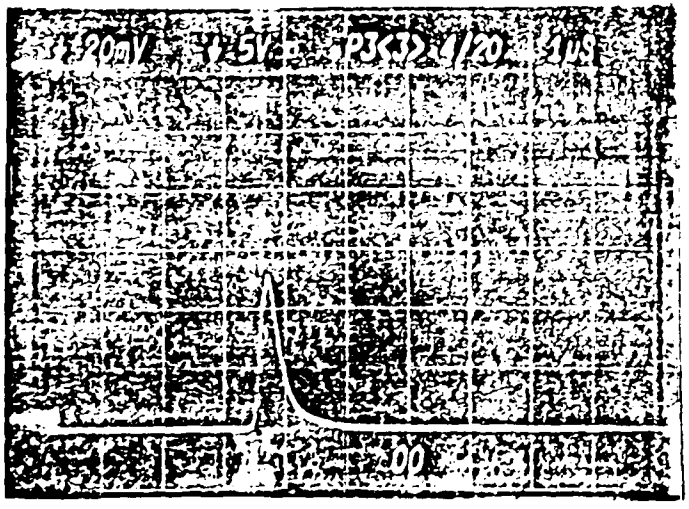

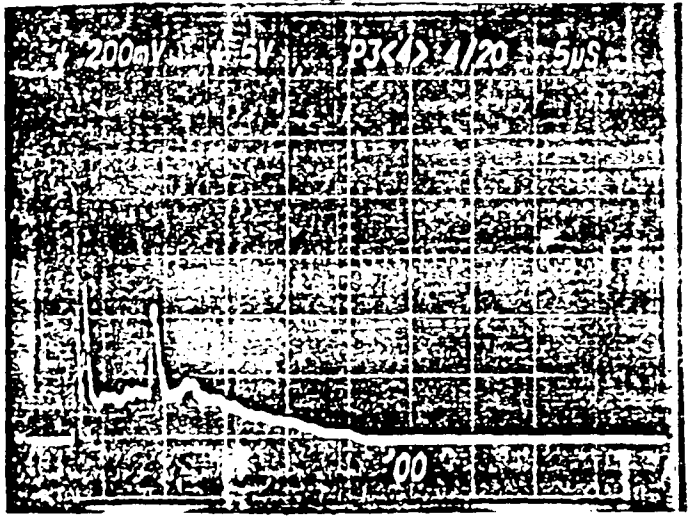

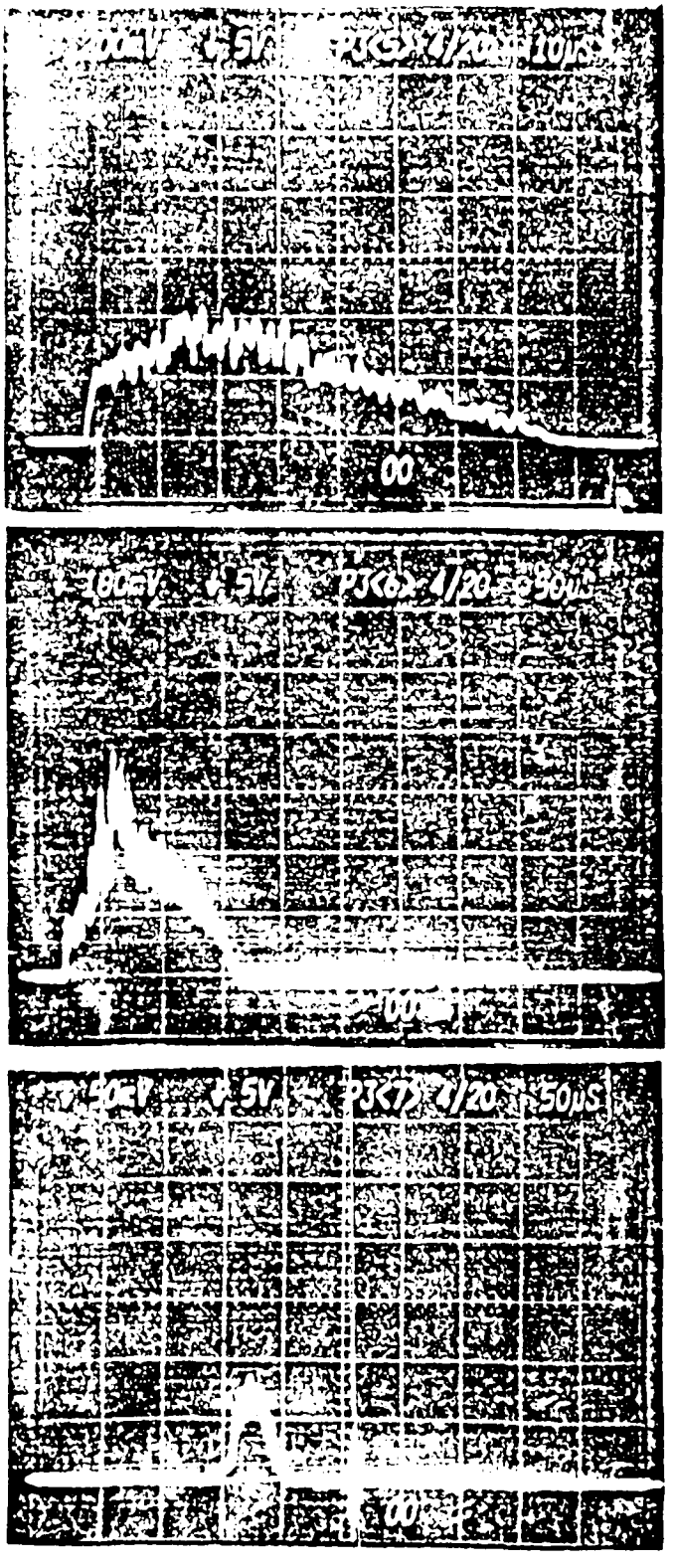

Table E.1 (Continued)

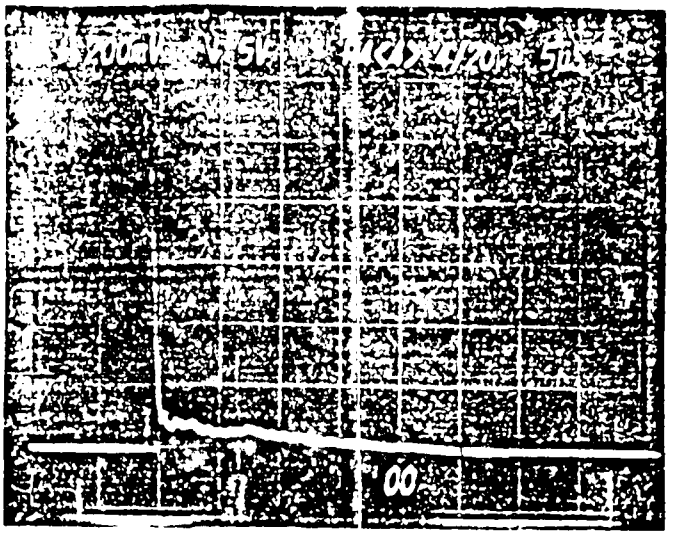

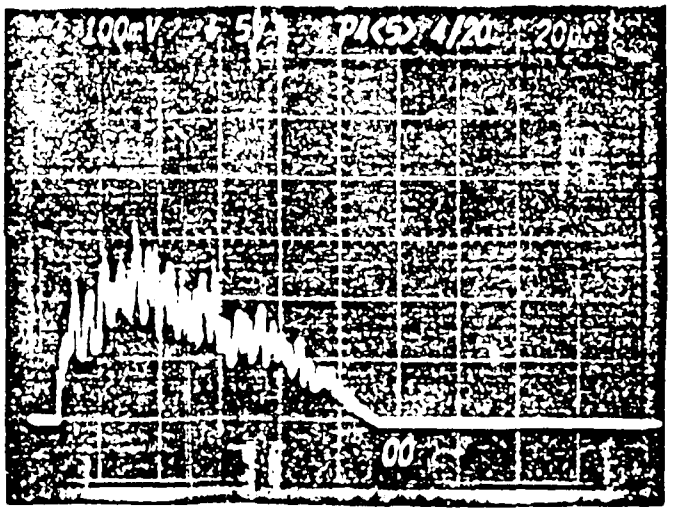

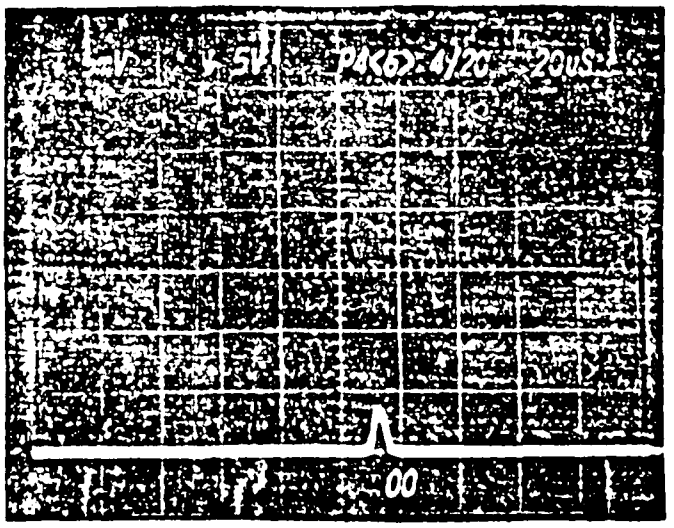

Table F.3 (Continued) 157

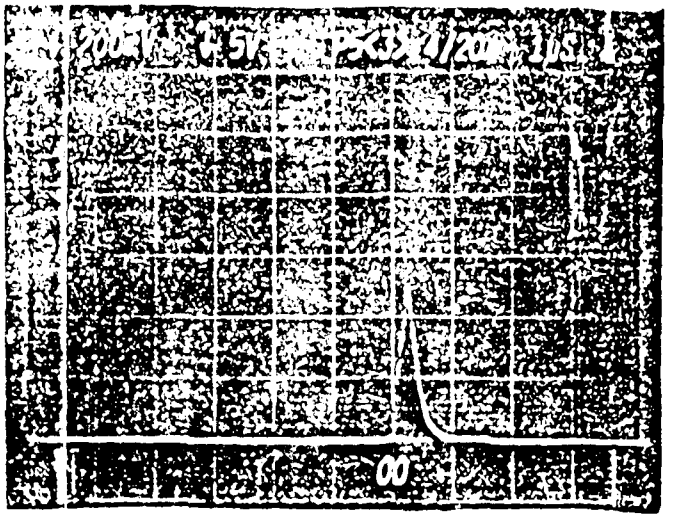

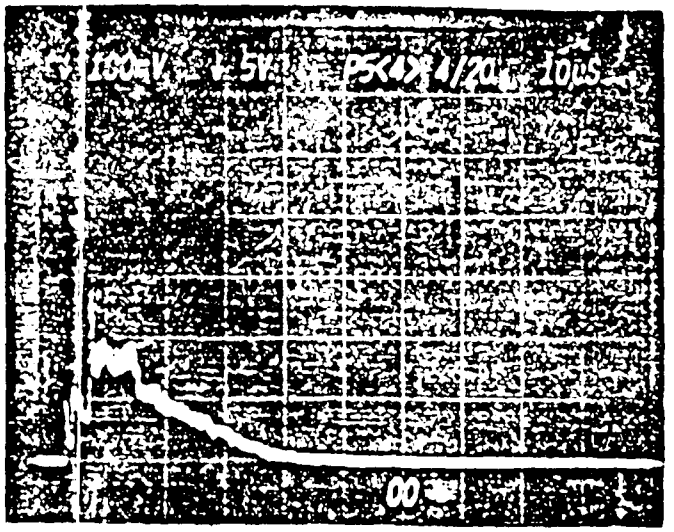

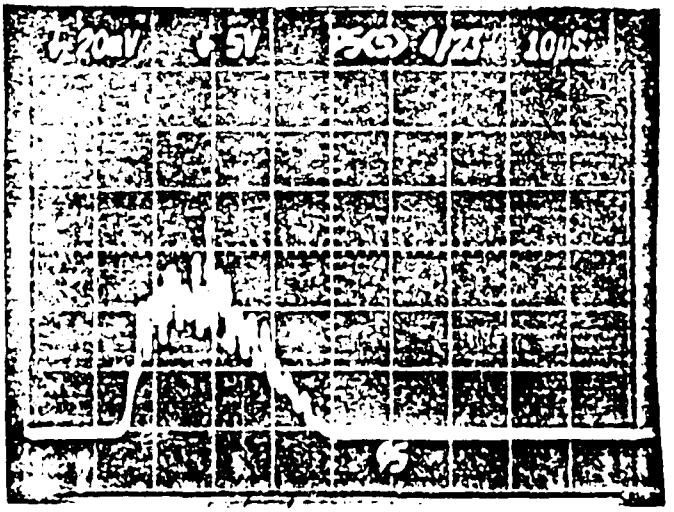

Table F.3 TEA photographes, $He:O_2:F_2:H_2$=20.8:1.0:4.6:1.2, 102 torr

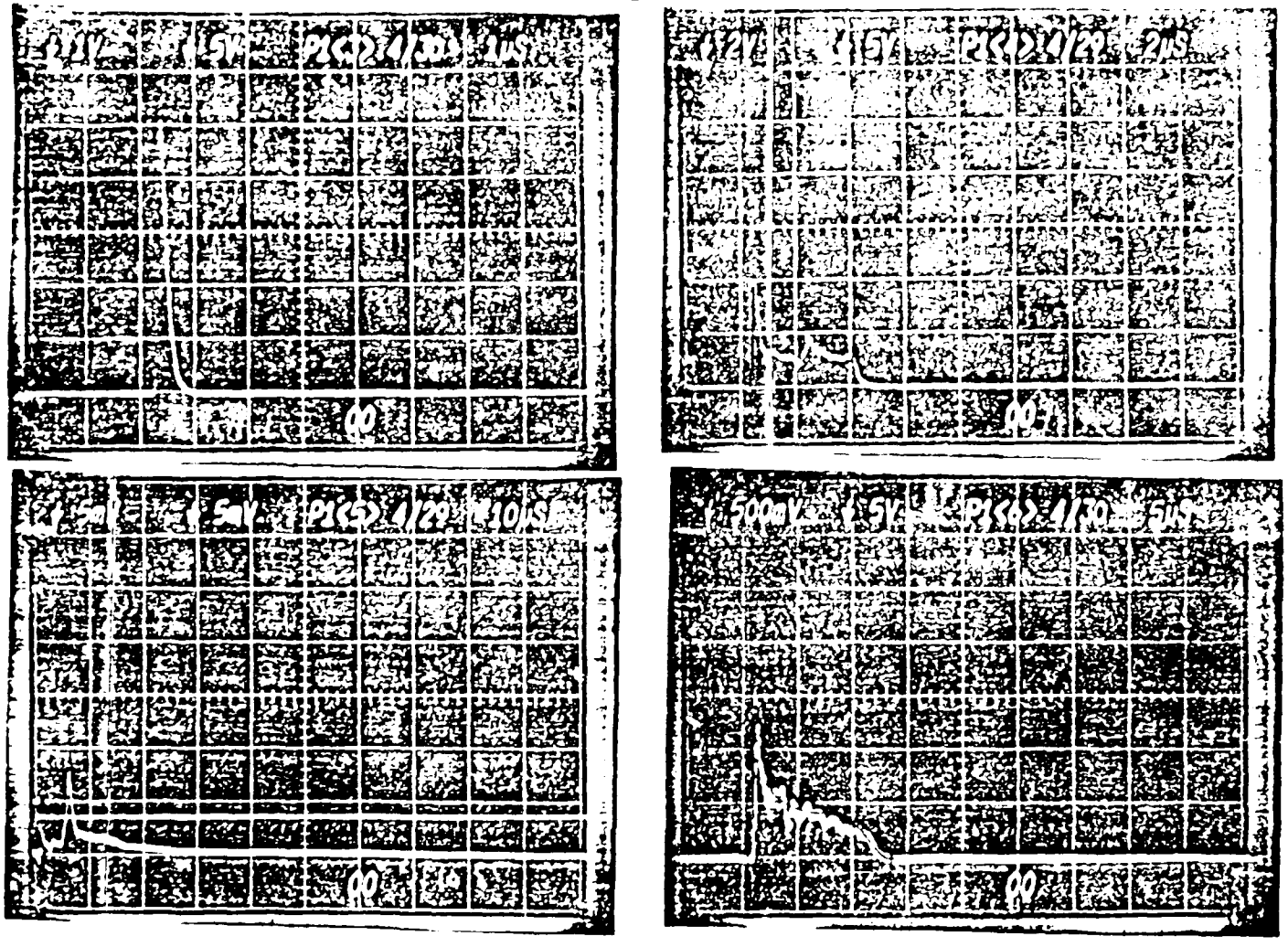

Table F.3 (Continued)

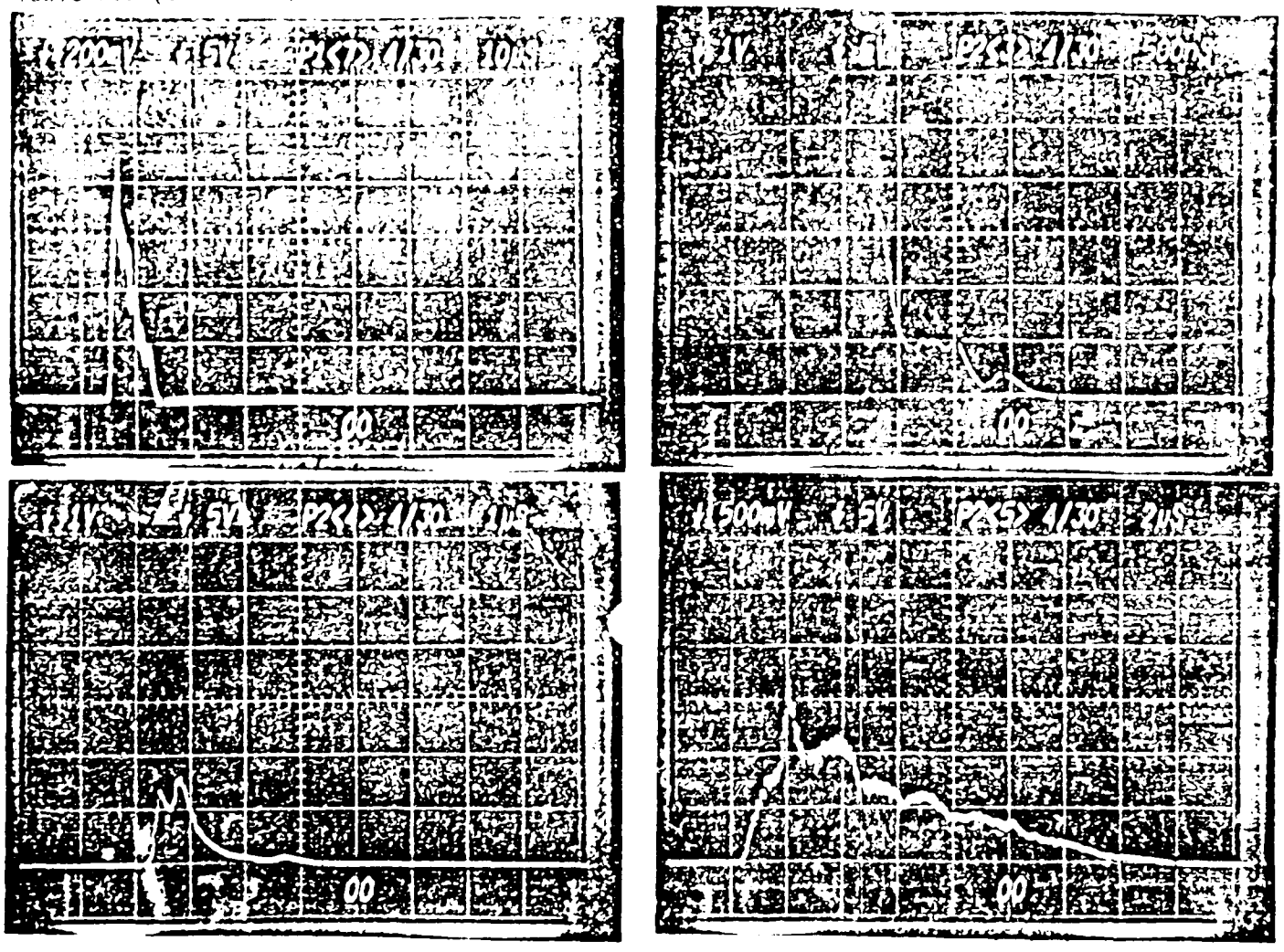

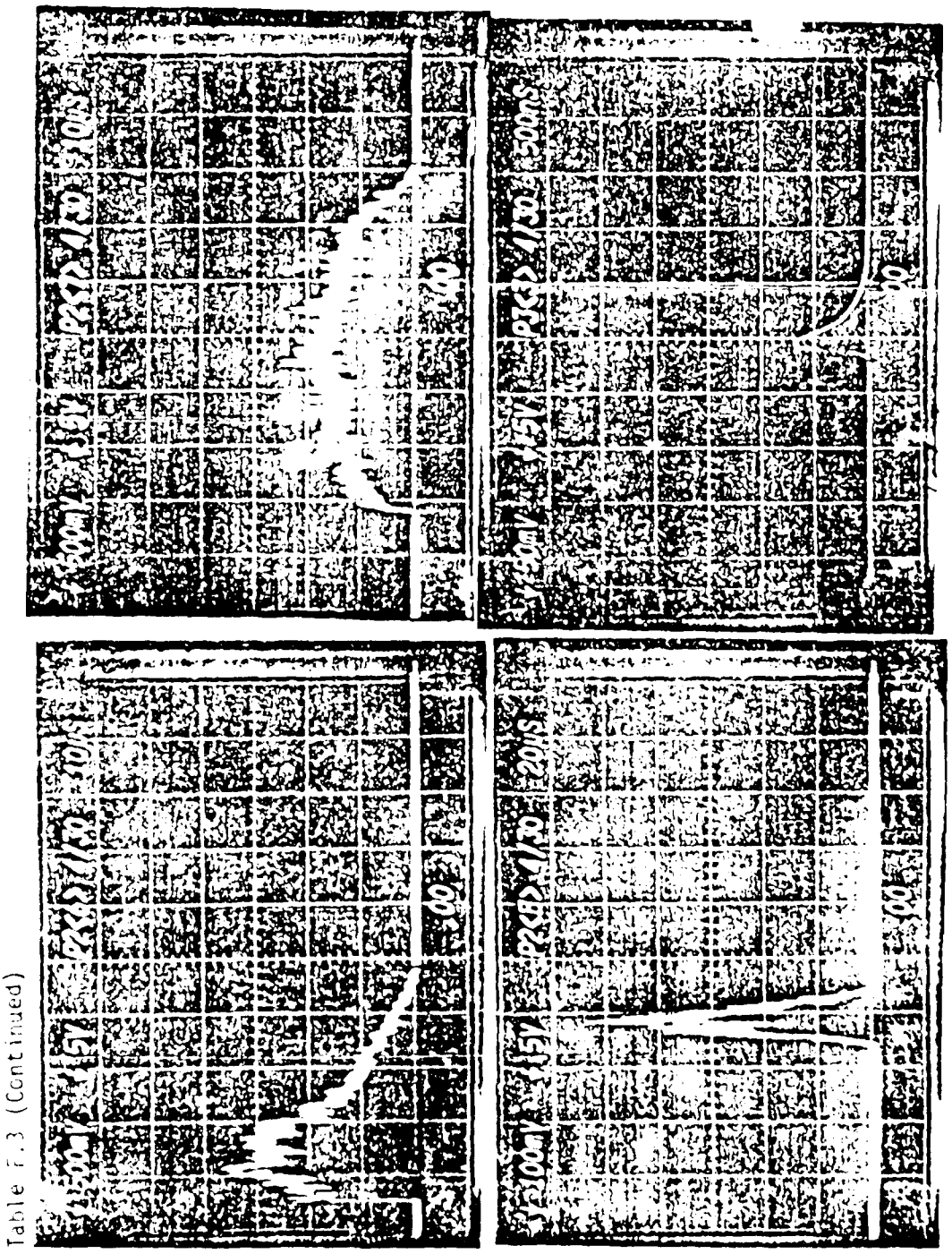

Table F.3 (Continued)

Table F.3 (Continued)

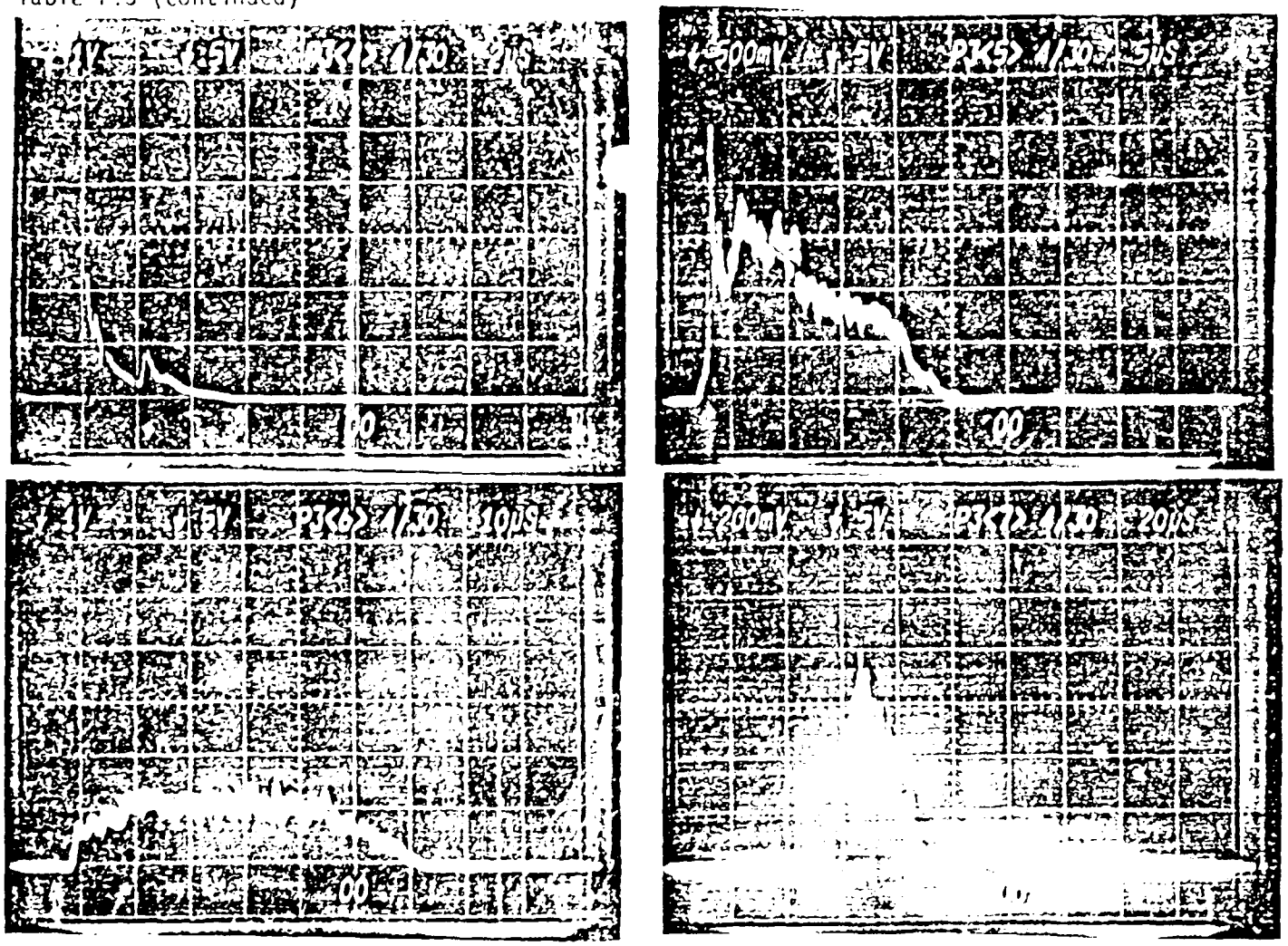

Table F.3 (Continued)

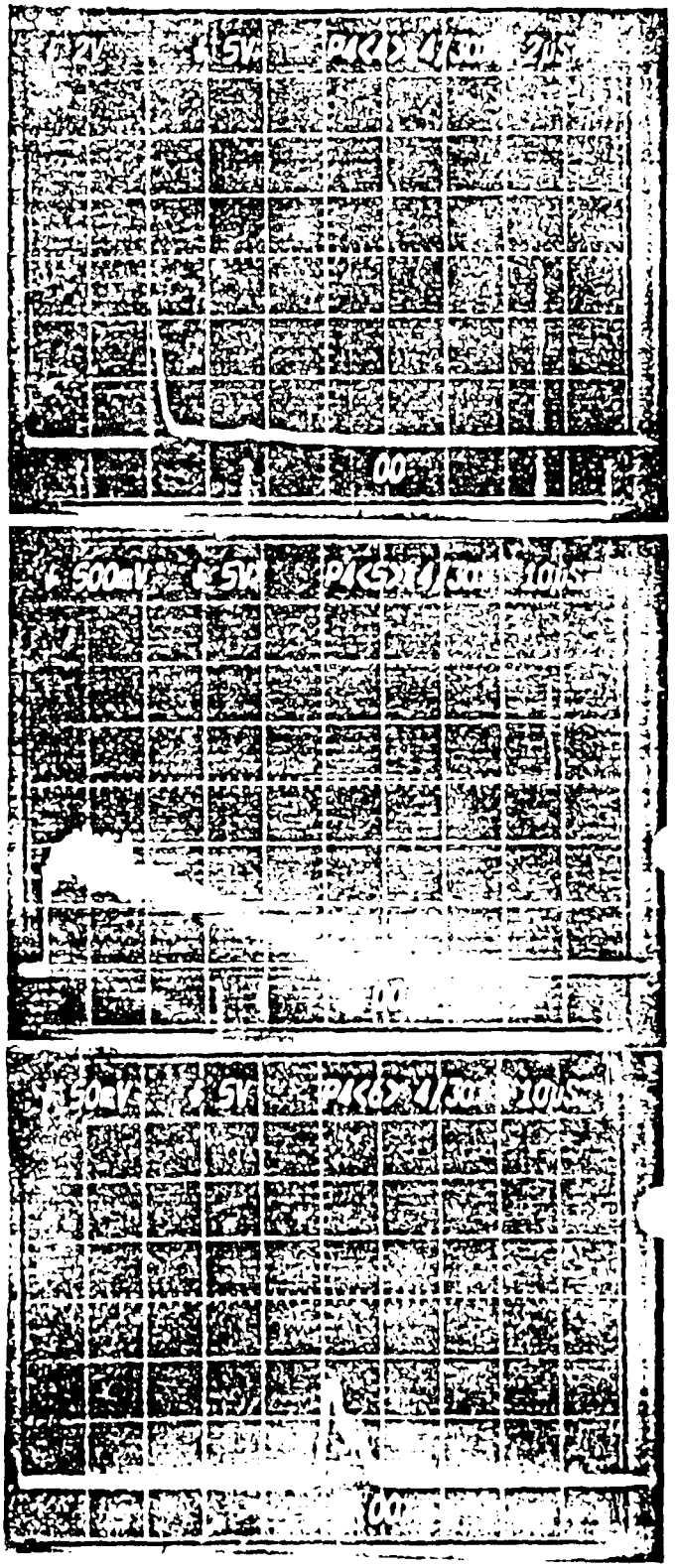

Table F.3 (Continued)

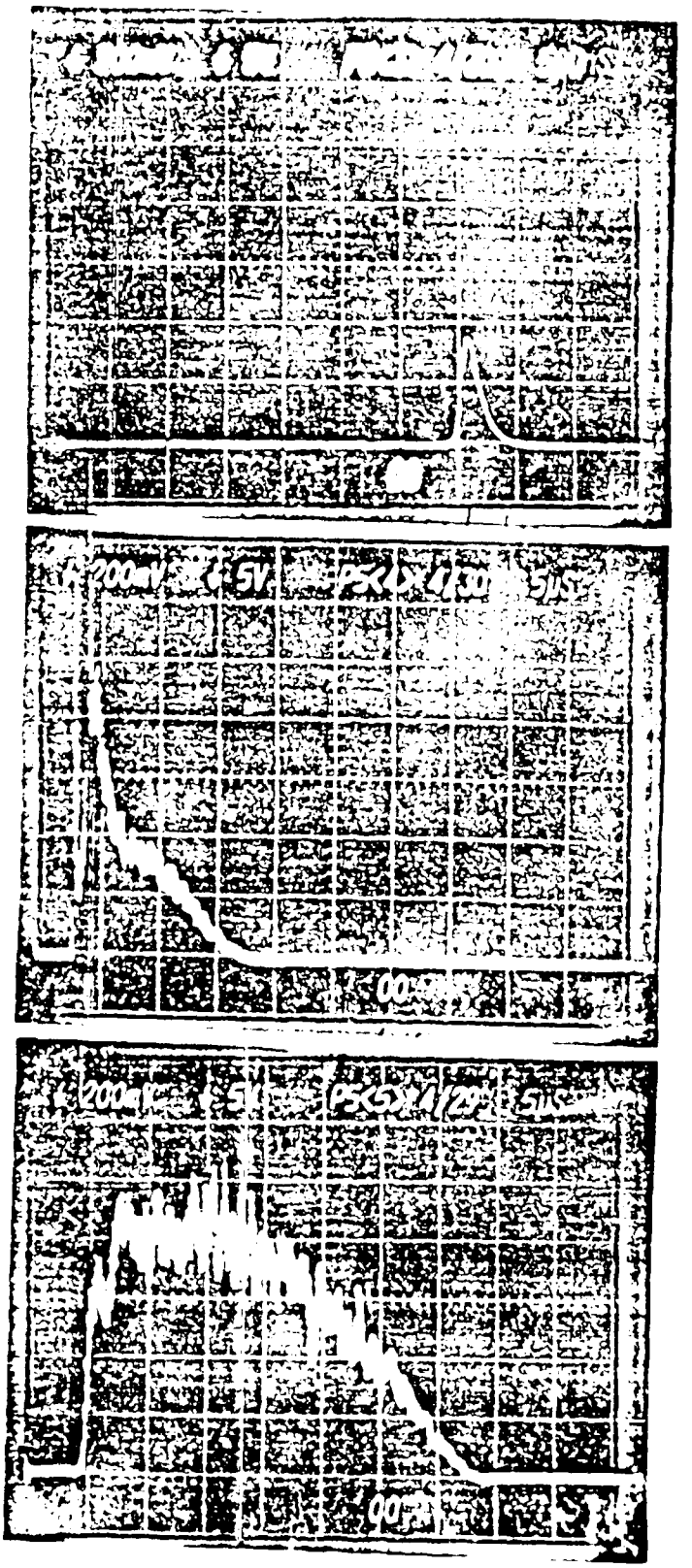

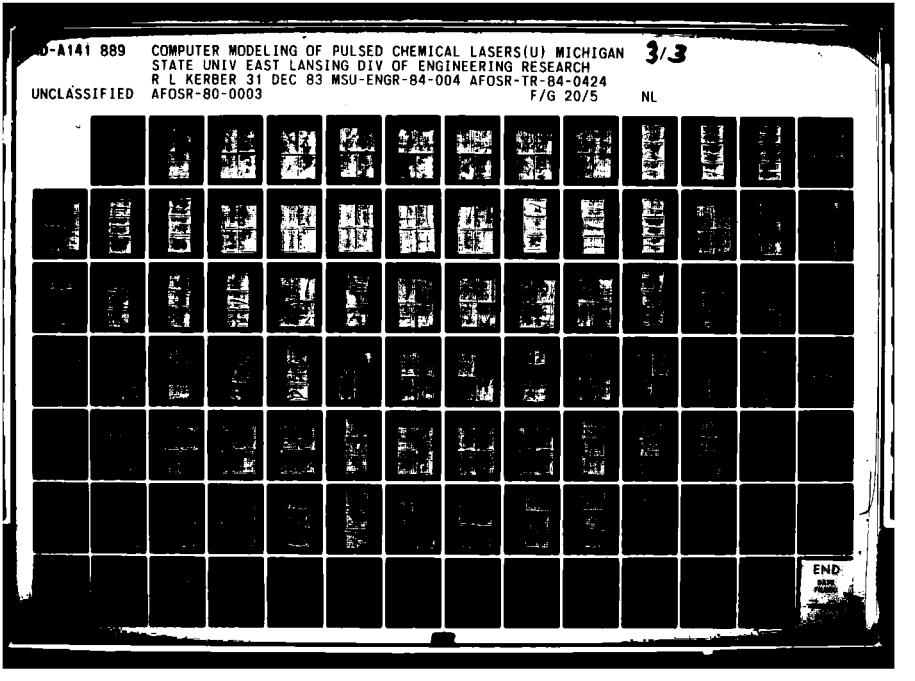
D-A141 889 COMPUTER MODELING OF PULSED CHEMICAL LASERS(U) MICHIGAN
STATE UNIV EAST LANSING DIV OF ENGINEERING RESEARCH
R L KERBER 31 DEC 83 MSU-ENGR-84-004 AFOSR-TR-84-0424
UNCLASSIFIED AFOSR-80-0003 F/G 20/5 NL
3/3
END

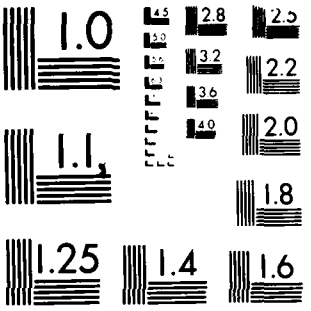

Table F.3 (Continued)

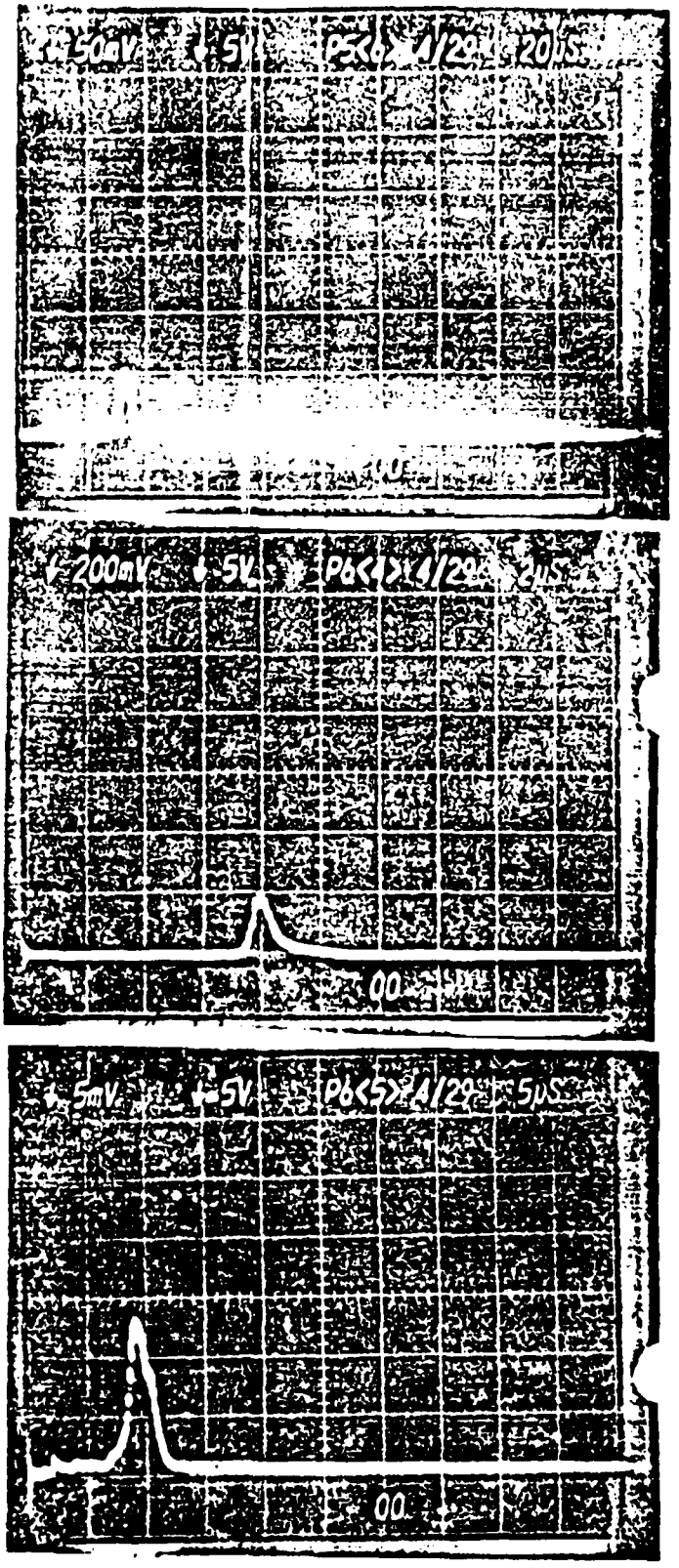

Table F.4 TRS photographes, He:O_2:F_2:H_2=20.8:1.0:4.6:1.2, 331 torr

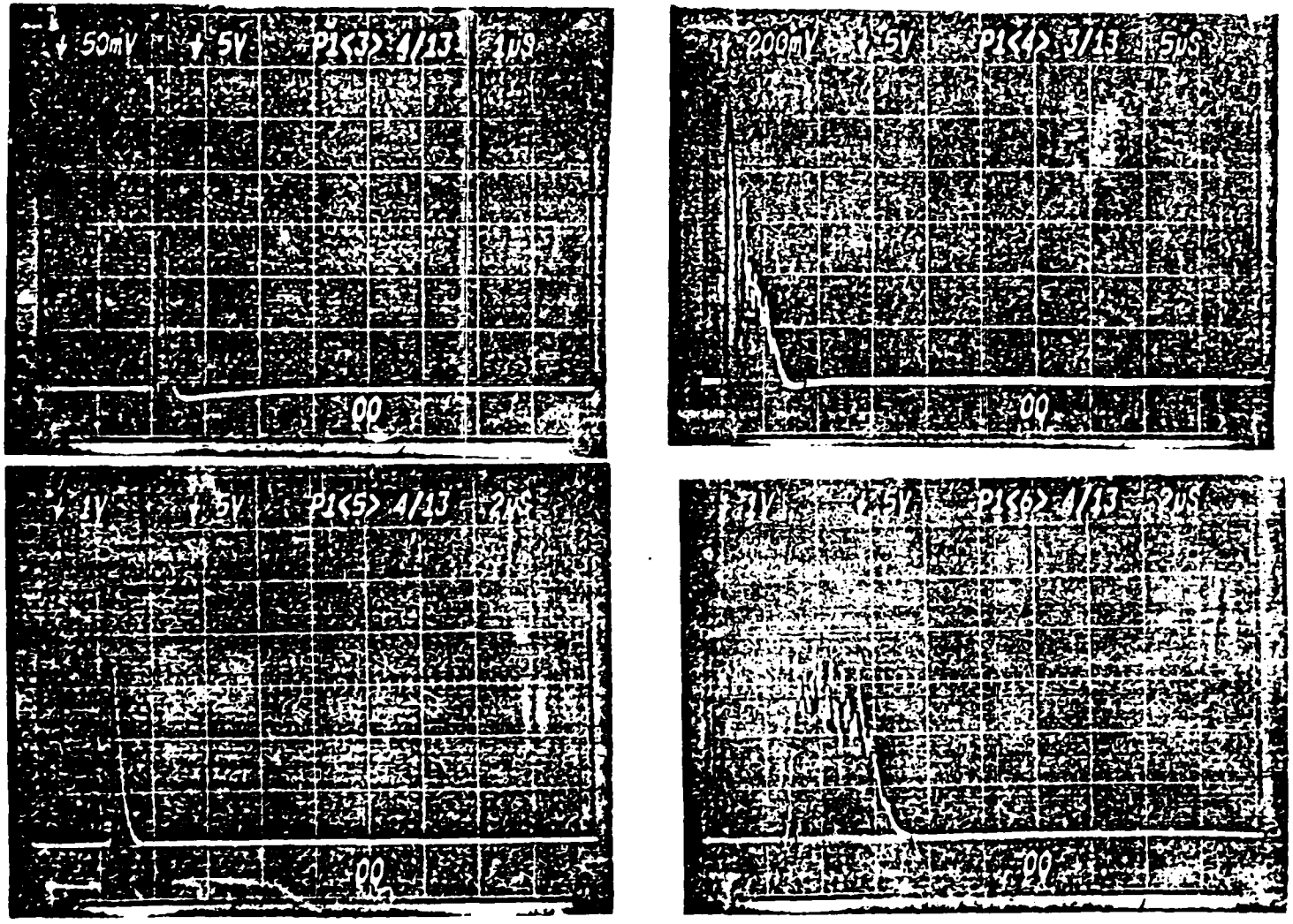

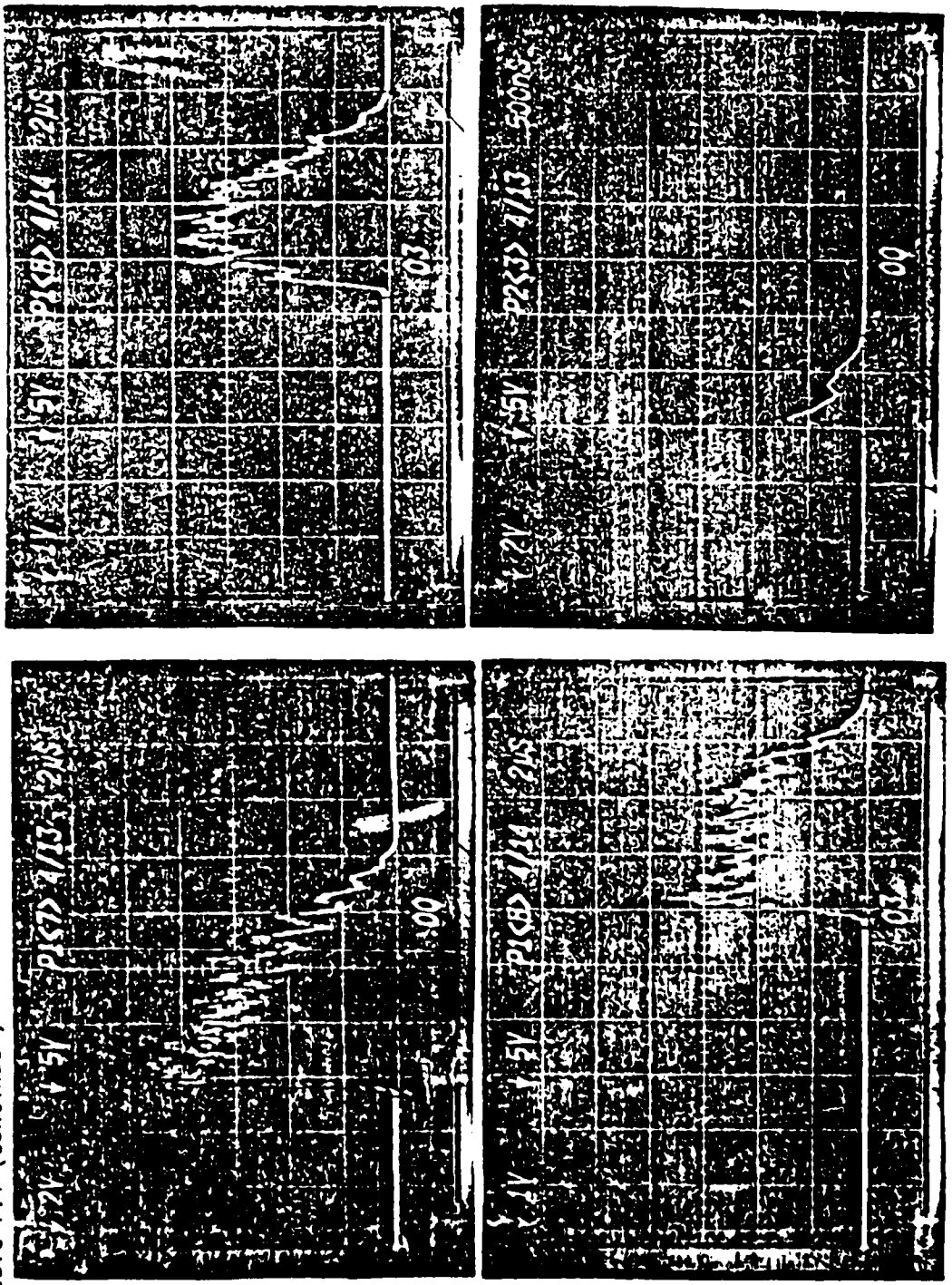

Table F.4 (Continued)

Table F.4 (Continued)

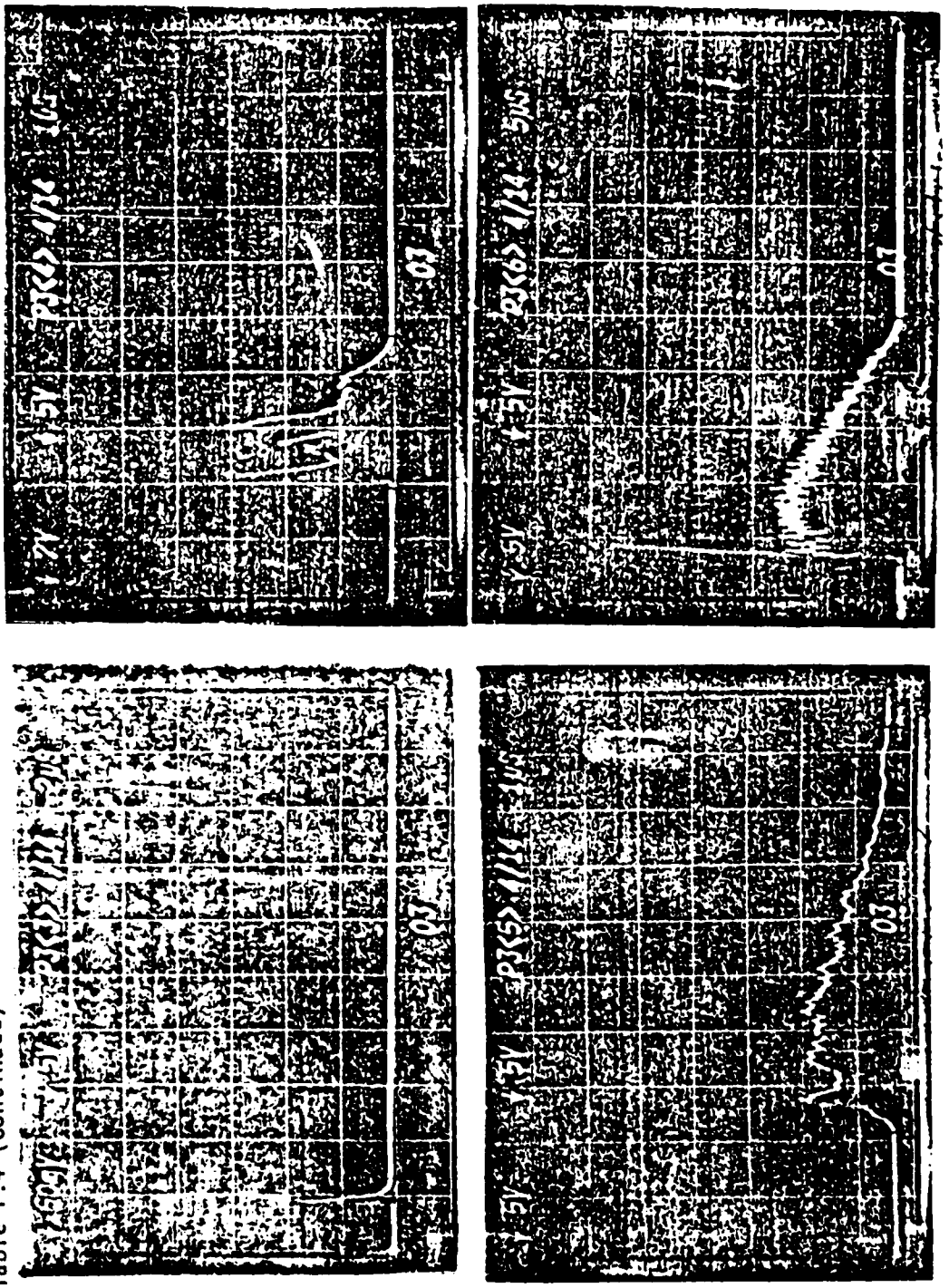

Table F.4 (Continued)

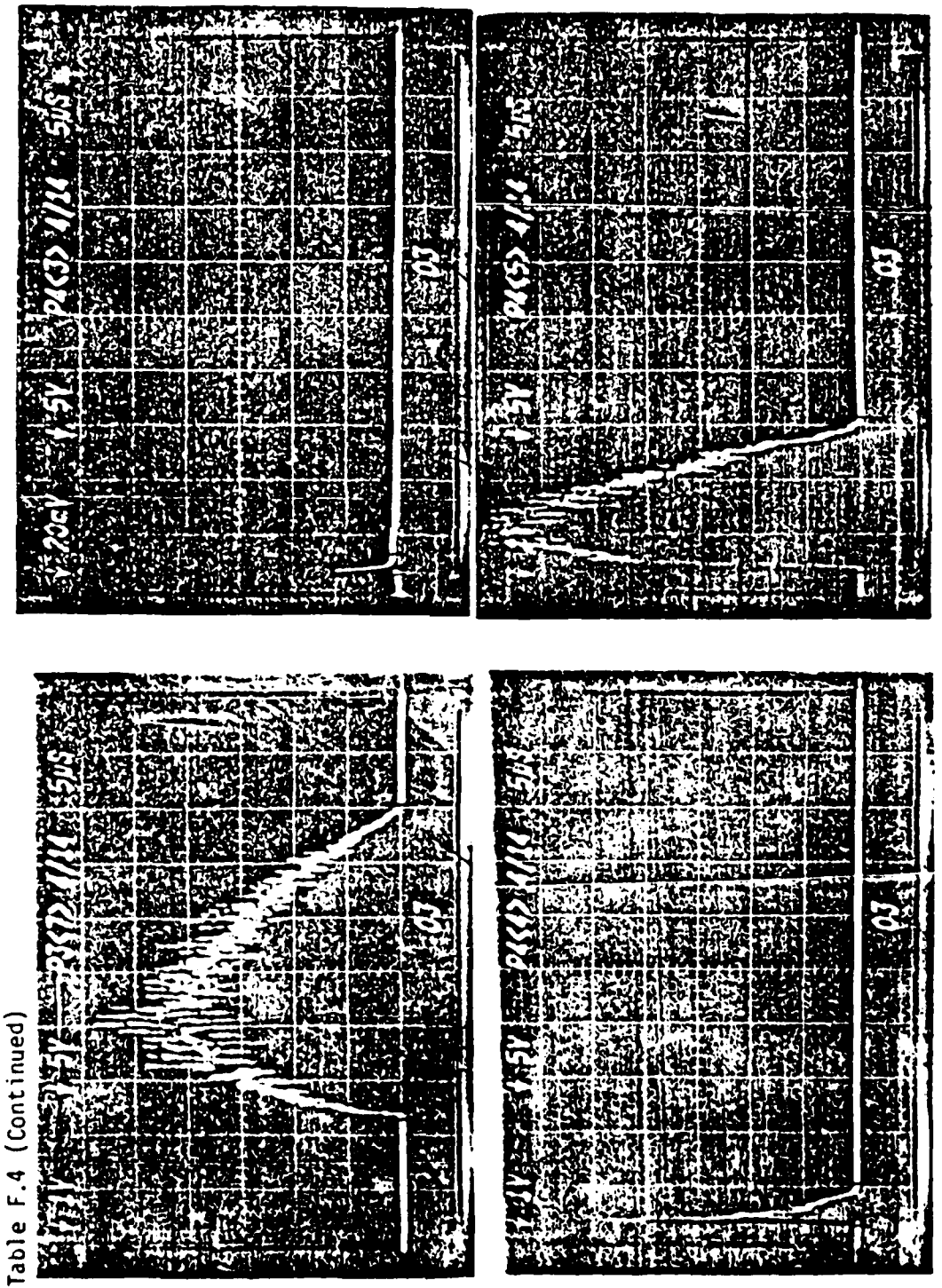

Table F.4 (Continued)

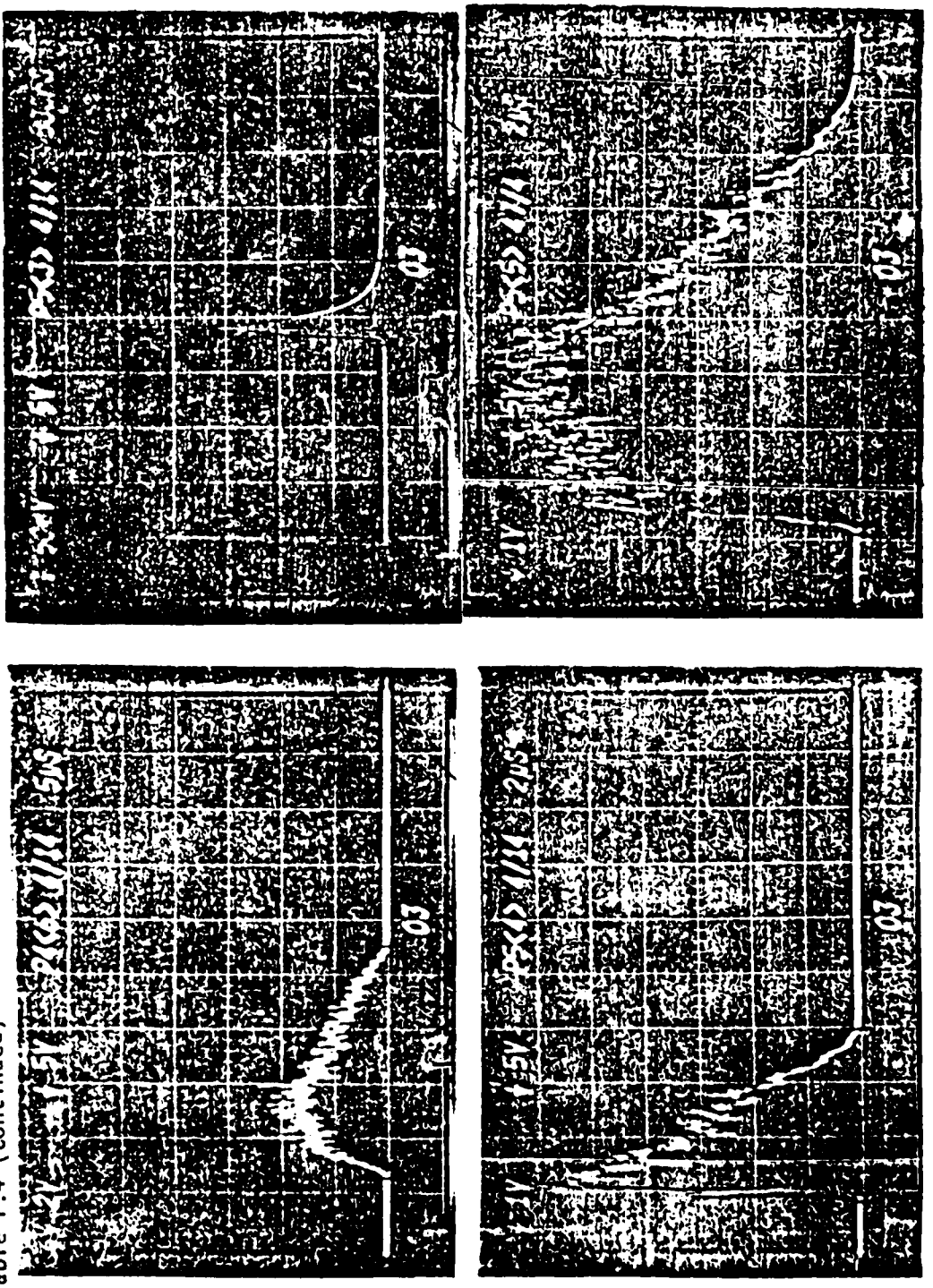

Table F.4 (Continued)

Table F.4 (Continued)

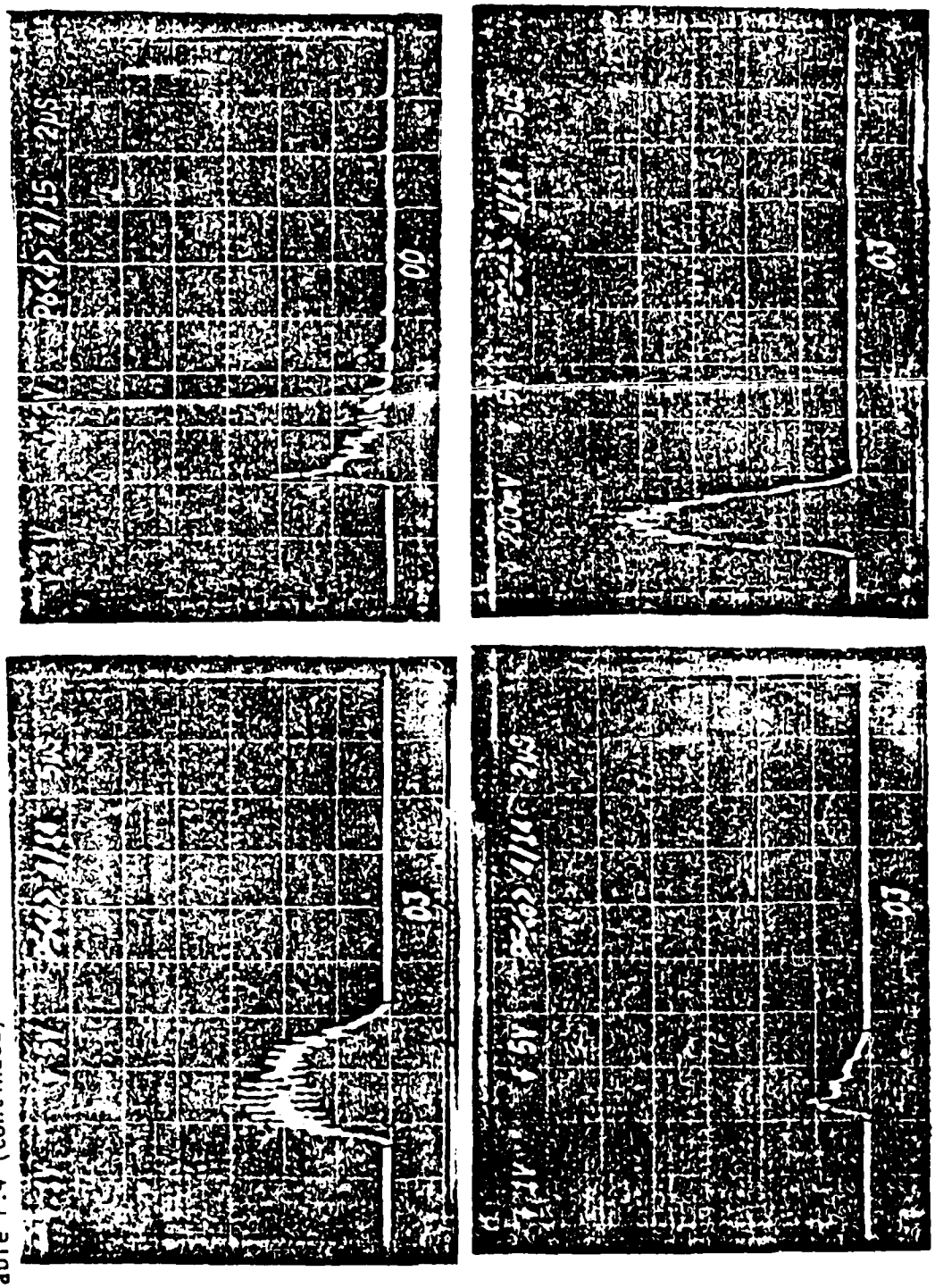

Table F.5 SSG photographes, $He:O_2:F_2:H_2$=22.0:1.0:2.7:1.0, 102 torr

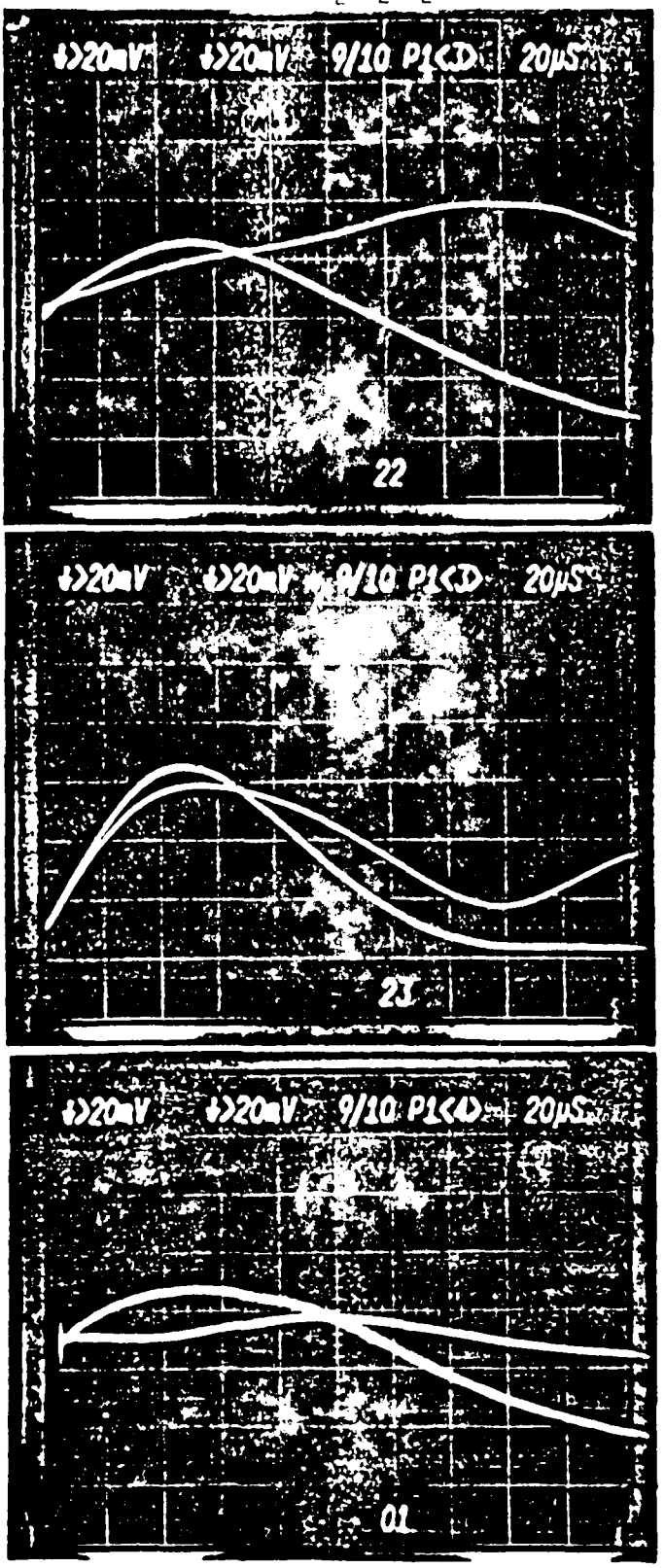

Table F.5 (Continued)

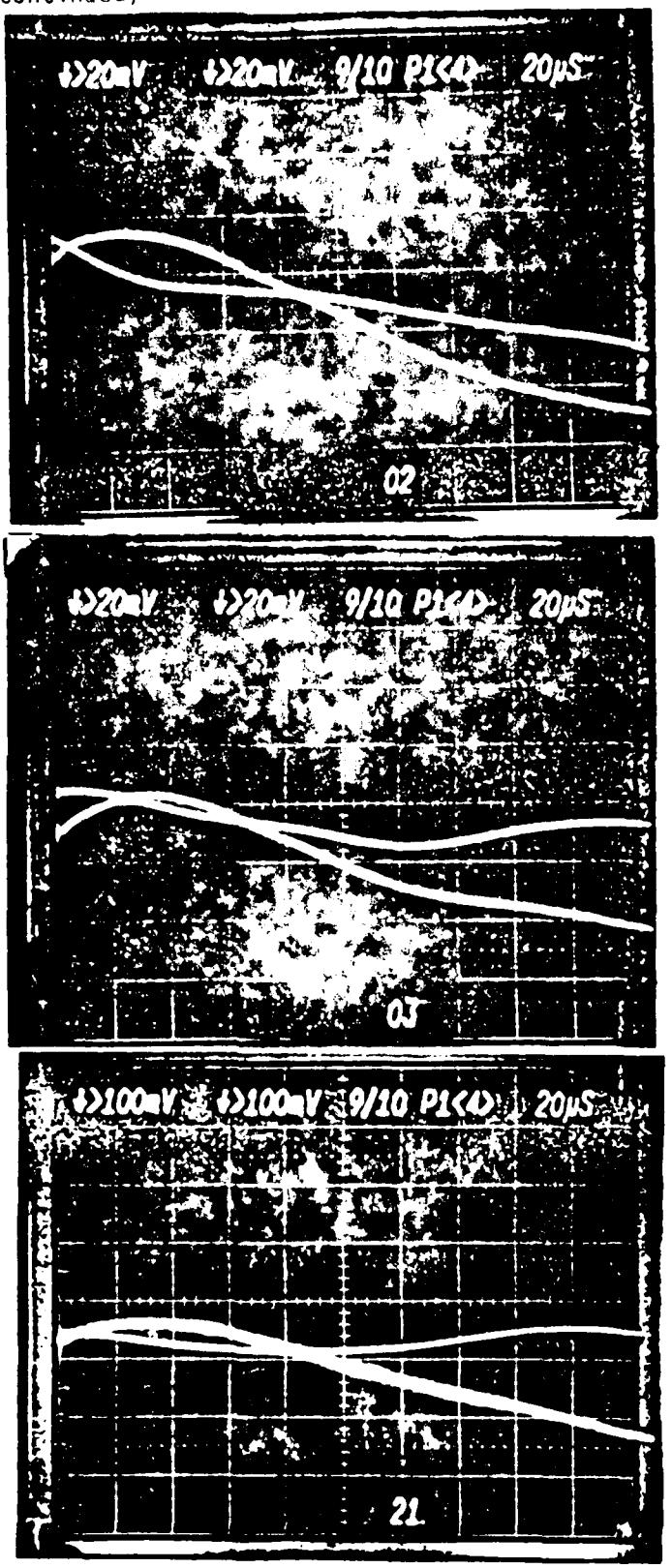

Table F.5 (Continued)

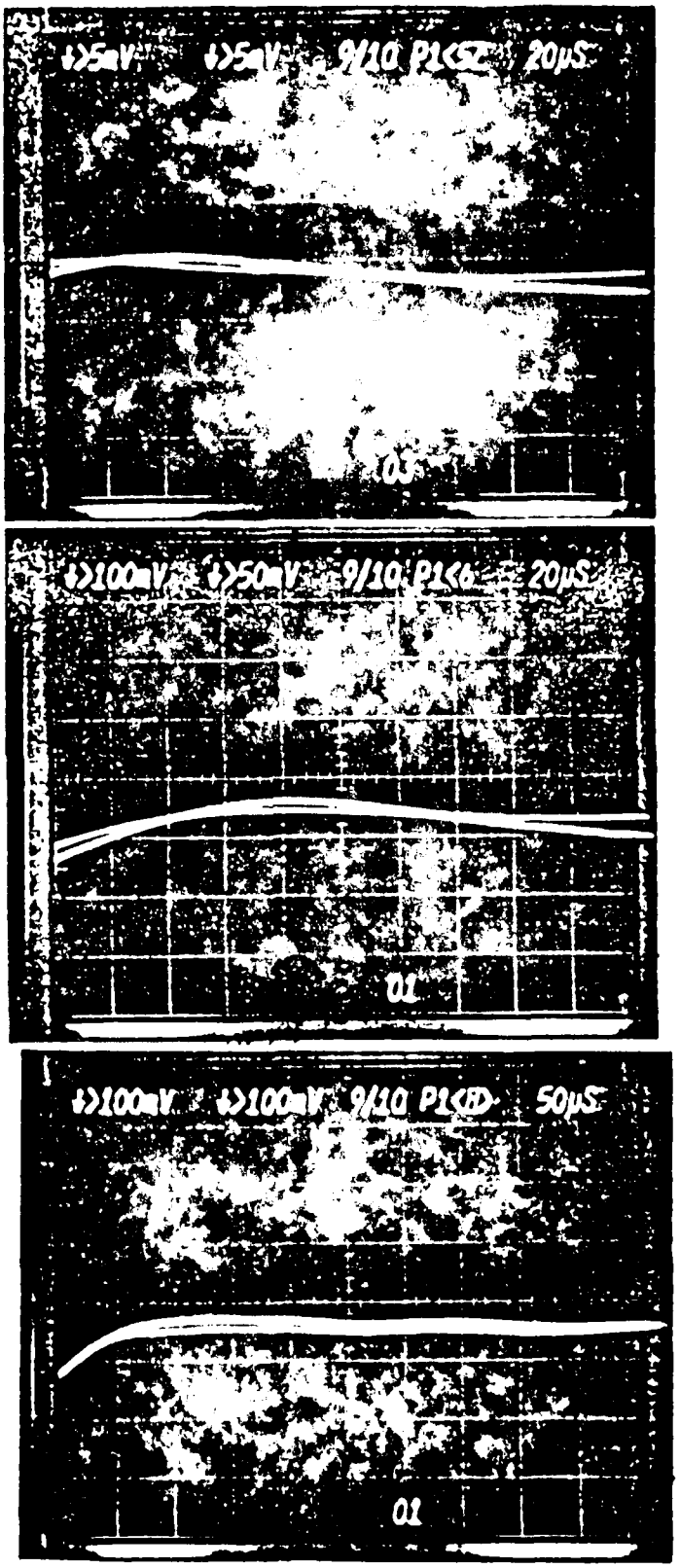

Table F.5 (Continued)

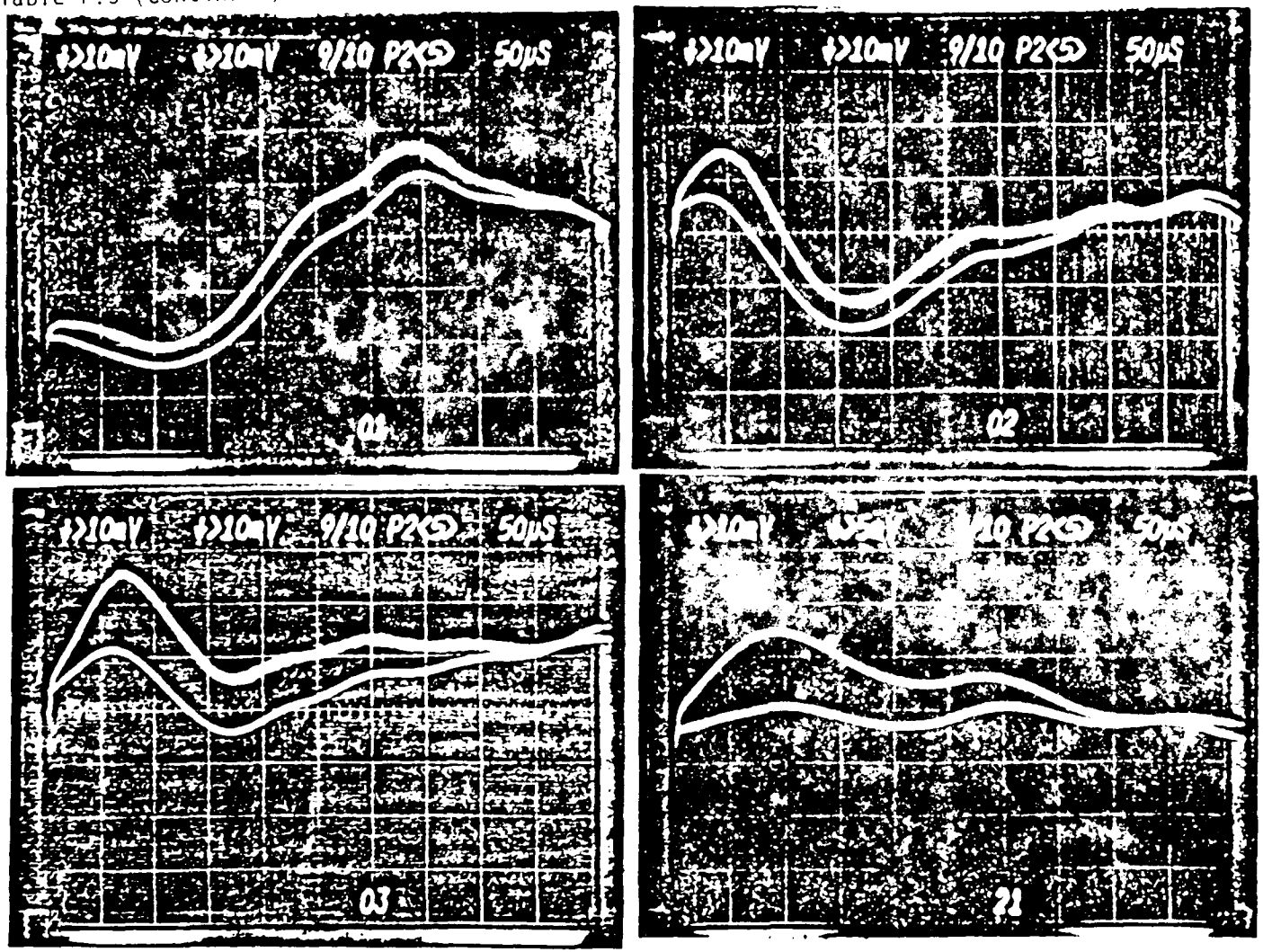

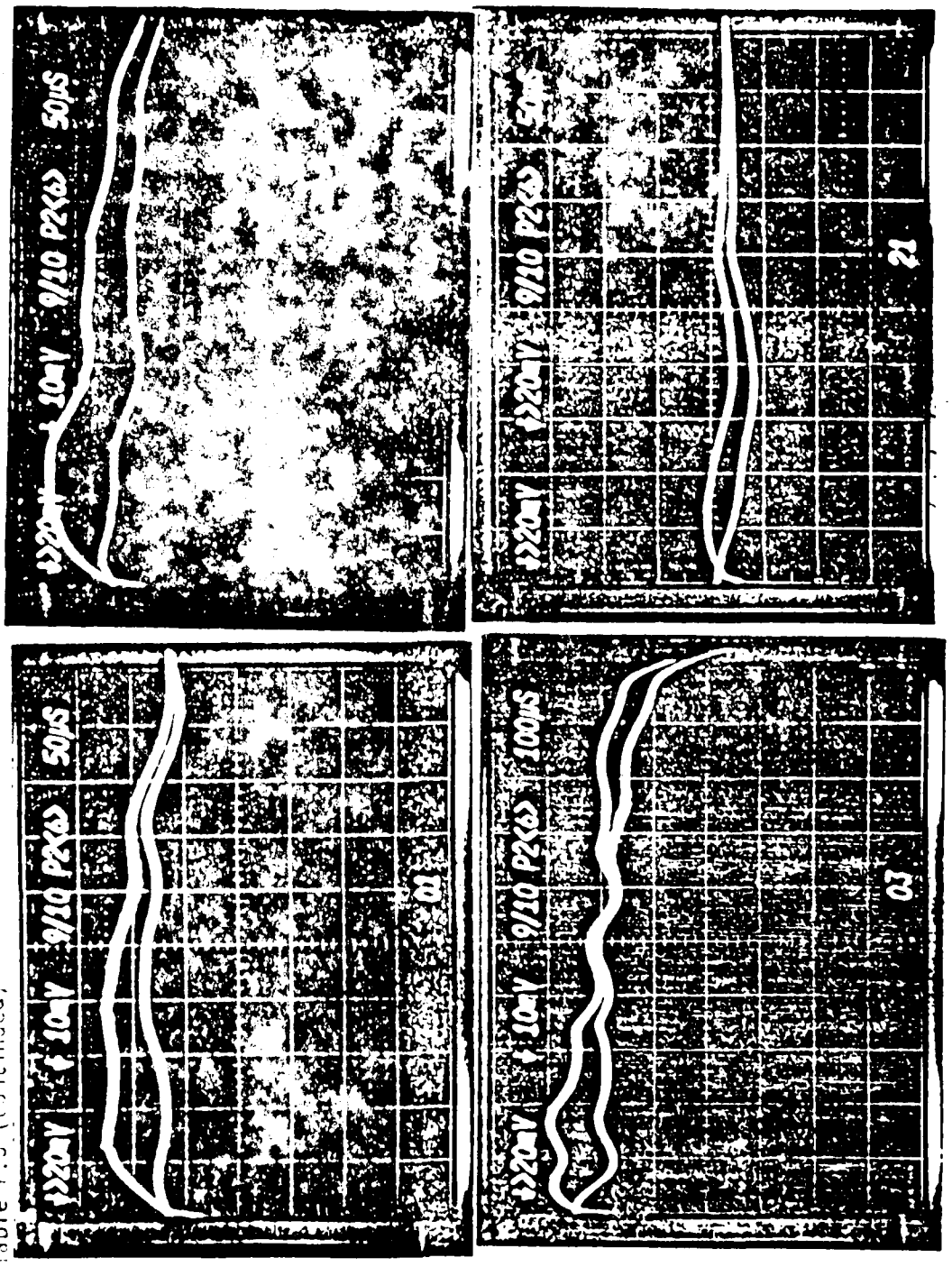

Table F.5 (Continued)

Table F.5 (Continued)

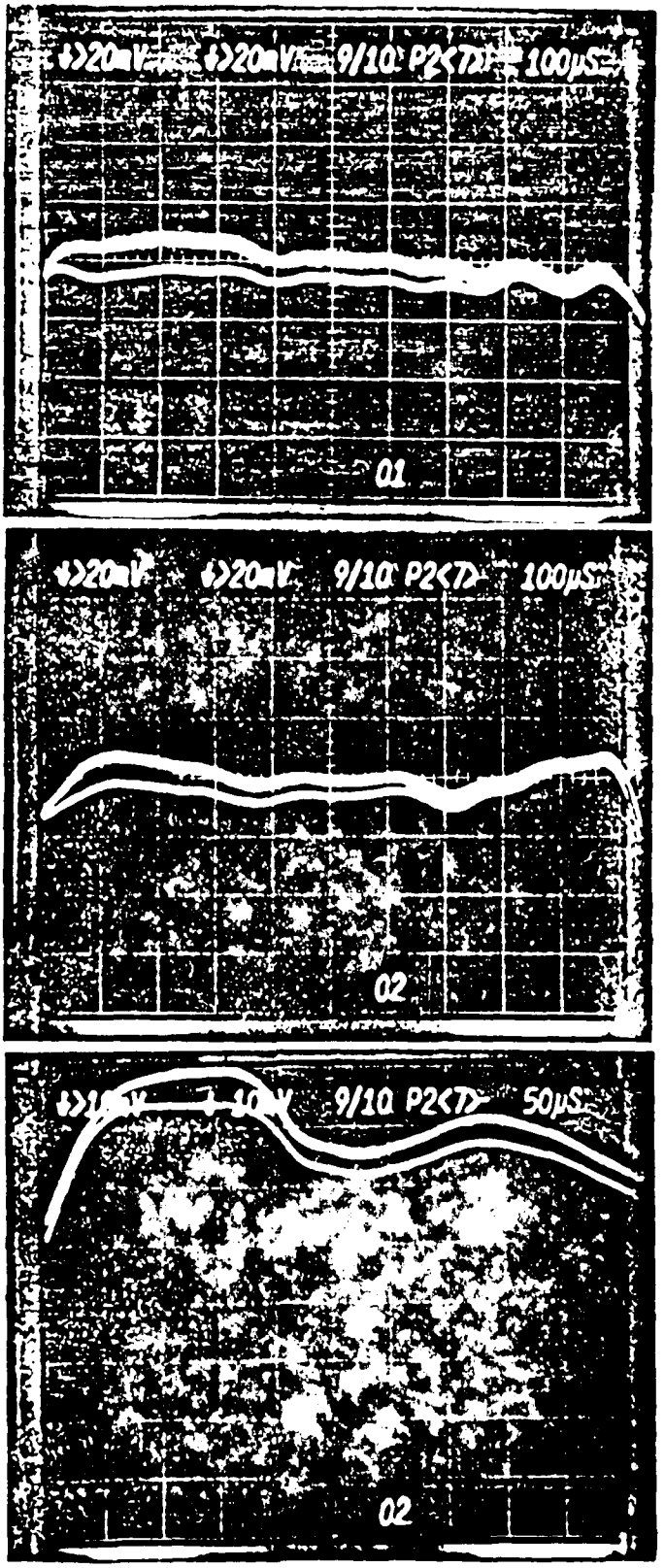

Table F.5 (Continued)

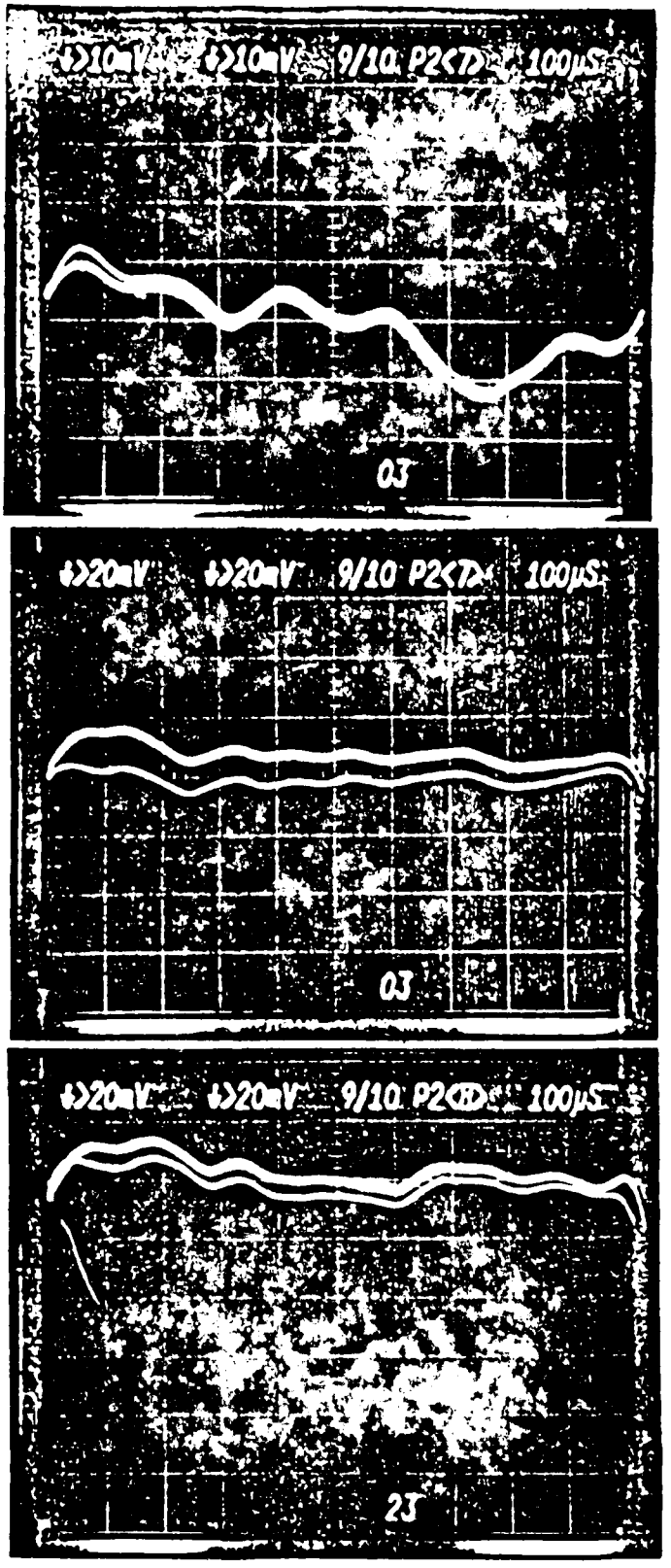

Table F.6 SSG photographes, $He:O_2:F_2:H_2$=22.0:1.0:2.7:1.0, 331 torr

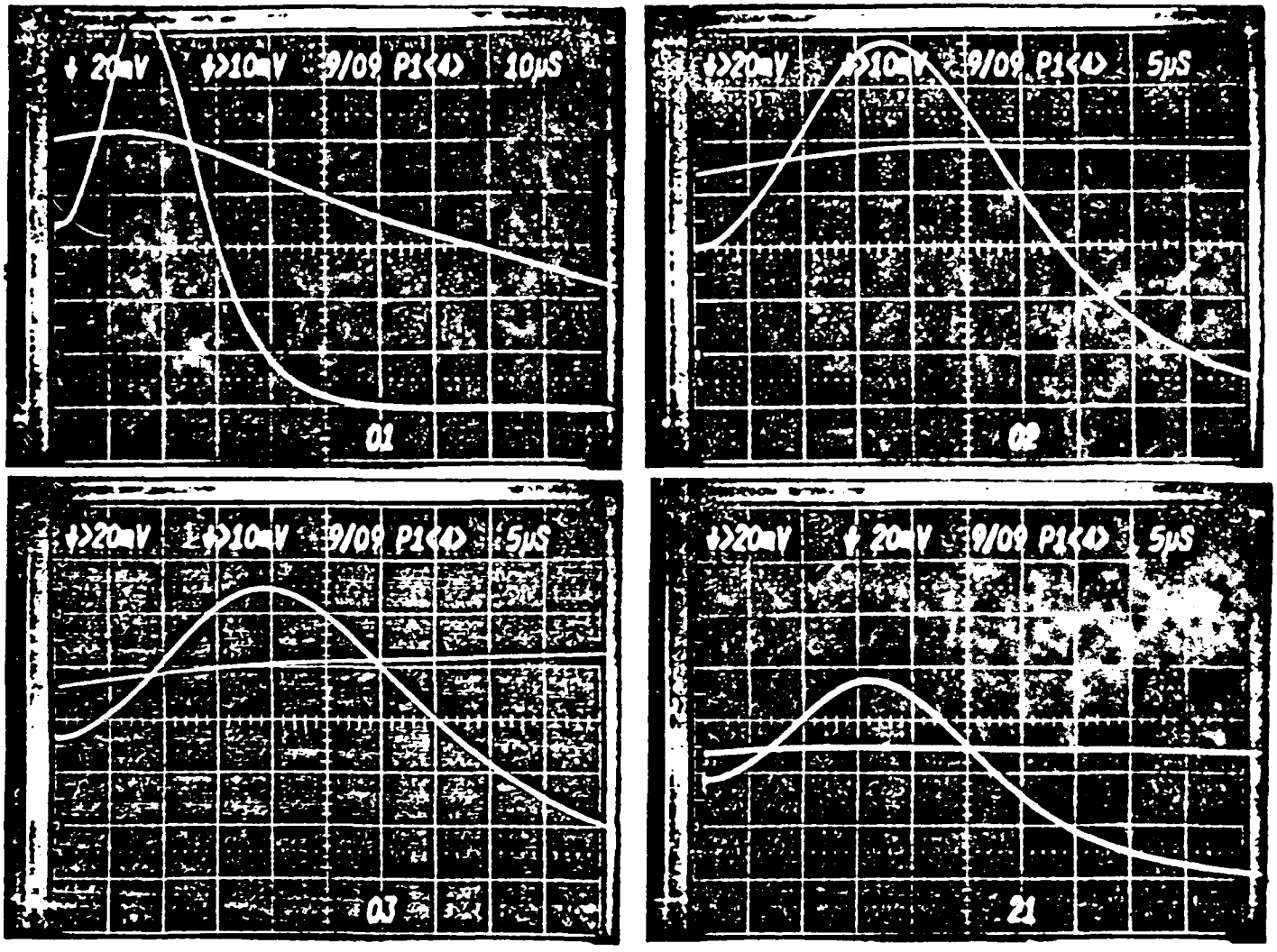

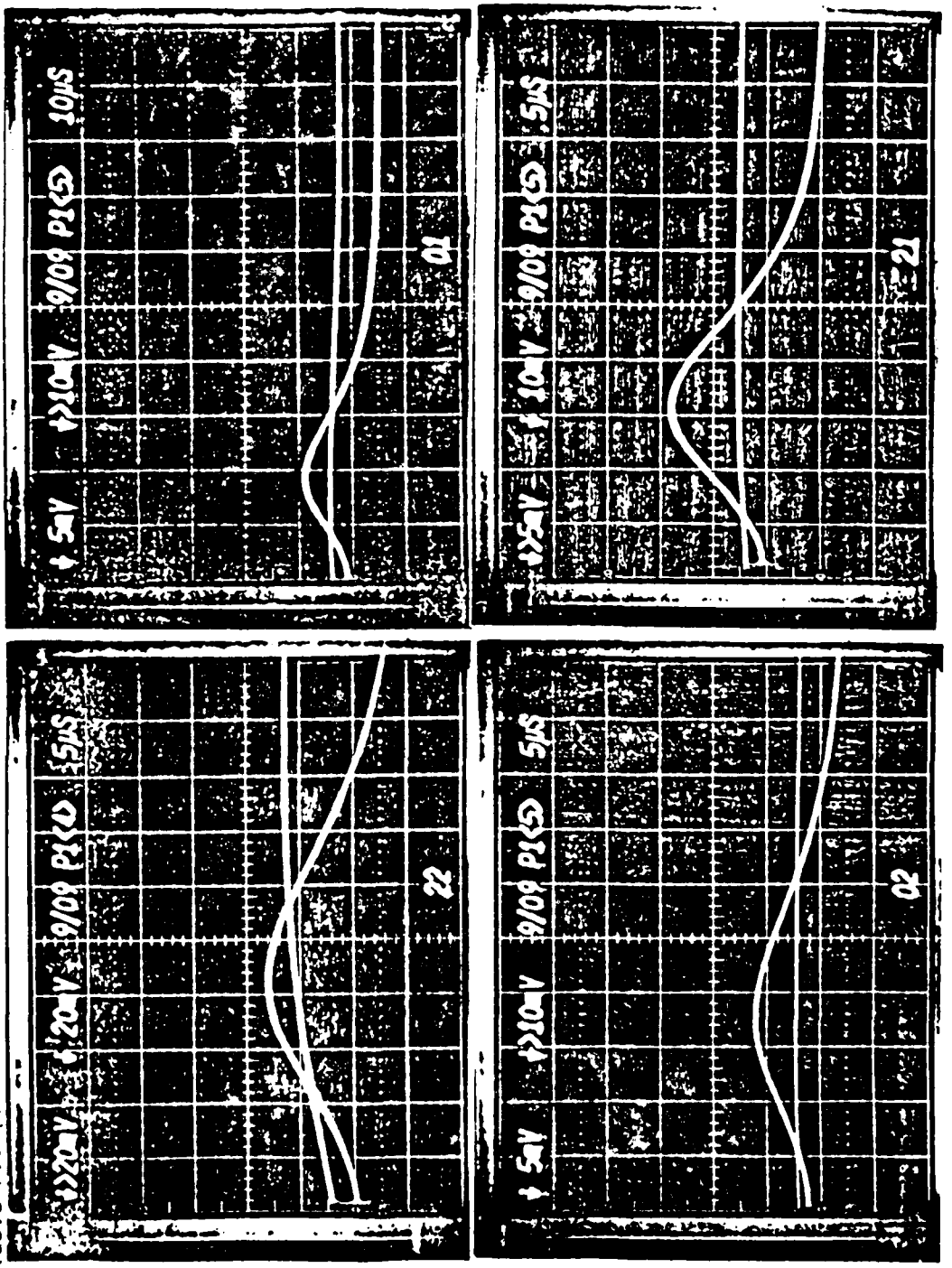

Table F.6 (Continued)

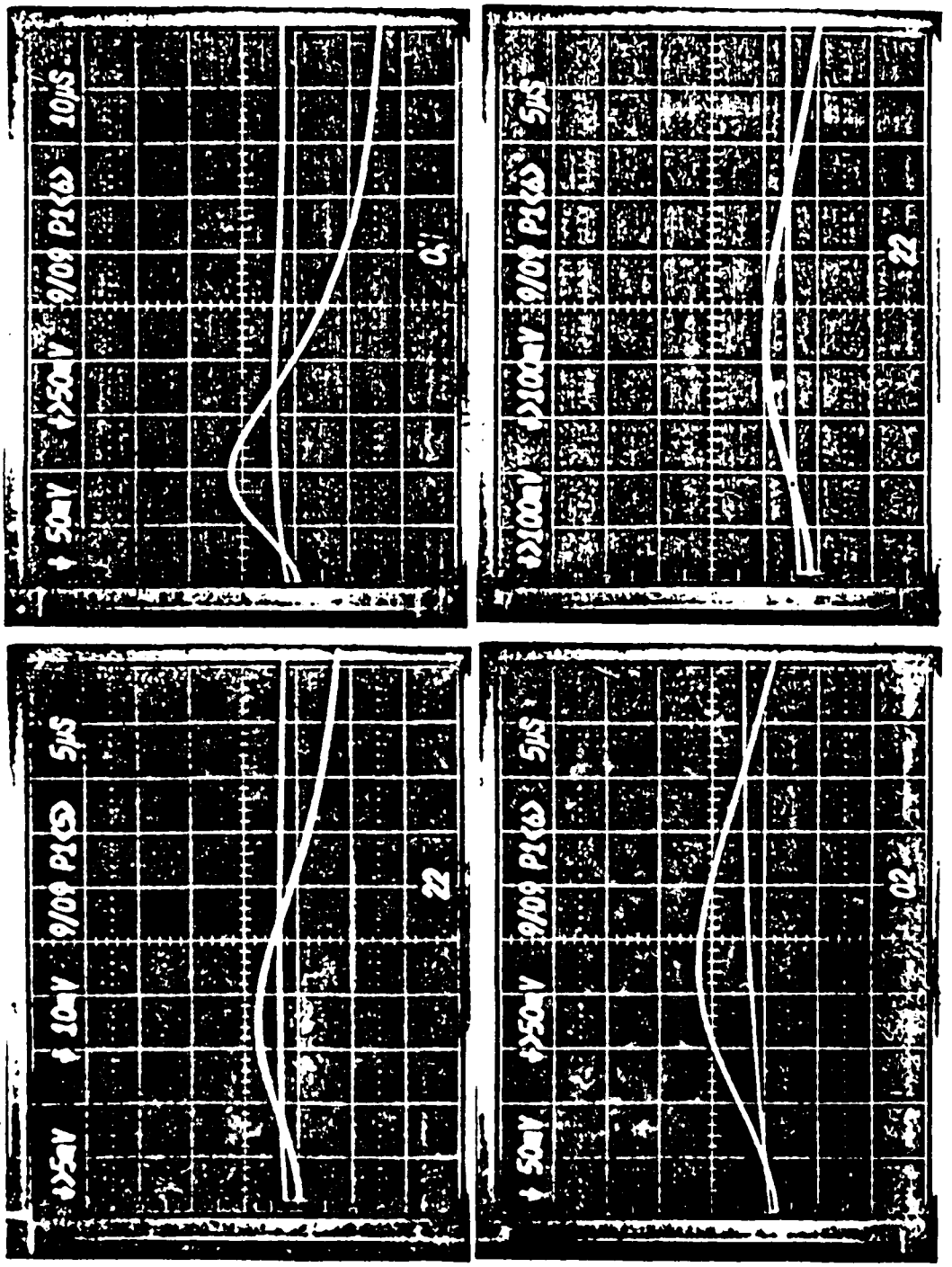

Table F.6 (Continued)

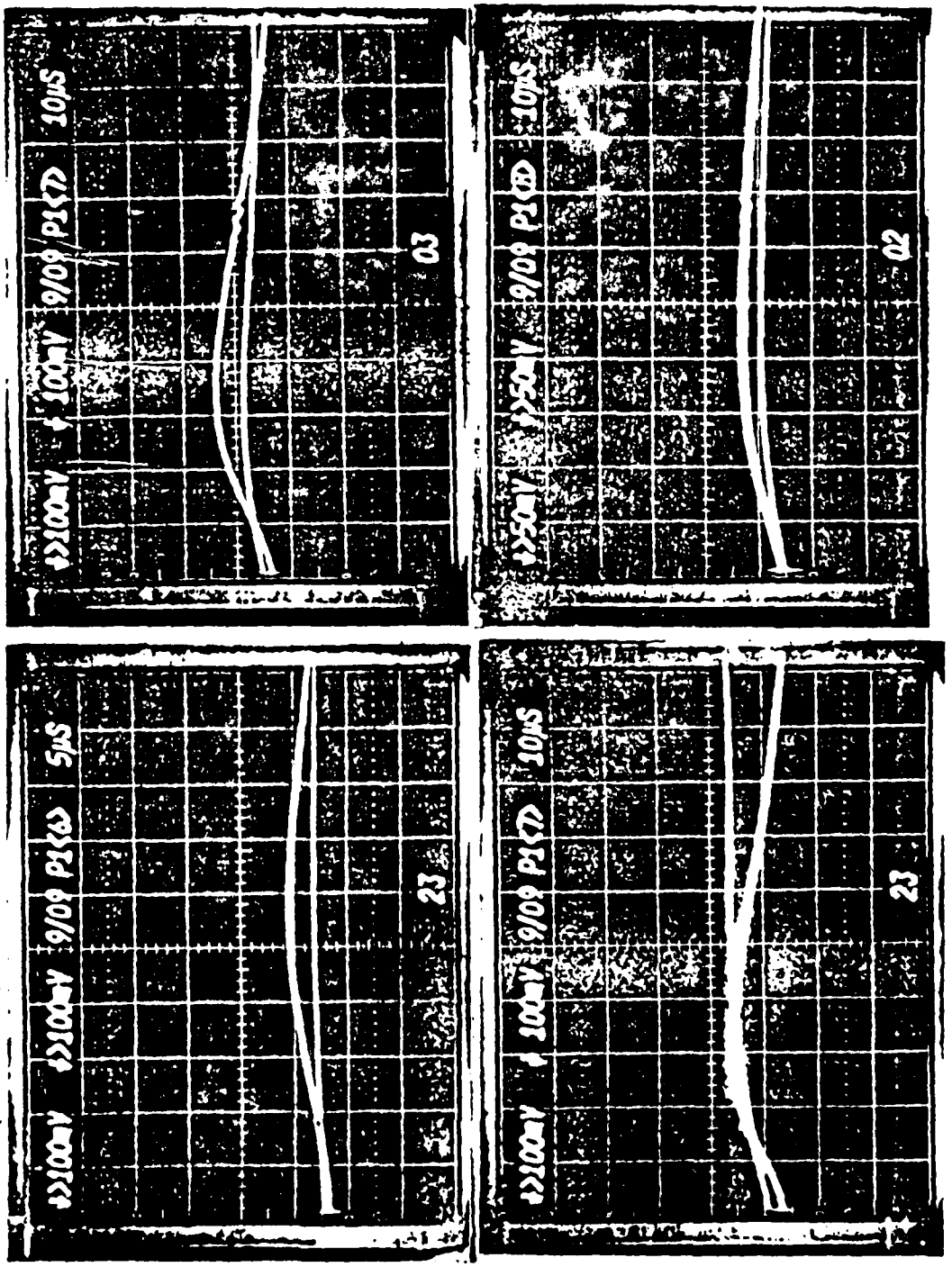

Table F.6 (Continued)

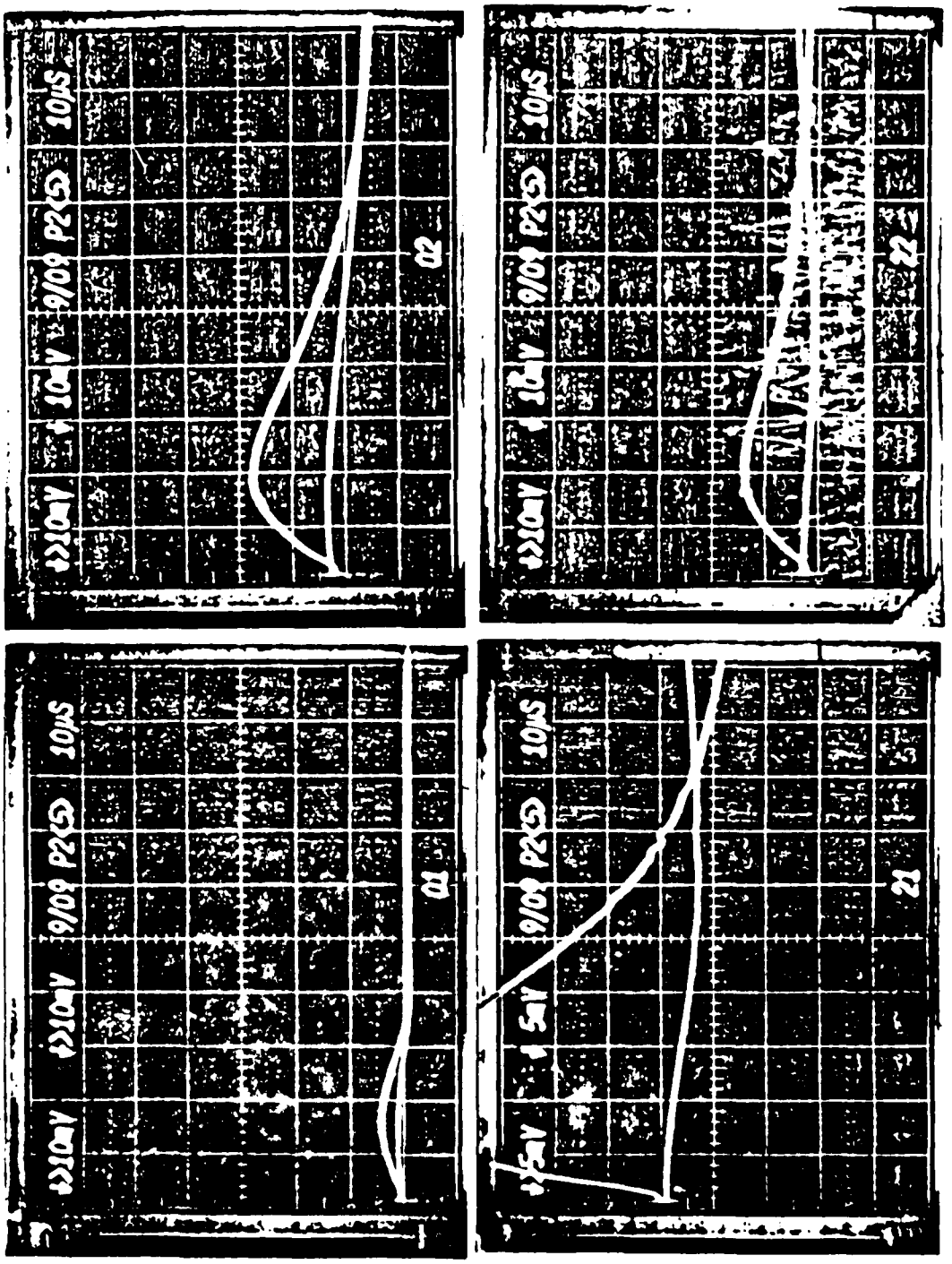

Table F.6 (Continued)

Table F.6 (Continued)

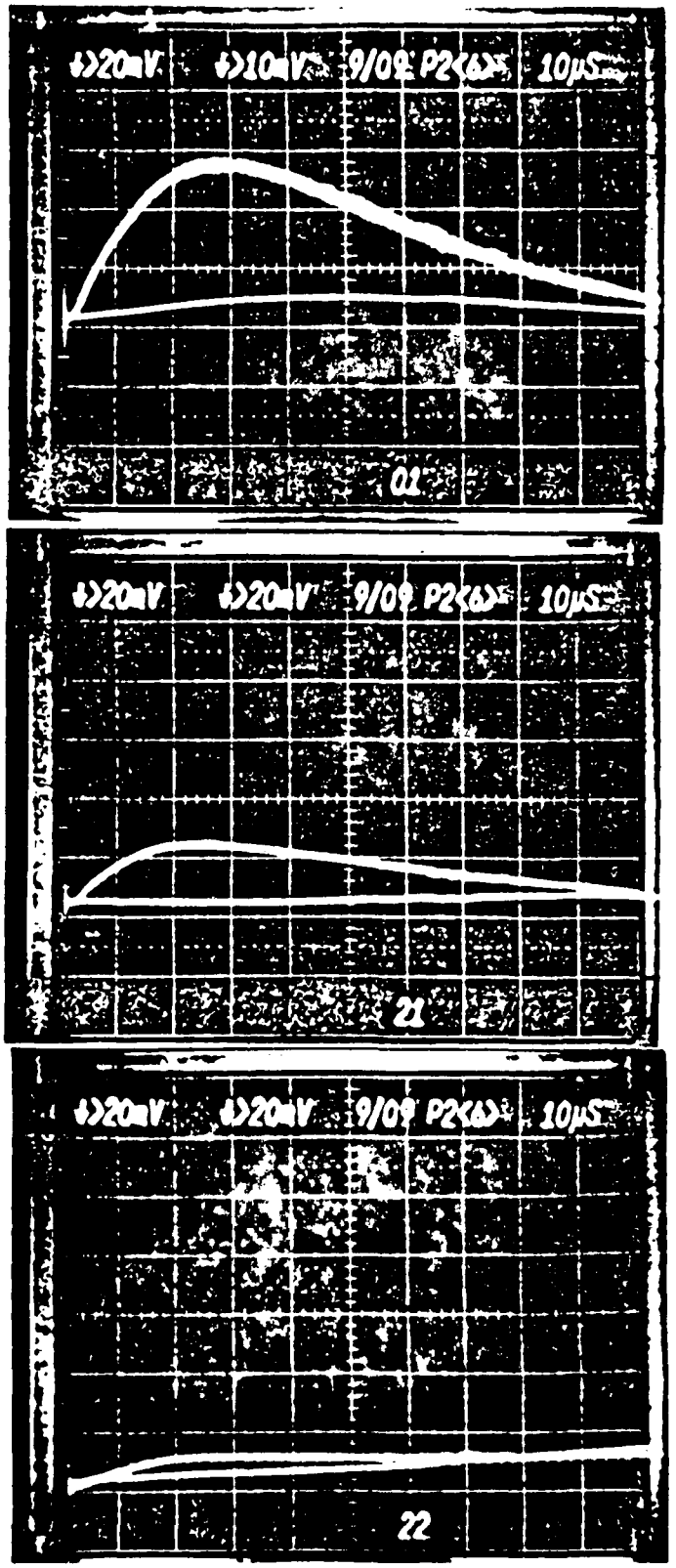

Table F.6 (Continued)

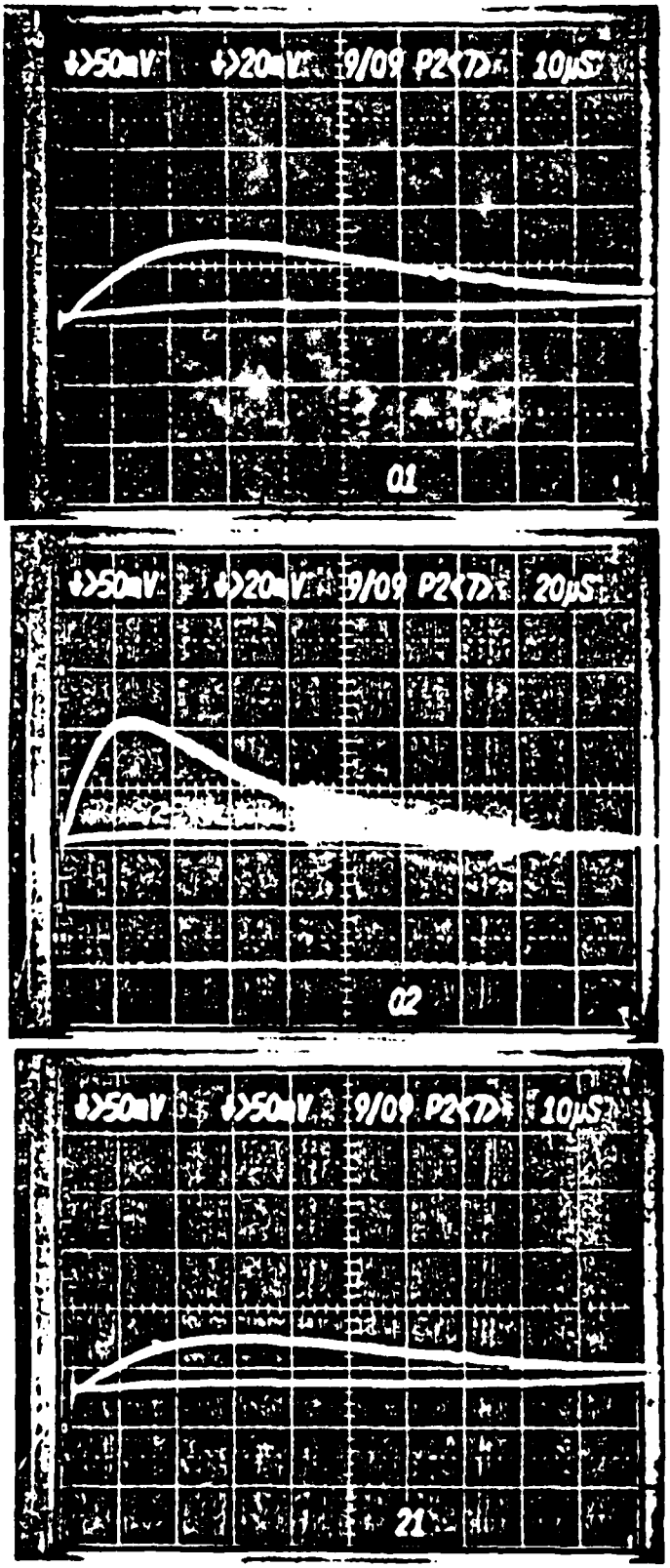

Table F.6 (Continued)

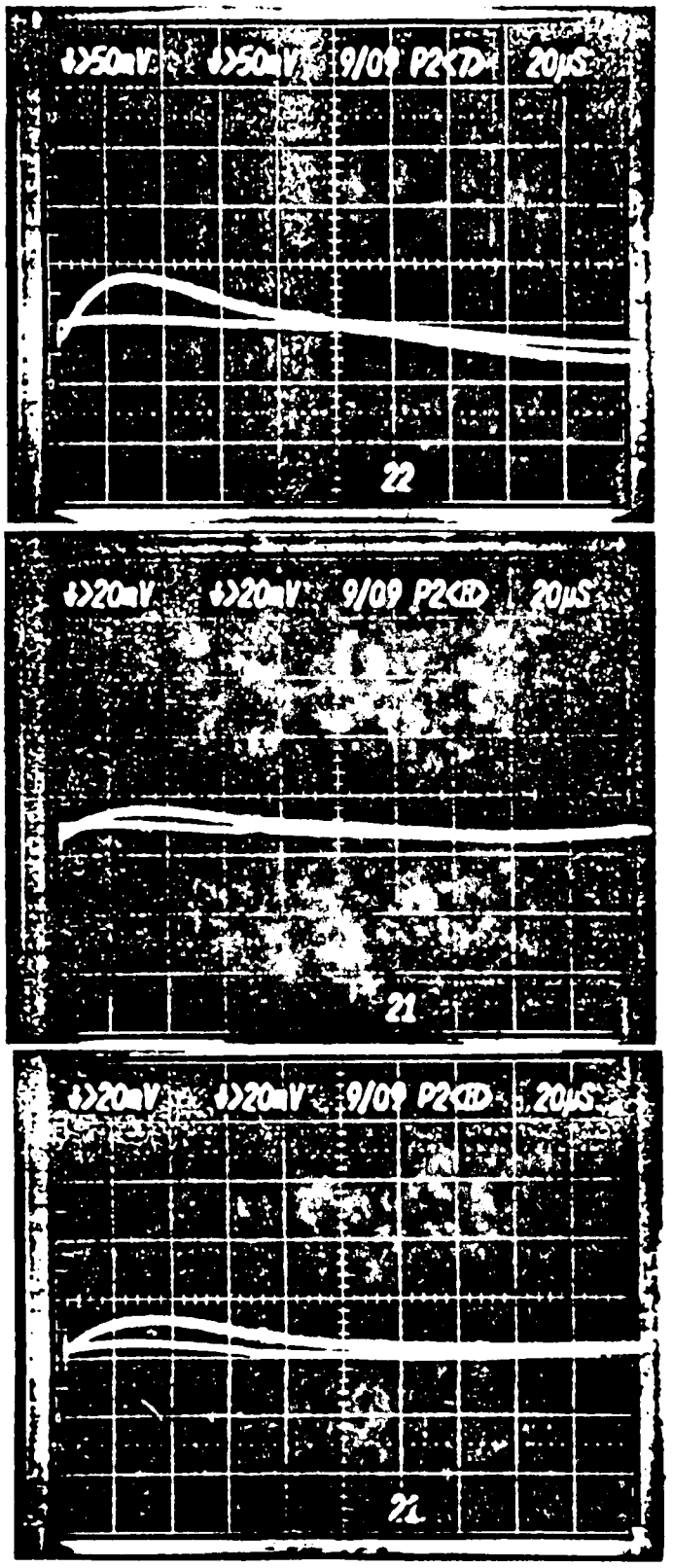

Table F.7 TRS photographes, $He:O_2:F_2:H_2$=22.0:1.0:2.7:1.0, 36 torr

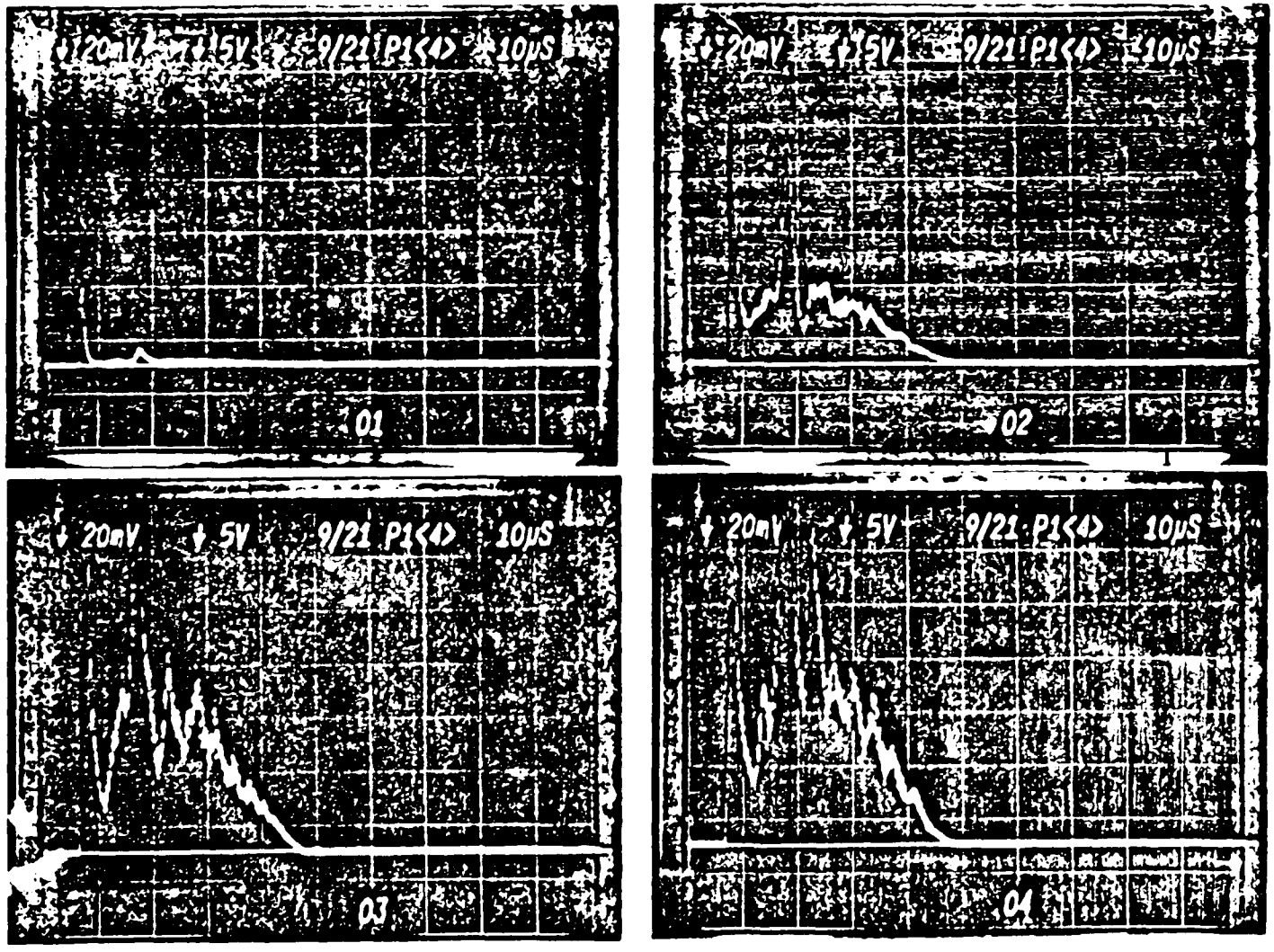

Table F.7 (Continued)

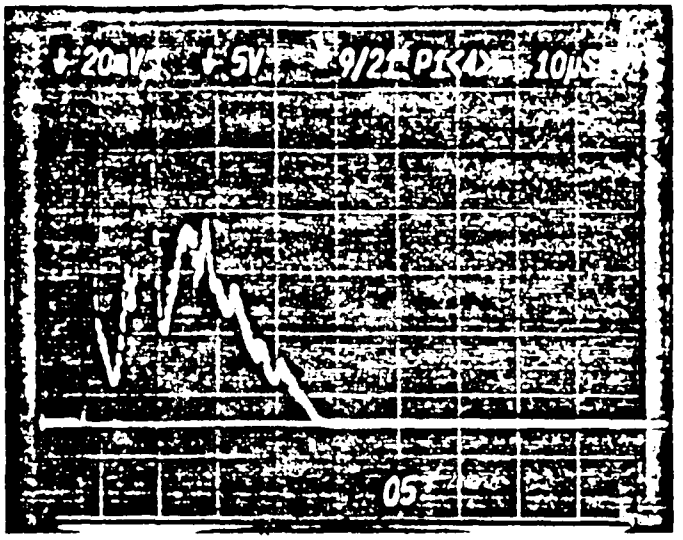

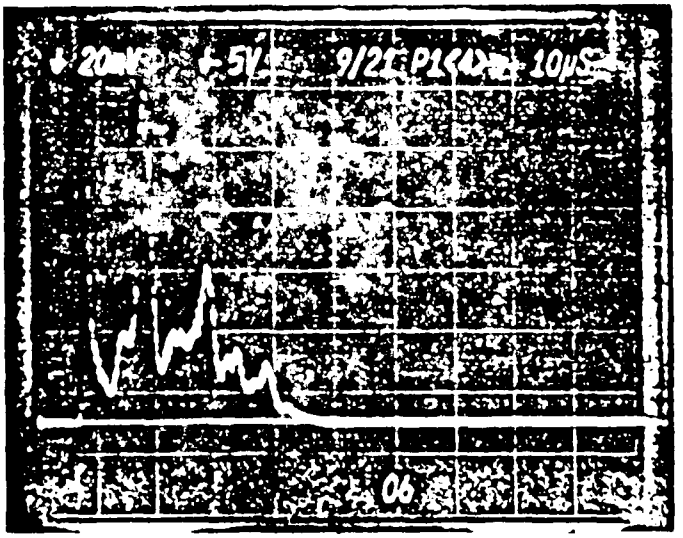

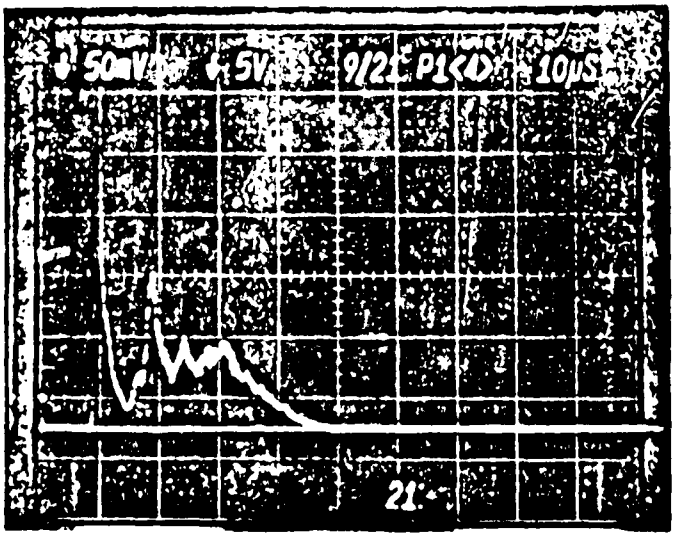

Table [illegible] (Continued)

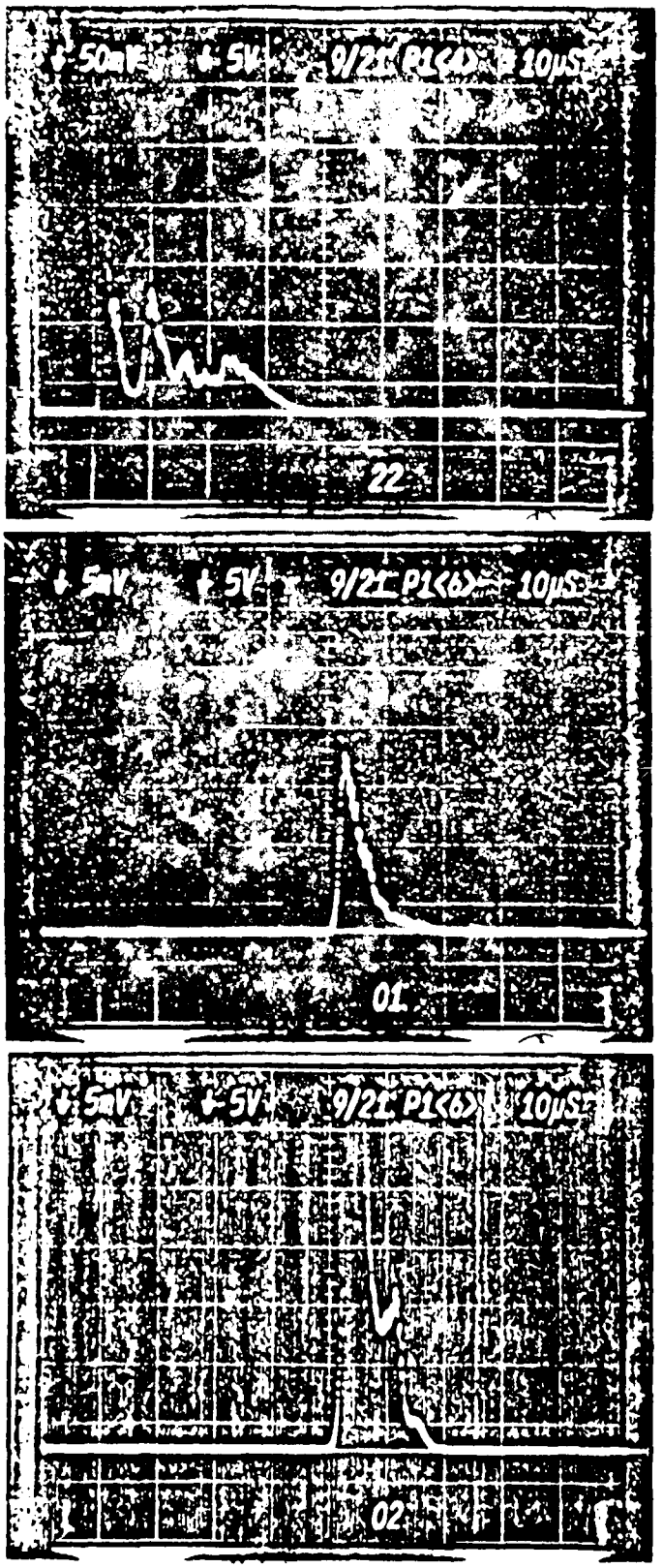

Table F.7 (Continued)

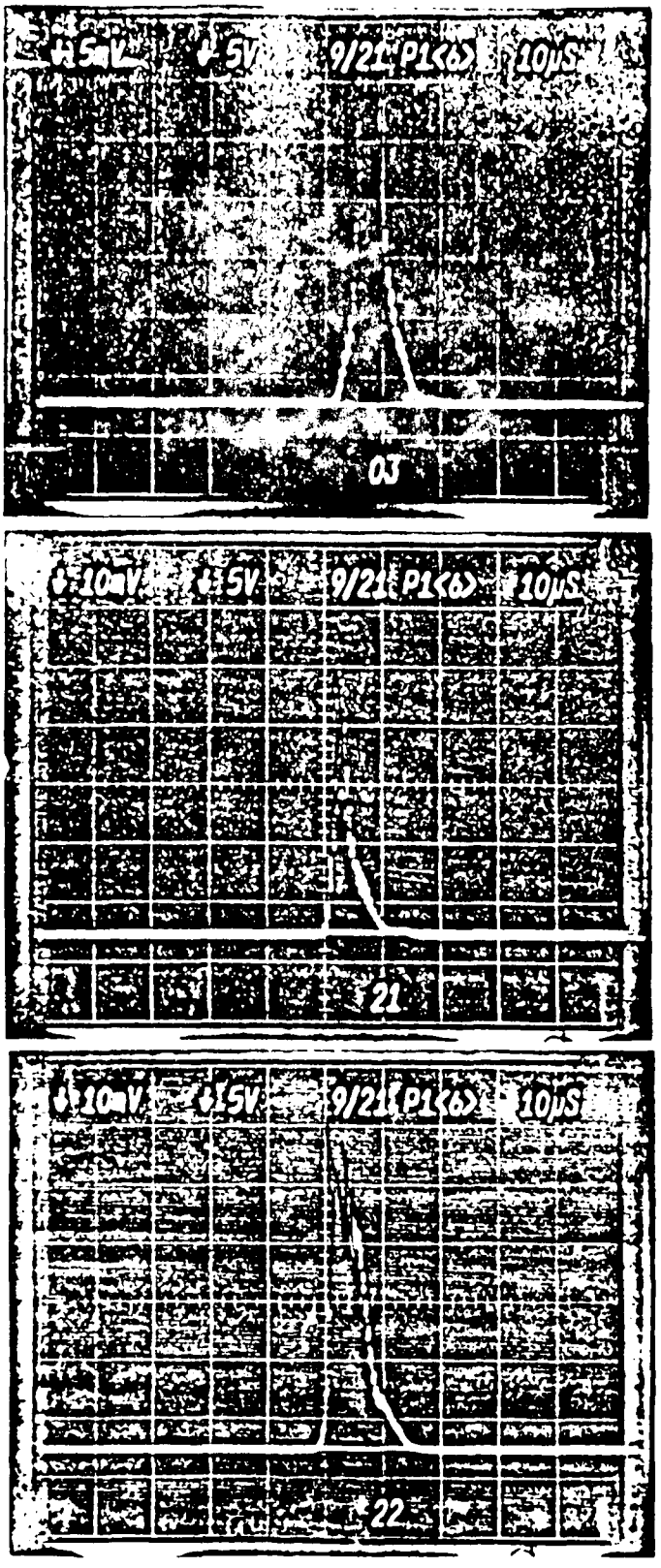

Table F.7 (Continued)

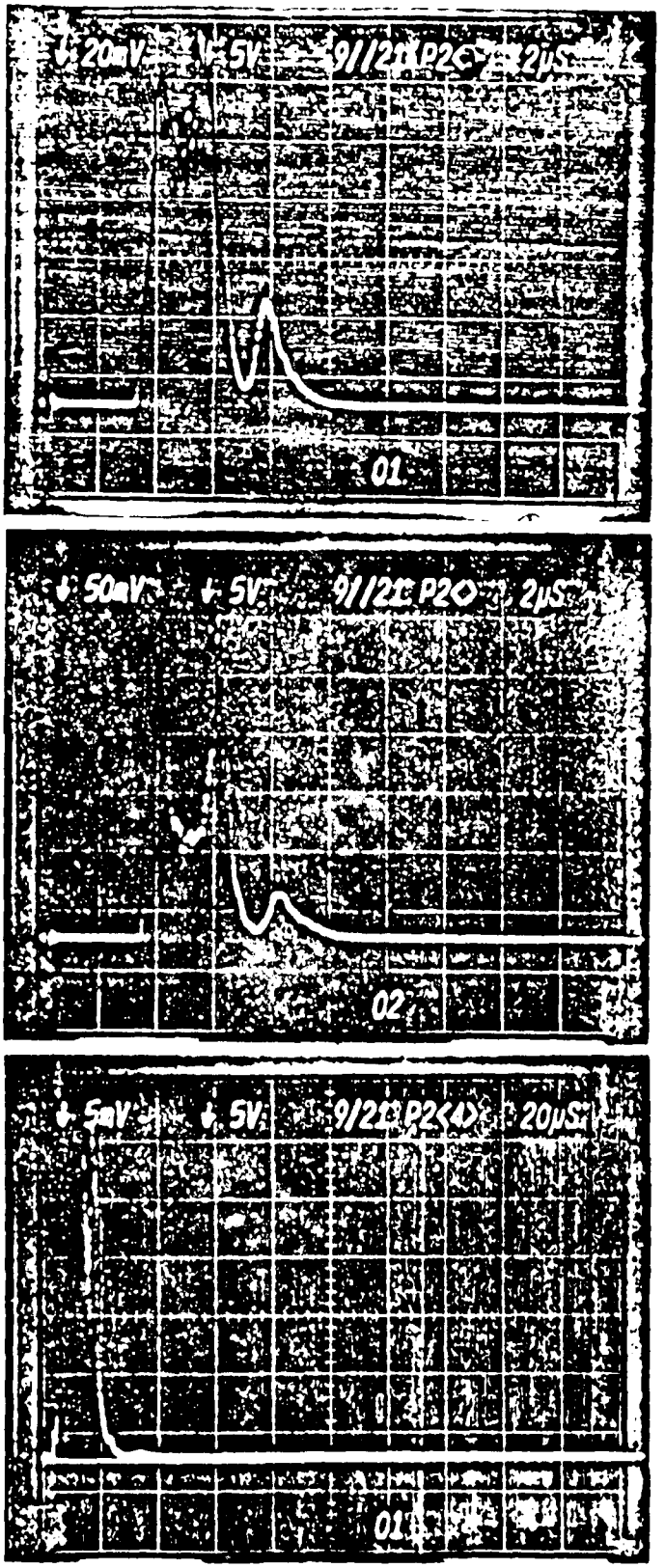

Table F.7 (Continued)

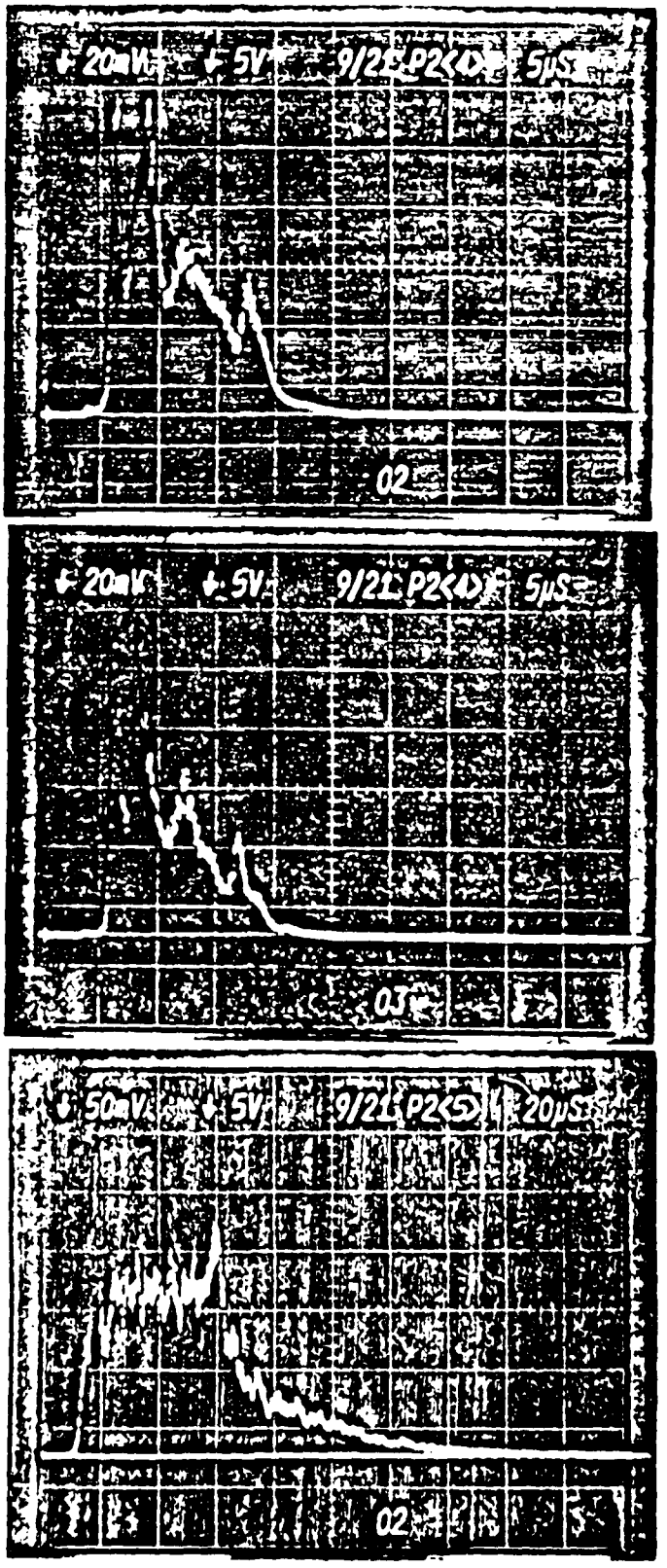

Table F.7 (Continued)

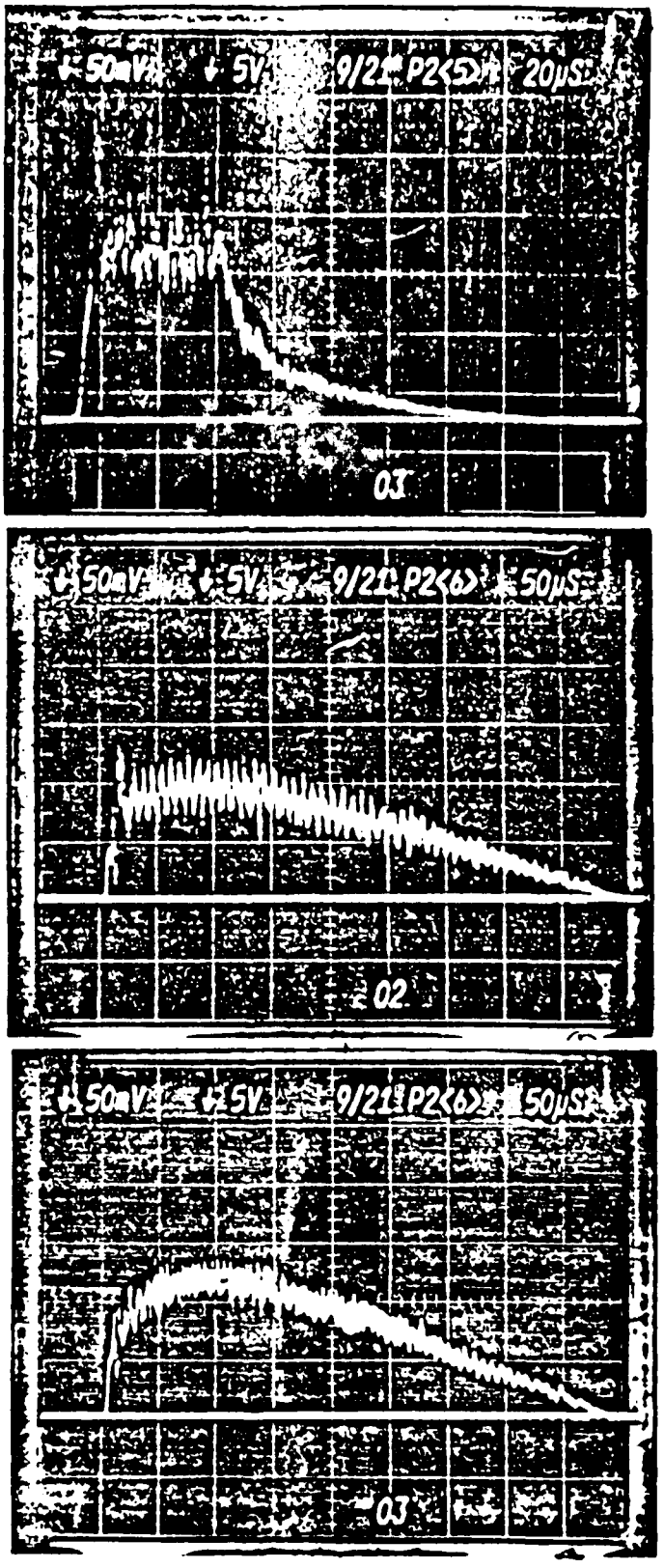

Table F.7 (Continued)

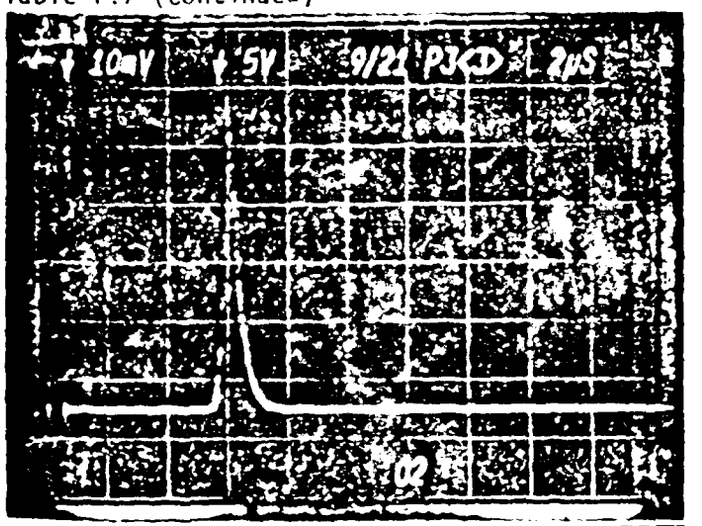

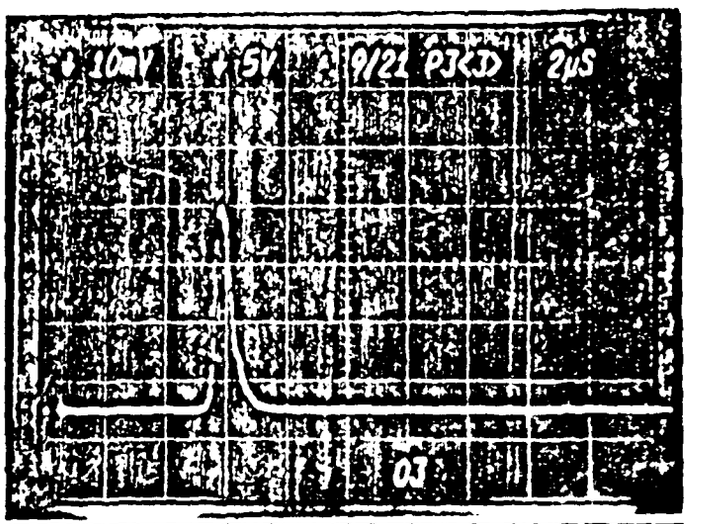

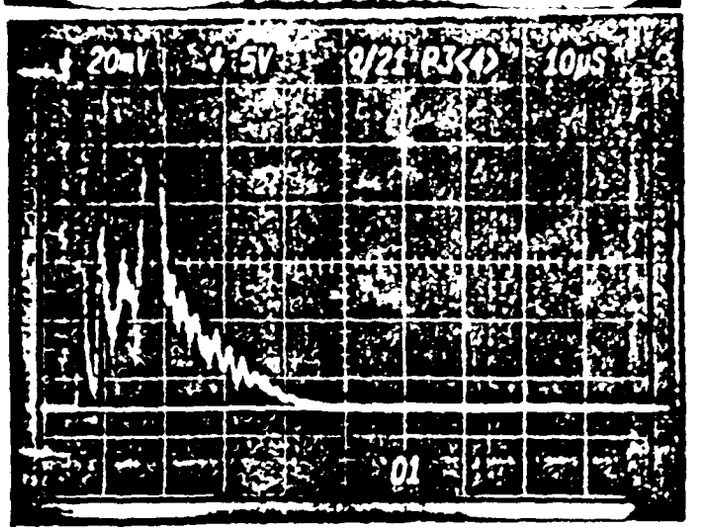

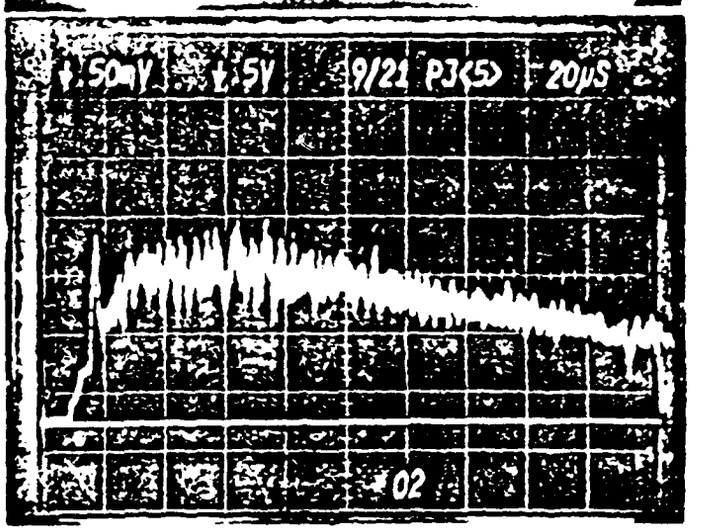

Table F.7 (Continued)

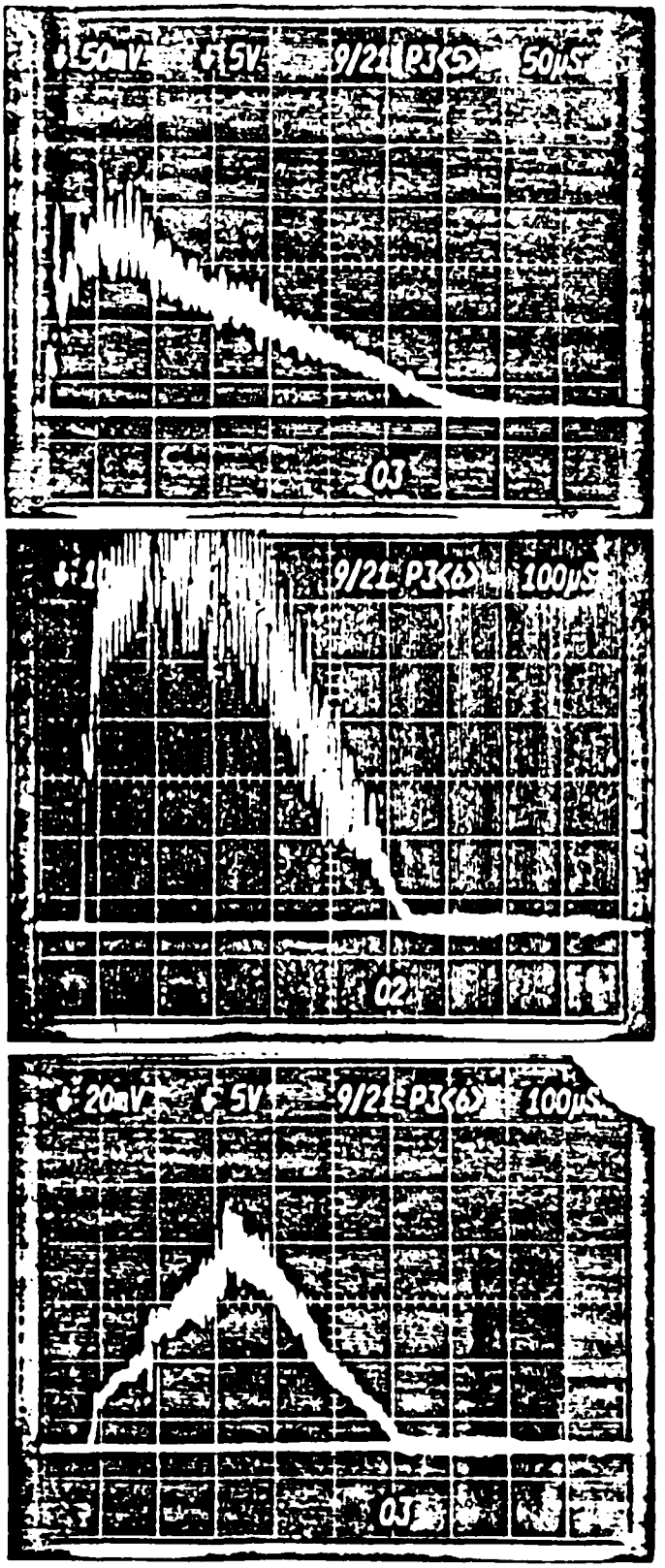

Table F.7 (Continued)

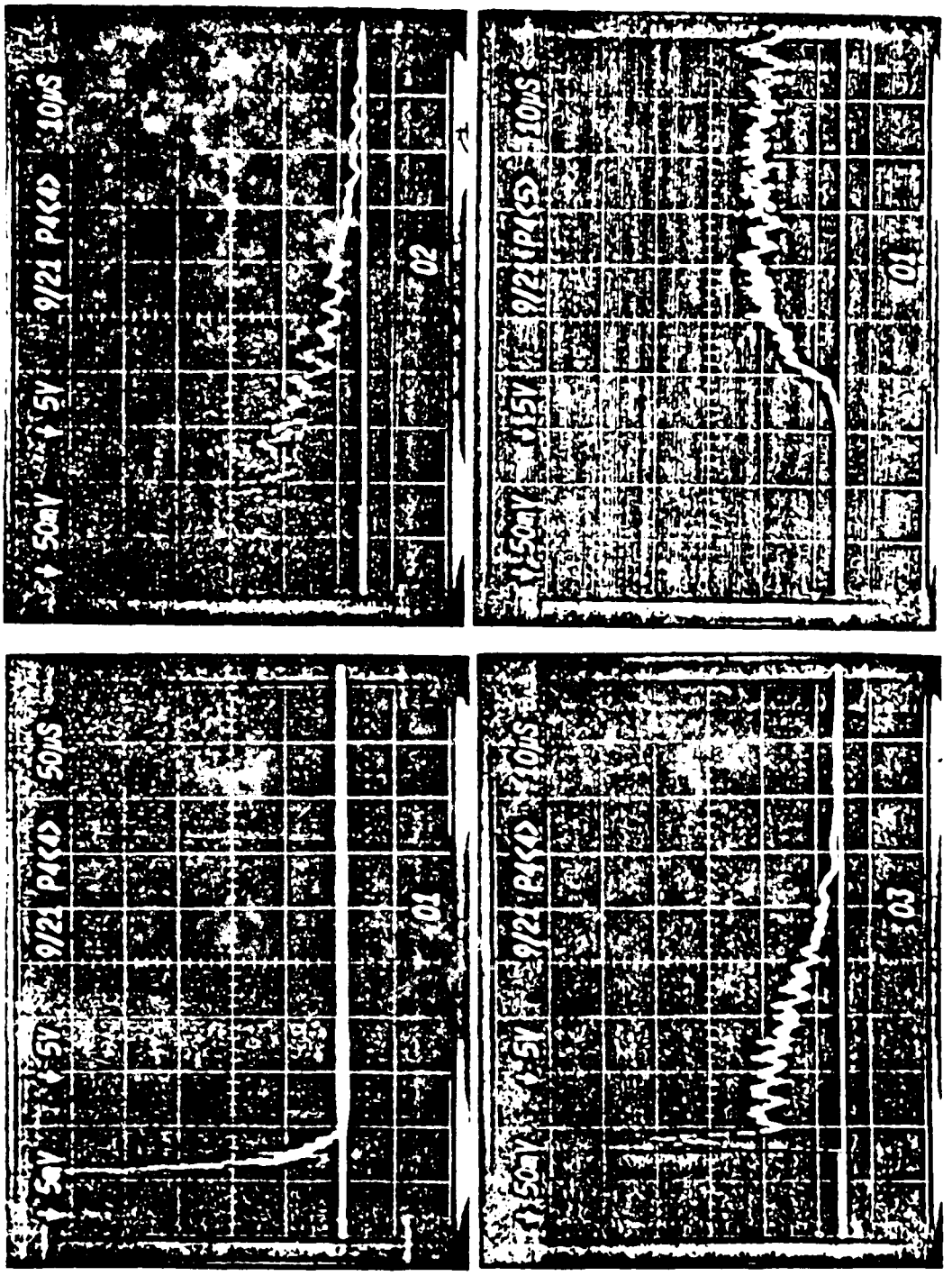

Table F.7 (Continued)

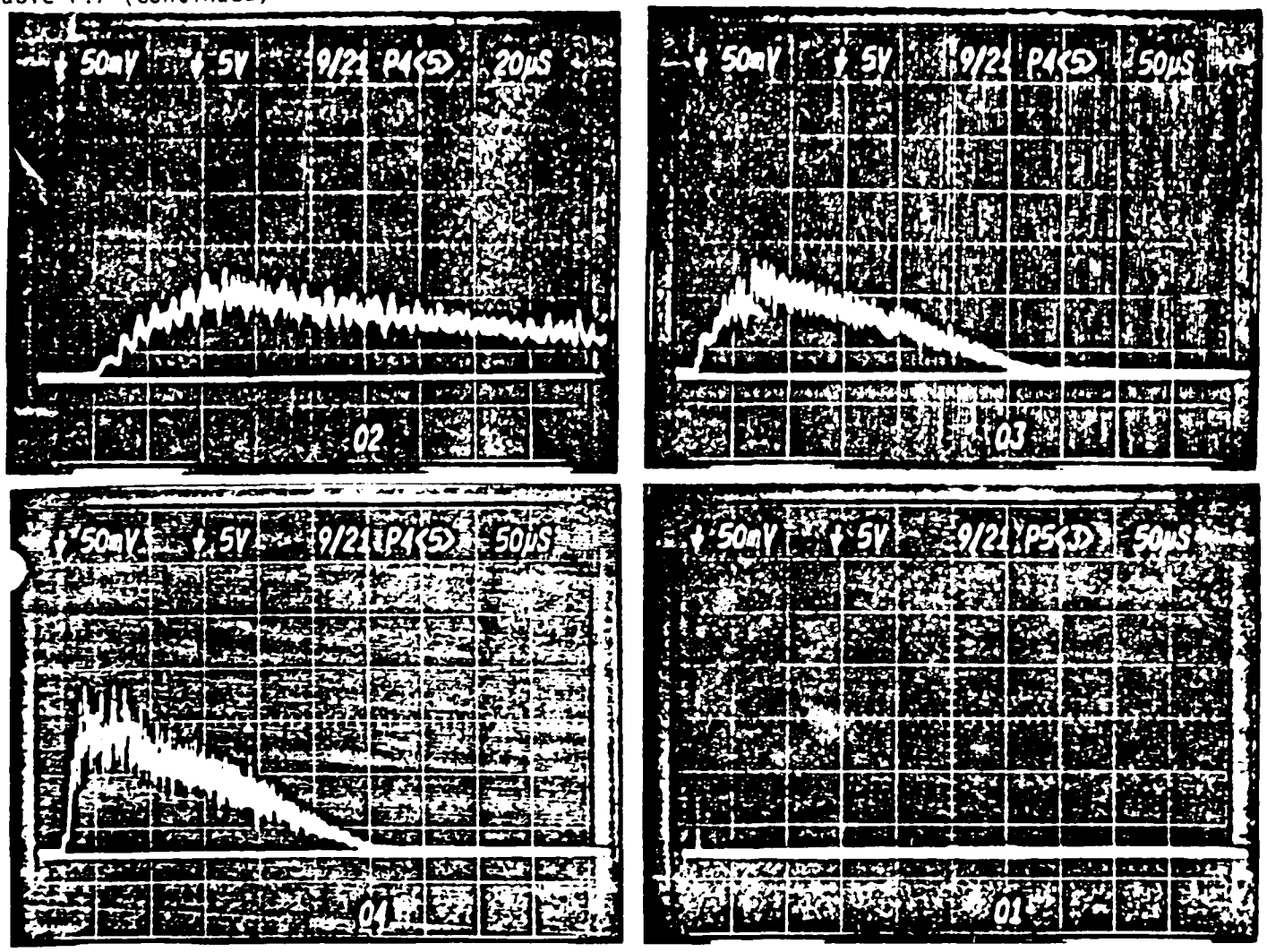

Table F.7 (Continued)

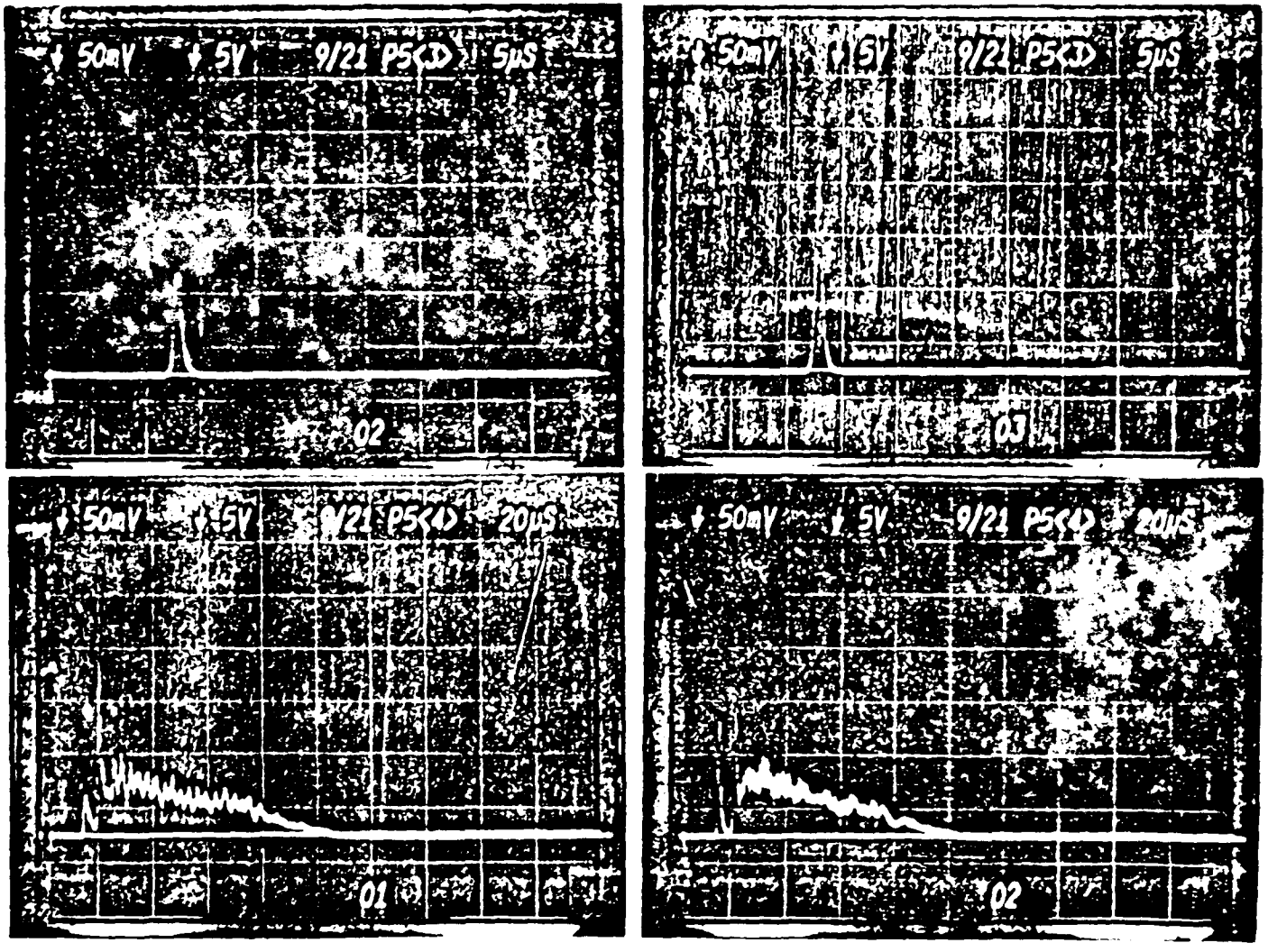

Table F.8 TRS photographes, $He:O_2:F_2:H_2$=22.0:1.0:2.7:1.0, 102 torr

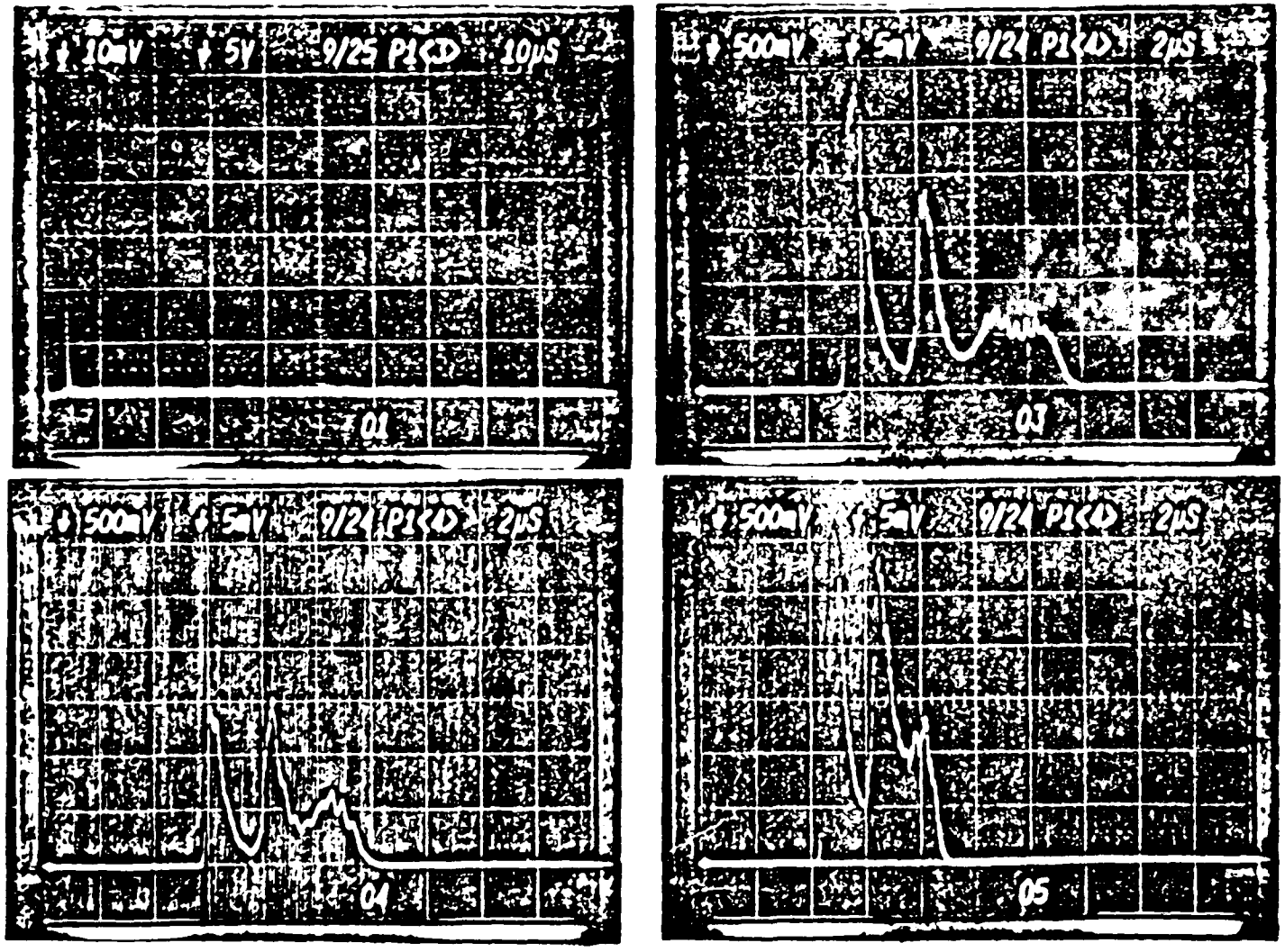

Table F.8 (Continued)

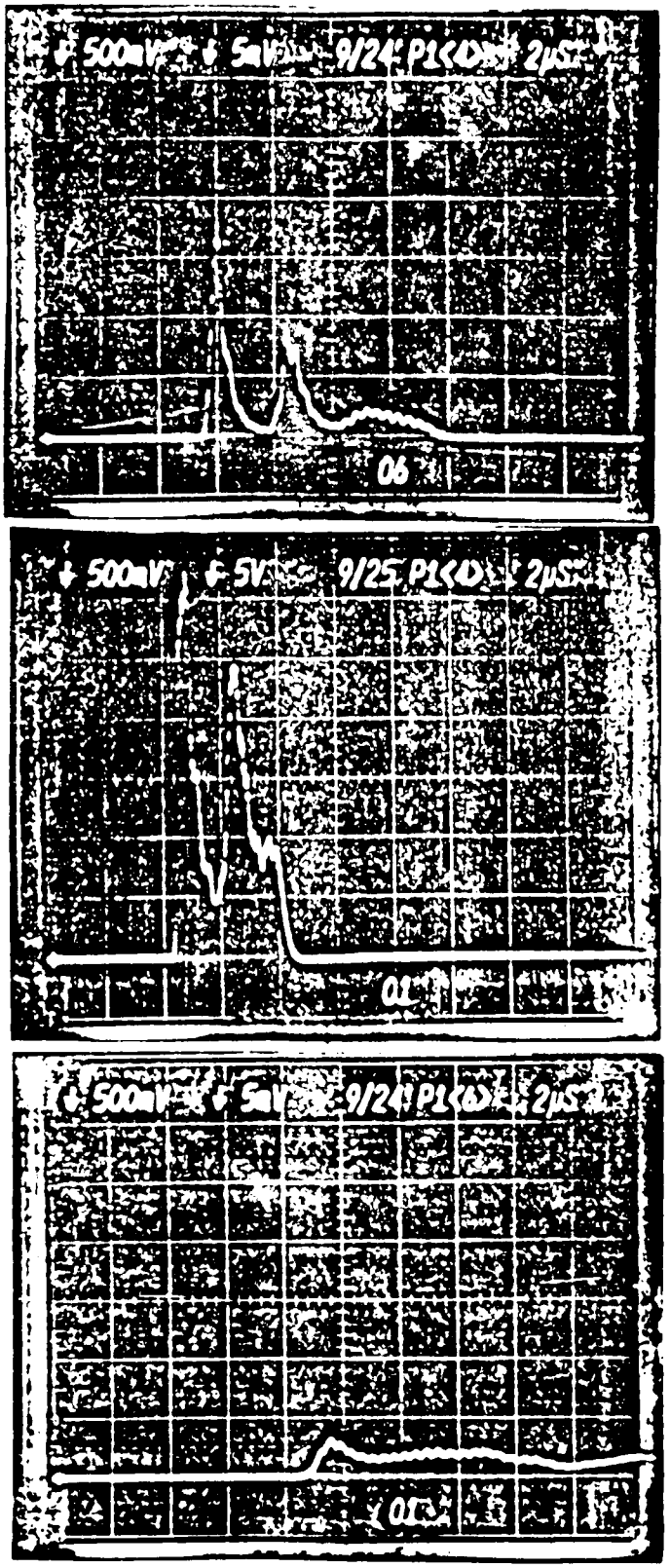

Table F.5 (Continued)

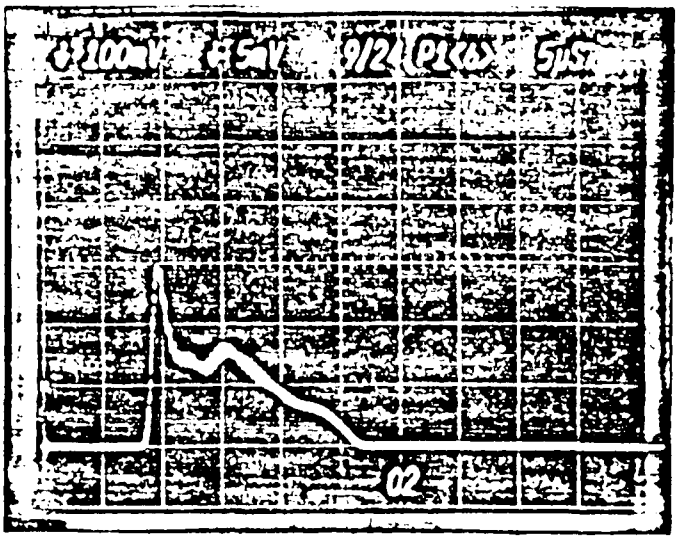

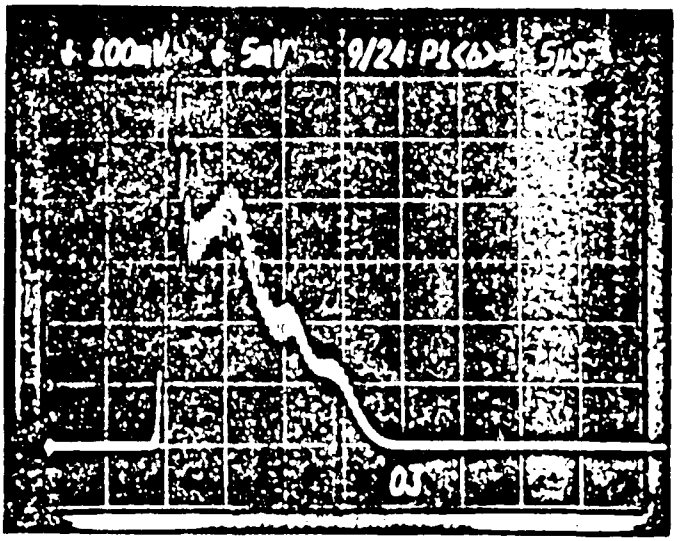

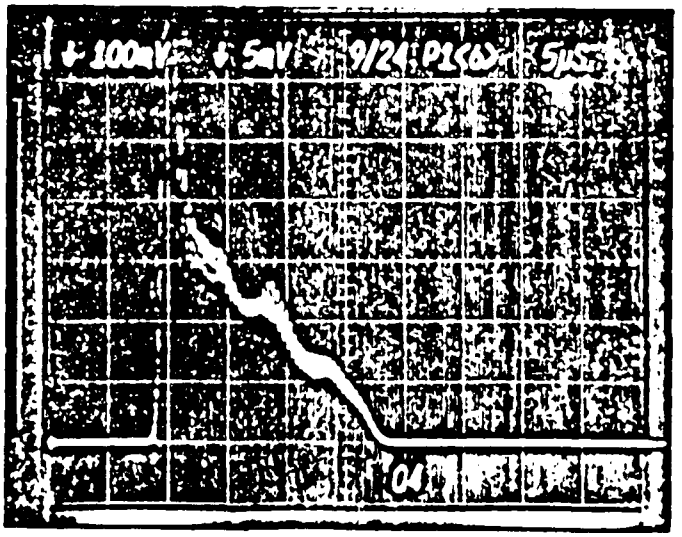

Table F.8 (Continued)

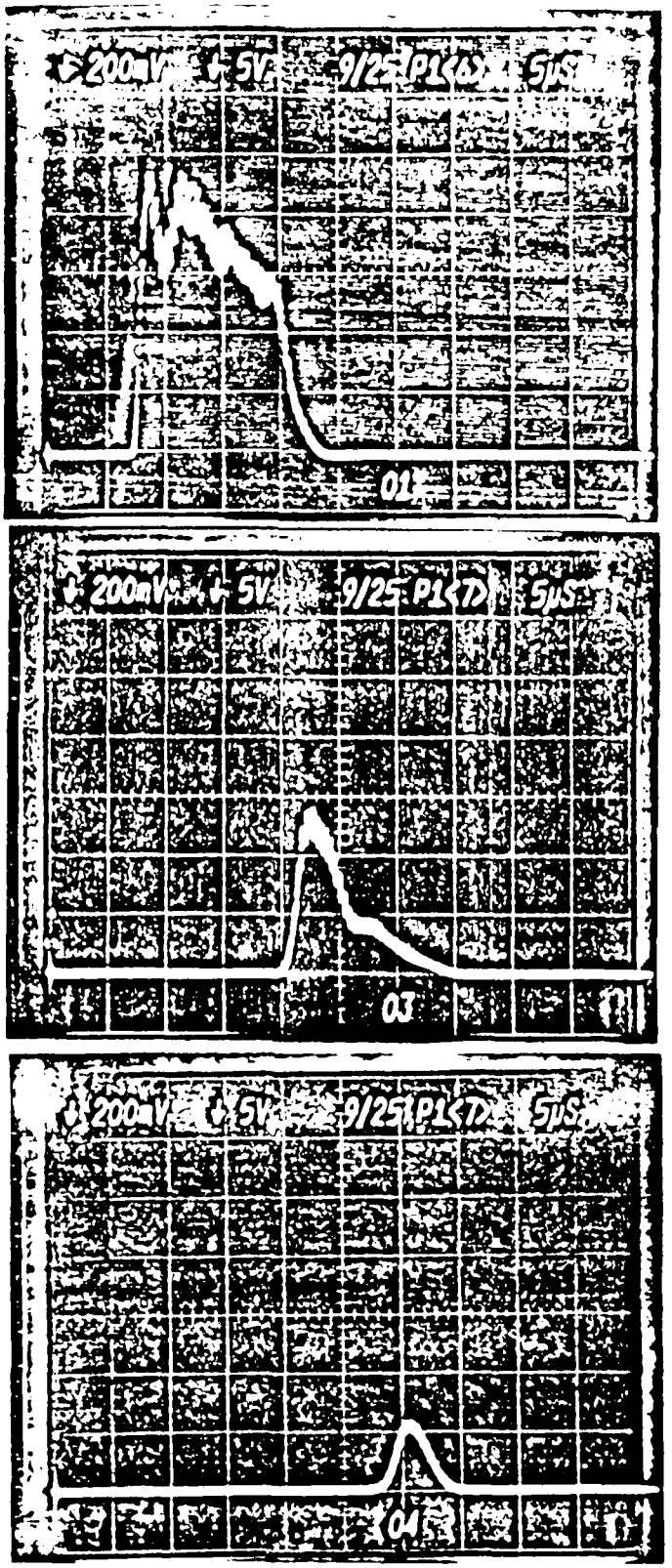

Table F.8 (Continued)

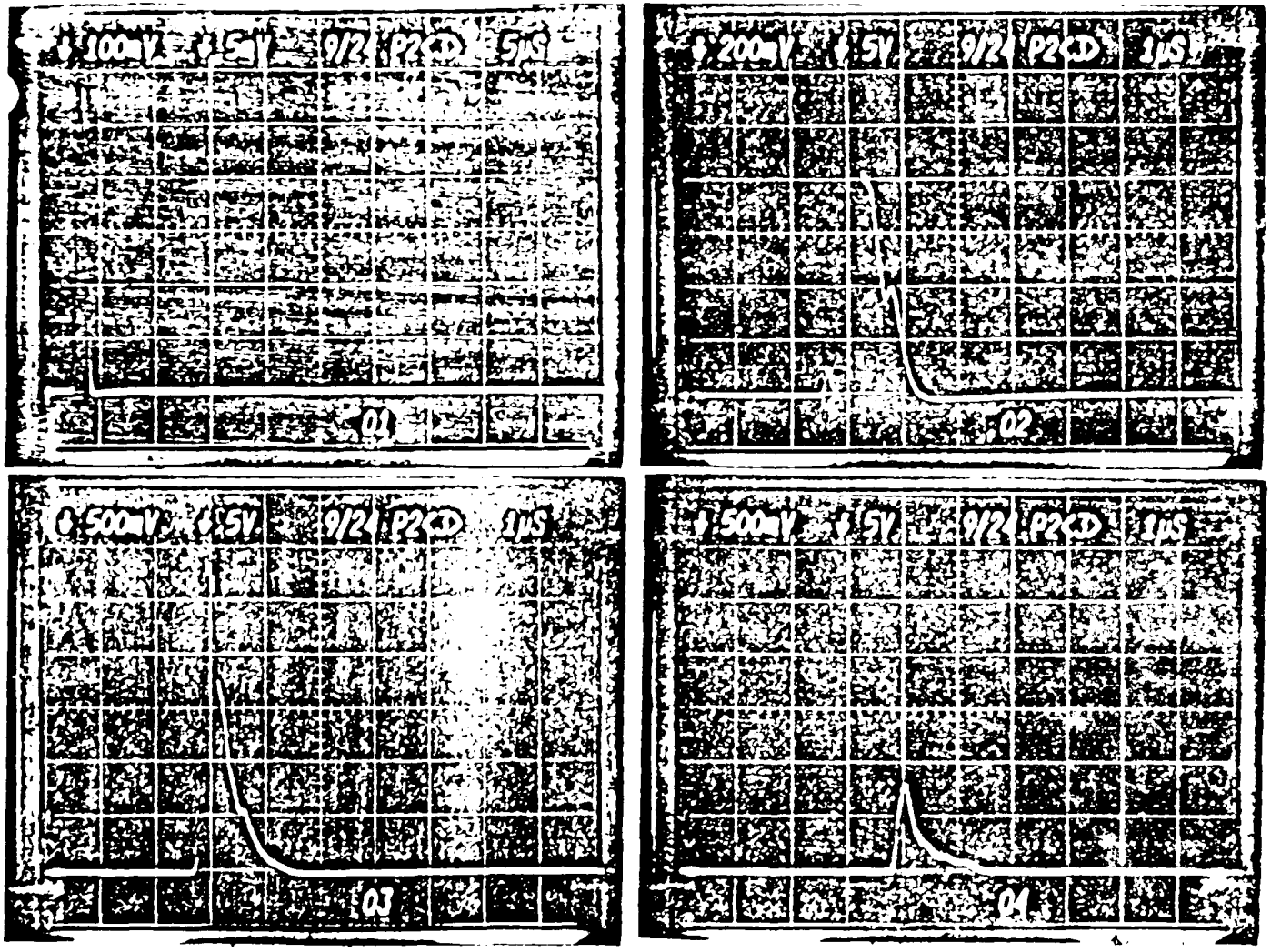

Table F.8 (Continued)

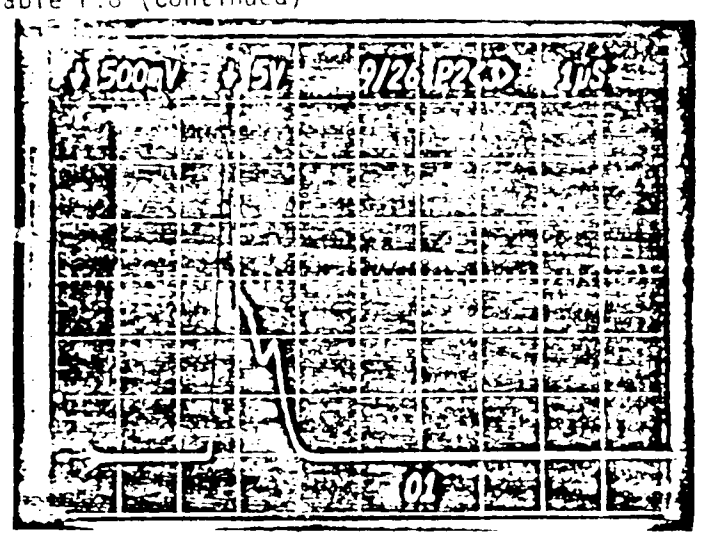

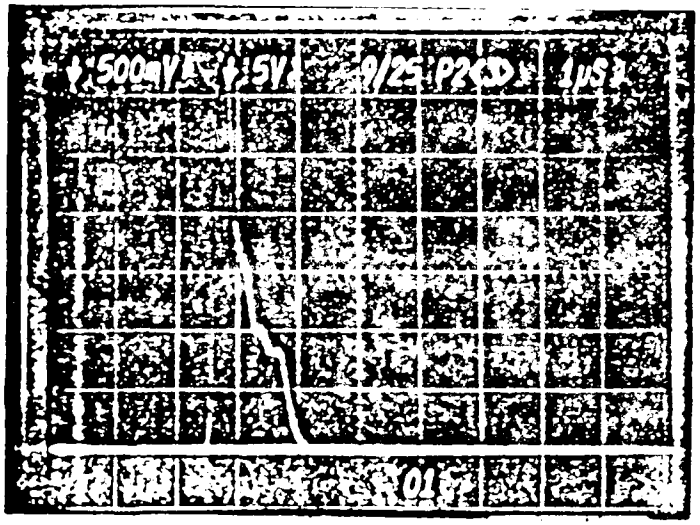

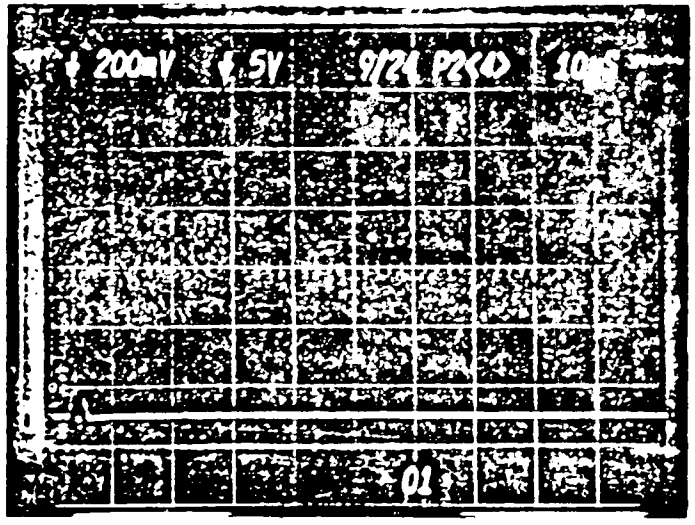

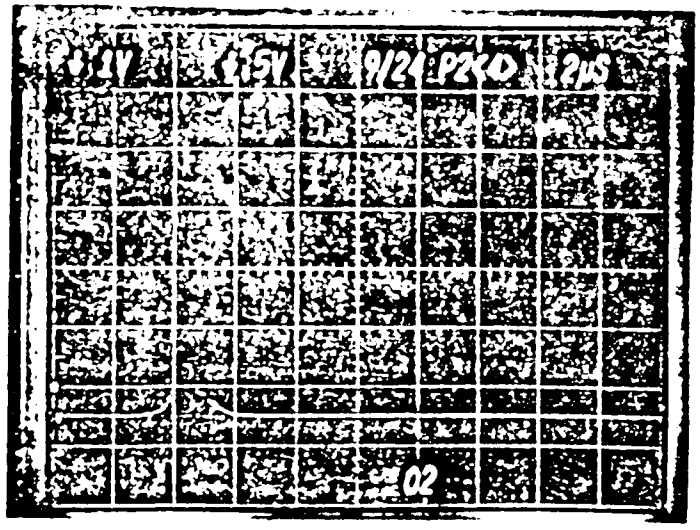

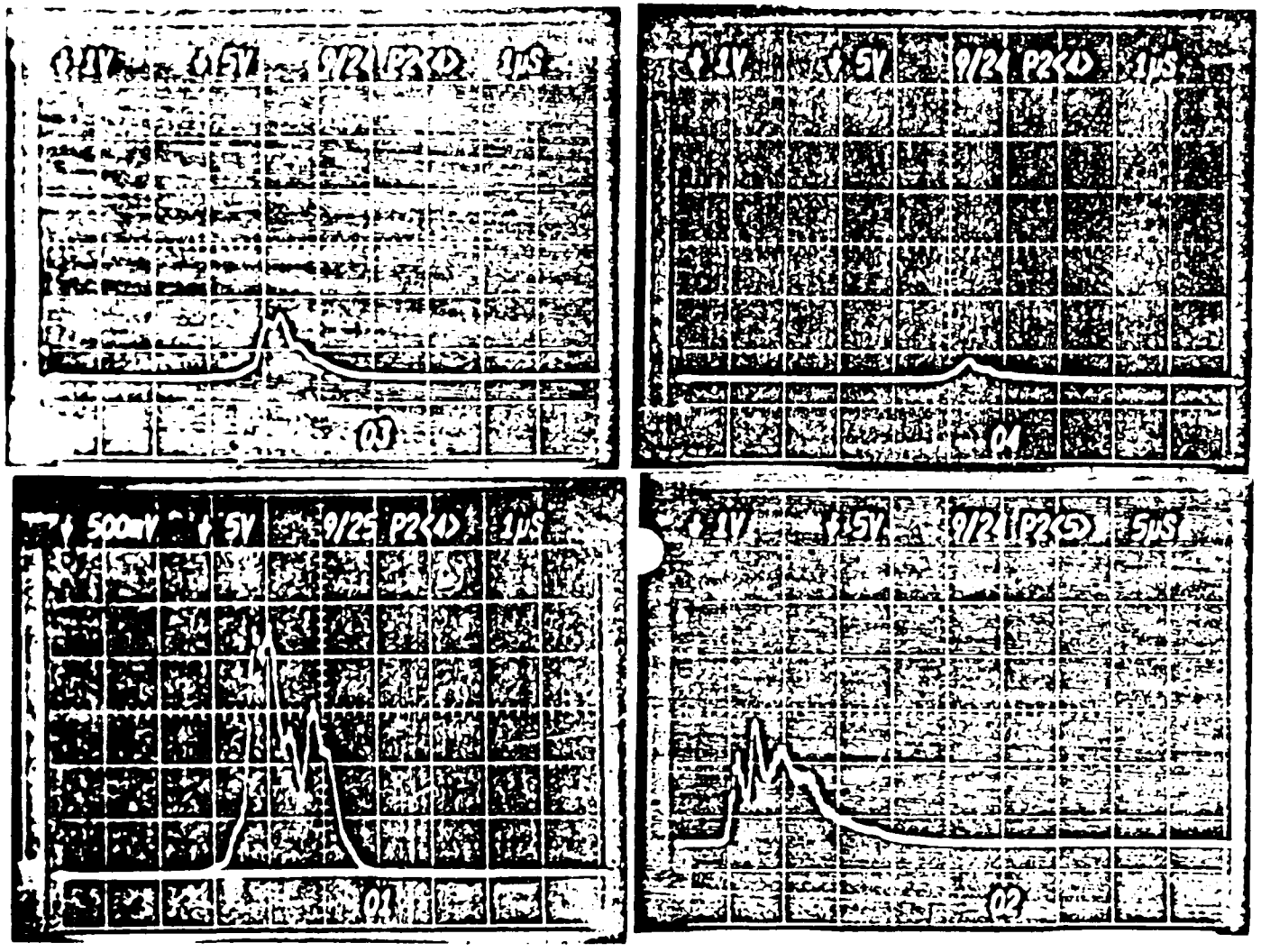
Q3
Q4
Q1
Q2

Table F.8 (Continued)

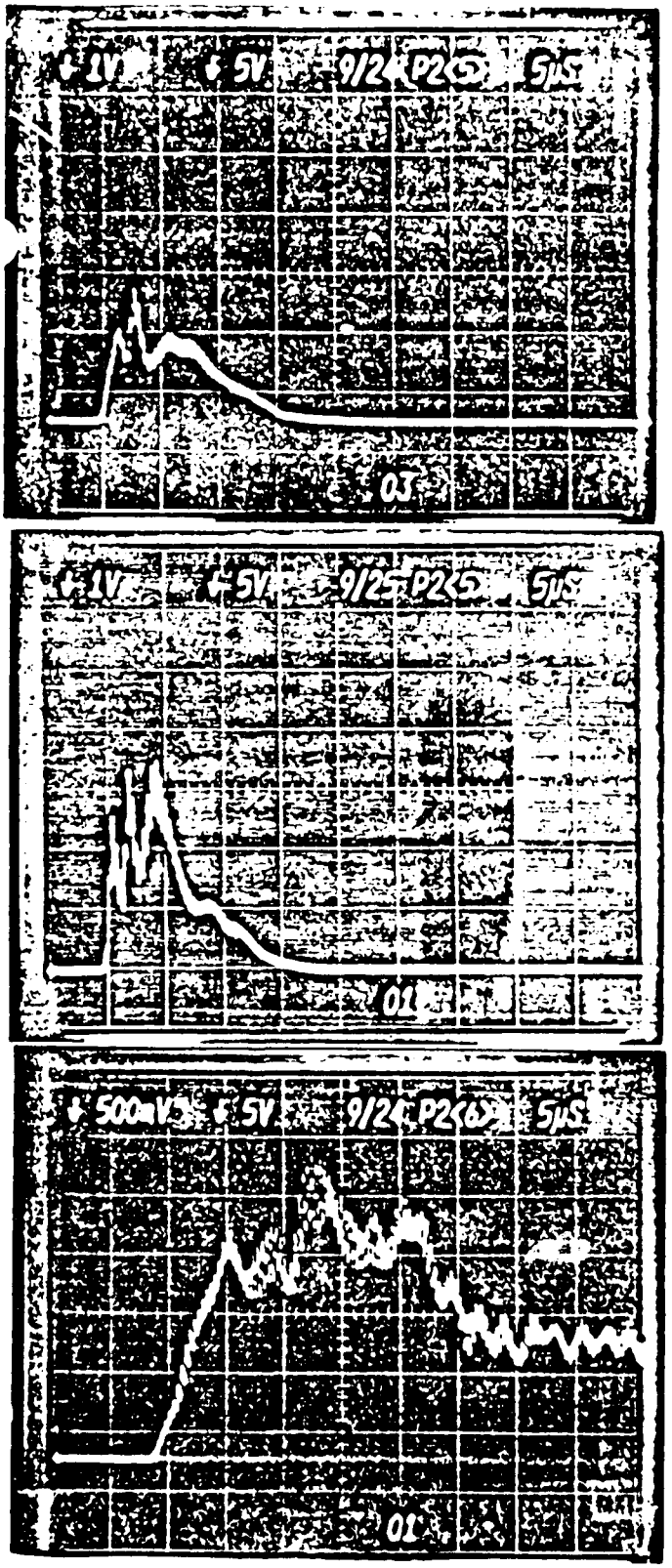

Table F.8 (Continued)

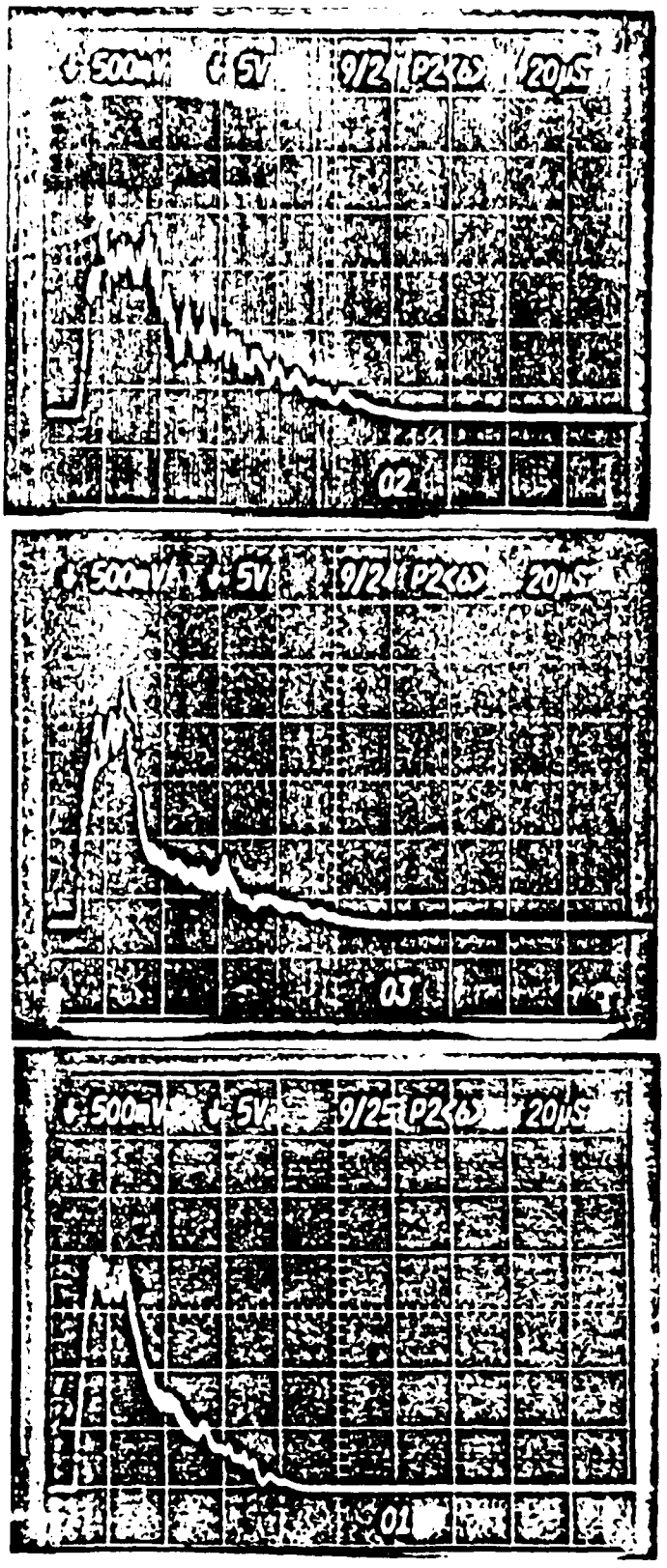

Table F.8 (Continued)

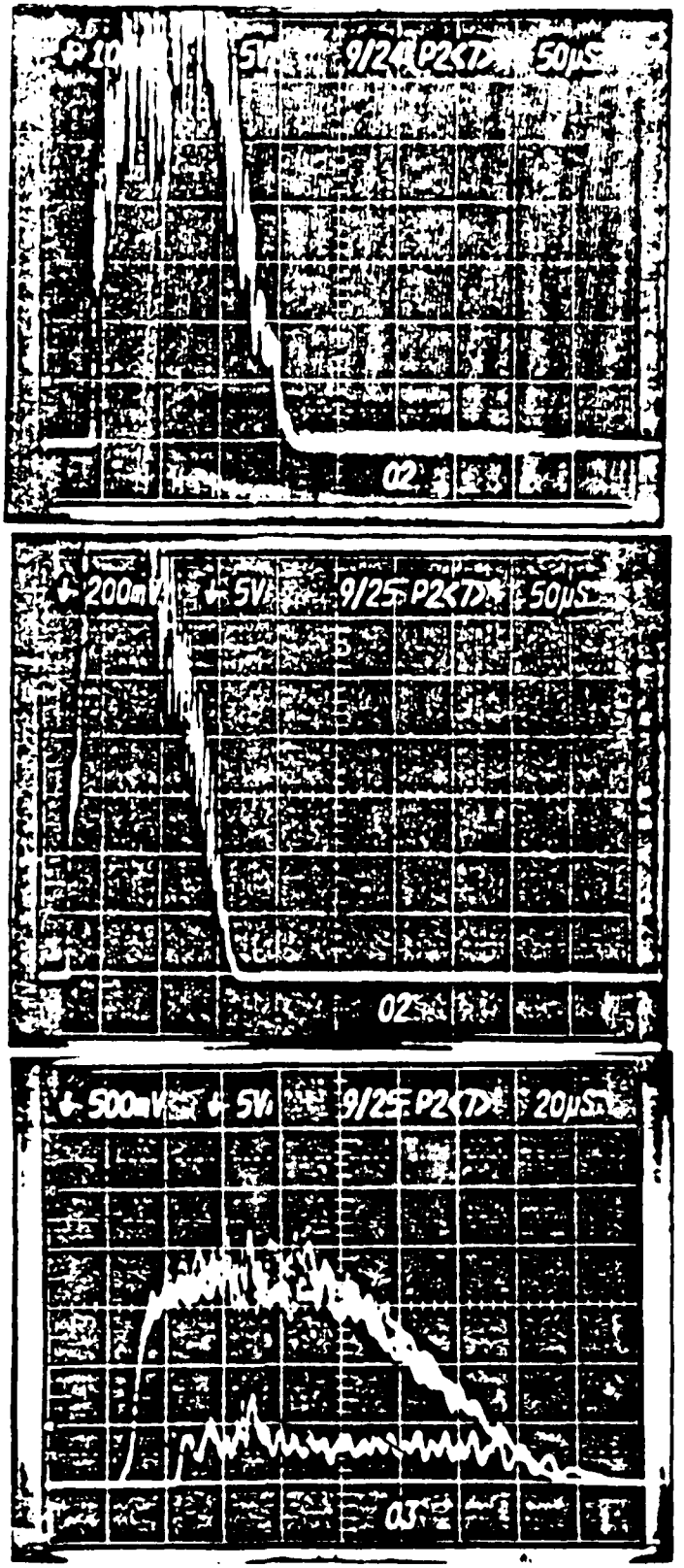

Table F.8 (Continued)

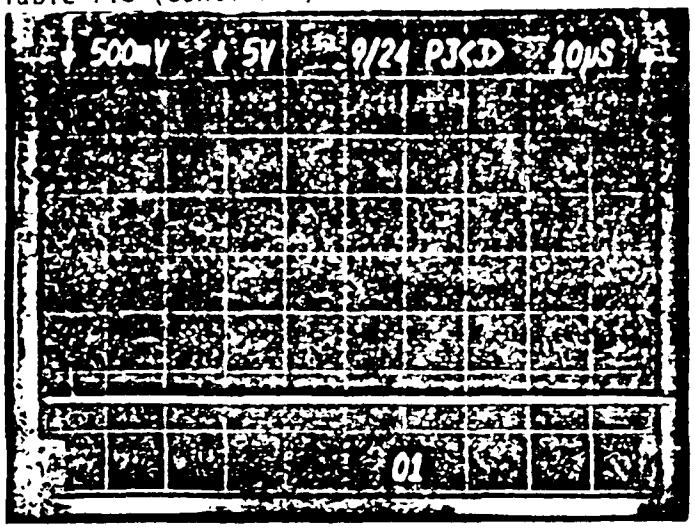

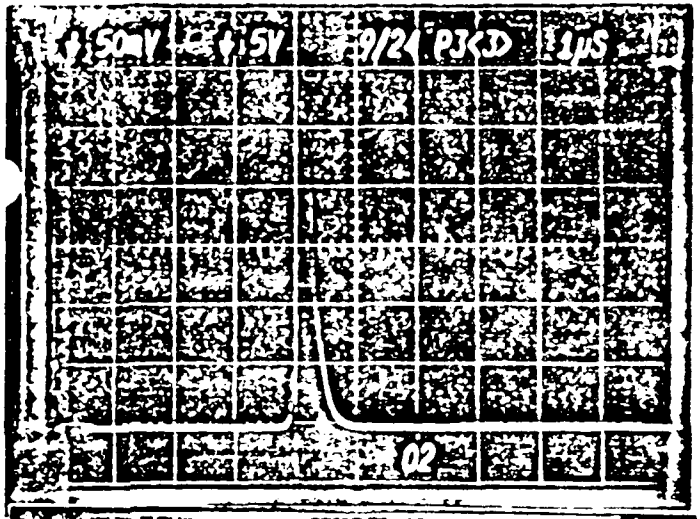

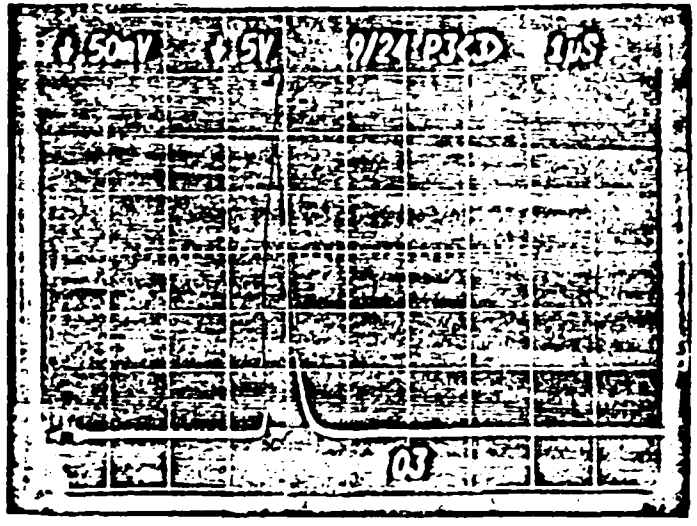

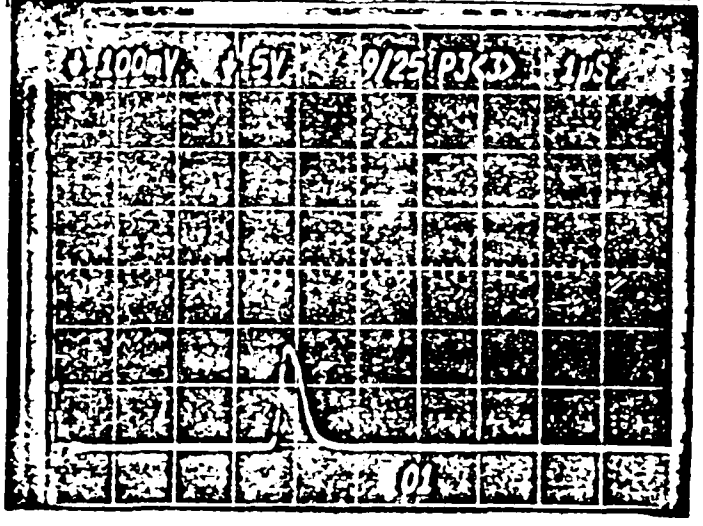

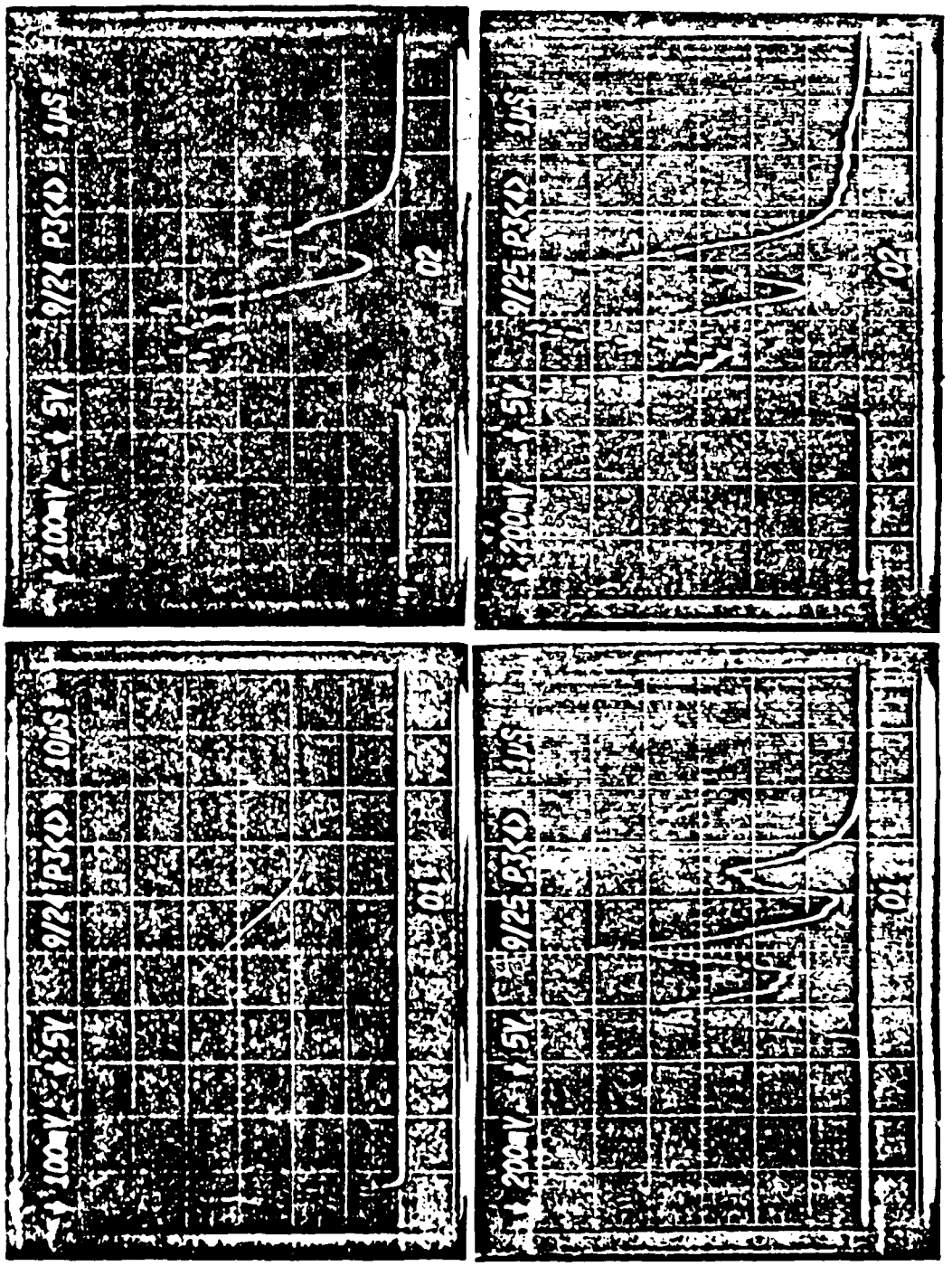

Table F.8 (Continued)

Table F.8 (Continued)

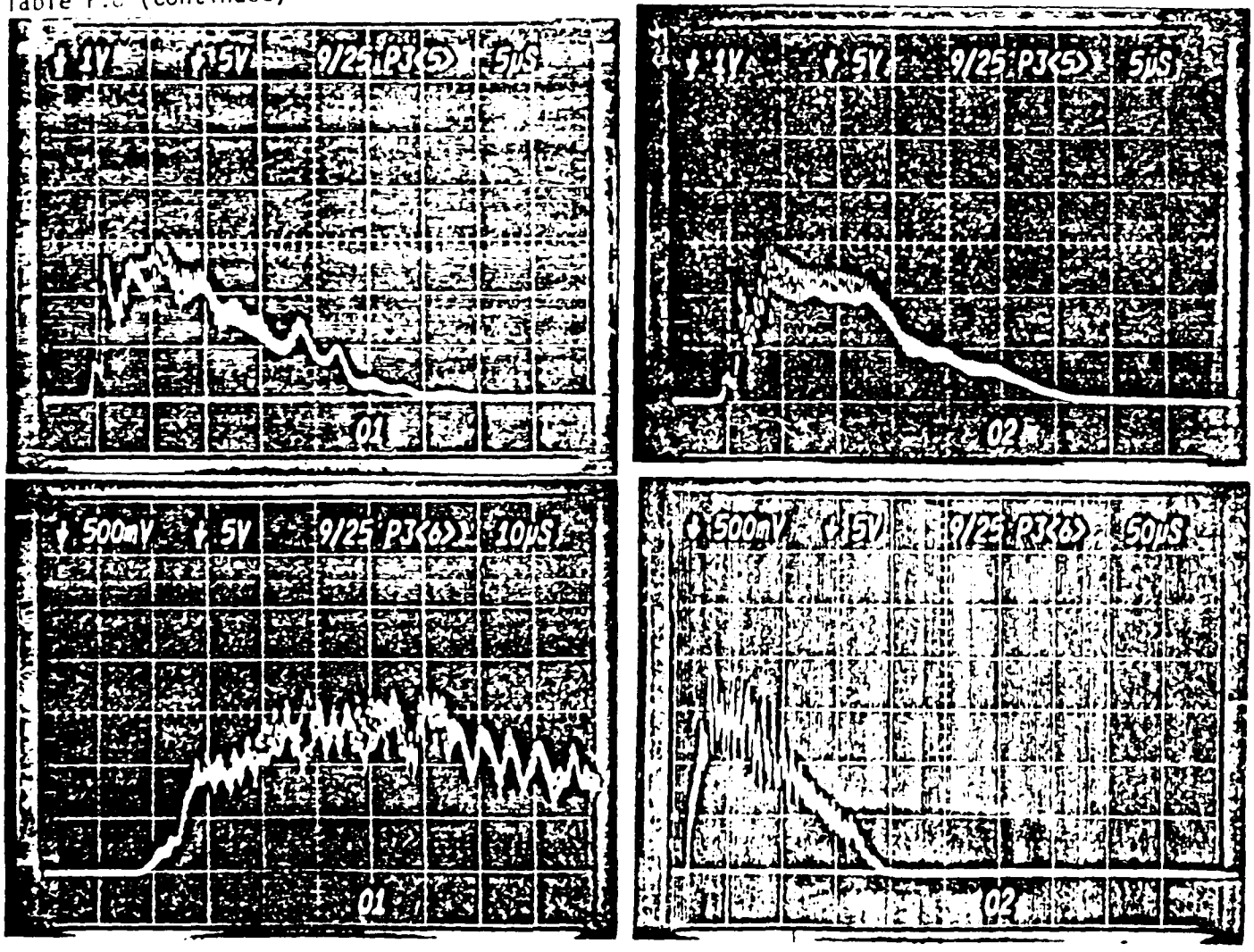

Table F.8 (Continued)

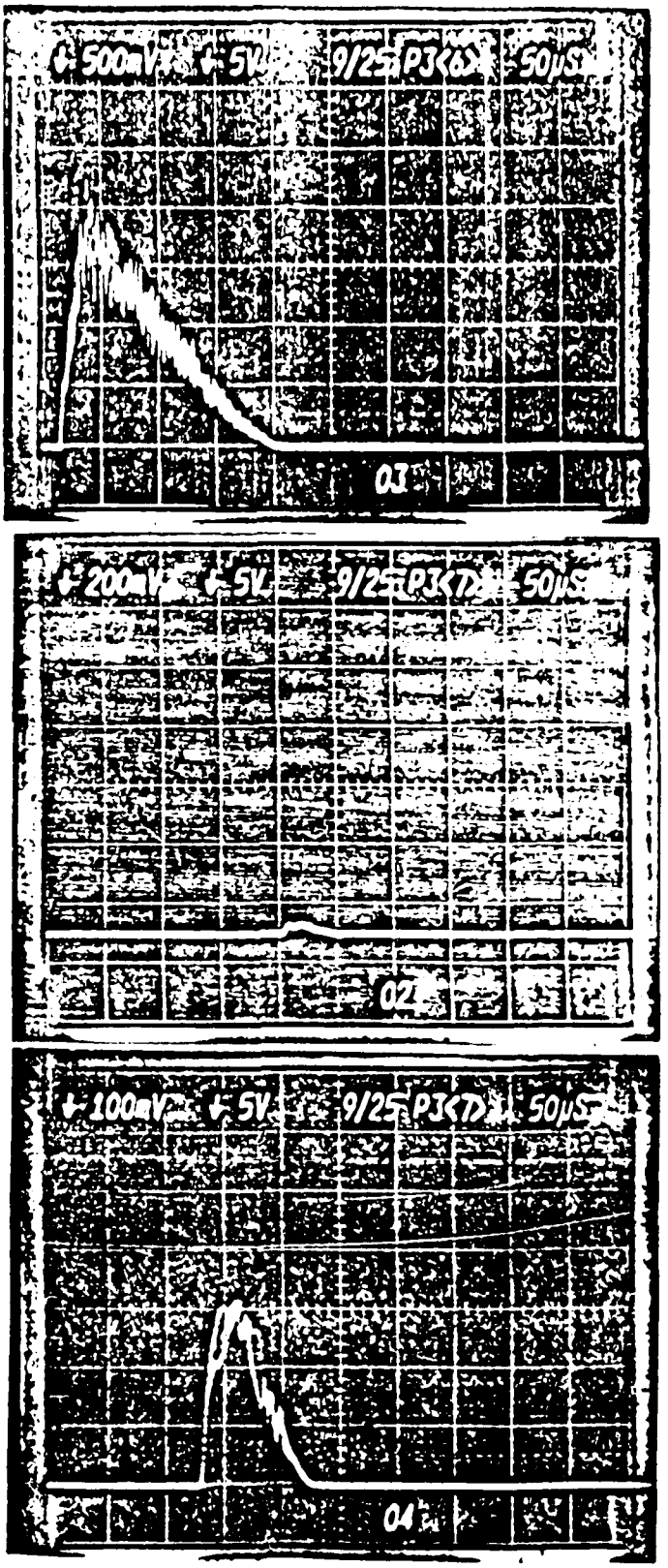

Table F.8 (Continued)

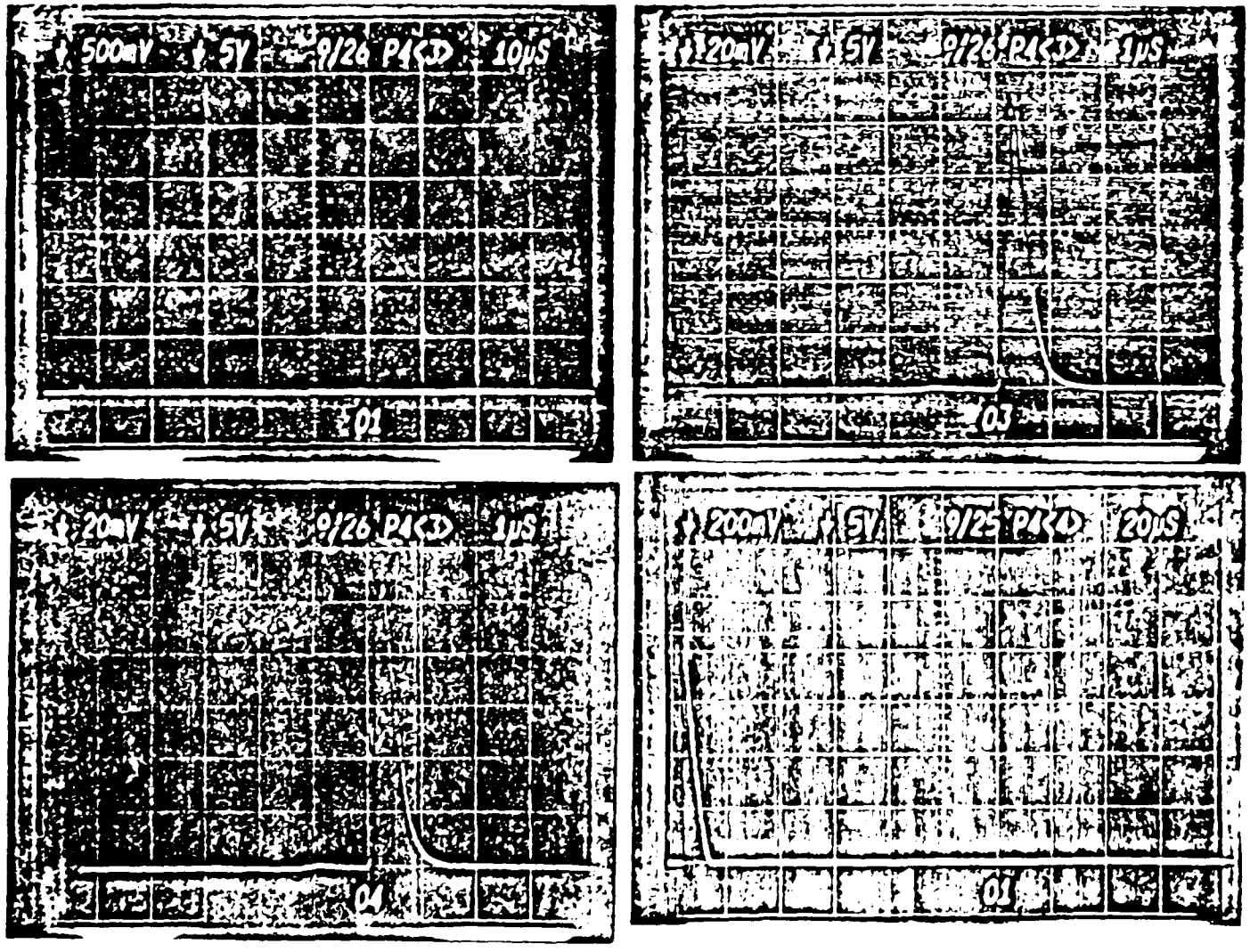

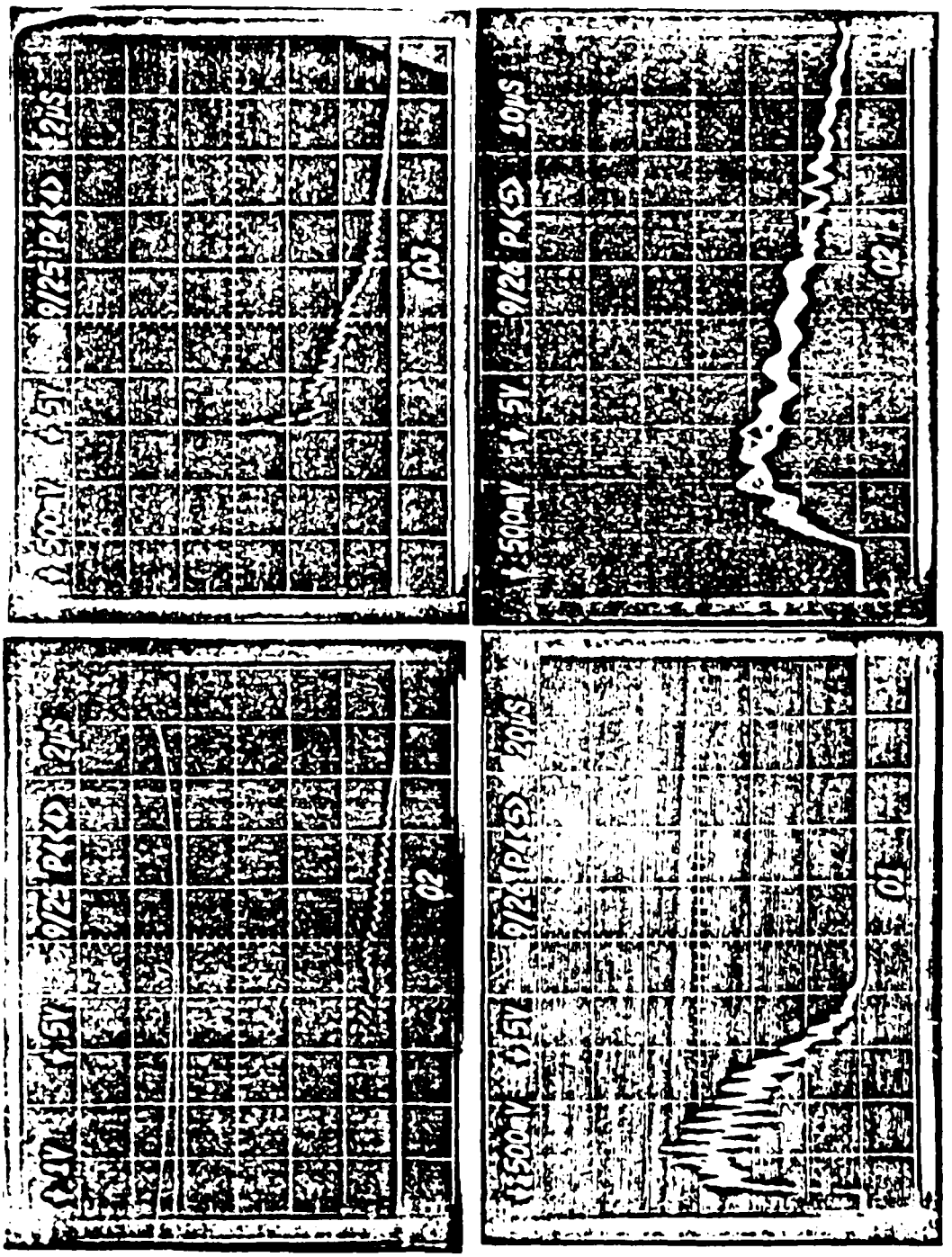

Table F.8 (Continued)

Table F.8 (Continued)

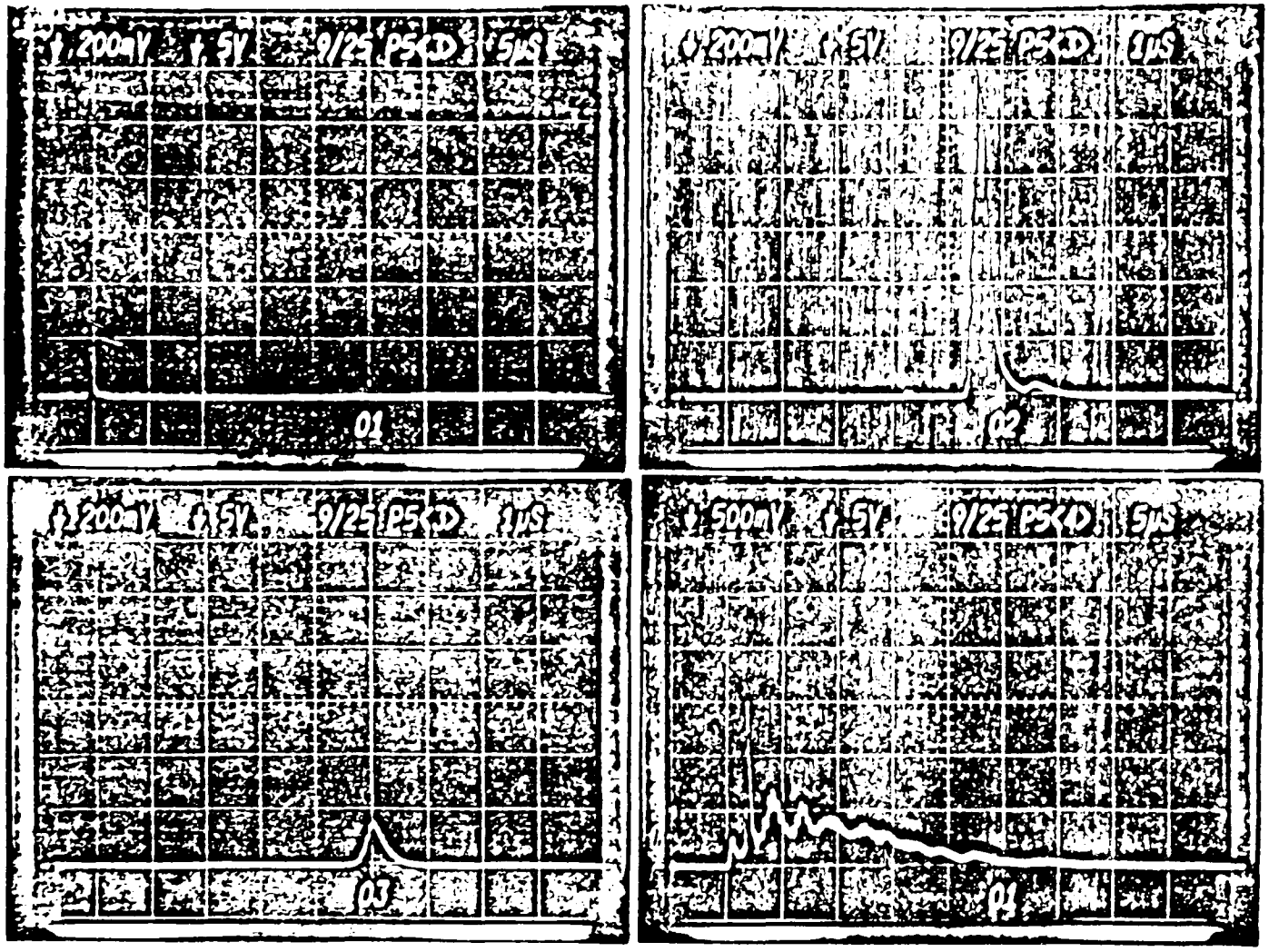

Table F.3 (Continued)

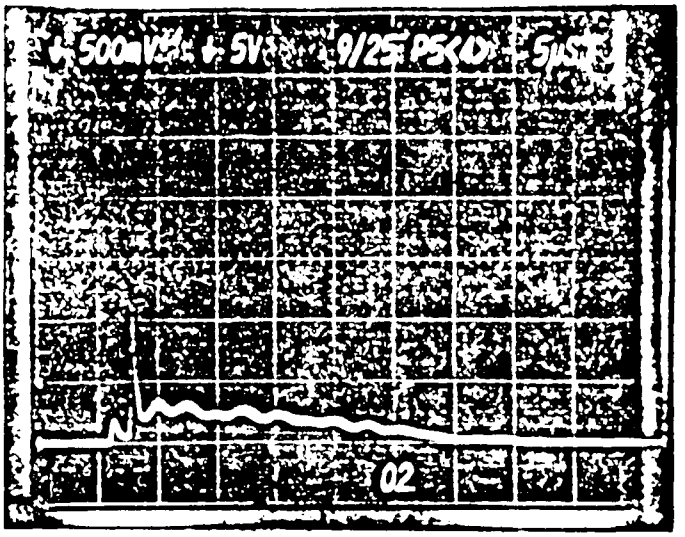

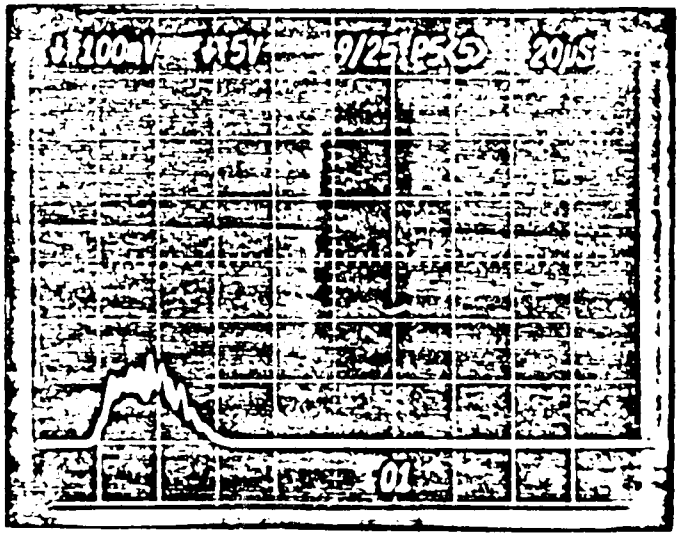

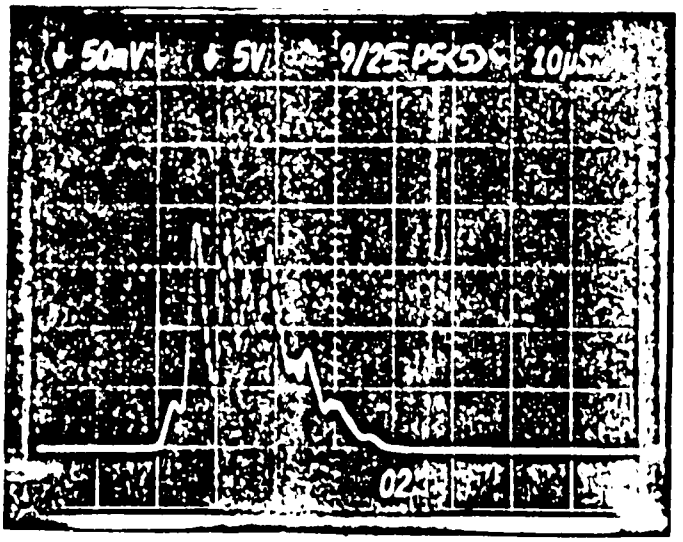

Table F.9 TRS photographes, $He:O_2:F_2:H_2$=22.0:1.0:2.7:1.0, 331 torr, R_0=0.81

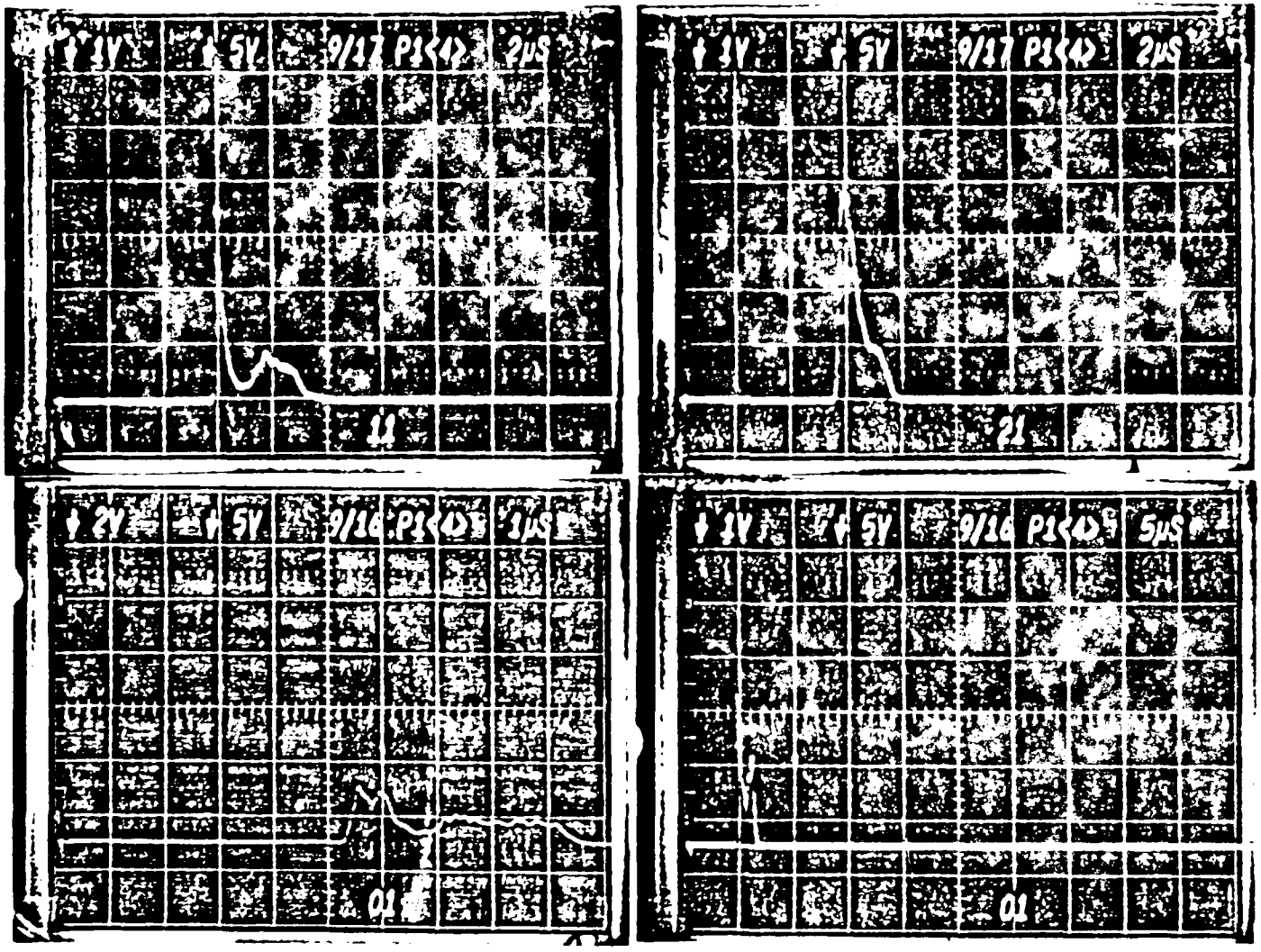

Table F.9 (Continued)

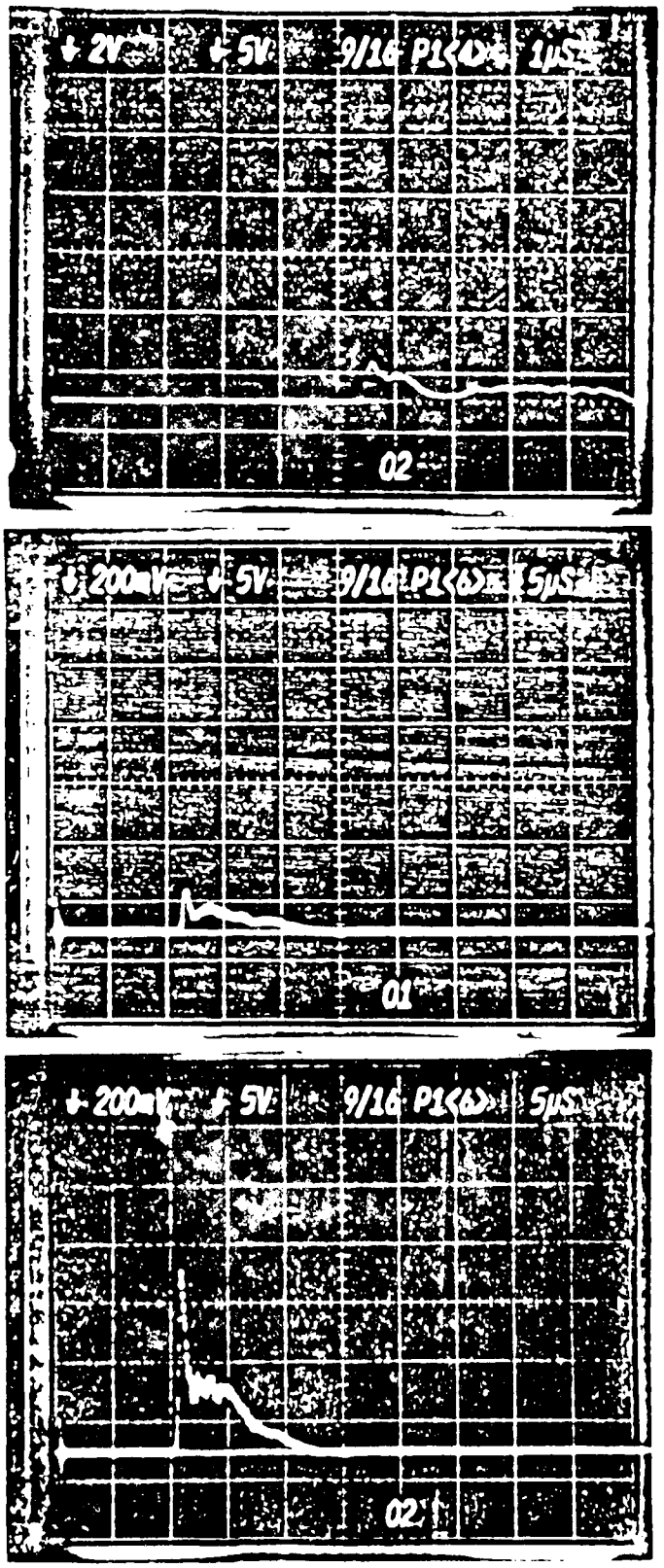

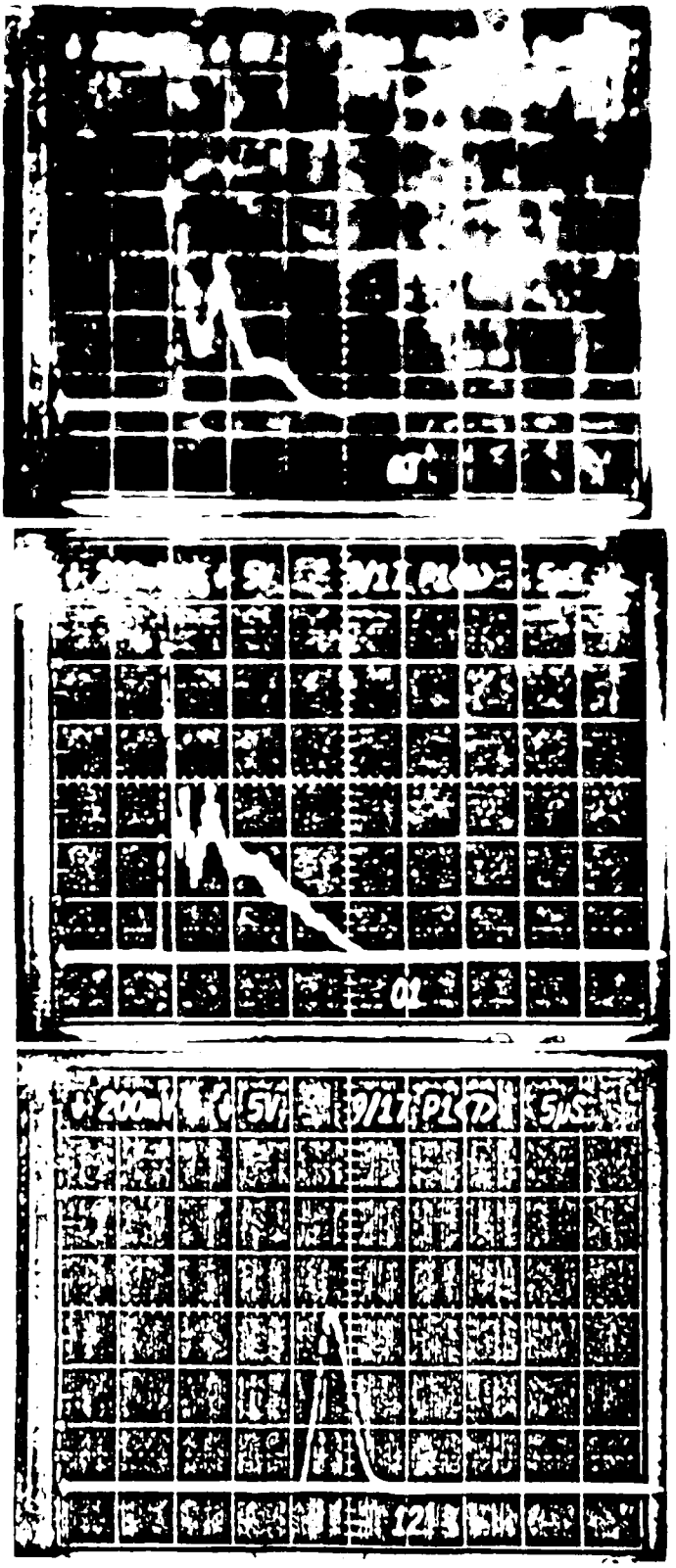

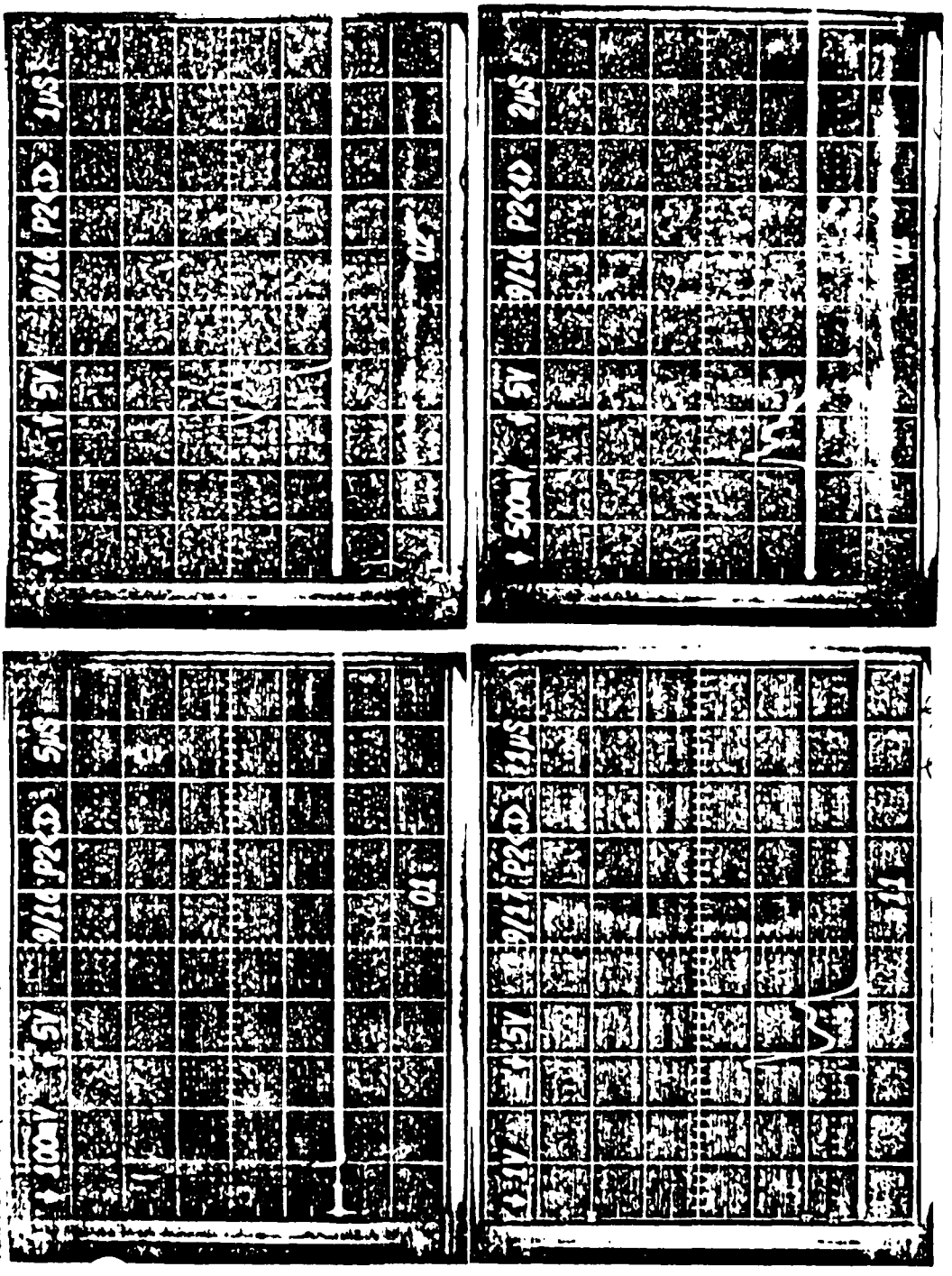

Table F.9 (Continued)

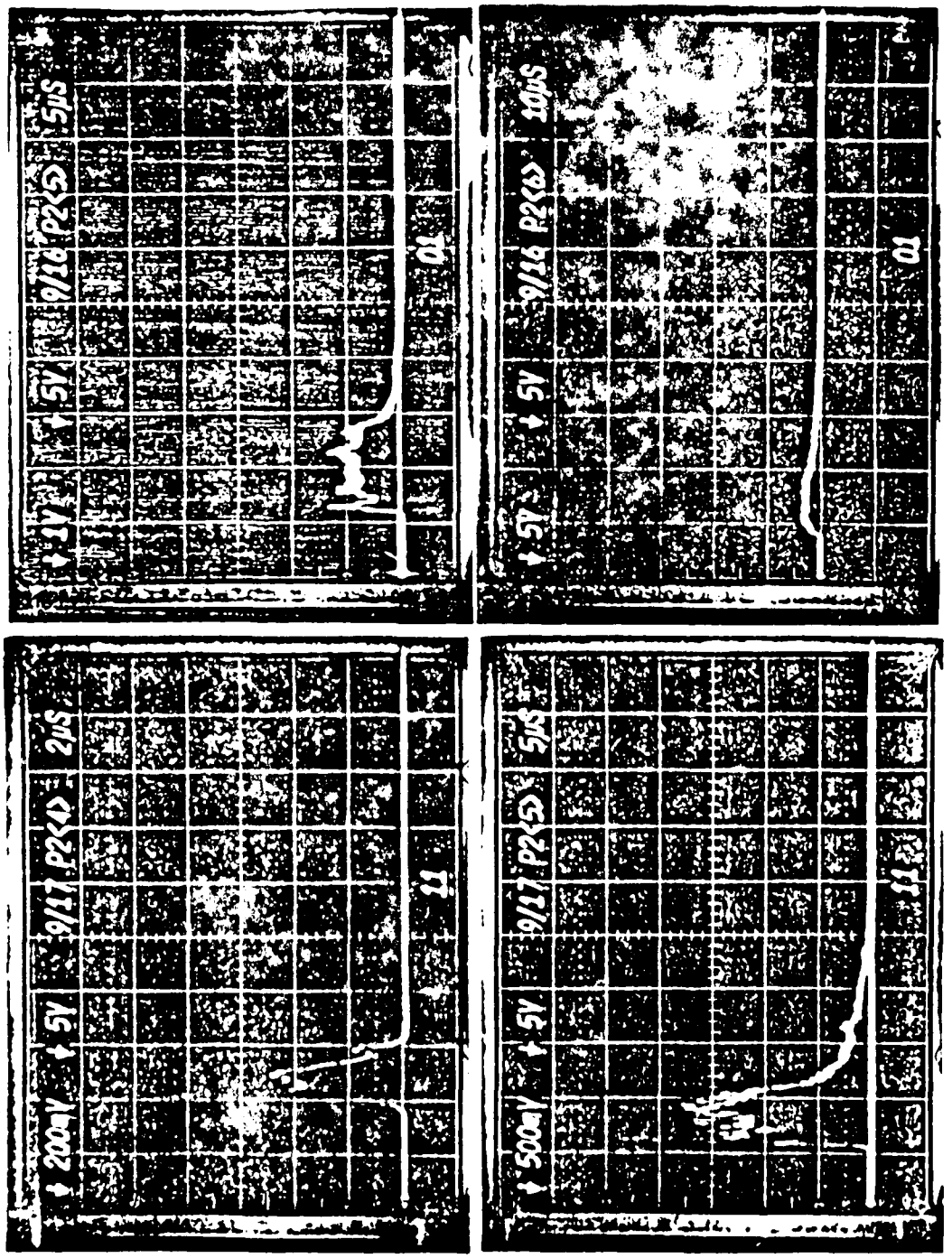

Table F.9 (Continued)

Table F.9 (Continued)

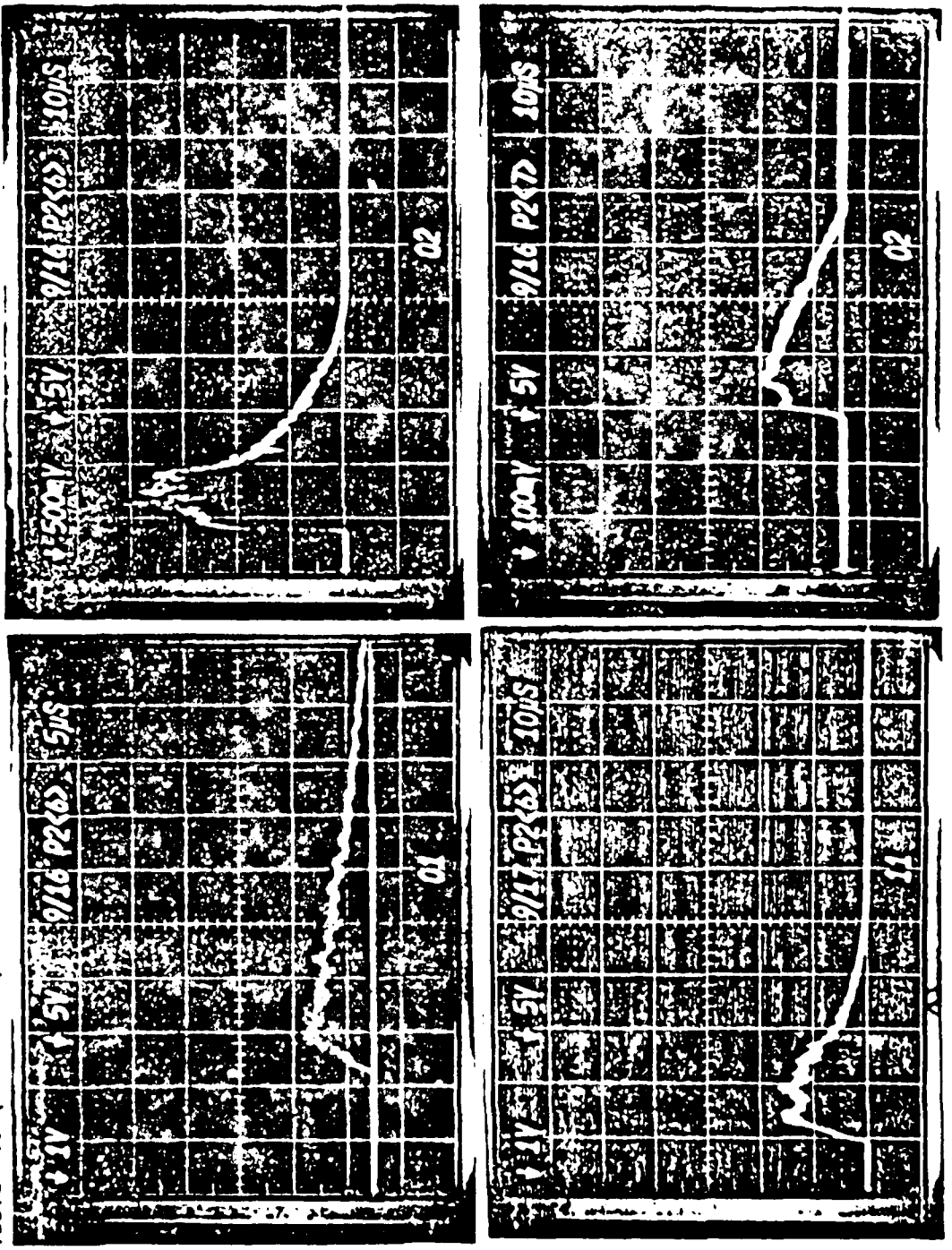

Table F.9 (Continued)

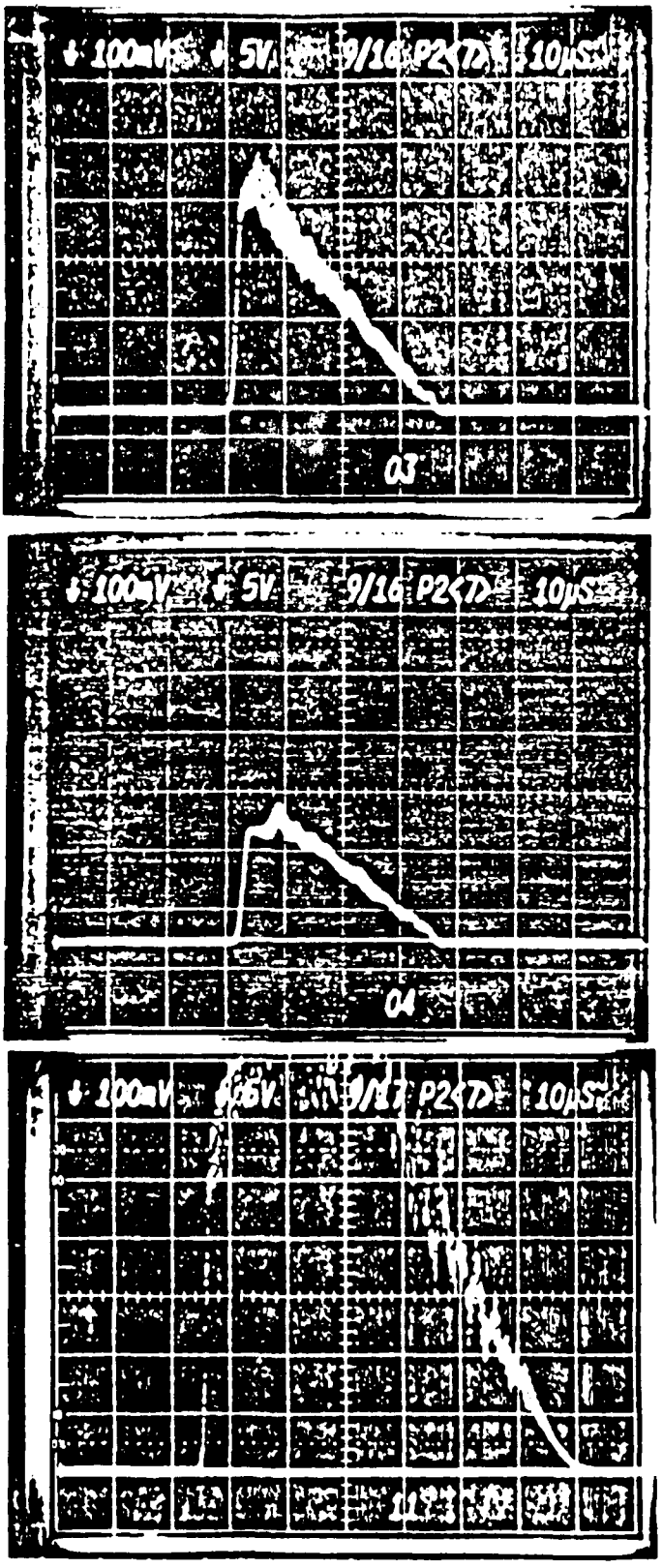

Table F.9 (Continued)

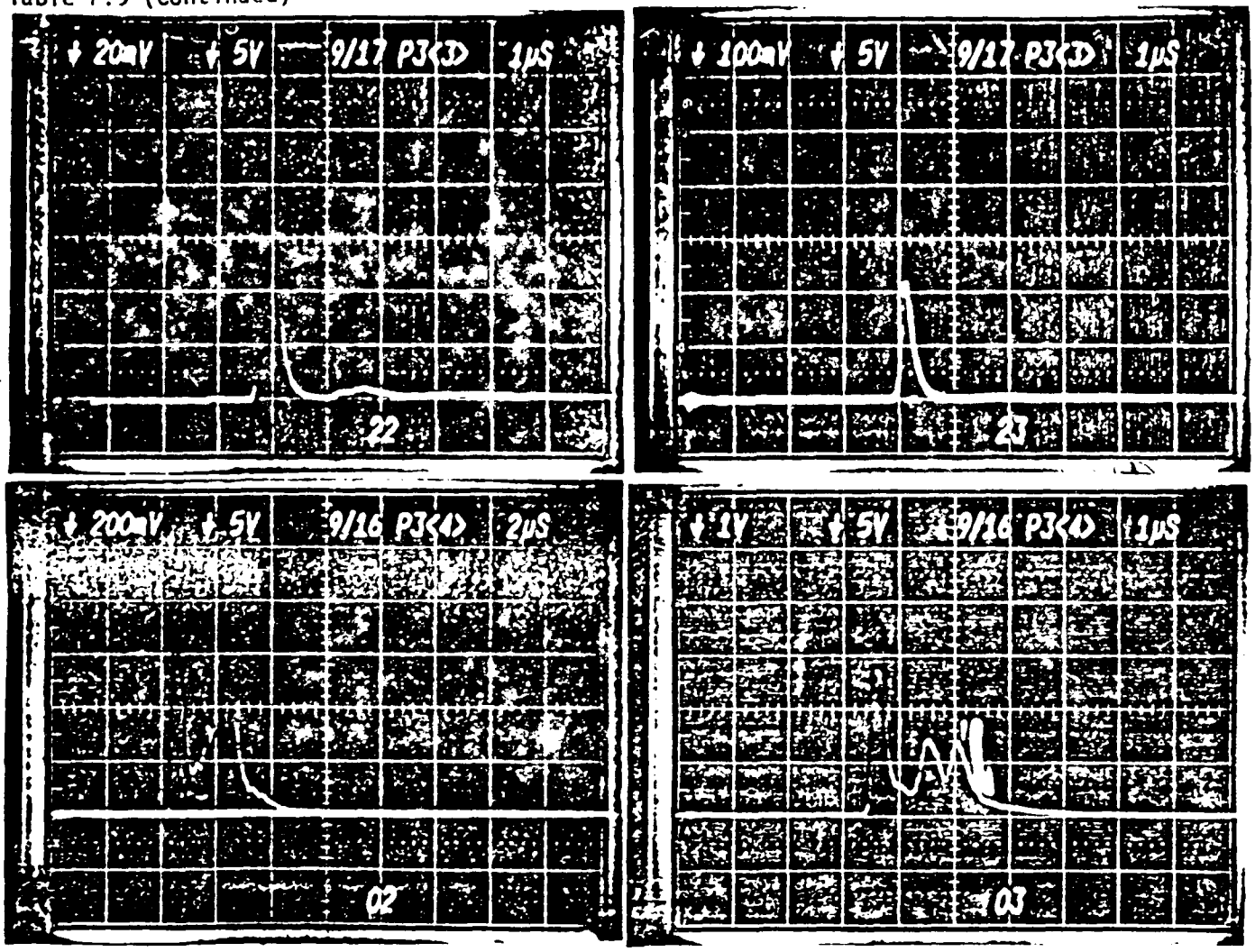

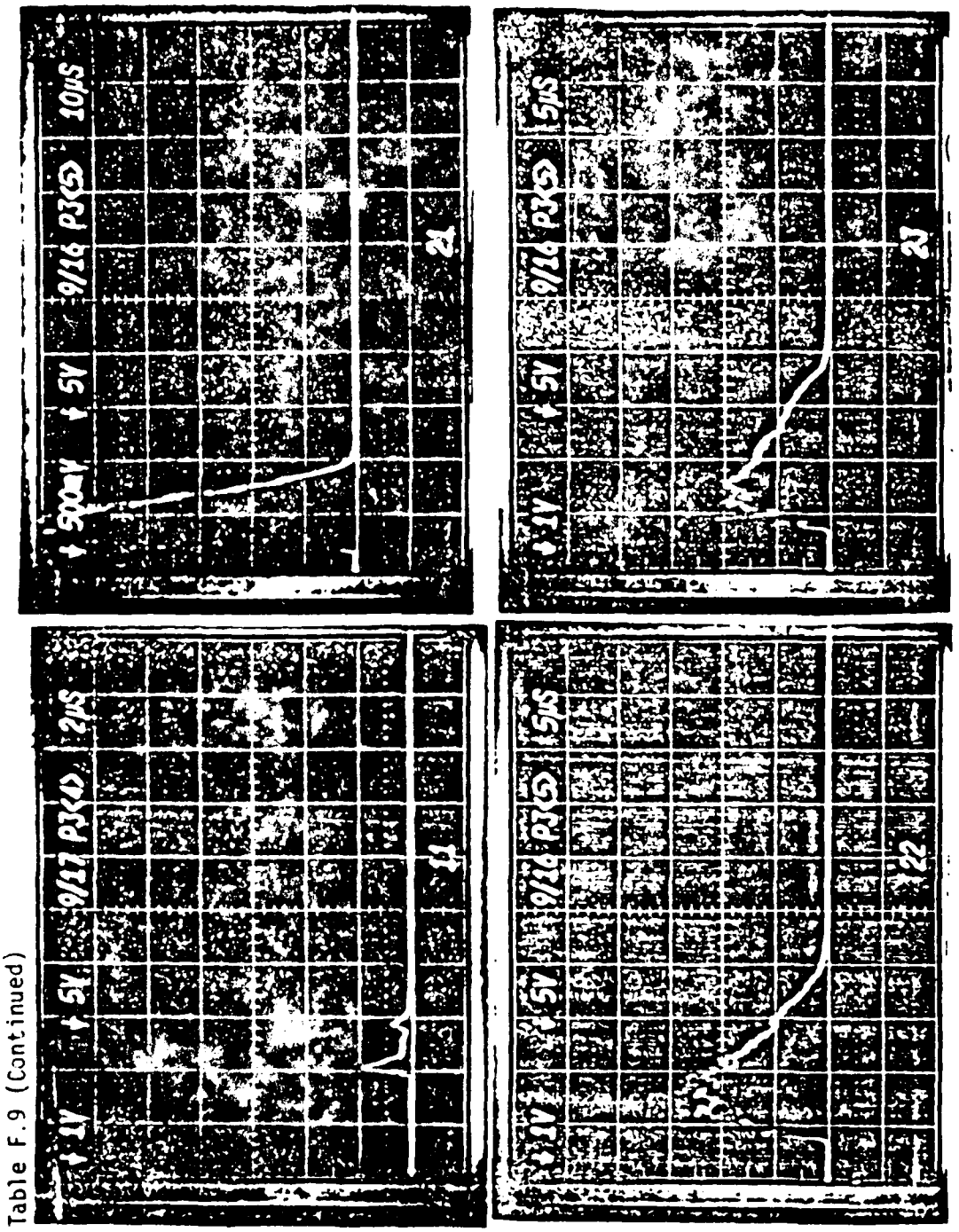

Table F.9 (Continued)

Table F.9 (Continued)

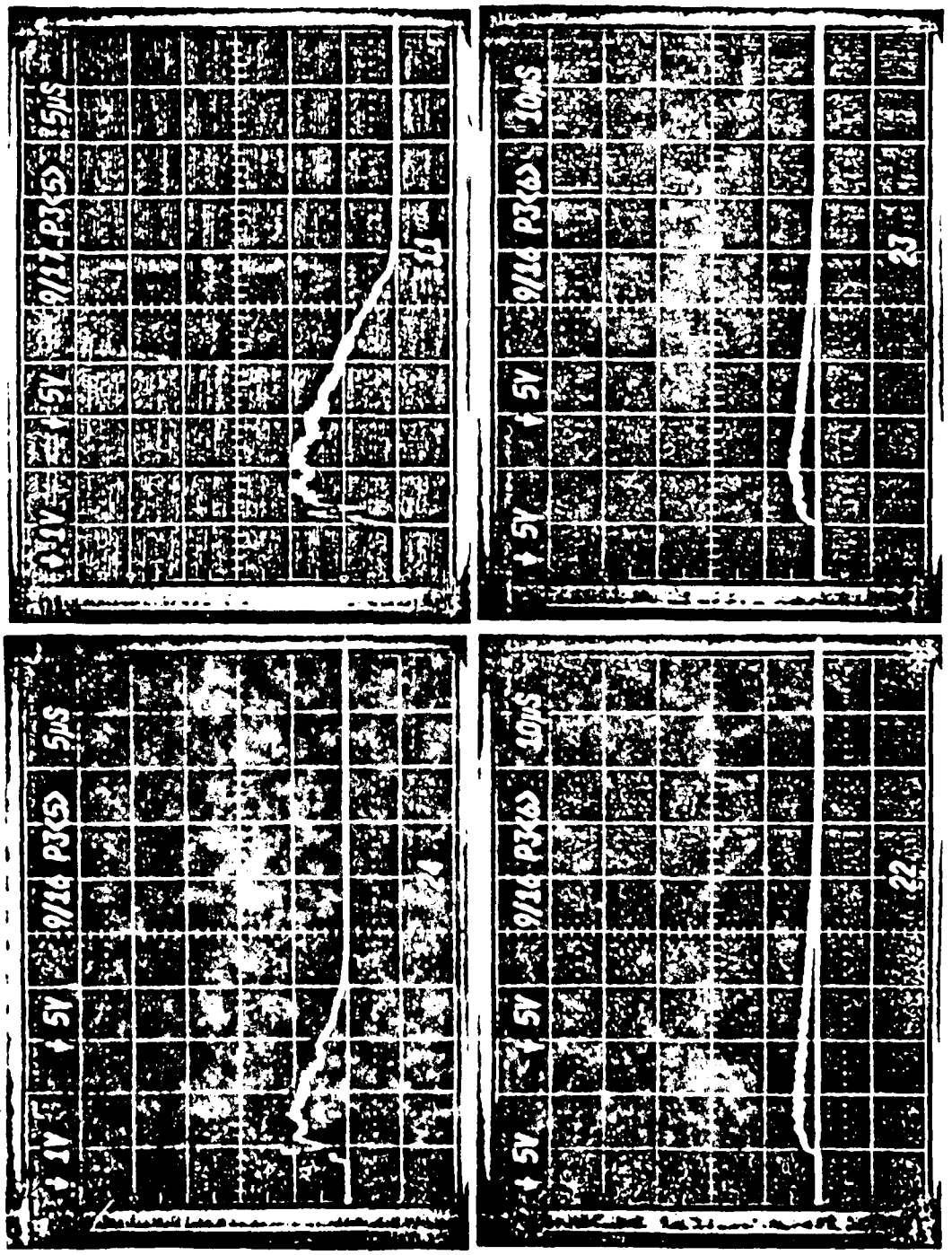

Table F.9 (Continued)

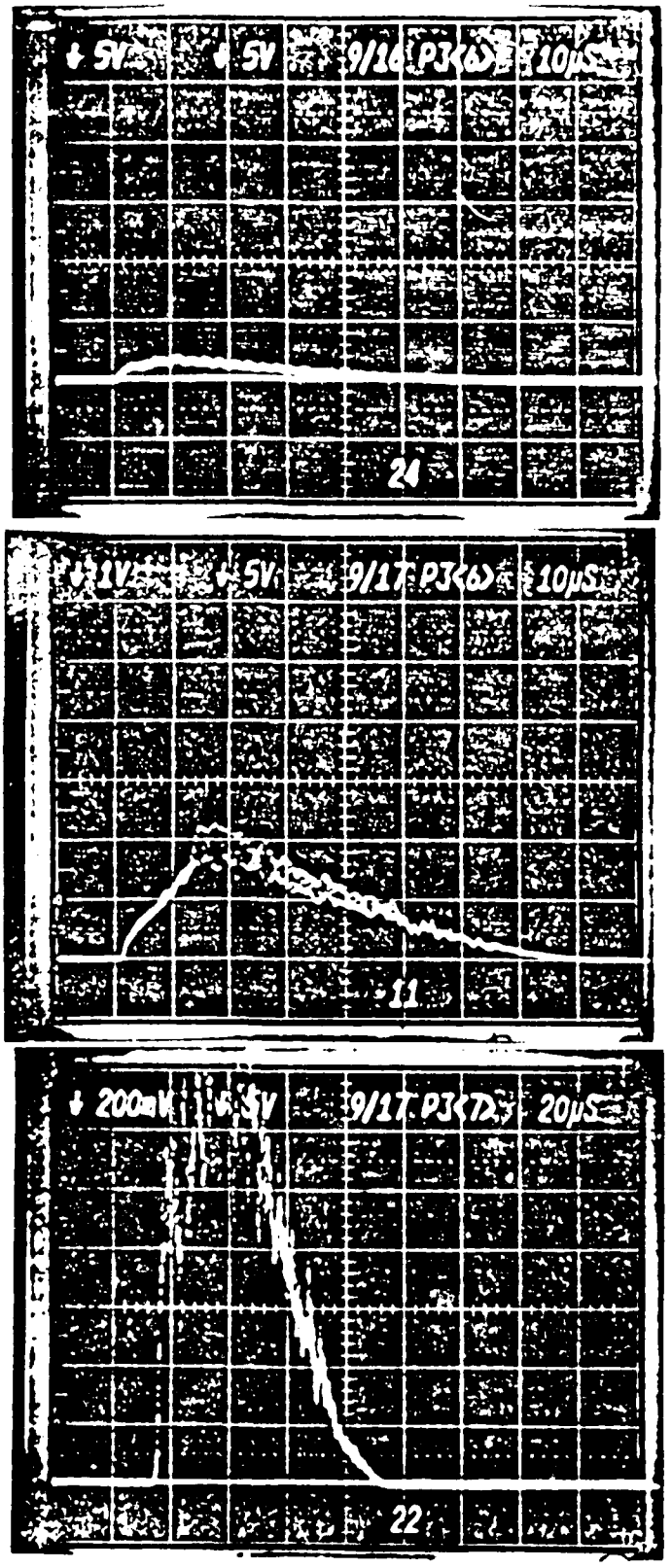

Table F.9 (Continued)

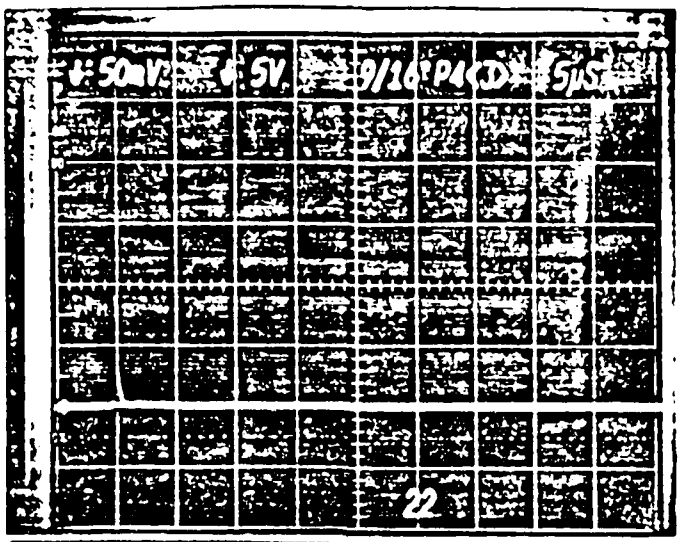

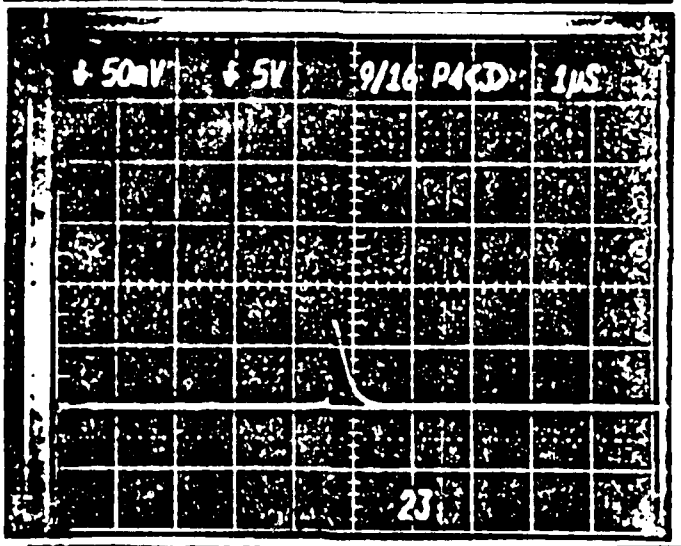

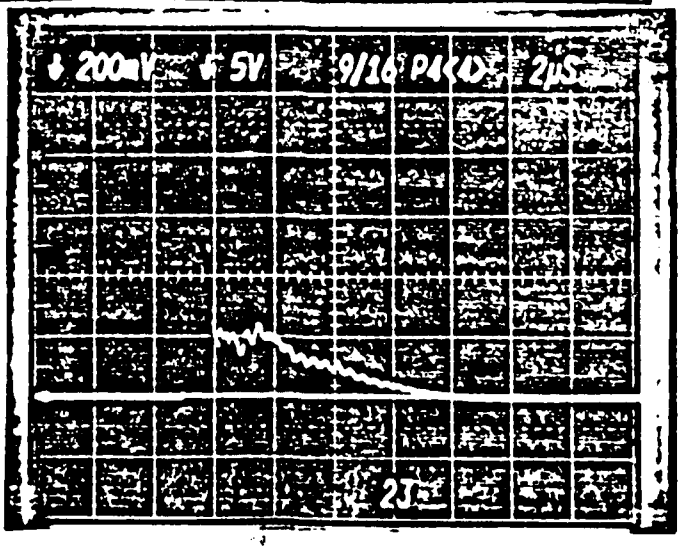

Table F.3 (Continued)

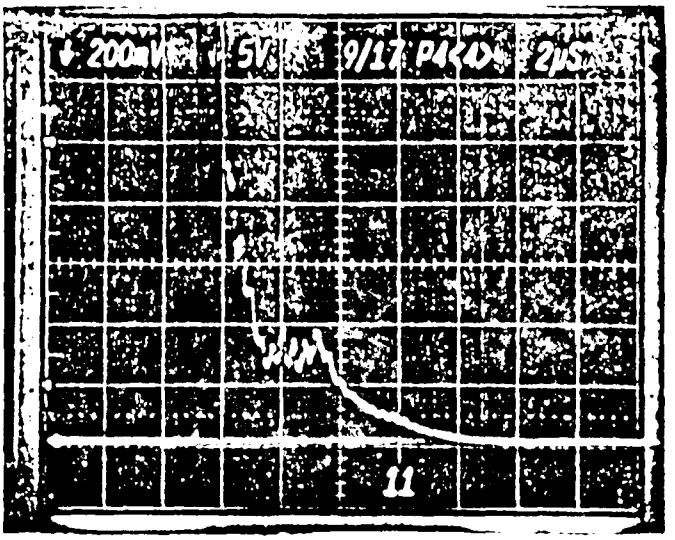

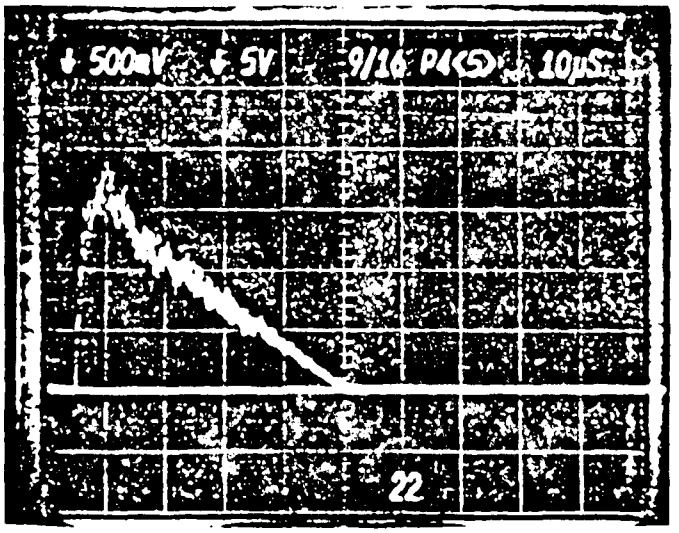

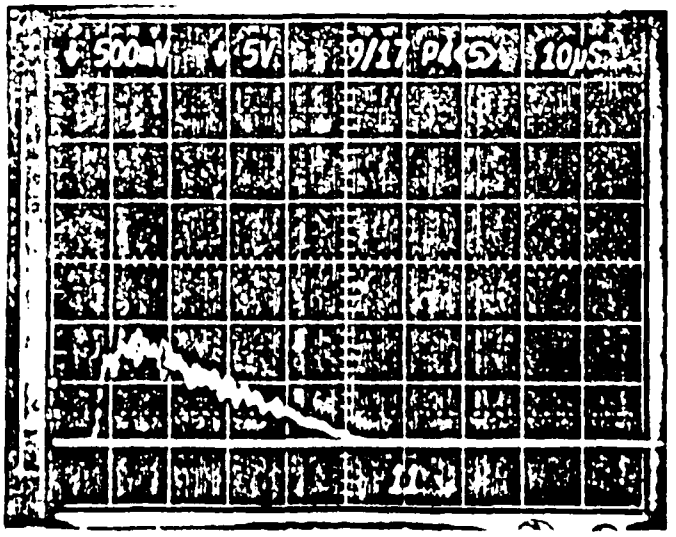

Table F.9 (Continued)

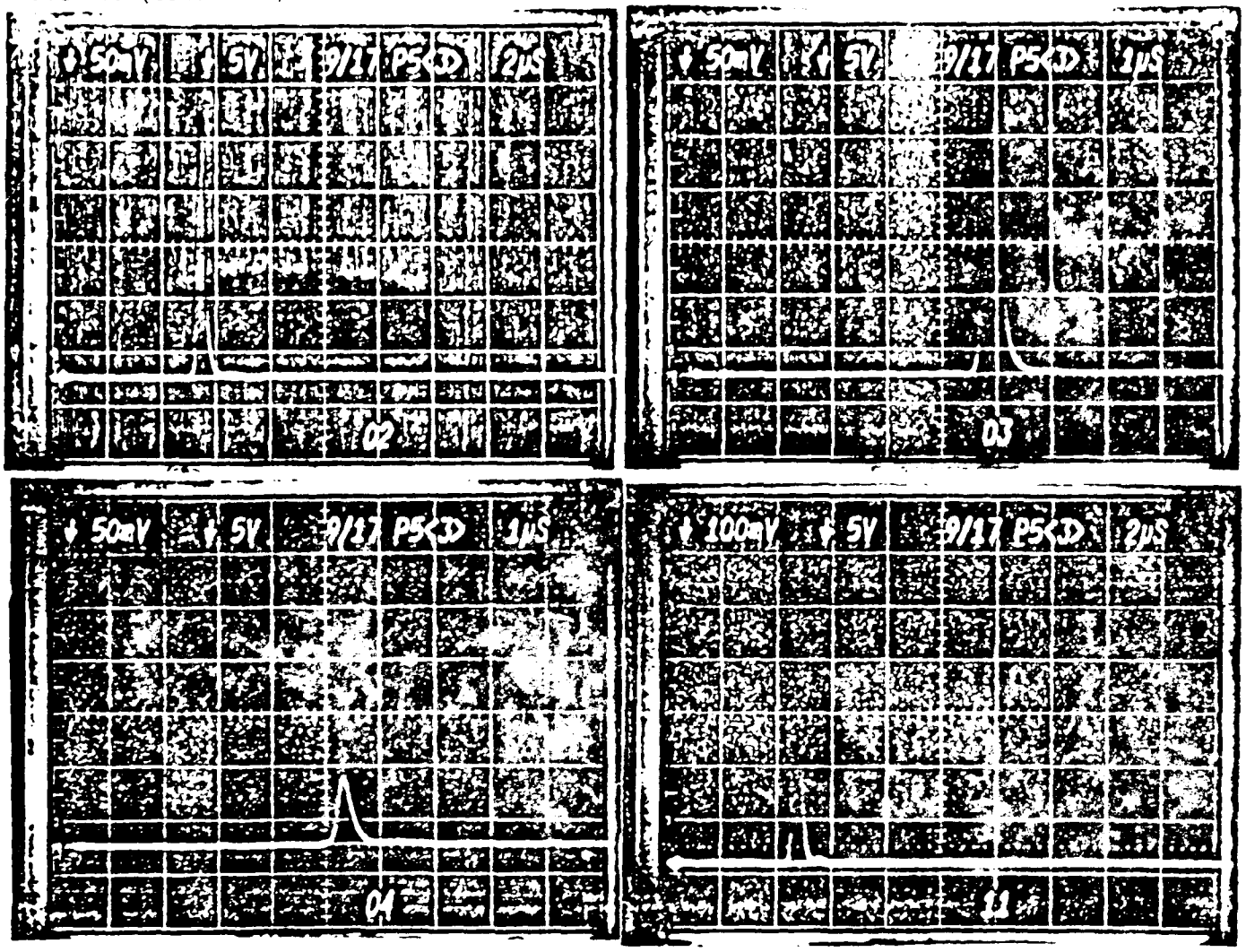

Table F.9 (Continued)

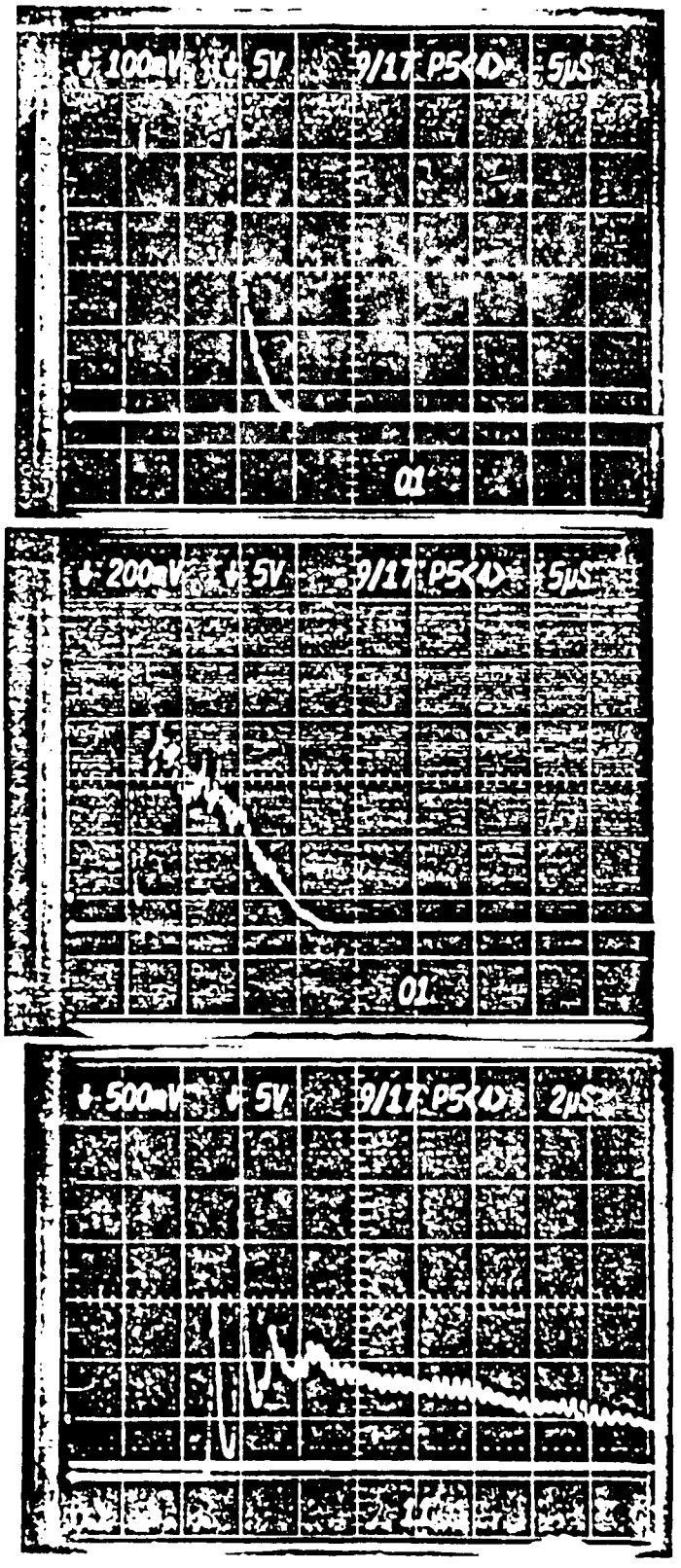

Table F.9 (Continued)

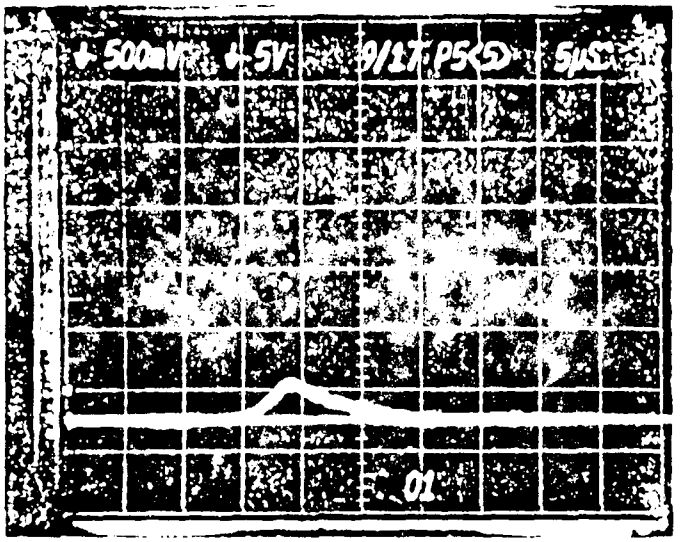

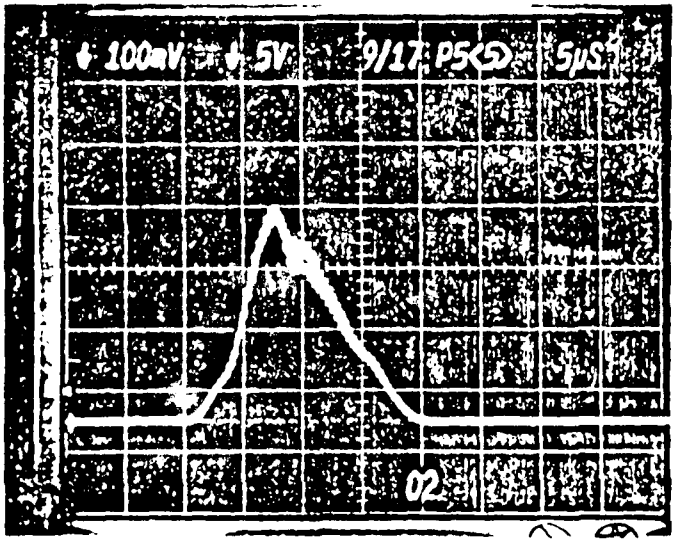

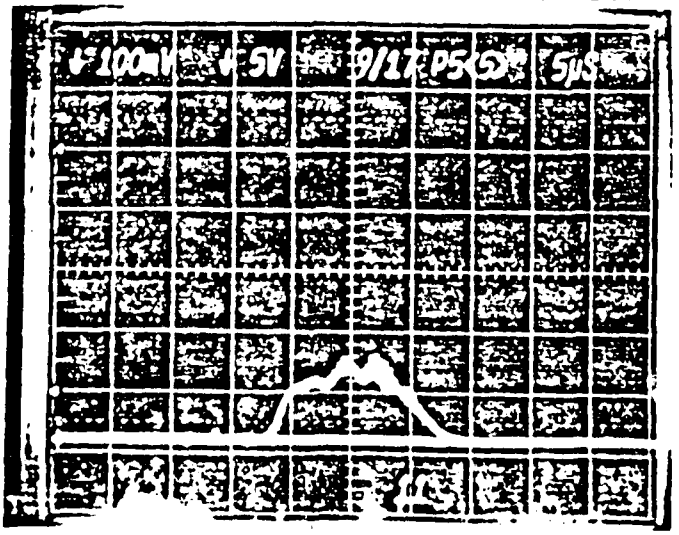

Table F.10 TRS photographes, $He:O_2:F_2:H_2$=22.0:1.0:2.7:1.0, 331 torr, R_0=0.97

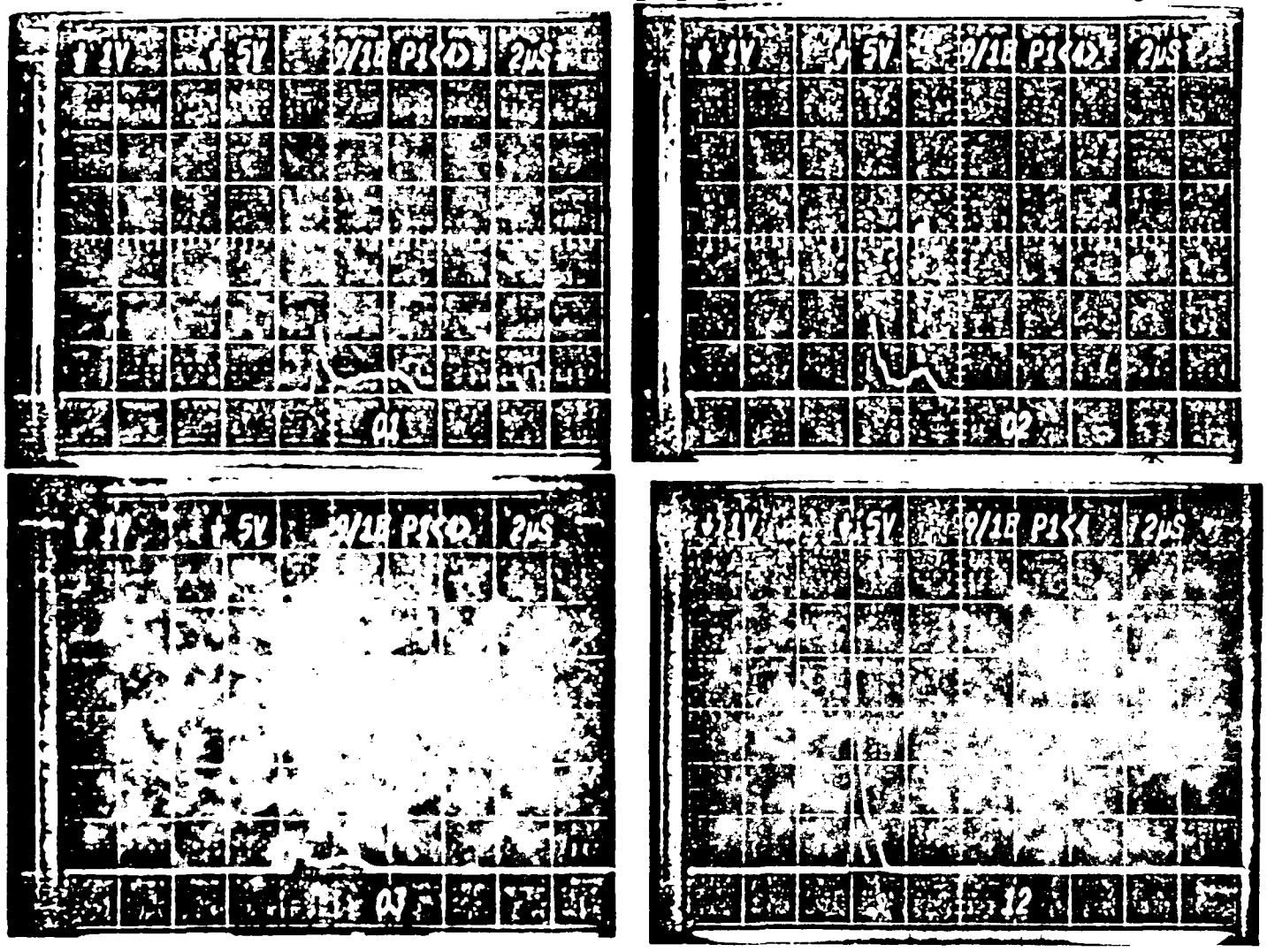

Table F.10 (Continued)

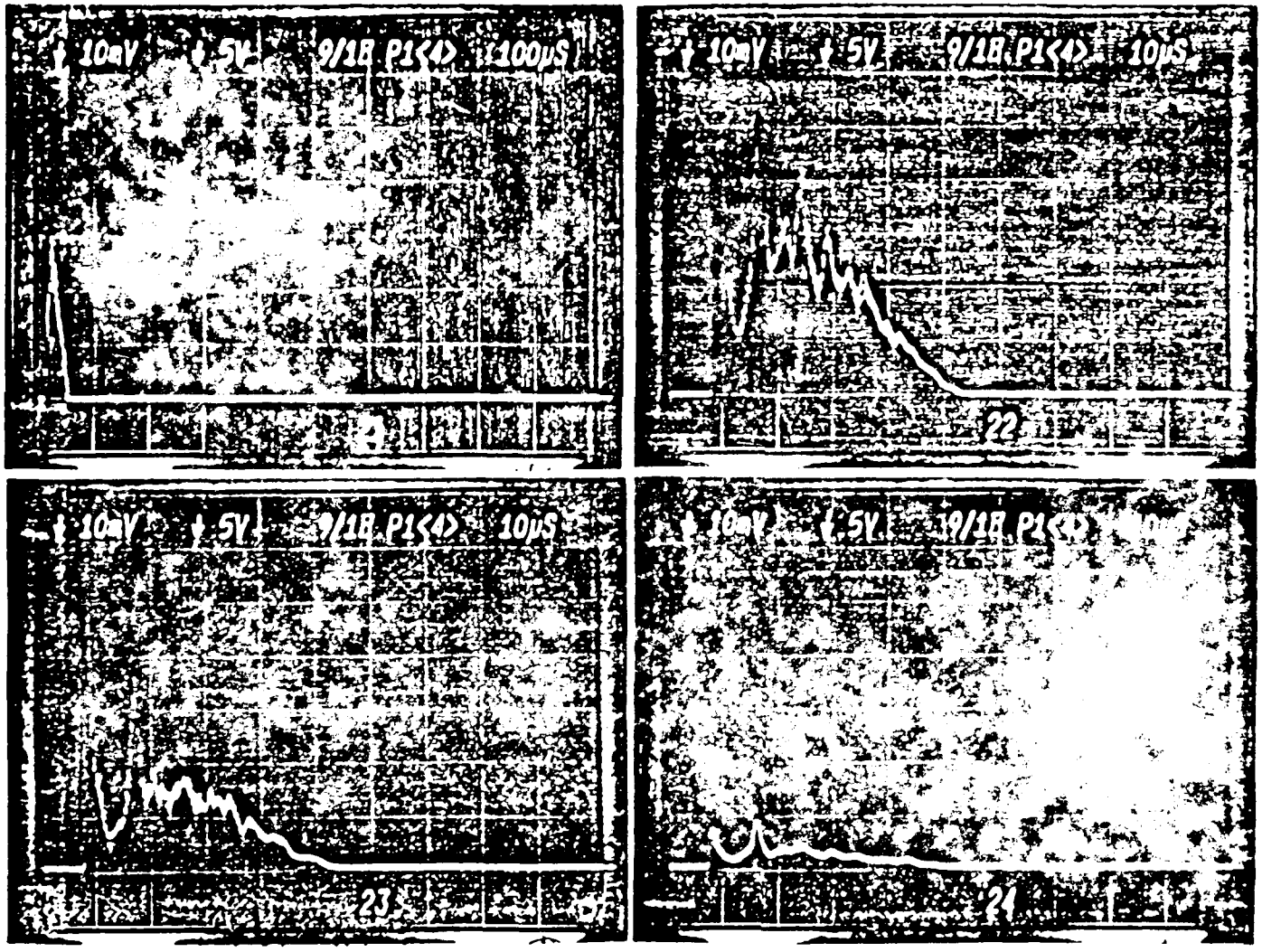

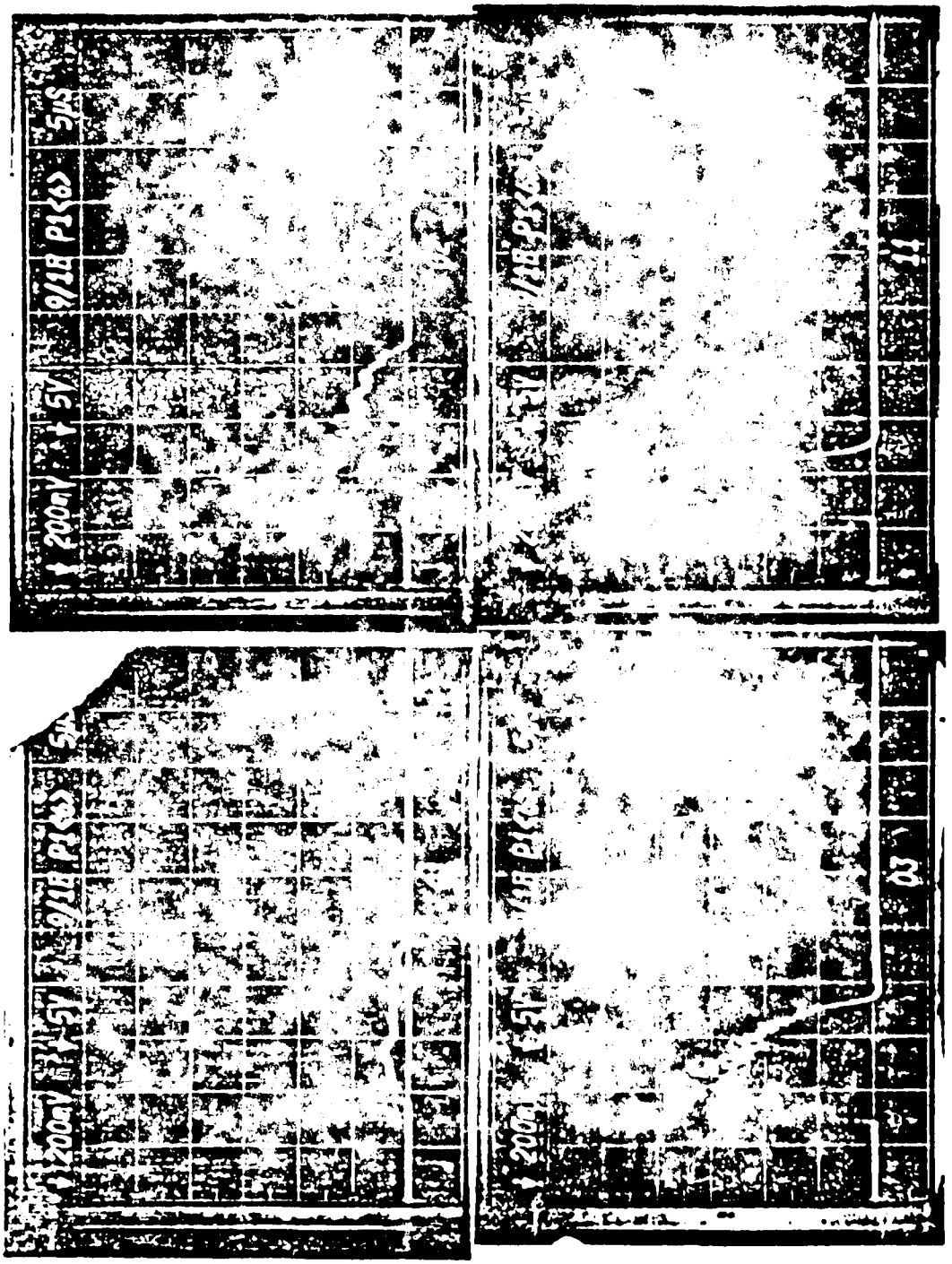

Table F.10 (Continued)

Table F.10 (Continued)

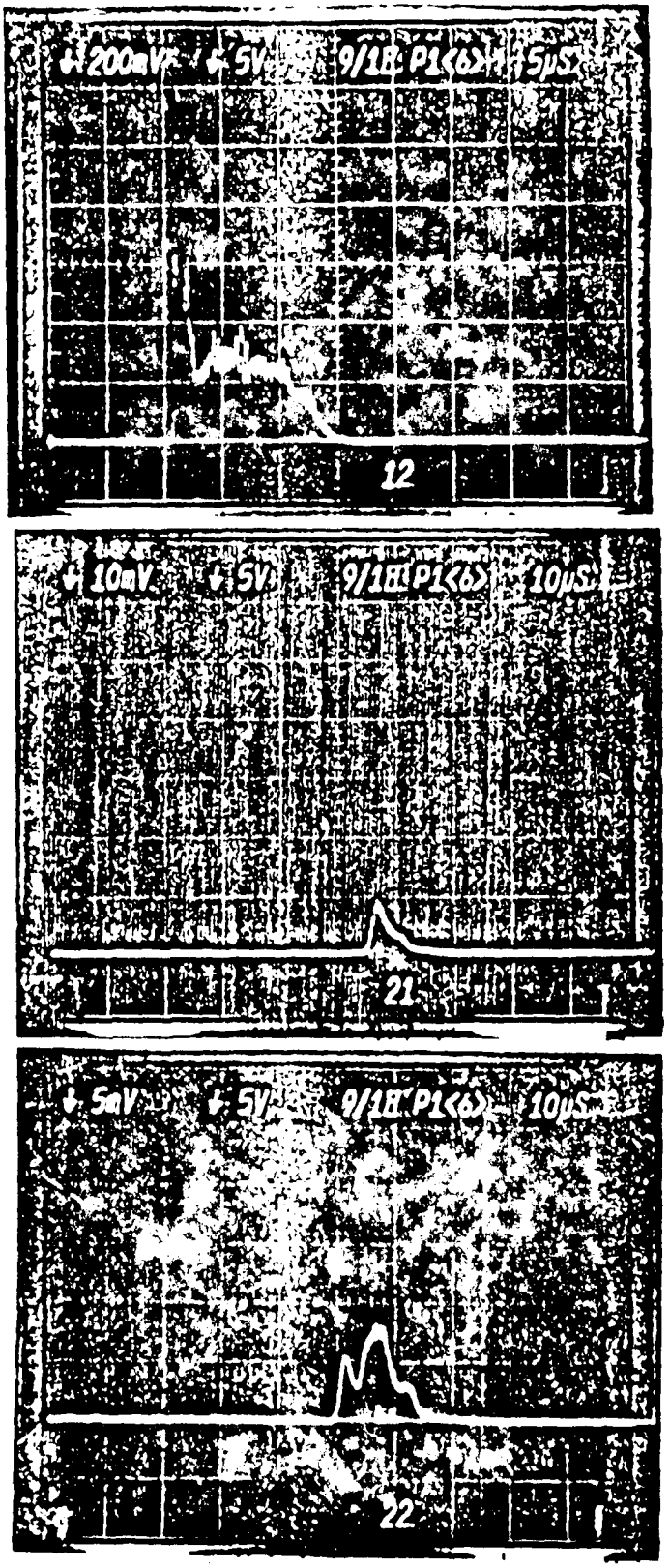

Table F.10 (Continued)

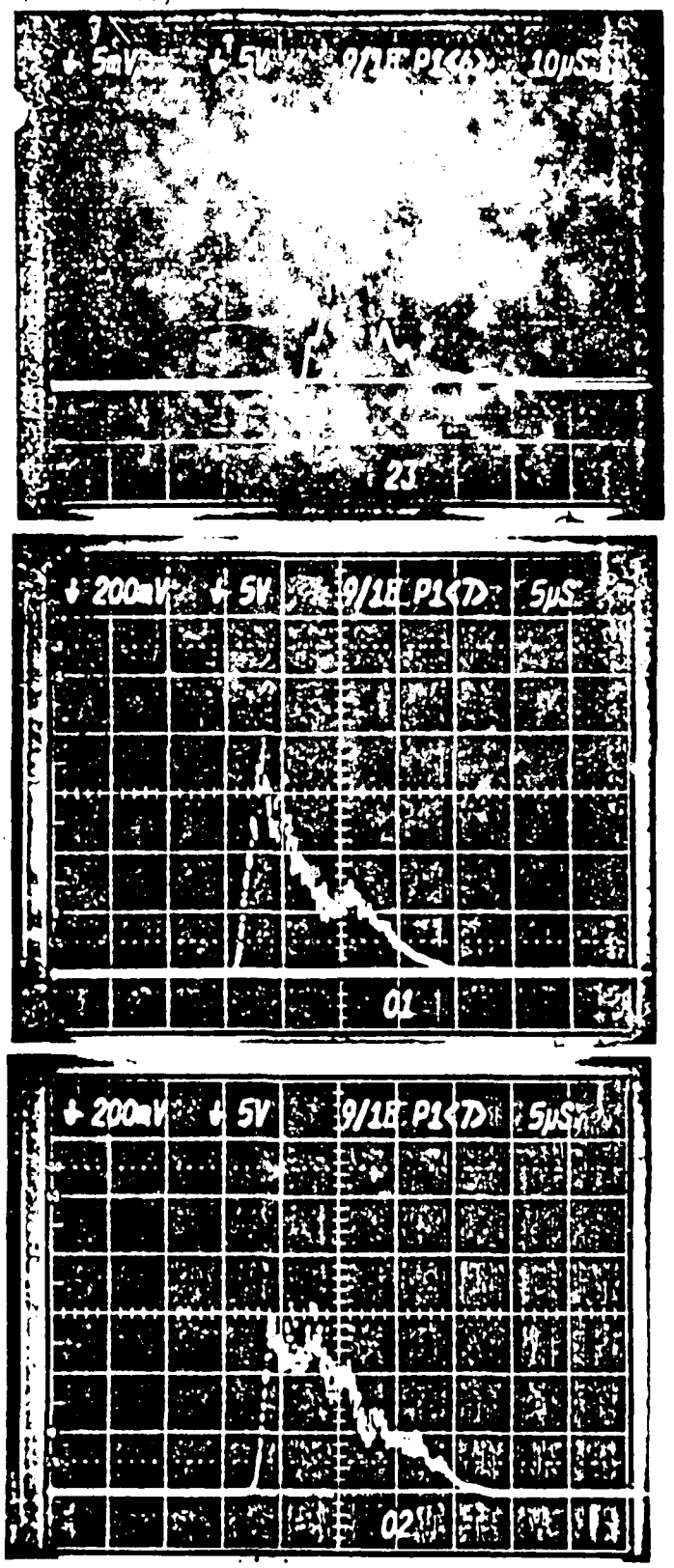

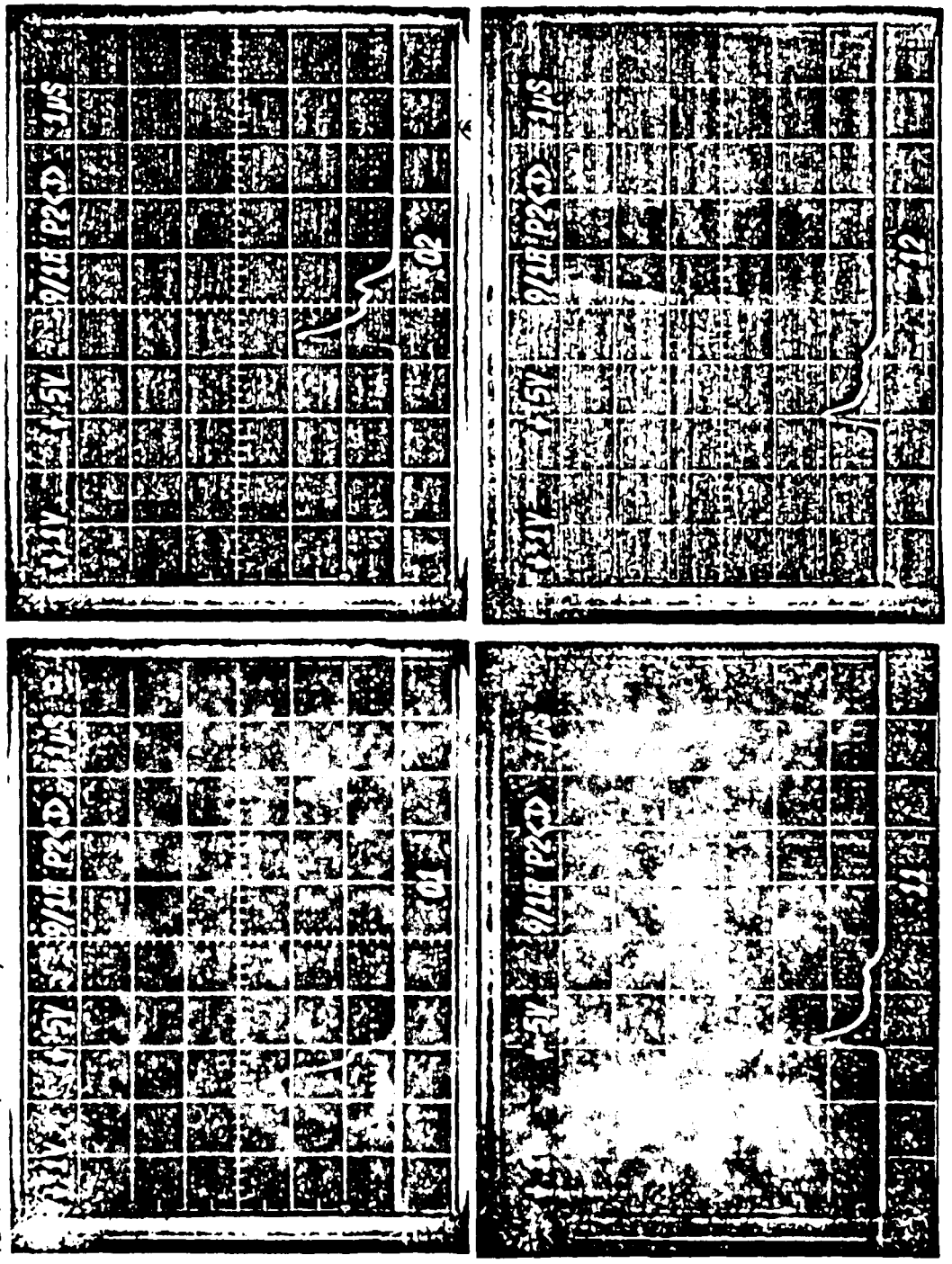

Table F.10 (Continued)

Table F.10 (Continued)

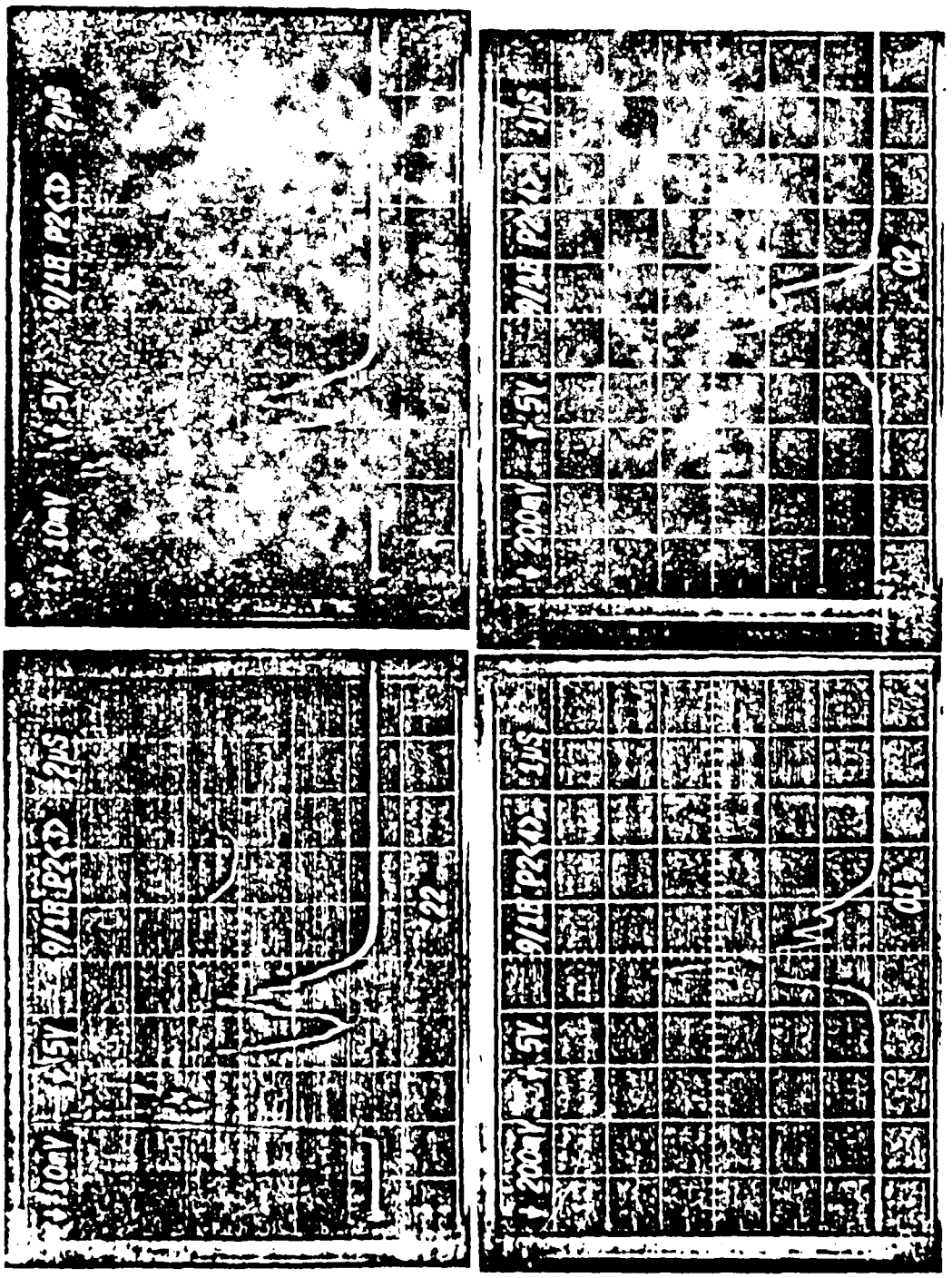

Table F.10 (Continued)

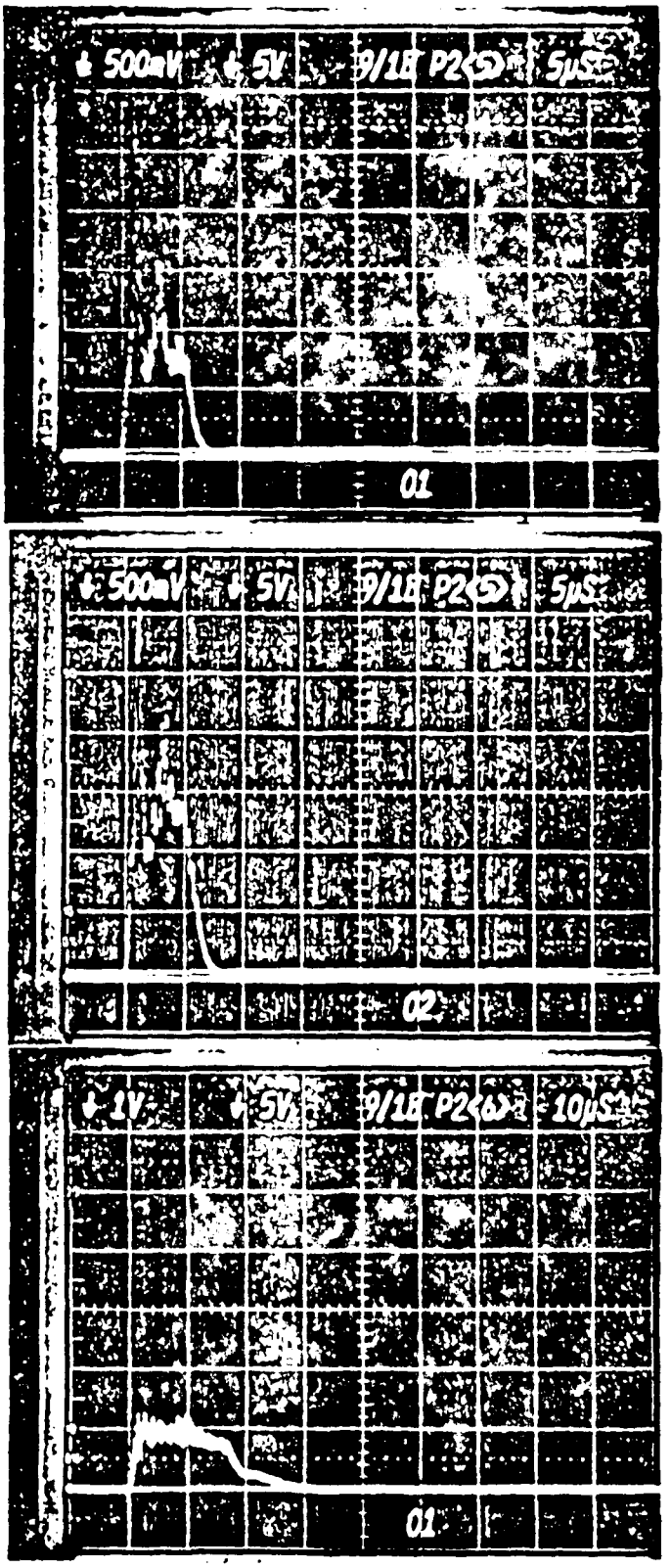

Table F.10 (Continued)

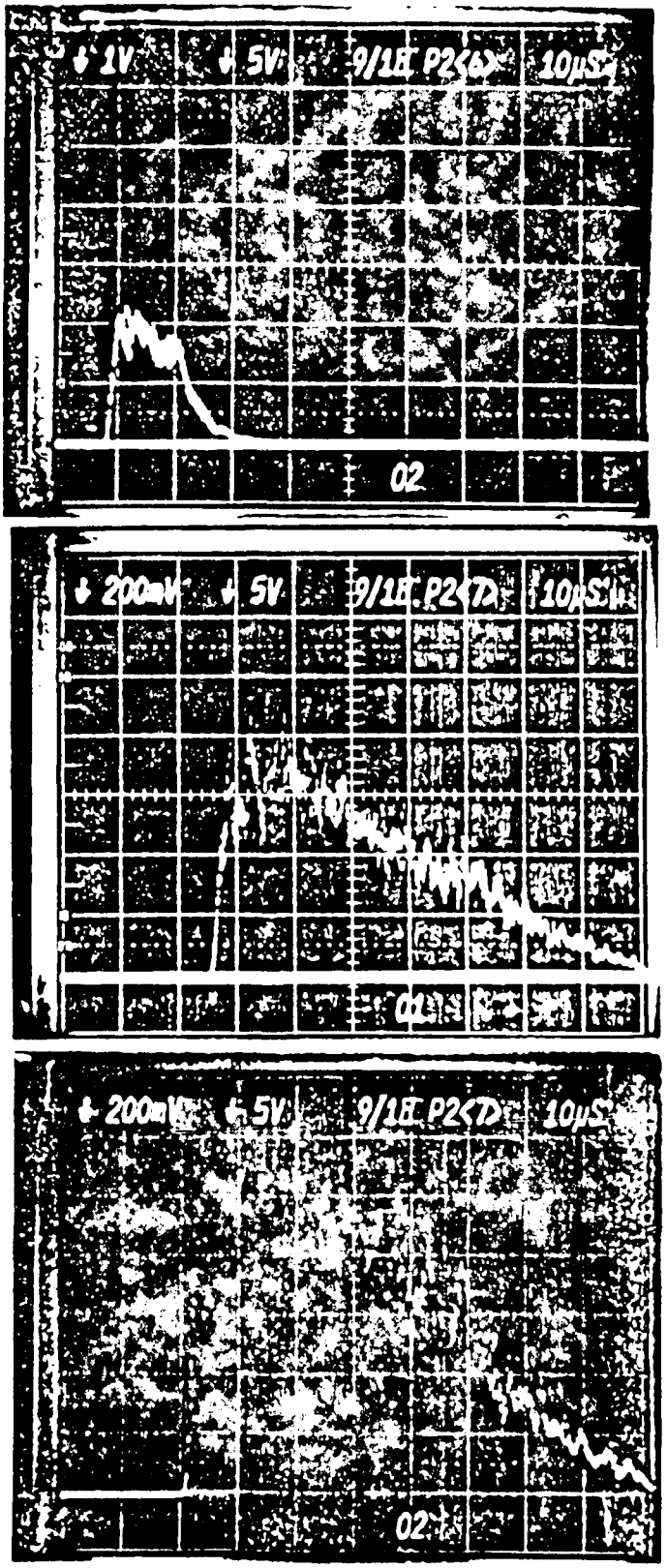

Table F.10 (Continued)

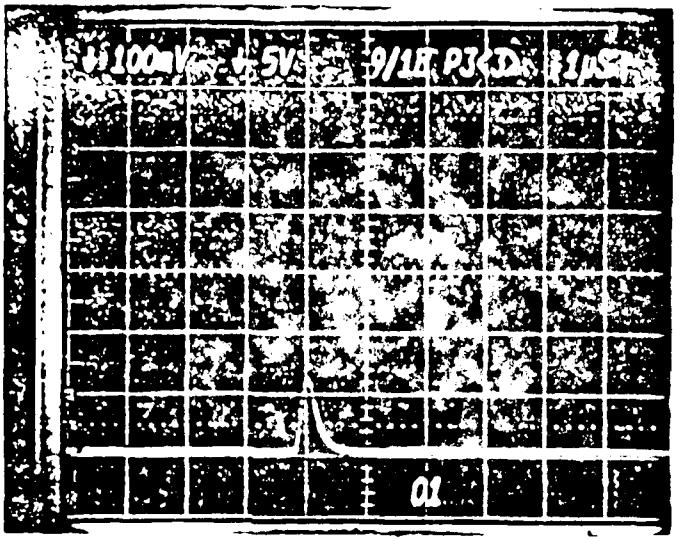

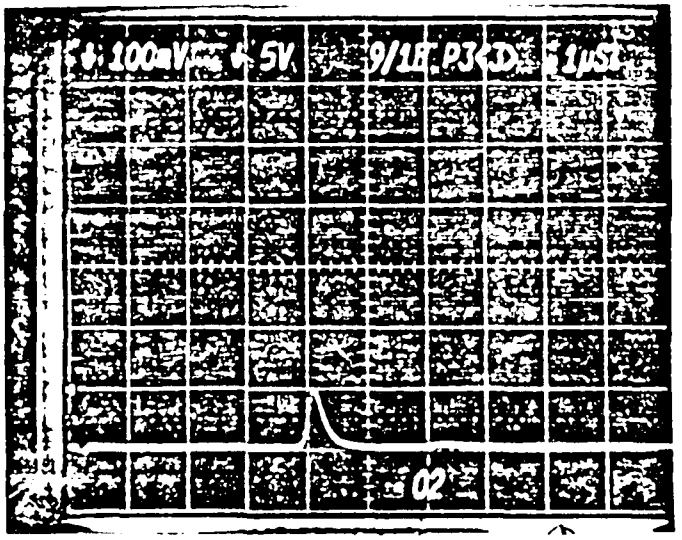

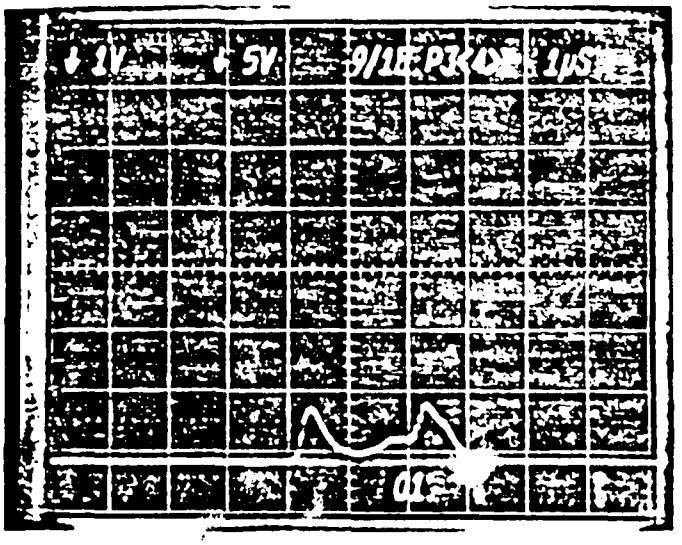

Table F.10 (Continued)

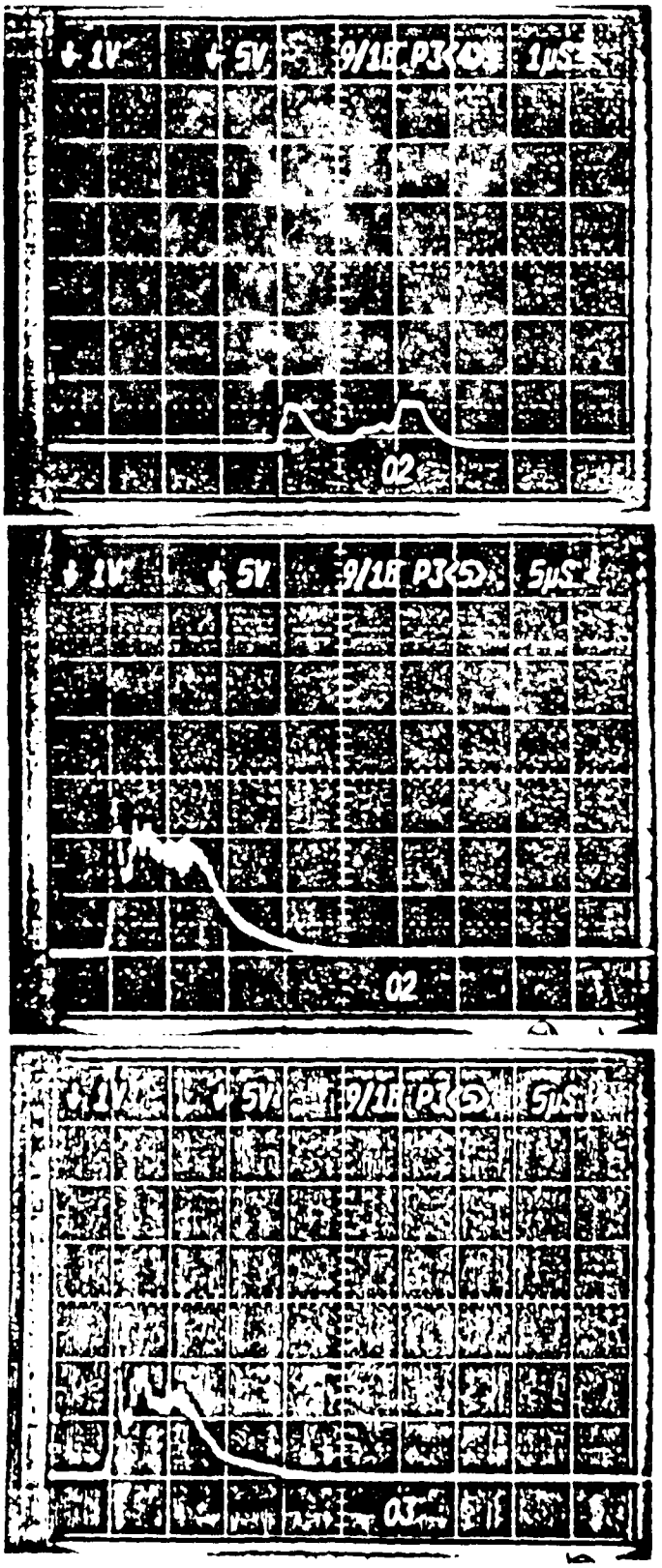

Table F.10 (Continued)

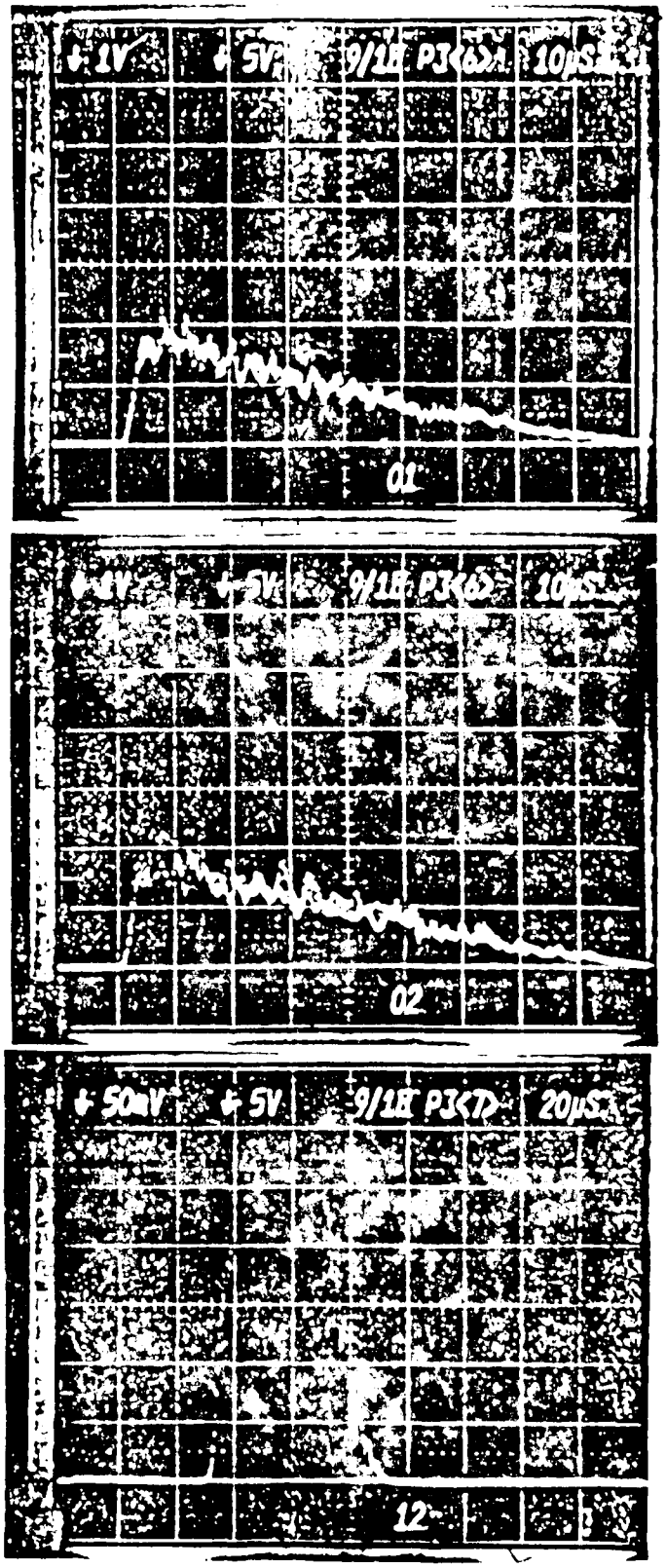

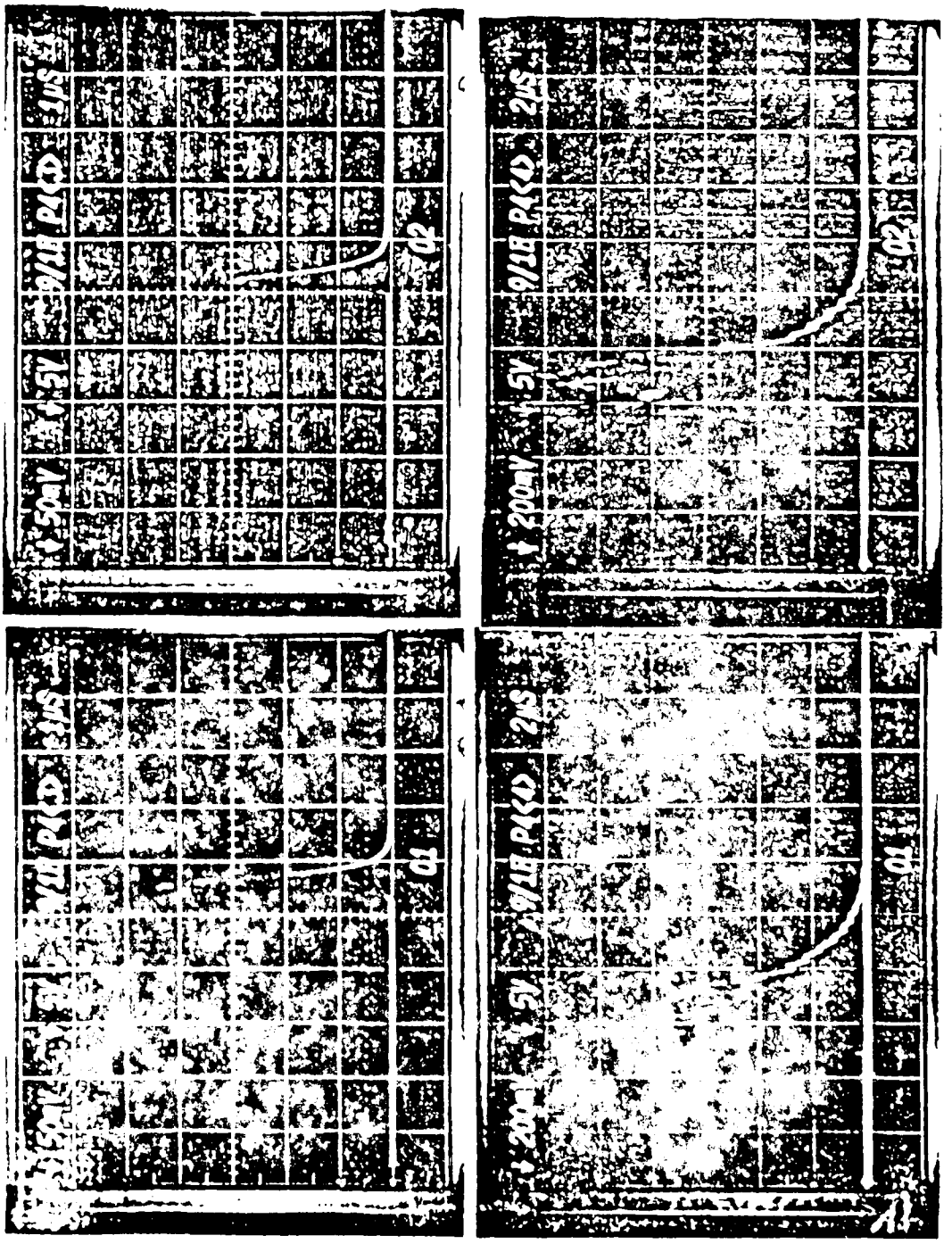

Table F.10 (Continued)

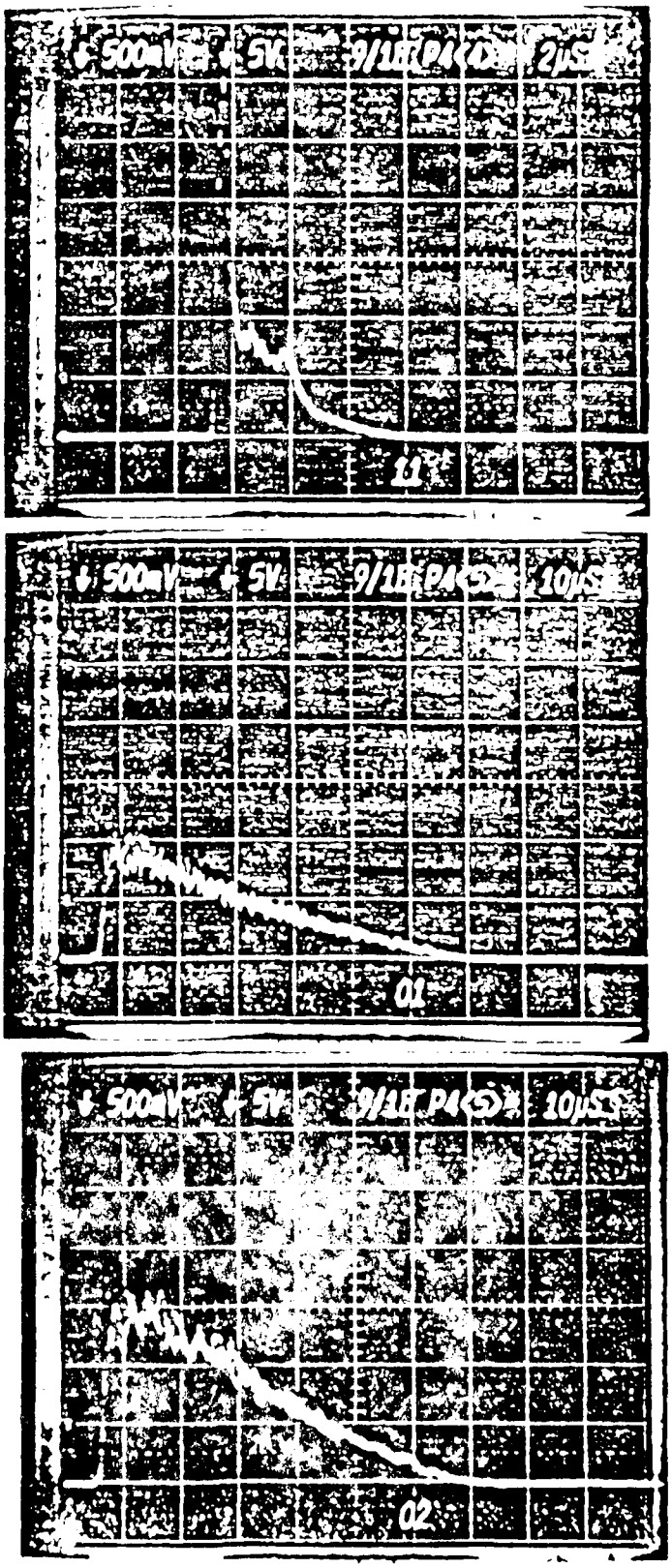

Table F.10 (Continued)

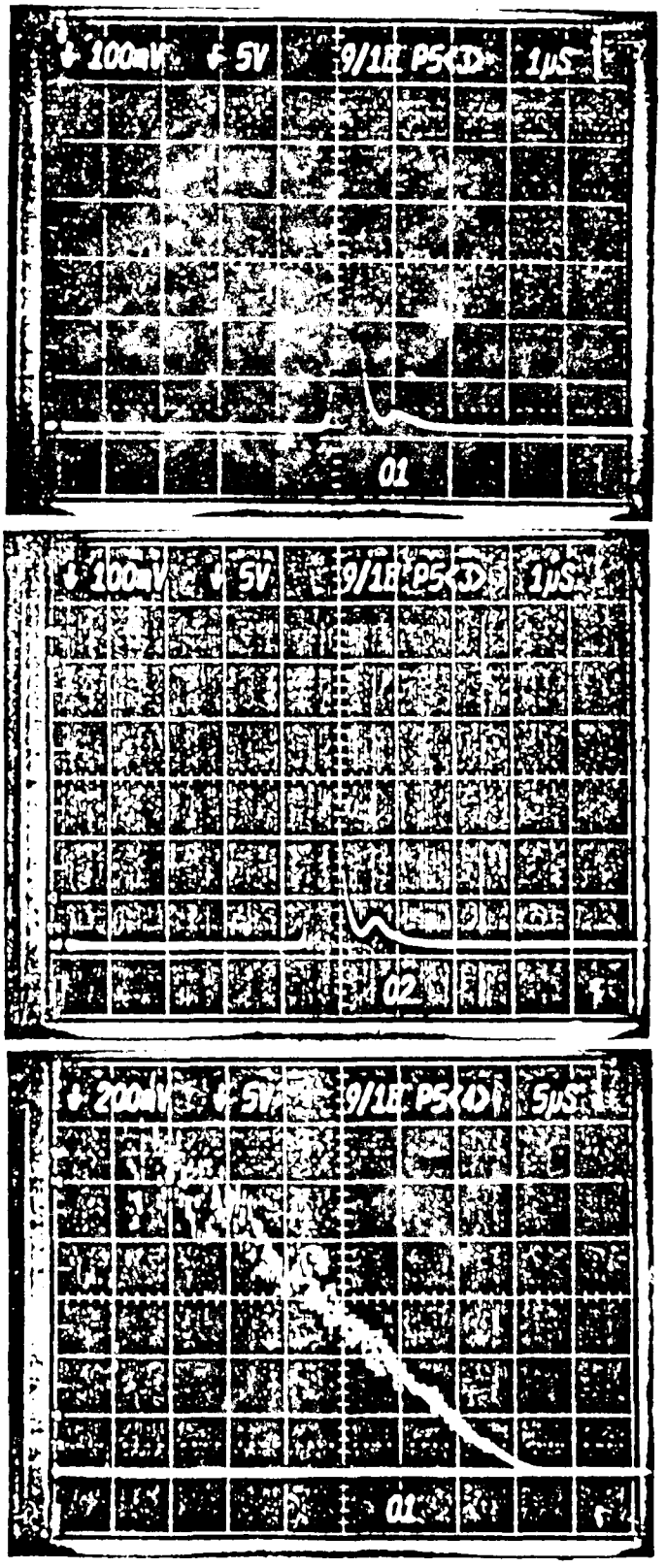

Table F.10 (Continued)

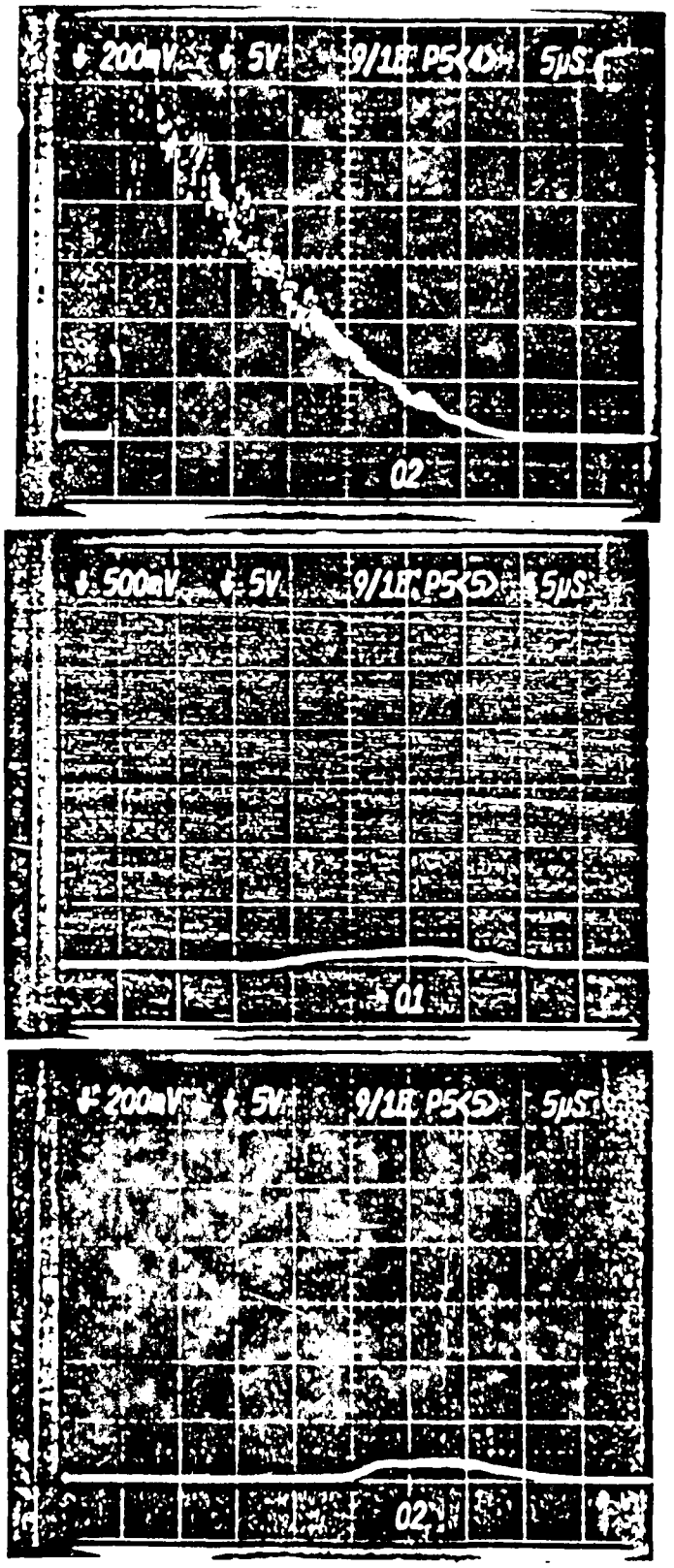

LIST OF REFERENCES

LIST OF REFERENCES

[1]. R. W. F. Gross and J. F. Bott, Handbook of Chemical Lasers, (New York: John Wiley and Sons, 1976).

[2]. J. V. V. Kasper and G. C. Pimentel, "HCl Chemical Laser," Phys. Rev. Lett. 14 (10), 352-354 (1965).

[3]. K. L. Kompa and G. C. Pimentel, "Hydrofluoric Acid Chemical Laser," J. Chem. Phys. 47 (2), 857-858 (1967).

[4]. O. D. Krogh and G. C. Pimentel, "Chemical Lasers from the Reactions of ClF and ClF_3 with H_2 and CH_4: A Possible Chain-Branching Chemical Laser," J. Chem. Phys. 56 (2), 969-75 (1972).

[5]. N. Jonathan, C. M. Meliar-Smith, S. Okuda, D. H. Slater, and D. Timlin, "Initial Vibrational Energy Level Distributions Determined by Infra-red Chemiluminescence II. The Reaction of Fluorine Atoms with Hydrogen Halides," Molec. Phys. 22 (4), 561-574 (1971).

[6]. K. G. Anlauf, J. C. Polanyi, W. H. Wong, and K. B. Woodall, "Distribution of Reaction Products III. Cl + HI, Cl + DI," J. Chem. Phys. 49 (11), 5189-5190 (1968).

[7]. J. C. Polanyi and K. B. Woodall, "Energy Distribution Among Reaction Products. VI. F + H_2, D_2," J. Chem. Phys. 57 (4), 1574-1586 (1972).

[8]. J. C. Polanyi and J. J. Sloan, "Energy Distribution Among Reaction Products. VII. H + F_2," J. Chem. Phys. 57 (11), 4988-4998 (1972).

[9]. O. M. Batovskii, G. K. Vasilijev, E. F. Makarov, and V. L. Talrose, "Chemical Laser Operating on Branched Chain Reaction of Fluorine with Hydrogen," Sov. Phys. JETP Lett. 9 (6), 200-201 (1969).

[10]. N. G. Basov, L. V. Kulakov, E. P. Markin, A. I. Nikitin, and A. N. Oraevskii, "Emission Spectrum of a Chemical Laser Using an H_2 + F_2 Mixture," Sov. Phys. JETP Lett. 9 (11), 375-378 (1969).

[11]. L. D. Hess, "Pulse Laser Emission Chemically Pumped by the Reaction Between Hydrogen and Fluorine," J. Chem. Phys. 55 (5), 2466-73 (1971).

[12]. N. R. Greiner, L. S. Blair, E. L. Patterson, and R. A. Gerber, "100 Gigawatt $H_2 + F_2$ Laser Initiated by an Electron Bean," IEEE J. Quant. Elec. QE-9 (9), 780 (1974).

[13]. R. L. Kerber, A. Ching, M. L. Lundquist, and J. S. Whittier, "An Efficiently Initiated Pulsed $H_2 + F_2$ Laser," IEEE J. Wuant. Elec. EQ-9 (6), 607-609 (1973).

[14]. J. V. Parker and R. R. Stephens, "Pulsed HF Chemical Laser with High Electrical Efficiency," Appl. Phys. Lett. 22 (9), 450-2 (1973).

[15]. S. Marcus and R. J. Carbone, "Gain and Relaxation Studies in Transversely Excited HF Lasers," IEEE J. Quant. Elec. QE-8 (7), 651-5 (1972).

[16]. D. H. Stone, "An Information Theory Approach to Hydrogen Halide Reaction Product Distributions," Ph.D. Thesis (1980).

[17]. S. N. Suchard, R. W. F. Gross, and J. S. Whittier, "Time-Resolved Spectroscopy of a Flash-Initiated $H_2 + F_2$ Laser," Appl. Phys. Lett. 19 (10), 411-3 (1971).

[18]. G. G. Dolgov-Savel'ev, V. A. Polyakov, and G. M. Chumak, "Laser Emission in the 2.8 Range Involving Vibration-Rotation Transitions in the HF Molecule," Sov. Phys. JETP 31 (4), 643-6 (1970).

[19]. N. R. Greiner, "Submicrosecond Pulses from a Hydrogen-Fluorine Laser with High Energy Density and Quantum Efficiency," IEEE J. Quant. Elec. QE-8 (12), 872-6 (1972).

[20]. N. Cohen, private communication.

[21]. J. K. Hancock and W. H. Green, "Vibrational Deactivation of HF(v = 1) in Pure HF and in HF-Additive Mixtures," J. Chem. Phys. 57 (11), 4515-4529 (1972).

[22]. W. R. Watkins, R. L. Spellicy, K. O. White, B. Z. Sojka, and L. R. Bower, "Water Absorption Coefficients at HF Laser Wavelengths (2.64-2.93 μm)," Appl. Opt. 18 (10), 1582-9 (1979),

[23]. R. L. Kerber, R. C. Brown, and K. A. Emery, "Rotational Nonequilibrium Mechanisms in Pulsed $H_2 + F_2$ Chain Reaction Lasers. 2: Effect of VR Energy Exchange," Appl. Opt. 19 (2), 293-300 (1980).

[24]. G. M. Jursich and F. F. Crim, "Vibrational Relaxation of HF (v = 3,4,5)," J. Chem. Phys. 74 (8), 4455-4464 (1981).

[25]. T. J. Foster and F. F. Crim, "Vibrational Relaxation of HF (v = 3,4,5) Between 300 and 700 K," J. Chem. Phys. 75 (8), 3871-5 (1981).

[26]. R. F. Heidner III, J. F. Bott, C. E. Gardner, and J. E. Melzer, "Absolute Rate Coefficients for F + H_2 and F + D_2 at 295K," J. Chem. Phys. 70 (10), 4509-14 (1979).

[27]. E. Wurzberg and P. L. Houston, "The Temperature Dependence of Absolute Rate Constants for the F + H_2 and F + D_2 Reactions," J. Chem. Phys. 72 (9), 4811-4 (1980).

[28]. G. G. Dolgov-Savel'ev, V. F. Zharov, Yu. S. Neganov, and G. M. Chumak, "Vibrational-Rotational Transitions in an H_2 + F_2 Chemical Laser," Sov. Phys. JETP 34 (1), 34-7 (1972).

[29]. V. T. Galochkin, S. I. Zavorotnyi, V. N. Kosinov, A. A. Ovchinnikov, A. N. Oraevskii, and N. F. Starodubtsev, "Investigation of the Characteristics of a Chemical HF Laser Excited by CO_2 Laser Pulses," Sov. J. Quant. Elec. 6 (1), 66-69 (1976).

[30]. H. Hokazono, K. Hishihuma, K. Watanabe, M. Obara, and T. Fujioka, "A High Efficiency HF(H_2/F_2) Chemical Laser Initiated with a Surface-Spark Ultraviolet Flash," J. Appl. Phys. 53 (3), 1359-63 (1982).

[31]. R. W. F. Gross, J. Cohen, and T. A. Jacobs, "HF Chemical Laser Produced by Flash Photolysis of $F_2O_2H_2$ Mixtures," J. Chem. Phys. 48 (8), 3821-2 (1968).

[32]. K. L. Kompa, J. H. Parker, and G. C. Pimentel, "UF_6 - H_2 Hydrogen Fluoride Chemical Laser: Operationa and Chemistry," J. Chem. Phys. 49 (10), 4257-64 (1968).

[33]. K. L. Kompa, P. Gensel, and J. Wanner, "New Hydrogen Fluoride Chemical Lasers," Chem. Phys. Lett. 3 (4), 210-12 (1969).

[34]. V. S. Burmasov, G. G. Dolgov-Savel'ev, V. A. Polyakov, and G. M. Chumak, "Quantum Yield of Generation of an H_2 + F_2 Mixture," ZhETF Pis. Red. 10 (1), 42-4 (1969).

[35]. A. N. Chester and L. D. Hess, "Study of the HF Chemical Laser by Pulse-Delay Measurements," IEEE J. Quant. Elec. QE-8 (1), 7-13 (1973).

[36]. P. Gensel, K. L. Kompa, and J. Wanner, "Flash Characteristics as an Important Parameter in Chemical Laser Experiments," Chem. Phys. Lett. 7 (6), 583-6 (1970).

[37]. L. D. Hess, "Chain Reaction Chemical Laser Using H_2-F_2-He Mixtures," Appl. Phys. Lett. 19 (1), 1-3 (1971).

[38]. J. Wilson and J. S. Stephenson, "Atmospheric-Pressure Pulsed Chemical Laser," Appl. Phys. Lett. 20 (2), 64-6 (1972).

[39]. S. N. Suchard, R. L. Kerber, G. Emanuel, and J. S. Whittier, "Effect of H_2 Pressure on Pulsed H_2 + F_2 Laser. Experiment and Theory," J. Chem. Phys. 57 (12), 5065-75 (1972).

[40]. D. B. Nichols, K. H. Wolstad, and J. D. McClure, "Time Resolved Spectroscopy of a Pulsed H_2 + F_2 Laser with Well-Defined Initial Conditions," J. Appl. Phys. 45 (12), 5360-6 (1974).

[41]. H. L. Chen, R. L. Taylor, J. Wilson, P. Lewis, and W. Fyfe, "Atmospheric Pressure Pulsed HF Chemical Laser," J. Chem. Phys. 61 (1), 306-18 (1974).

[42]. S. N. Suchard, "Lasing from the Upper Vibrational Levels of a Flash-Initiated H_2 + F_2 Laser," Appl. Phys. Lett. 23 (2), 68-70 (1973).

[43]. V. P. Borisov, S. D. Velikanov, S. B. Kormer, M. V. Sinitsyn, and Yu. N. Frolov, "Investigation of Spectral and Time Characteristics of a HF Chemical Laser," Sov. J. Quant. Elec. 7 (2), 187-90 (1977).

[44]. M. Obara and T. Fujioka, "Time-Resolved Spectroscopic Studies on the TE HF Chemical Lasers Using the Mixtures of SF_6/H_2 and SF_6/CH_4," Jap. J. Appl. Phys. 13 (4), 675-583 (1974).

[45]. N. G. Basov, V. T. Galochkin, L. V. Kulakov, E. P. Markin, A. I. Nikitin, and A. N. Oraevskii, "Chemical Lasers Utilizing Mixtures of Fluorine or Nitrogen Fluorides with Deuterium," Sov. J. Quant. Elec. 1 (4), 348-54 (1972).

[46]. W. H. Green and M. C. Lin, "Pulse-Discharge-Initiated Chemical Lasers. III. Complete Population Inversion in HF," J. Chem. Phys. 54 (7), 3222-3 (1971).

[47]. T. V. Jacobson, G. H. Kimbell, and D. R. Snelling, "A High-Repetition-Rate Chemical HF Laser," IEEE J. Quant. Elec. QE-9 (4), 496-7 (1973).

[48]. H. Pummer, W. Breitfeld, H. Wedler, G. Klement, and K. L. Kompa, "Parameter Study of a 10-J Hydrogen Fluoride Laser," Appl. Phys. Lett. 22 (7), 319-20 (1973).

[49]. S. Marcus and R. J. Carbone, "Performance of a Transversely Excited Pulsed HF Laser," IEEE J. Quant. Elec. QE-7 (10), 493-4 (1971).

[50]. N. R. Greiner, "Time-Resolved Output Spectrum from a Hydrogen Fluoride Laser Using Mixtures of SF_6 and HI," IEEE J. Quant. Elec. QE-11 (10), 844-5 (1975).

[51]. C. J. Ultee, "Pulsed Hydrogen Fluoride Lasers," IEEE J. Quant. Elec. QE-6 (10), 647-8 (1970).

[52]. N. G. Basov, V. T. Galochkin, V. I. Igoshin, L. V. Kulakov, E. P. Martin, A. I. Kikitin, and A. N. Oraevsky, "Spectra of Stimulated Emission in the Hydrogen-Fluorine Reaction Process and Energy Transfer from DF to CO_2," Appl. Opt. 10 (8), 1814-20 (1971).

[53]. G. G. Dolgov-Savel'ev and A. A. Podminogin, "Pulsed Laser Utilizing a Fluorine and Hydrogen Mixture," Sov. J. Quant. Elec. 2 (4), 348-352 (1973).

[54]. K. J. Pettipiece, "A TEM_{00} Short Pulse KF Oscillator," Chem. Phys. Lett. 14 (2), 261-3 (1972).

[55]. W. H. Green and M. C. Lin, "Pulsed Discharge Initiated Chemical Lasers-Part II: HF Laser Emission from NF_3 and N_2F_4 Systems," IEEE J. Quant. Elec. QE-7 (2), 98-101 (1971).

[56]. A. A. Podminogin, "Hydrogen Fluoride (Deuterium Fluoride) Pulsed Laser," Sov. J. Quant. Elec. 3 (3), 229-31 (1973).

[57]. T. F. Deutsch, "Laser Emission from HF Rotational Transitions," Appl. Phys. Lett. 11 (1), 18-20 (1967).

[58]. D. P. Akitt and J. T. Yardley, "Far-Infrared Laser Emission in Gas Discharges Containing Boron Trihalides," IEEE J. Quant. Elec. QE-6 (2), 113-6 (1970).

[59]. O. R. Wood, E. G. Burkhardt, M. A. Pollack, and T. J. Bridges, "High Pressure Laser Action in 13 Gases with Transverse Excitation," Appl. Phys. Lett. 18 (4), 112-5 (1971).

[60]. O. R. Wood and T. Y. Chang, "Transverse-Discharge Hydrogen Halide Lasers," Appl. Phys. Lett. 20 (2), 77-9 (1972).

[61]. J. H. Smith and D. W. Robinson, "Chemical Pumping of Pure Rotational HF Lasers," J. Chem. Phys. 74 (9), 5111-5 (1981).

[62]. E. R. Sirkin and G. C. Pimentel, "HF Rotational Laser Emission through Photoelimination from Vinyl Fluoride and 1,1-Difluoroethene," J. Chem. Phys. 75 (2), 604-12 (1981).

[63]. T. F. Deutsch, "Gain Measurements on Uniformly Excited HF/DF TEA Lasers," IEEE J. Quant. Elec. QE-10 (1), 84-7 (1974).

[64]. C. R. Jones, "Gain and Energy Measurements on an HF/DF Electrically Pulsed Chemical Laser," Appl. Phys. Lett. 22 (15), 653-5 (1973).

[65]. R. A. Chodzko, D. J. Spencer, and H. Mirels, "Zero-Power Gain Measurements in a CW HF Laser Using a Pulsed-Probe Laser," IEEE J. Quant. Elect. QE-9 (5), 550-3 (1973).

[66]. S. N. Suchard, "Small-Signal Gain and Time-Resolved Spectroscopy of the D_2-F_2/CO_2 Pulsed Chemical Transfer Laser System," J. Quant. Elec. QE-10 (1), 87-9 (1974).

[67]. L. J. Denes and L. A. Weaver, "Laser Gain Characterization of Near-Atmosphere CO_2/N_2/He Glows in a Planar Electrode Geometry," J. Appl. Phys. 44 (9), 4125-36 (1973).

[68]. R. C. Brown, "A Theoretical Assessment of Vibrational to Rotational Energy Exchange in the Hydrogen Fluoride Chemical Laser," Ph.D. Thesis (1980).

[69]. J. J. T. Hough, "A Theoretical and Experimental Investigation of the Mechanisms of the Hydrogen Fluoride Pulsed Chemical Laser," Ph.D. Thesis (1975).

[70]. R. L. Kerber, G. Emanuel, and J. S. Whittier, "Computer Modeling and Parametric Study of a Pulsed H_2 + F_2 Laser," Appl. Opt. 11 (5), 1112-23 (1972).

[71]. N. Cohen, M. A. Kwok, R. L. Wilkins, and J. F. Bott, "The Status of Rotational Disequilibrium in HF Chemical Lasers," (to be published).

[72]. M. C. Potter and J. F. Foss, Fluid Mechanics, (New York: The Ronald Press Company, 1975).

[73]. D. J. Spencer, J. A. Beggs, and H. Mirels, "Small Scale HF(DF) Chemical Laser," J. Appl. Phys. 48 (3), 1206-1211 (March 1977).

[74]. R. C. Brown and R. L. Kerber, "Parametric Study of Rotational Nonequilibrium Models of Pulsed HF and DF Chain Reaction Chemical Lasers," Michigan State University Technical Report, MSU-ENG-80-013 (January 1980).

[75]. W. K. Jaul and R. L. Kerber, "A Theoretical Assessment of the Kinetic Limitations of the Chemically Pumped HF Optical Resonant Transfer Laser," Michigan State University Technical Report, MSU-ENG-82-018 (September 1982).

[76]. M. F. Weisbach, V. R. Buonadonna, C. J. Artura, W. B. Shepherd, J. E. Schrader, and J. D. McClure, "PHOCL-50: A 50 Liter Photoinitiated Chemical Laser," Boeing Report D180-24898-1, Boeing Corporation, Seattle, Washington (November 1978).

[77]. J. S. Whittier and R. L. Kerber, "Performance of an HF Chain-Reaction Laser with High Initiation Efficiency," IEEE J. Quant. Elec. QE-10 (11), 844-7 (1974).

[78]. J. B. Levy and B. K. W. Copeland, "The Kinetics of the Hydrogen-Fluoride Reaction. II. The Oxygen-Inhibited Reaction," J. Phys. Chem. 69 (2), 408-16 (1965).

[79]. R. L. Taylor, P. F. Lewis, and J. Cronin, "A Mechanism for the Photochemical Induced Combustion of H_2/F_2 Mixtures Inhibited by O_2," J. Chem. Phys. 73 (5), 2218-23 (1980).

[80]. R. A. McClatchey, W. S. Benedict, S. A. Clough, D. E. Burch, R. F. Calfee, K. Fox, L. S. Rothman and J. S. Garing, "Air Force Cambridge Research Laboratory Atmospheric Absorption Line Parameter Compilation," AFCRL-TR-73-0096 (1973).

[81]. R. T. Lagemann and E. A. Jones, "The Infrared Spectrum of Sulfur Hexafluoride," J C P 19(5), 534-6 (1951).

[82]. H. R. Carlon, "Infrared Absorption Coefficient (3-15 μm) for Sulfur Hexafluoride (SF_6) and Freon (CCl_2F_2)," A O 18(10), 1474-5 (1979).

[83]. G. Herzberg, Molecular Spectra and Molecular Structure III. Electronic Spectra and Electronic Structure of Polyatomic Molecules, (Princeton: D. Van Nostrand Co., Inc. 1967).

[84]. G. B. King, private communication.

[85]. G. Guelachvili, "Absolute Wavenumber Measurements of 1-0, 2-0, HF and 2-0, $H^{35}Cl$, $H^{37}Cl$ Absorption Bands," Opt. Comm. 19(1), 150-4 (1976).

[86]. W. Lafferty, private communication.

[87]. F. E. Frawey and K. N. Rao, "High Resolution Infrared Spectra of Water Vapor," J. Mol. Spec. 29(3), 348-64 (1969).

[88]. C. J. Ultee, "Compact Pulsed HF Lasers," Rev. Sci. Instr. 42(8), 1174-6 (1971).

[89]. R. V. Jacobson, G. H. Kimbell and D. R. Swelling, "A High Repetition-Rate Chemical HF Laser," IEEE J. QEL QE-9(4), 496-7 (1973).

[90]. D. D. Krogh and G. C. Pimentel, "ClF_x-H_2 Chemical Lasers (x = 1,3,5): Vibrational-Rotational Emission by HF from States with High Rotational Excitation," J. Chem. Phys. 67 (7), 2993-3001 (1977).

[91]. N. Skribanowitz, I. P. Herman, R. M. Osgood, M. S. Feld, and A. Javan, "Anisotropic Ultrahigh Gain Emission Observed in Rotational Transitions in Optically Pumped HF Gas," Appl. Phys. Lett. 20 (11), 428-31 (1972).

[92]. J. Butler, private communication.

[93]. W. Q. Jeffers, private communication.

[94]. L. Kanke, private communication.

[95]. N. Cohen, "A Review of Rate Coefficients in the H_2 + F_2 Chemical Laser System-Supplement (1977)," TR-78-41, The Aerospace Corporation, El Segundo, California (June 1978).

[96]. R. L. Wilkins, "Mechanisms of Energy Transfer in Hydrogen Fluoride Systems," J. Chem. Phys. 67 (12), 5838-54 (1977).

[97]. F. E. Bartoszek, D. M. Manos, and J. C. Polanyi, "Effect of Changing Reagent Energy. X. Vibrational Threshold Energies for Reaction Paths HF(v)+D, F+HD and H+DE," J. Chem. Phys. 69 (2), 933-5 (1979).

[98]. H. A. Watts, private communication.

[99]. R. L. Kerber and J. J. T. Hough, "Rotational Nonequilibrium Mechanisms in Pulsed H_2 + F_2 Chain Reaction Lasers. I: Effect on Gross Laser Performance Parameters," Appl. Opt. 17 (15), 2369-80 (1978).

[100]. P. A. Lovoi, R. Maynard, and B. Smith, "Flashlamp Efficiency for Photoinitiation in HF/DF Lasers," Proceedings International Conference on Lasers 1979, 530, (December 1979).

[101]. M. J. Berry, "A Comparison of Photolytic Fluorine-Atom Sources for Chemical Laser Studies," Chem. Phy. Lett 15 (2), 269-73 (1972).

[102]. W. B. Gretner, "A Thermal Actinometer for Flash Photolysis," Chem. Phys. Lett. 16 (2), 324-7 (1972).

[103]. S. N. Suchard and D. G. Sutton, "Laser Actinometry of Flash-Photolyzed H_2/F_2/He Mixtures," IEEE J. Quant. Elec. QE-10 (5), 430-3 (1974).

[104]. B. D. Crane, Ph.D. Thesis, 1980.

[105]. N. Cohen, private communication.

[106]. S. J. Leone, private communication.

[107]. G. Emanuel, W. D. Adams, and E. B. Turner, "PESALL-1: A Chemical Laser Computer Program," TR-0172(2776)-1, The Aerospace Corporation, El Segundo, CA (March 1972).

[108]. R. L. Wilkins, "Vibration-Rotation Bands of HF and DF," TR-0077(2063)-7, The Aerospace Corporation, El Segundo, CA (September 1977).

[109]. J. J. T. Hough, "Lorentz Broadening in the Modeling of the HF Chemical Laser," Appl Opt 16 (8), 2297-2307 (1977).

[110]. R. E. Meredith and F. G. Smith, "Investigations of Fundamental Laser Processes Vol. II. Computations of Electric Dipole Matrix Elements for Hydrogen Fluoride and Deuterium Fluoride," 84130-39-T(II), The Environmental Research Institute of Michigan, Ann Arbor, MI (November 1971).

[111]. J. M. Herbelin and G. Emanuel, "Einstein Coefficients for Diatomic Moelcules," J Chem Phys 60 (2), 689-696 (1974).

[112]. L. F. Shampine, H. A. Watts, and S. M. Davenport, "Solving Nonstiff Ordinary Differential Equations-The State of the Art," SIAM Review 18 (3), 376-411 (1976).

[113]. E. B. Turner, G. Emanuel, and R. L. Wilkins, "The NEST Chemistry Computer Program, Vol. I," TR-0059(6240-01)-1, The Aerospace Corporation, El Segundo, CA (July 1970).

[114]. F. Daniels and R. A. Alberty, Physical Chemistry, 4th edition, (New York: John Wiley and Sons, 1975).

[115]. H. K. Steunenberg and R. C. Vogel, "The Absorption Spectrum of Fluorine," J Amer Chem Soc 78 (5), 901-902 (1956).

[116]. A. Yariv, Quantum Electronics, 2nd edition (New York: John Wiley and Sons, 1975).


ATE
LMED